Proceedings of the International Conference on Climate Change and Sustainability Engineering in ASEAN (CCSE-ASEAN) 2019

Enhancing the Role of Engineering in Climate Change Mitigation and Sustainable Development in ASEAN Region

Jember, Indonesia
13 November 2019

Hosted by

https://ccse-asean.org

Sponsored by

Faculty of Engineering
Universitas Jember

School of Engineering
University of San Carlos

Proceedings of the International Conference on Climate Change and Sustainability Engineering in ASEAN (CCSE-ASEAN) 2019

Enhancing the Role of Engineering in Climate Change Mitigation and Sustainable Development in ASEAN Region

Steering Committee

Dr. Ir. Entin Hidayah, M.UM (Universitas Jember)
Prof. Evelyn B. Taboada, Ph.D (University of San Carlos)
Engr. Ricardo L. Fornis (University of San Carlos)
Engr. Luis K. Cabatingan (University of San Carlos)
Dr. Eng. Triwahju Hardianto (Universitas Jember)
Syamsul Arifin, S.T., M.T. (Universitas Jember)
Sumardi, S.T., M.T. (Universitas Jember)

Organizing Committee

General Chair	:Dr. Eng. Triwahju Hardianto (Universitas Jember)
Vice Chair	:Luzvisminda M. Bellotindos, Ph.D. (University of San Carlos)
Vice Chair	:Boy Arief Fachri, S.T.,M.T., Ph.D (Universitas Jember)
Scientific Committee	:Prof. Dr. Ir. Bambang Sujanarko, M.M. (Universitas Jember)
	Mahros Darsin, S.T., M.Sc, Ph.D (Universitas Jember)
Scientific Publication	:Ir. Khairul Anam, S.T., M.T., Ph.D (Universitas Jember)
Funding	:Syamsul Arifin, S.T., M.T. (Universitas Jember)
Tour	:Dr. Yeny Dokhikah, S.T., M.T. (Universitas Jember)
Public Relation & Information Technology	:Abdur Rohman, Ph.D (Universitas Jember)
	Ivan Augusta Farizkha, M.T. (Universitas Jember)
	Widya Cahyadi, M.T. (Universitas Jember)
	Andrita C. Eska, M.T. (Universitas Jember)
	Dedy W Herdiyanto, M.T. (Universitas Jember)
	Devita A. Larasati, S.T., M.Sc. (Universitas Jember)
	Fanteri Aji Dharma, S.T., M.S. (Universitas Jember)

Reviewers

Prof. Dr. Ir. Bambang Sujanarko (Universitas Jember)
Prof. Dr. Saiful Bukhori (Universitas Jember)
Dr. Ian Dominic Tabañag (University of San Carlos)
Engr. Aure Flo Oraya, B.S., M.S. (University of San Carlos)
R.A. Ilyas, Ph.D (Universiti Teknologi Malaysia)
Sri Wahyuni, S.T., M.T., Ph.D (Brawijaya University)
Dr. Eng. Mega Nur Sasongko (Brawijaya University)
Ir. Hadi Suyono, S.T., M.T., Ph.D., IPM (Brawijaya University)
Sutrasno Kartohardjono, Ph.D (Universitas Indonesia)
Dr. I Gede Tunas (Universitas Tadulako)
Dr. Willyanto Anggono, S.T., M.Sc (Petra Christian University)
Diky Siswanto, S.T., M.T., Ph.D (Universitas Widyagama Malang)
Dr. Retno Wulandari, S.T., M.T. (Universitas Negeri Malang)

Publisher

Editorial Staff

Cover: Design by Arif Hidayatulloh and Abdur Rohman with Inkscape. Photo by Pia Britton from Pexels

Foreword

Strengthening the response to the threat of climate change has been a major international goal in the last decade. It is the sole aim of the Paris Agreement and a goal in the UN Sustainable Development Goals. The climate change has been a more critical issue in regions with tropical climates such as ASEAN member countries. The International Conference on Climate Change and Sustainability in ASEAN 2019 (CCSE-ASEAN 2019) is an effort to discuss the best response to the climate change that would certainly pose significant threats to sustainable development in Southeast Asia. This conference aims at encouraging rich discussions and continuous collaborations among researchers, engineers, leaders in regional government and industries, and students on enhancing the role of the engineering field with its major innovations in ASEAN countries to mitigate climate change impacts.

CCSE-ASEAN 2019 received 171 submissions of abstracts and full papers. On the basis of a single-blind review process, in which two or three independent reviewers were assigned for each submission, 100 full papers were accepted for oral presentation. The presenters at CCSE-ASEAN 2019 came from several countries including Indonesia, Philippines, Japan, China, and Iraq. The authors presented original scientific reports on varied topics but highly relevant to climate change and sustainability studies.

Based on the recommendation of CCSE ASEAN 2019 Scientific Committee and the authors' consent, the papers presented at CCSE-ASEAN 2019 had been submitted to several publication outlets. Fifty three papers have been published in *AIP Conference Proceedings*. A paper has been published in the *International Journal of Renewable Energy Development* (IJRED). Nine papers have been accepted for publication in *Journal of Energy, Mechanical, Material, and Manufacturing Engineering* (JEMMME). A paper has been accepted for publication in *Jurnal Teknik Sipil dan Perencanaan* (JTSP).

This proceeding is a collection of 26 papers. Application of some emerging technologies, including smart facial and wood types detection, real-time monitoring of volcanoes, and power plants, and rectenna are reported in eight papers. Four papers are on bio-based chemicals discussing coffee residue composites, diesel and coconut oil, and sugar cane fiber. Furthermore, there are two papers on photovoltaic systems, three papers on advanced materials, and a paper on flood detection. Other papers discussed other topics, including ergonomic chairs, honey filter machines, and Sustainable Development Goals. We sincerely thank all authors who have submitted their papers to CCSE-ASEAN 2019 especially to the authors who patiently wait for the publication process.

Our deep gratitude goes to the authors and the reviewers for their dedicated work. We sincerely thank all keynote speakers for their insightful lectures in the plenary session. We would also thank all committee members of CCSE-ASEAN 2019 for their continuous hard work and cooperation, and we thank our sponsors for their support. We do hope that all the participants of CCSE-ASEAN 2019 would gain meaningful inspiration and fruitful collaboration from the conference.

Chair of CCSE-ASEAN 2019

Dr. Eng. Triwahju Hardianto

Table of Contents

Chapter 3: Advanced Materials

Chapter 4: Sustainable Energy

Chapter 5: Disaster Management

Chapter 6: Miscellaneous Engineering

Design Real Time Monitoring of Volcanos Based On Hydrogen Autonomy

Johan Pamungkas[1, a)] and Hery Teguh Setiawan[2, b)]

[1,2] Universitas Tidar
Jalan Kapten Suparman No. 39 Potrobangsan, Magelang Utara 56116, Jawa Tengah

a)johan@untidar.ac.id
b)hery.teguh.s@untidar.ac.id

Abstract. Wireless Sensor Network is a wireless communication technology that can be used for remote sensing because with the WSN it is possible to build a monitoring technology that can consist of two or more sensor nodes scattered in a particular monitoring area and coordinated by the cluster head if the topology used is Clustering Topology. The sensor node in WSN functions as one component that has the function to transmit data and receive data, the current technology that can represent the latest WSN technology is XBee3 which is a WSN module that experiences improved performance both in terms of hardware or software, but which remains a the problem that occurs is the limited resources used in the sensor node itself because the sensor node in the WSN serves to carry out the process of communication or sensing continuously especially in the volcano real-time monitoring system that requires a good level of reliability, accuracy and integrated. For this reason, a Real-Time Monitoring Volcano system is used that uses WSN which is supported by Hydrogen Autonomy which is used as a resource on sensor nodes and cluster heads, which will also be observed in the use of power through power monitors so that sensor nodes are known. Measurements are made with several scenarios for the XBee3 module, for conditions when sending data, receiving data, Lost of Sight (LOS), and Non-Lost of Sight (NLOS).

INTRODUCTION

Wireless Sensor Network (WSN) has the potential to be developed in various sectors such as transportation, remote sensing, or geological disaster mitigation. Many studies have been conducted on studying and developing WSN. Some hardware developments were resulting in the prospect of developing low-cost WSN using low power and minimalist design which can be used in all remote sensing needs. In addition, the developments were conducted by combining a great number of sensor nodes and artificial intelligence in network management to realize the optimal system. Thus, it is possible to optimally, reliably and efficiently carry out the process of data collection, data processing, data analysis, and dissemination of obtained information. Wireless Sensor Network is a large scale network consisting of various types of networks connected. Sensor data is shared among sensors. Sensor data is used as input to distribute estimates of information data which is then extracted according to needs to obtain relevant information from each sensor installed, to increase the accuracy level, to suppress the cost, and to modify the sensor node deployments easily.

In the previous study, the Design of Real-Time Monitoring Based on Wireless Sensor Network on the Volcanic Eruption Disaster Mitigation concluded that there are several problems which need to be considered when using the Wireless Sensor Network. First, the number of nodes needed in the deployment process gives the most significant influence because the number of nodes installed is mainly used for sensing process (obtaining data). It is necessary to determine the size or area of the environmental range as well as the amount of sampling frequency needed. In general, a system consists of more Wireless Sensor Network nodes installed has a better quality of the obtained data and the greater energy or power used. [1]

The increasing attention on the progress of autonomous energy in sensing systems and computing systems that operate in a monitoring system makes studies in the search for alternative sources of electrical power, power

conversion, and energy harvesting become the future key technology. It is because the ultimate goal of this is to combine the latest update energy generation technologies with the existing system. This paper introduces an embedded system that increases the availability of supporting energy through fuel cell technology, hereinafter referred to as Hydrogen Autonomy. Hydrogen Autonomy is the generation of hydrogen chemical energy into mechanics through either internal or external hydrogen combustion processes. Thus, a source that can supply energy independently of a system can be produced. Hydrogen autonomy can be used as a source of fuel cell generator. This study aimed to review whether hydrogen autonomy technology can be used and has the potential to be used in the volcanic real-time monitoring system, to classify power supply methods, to distribute power at nodes, and to transmit the energy for wireless sensor network.

PREVIOUS RESEARCH

A previous study entitled Power Consumption and Maximizing Network Lifetime during Communication of Sensor Node in Wireless Sensor Networks provided a general description of how power consumption on sensor nodes are used for monitoring, sensing, and communicating between nodes and other nodes as well as the amount of power used in processing data. An analysis of power consumption on sensor nodes was performed in this study using scenario influenced by several factors in the use of power at sensor nodes. These factors include the use of power when the sensor node senses, the power consumption during the process of sensor nodes sensing data, and the power consumption when one node and another node communicate (transmit sensing data). [2]

Whereas a study entitled "A Portable Hybrid Hydrogen Fuel Cell-Battery Power Unit For Wireless Sensor Network" showed the results of the analysis of Multi Energy Harvesting architecture used in hybrid equipment for a low power system that can configure high levels. Architecture combined with an efficient energy harvesting system and micro fuel cell technology increased the efficiency of the converter used up to 86%. Moreover, this study showed the matching level of impedance level that exists in the maximum power transfer and different airflow speeds using the Buck-Boost Converter Type operated in discontinued mode. Therefore, the studied architecture showed that the system could manage power usage by using very low power microcontrollers to recognize environmental conditions. Thus, the parameters of the Maximum Power Point Tracking (MPPT) and the level of energy use can be monitored properly (Magno, Brunelli, Benini, 2014). The nature of solar panels output or so-called as photovoltaic (PV) panels is in the form of currents and voltages which are non-linear and highly dependent on natural conditions (including temperature and radiation received). Therefore, the characteristics of the Non-Linear PV found it difficult to get the maximum PV power using Maximum Power Point Tracking (MPPT) method.[3]

Wireless Sensor Network (WSN)

Wireless Sensor Network (WSN) is a technology which i sable to carry out monitoring by widely sharing and enabling Wireless communication. Wireless technology provides some advantages when it is used for the implementation of a wide range of system.
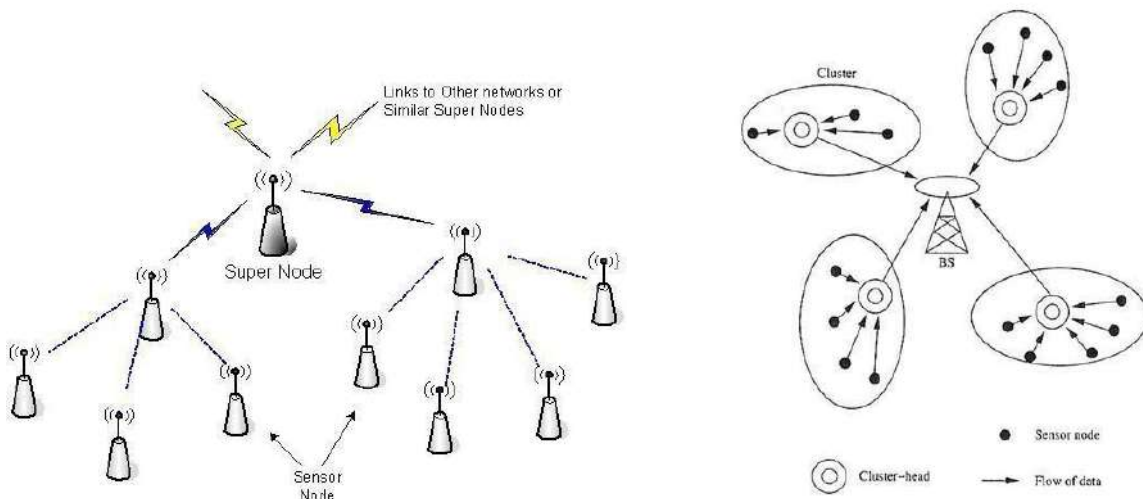
FIGURE 1. (a) Wireless Sensor Network, (b) Clustering Topology of Wireless Sensor Network
Sources of Figures: [11]

Clustering topology as shown in Figure 1(b) has different characteristics compared to other topologies such as:
a. Clustering topology groups sensor nodes into clusters.
b. Each cluster created is managed by the coordinator node or referred to as the cluster head.
c. The cluster head only has the function of sending data to the Base Station.
d. Data Fusion or the integration of some data received by each cluster head represent sesveral sensor nodes spread over a certain location.

WSN XBee3 Pro 802.15.4

XBee3 Pro is an RF module that has a working frequency at 2.4 GHz by the datasheet. Sending data on the XBee module will require a power supply of 2.1 to 3.6 VDC. Besides, the XBee3 module will overload with a current of 135 mA at the time of delivery and 15 mA at the time of reception with a range of 90m for NLOS and 32000m during the LOS. The Wireless Sensor Network module is an improvement from the previous model. The followings are the technical specification data of XBee3 Pro.

Fuel Cell

Fuel Cell is a simple technology used to make an electrochemical energy conversion device that will convert heat hydrogens in its process and oxygen into the water to simultaneously produce electrical energy. Fuel Cells used for implementation on the Real-Time Volcano Monitoring System power supply is PEM (Proton Exchange Membrane). 2 types of fuel cells that can be used to support the real-time volcanic monitoring system that uses hydrogen or methanol fuel. Both products can produce a capacity of up to 5 kW where the configuration of the Fuel Cell itself can be adjusted according to the needs tailored to the needs of each sensor node that is scattered and adjusted to its location. PEM Fuel Cell works with an electrolyte polymer in the form of a thin permeable layer. The efficiency ranges from 40 to 50 percent with the operating temperature around 80°C (around 175 °F). The output of Fuel Cell ranges from 50 to 250 kW. Solid flexible Electrolyte will not leak or crack. These membrane cells work at fairly low temperatures.
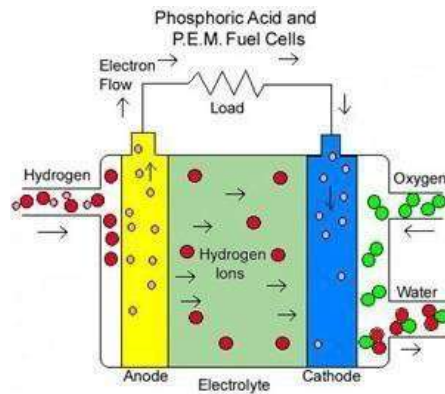
FIGURE 2. PEM Fuel Cell
Source of Figure:[12]

Fuel Cells used for implementation on the Real-Time Volcano Monitoring System power supply is PEM (Proton Exchange Membrane). 2 types of fuel cells that can be used to support the real-time volcanic monitoring system, hydrogen and methanol fuel. Both products can produce a capacity of up to 5 kW. The configuration of the Fuel Cell can be adjusted according to the needs tailored to the needs of each sensor node scattered and adjusted to its location. PEM Fuel Cell works with an electrolyte polymer in the form of a thin permeable layer. The efficiency ranges from 40 to 50 percent. Meanwhile, the operating temperature is around 80 °C (around 175 °F). The output of this Fuel Cell ranges from 50 to 250 kW. Solid Flexible Electrolyte will not leak or crack.

HES Aerostack is a Fuel Cell technology that uses Hydrogen-based Aerial Autonomy technology that has several types of energy output produced, including 250 Watt, 500 Watt, 1000 Watt, 1500 Watt, and 2000 Watt. Aerostak is a complete power device that also includes PEM Cell Stak, Electronic Instrumentation Control, shock-resistant case, integrated air conditioner, and LiPo Hybrid Electronic Card. Besides the above mentioned, the strength of Aerostack is having alight weight. The followings are the Aerostak HES Technical Specifications Data.

TABLE 2. Aerostack Technical Specification Data

Stack Design	45 Cells
Stack Rated Power	500 Watt
Stack Peak Power	600 Watt
Stack Voltage Range	27.0 V – 42.8 V
Stack Current Range	0 -25 A
Air Input Temperature	0 -35 C
Cooling	Integrated Fan
Total FC System Weight	1300 gram
FC System Dimensions	194 mm x 105 mm x 166 mm
Hydrogen Input Pressure	0.6 – 0.8 Bar
Hydrogen Purity Required	99999%
Hydrogen Max. Consumption	< 7.6 L/Min
Start-Up Time	< 30 s
Suggested Hybrid LiPo	8S

RESEARCH METHODS

The following are the steps that had been implemented. In this paper, an experimental scenario was made, consisting of several stages. The following are the steps that have been implemented.

A. System Design

In this study, each sensor node and cluster had used Xbee3 Pro that worked at 2.4 GHz frequency connected with Aerostack modeled the same as the basic concept of clustering topology network. Each cluster consisted of 2 cluster heads while each cluster heads will set 4-8 WSNs. The test on the Module Xbee3 Pro was conducted to find out the amount of power consumption when sending data, receiving data, on a Stand-By Mode, and during the Power Consumption Test (Energy Consumption) on each sensor node. The sensor node architecture can be seen in Figure 5.
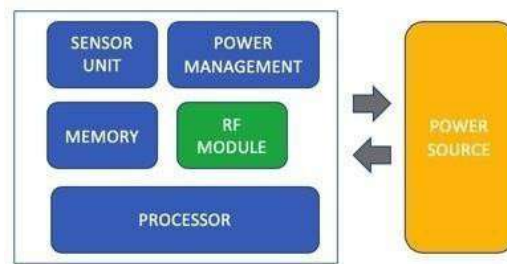
FIGURE 4. Sensor Node Architecture

B. The Test of Wireless Sensor Network Module Xbee3

The test of Xbee3 module was done to find out the amount of power consumption when sending data, receiving data, and on the Stand-By Mode.

C. *NLOS, LOS, and Power Consumption*

D. The Test of Receive Threshold and Transmitter Power

    a. Receive Threshold (Rx)
        Receive Threshold was the smallest power signal used to detect and receive transmitted data package.

    b. Transmitter Power (Tx)
        When a transmitter performs the process of sending information signals to a receiver, the transmitter expended power to carry out the transmission process. We can use this formula

$$Tx\ Power = V_{tx} I_x\ T \qquad (1)$$

Thus, transmitter power could be defined as the amount of power needed by a transmitter to transmit an information signal. Where, V is Voltage (Volt), I is Current (A) and T is Time (s).

EXPERIMENTS RESULT

Based on the testing at the Telecommunications Laboratory of Faculty of Engineering, Tidar University, the initial results from the testing of power consumption for each sensor node can be seen in Table III.

TABLE 3. Energy Consumption Of Wireless Sensor Network XBee3

Configuration	C1	C2	C3	C4
Tx Operating Current	130.0 mA	129.7 mA	128.4 mA	128.6 mA
Rx Operating Current	15 mA	14.9 mA	14.6 mA	14.6 mA
Standby Current	2 µA	2 µA	2 µA	2 µA
Charge Time (Single bit Transmitted)	0.582638889	0.584722222	0.630555556	0.626388889
Outdoor RF (LOS)	3200 m	3200 m	3198 m	3198
Indoor RF (NLOS)	90 m	90 m	90 m	90 m

From Table III, it can be inferred that the preliminary test showed that the power consumption for each sensor node indicated the amount of current used for data transmission (transmitter). It is known that the magnitude of the current operation was in the range of 128.4 mA – 130 mA. Meanwhile, in the receiving process (receiver), each node showed values ranging from 14.6 mA to 15 mA. The overall Standby Current was stable at 2µA.

TABLE 4. Result Test of NLOS Sensor Node Xbee3 C1-C4

Node Server Position	Node Server Position	Distance	Package Received	Energy Consumption (Tx/Rx)
Telecommunications Laboratory	Telecommunications Laboratory	10 m	Sent	60.75 mA/ 6.9 mA
Telecommunications Laboratory	Telecommunications Laboratory	20 m	Sent	60.75 mA/ 7.1 mA
Telecommunications Laboratory	Telecommunications Laboratory	30 m	Sent	60.90 mA/ 7.2 mA
Telecommunications Laboratory	Electronics Laboratory	40 m	Sent	67.00 mA/ 7.5 mA
Telecommunications Laboratory	Electronics Laboratory	50 m	Sent	65.95 mA/ 7.3 mA
Telecommunications Laboratory	Computer Laboratory	60 m	Sent	67.05 mA/ 7.5 mA
Telecommunications Laboratory	Computer Laboratory	70 m	Sent	67.05 mA/ 7.4 mA
Telecommunications Laboratory	Computer Laboratory	80 m	Sent	67.50 mA/ 7.5 mA
Telecommunications Laboratory	Computer Laboratory	90 m	Sent	67.50 mA/ 7.5 mA
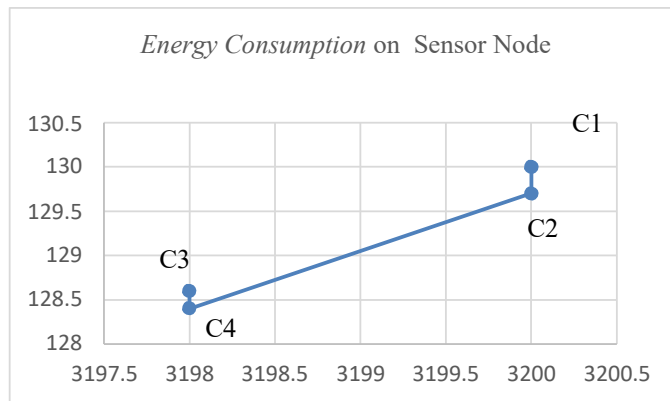
FIGURE 5. Result Test Of Energy Consumption on each Sensor Node

From figure 5 above, it can be inferred that the energy consumption of NLOS testing on each Sensor Node showed a similar result, between a range of 60.75 mA to 67.50 mA. The difference occurs when the sensor node condition was unstable due to the upload or download conditions. The sensor node was placed with the same distance but different positions.

TABLE 5. Result Test of LOS Sensor Node Xbee3 C1-C4

Distance	Package	C1	C2	C3	C4
250 m	@3330.0250#	Sent	Sent	Sent	Sent
500 m	@3330.500#	Sent	Sent	Sent	Sent
750 m	@3330.0750#	Sent	Sent	Sent	Sent
1000 m	@3330.1000#	Sent	Sent	Sent	Sent
1250 m	@3330.1250#	Sent	Sent	Sent	Sent
1500 m	@3330.1500#	Sent	Sent	Sent	Sent
1750 m	@3330.1750#	Sent	Sent	Sent	Sent
2000 m	@3330.2000#	Sent	Sent	Sent	Sent
2250 m	@3330.2250#	Sent	Sent	Sent	Sent
2500 m	@3330.2500#	Sent	Sent	Sent	Sent
2750 m	@3330.2750#	Sent	Sent	Sent	Not Sent
3000 m	@3330.3000#	Sent	Not Sent	Sent	Not Sent
3250 m	@3330.3250#	Not Sent	Not Sent	Not Sent	Not Sent

The test on the distance range of XBee3 Pro using the Line-of-Sight (LOS) method by sending several characters changing the distance from the cluster head to the sensor node. The results of the range testing using the LOS method on each sensor node can be seen in Table V above.

Proceedings of CCSE ASEAN 2019

Receive Threshold (Rx) and Transmitter Power

Rx Threshold became the receiver of the signal sent by the transmitter with a signal power which value was greater than Rx Tresh. Thus, based on technical specification data from XBee3 the following data were obtained it, from experiments and testing on hardware based on planned scenarios , the results are 10.3 W. Whereas for Transmitter Power, it is obtained at 486 KJoule.

Energy Consumption

From the results of this research, it can be inferred that the sensor node can transmit through testing using clustering topology known as a single-hop or multi-hop. After that, several hours of the test was conducted when the Sensor Node was in LOS condition with a capacity of 135 mA. The measurement took place when the power source was in a closed-circuit voltage position using a measured multimeter of 9.6 Volts. After making an hour of measurement, the battery capacity was remeasured to reduce the voltage to 8.5 Volts.

Summary

Hydrogen Autonomy can be used as an alternative or an improvement in the real-time monitoring system of volcanoes. The real-time monitoring system has been experiencing constraints in the accepted energy consumption because it requires more power (power energy) since the sensor nodes work optimally when working continuously. Also, a WSN system is made in real-time. Thus, indirectly all sensor nodes work continuously. However, the memory management used in the process of storing data sensing from each sensor node needs to be considered.

REFERENCES

[1.] J. Pamungkas,and Wirawan. Desain Real Time Monitoring Berbasis Wireless Sensor Network Upaya Mitigasi Bencana Erupsi Gunungapi. Jurnal Nasional Teknik Elektro dan Teknologi (JNTETI), Vol. 4, No. 3. (2015). August

[2.] Dutta, S, Gupta, S, and Das, M.K. Power Consumption and Maximing Network Lifetime during Communcation of Sensor Node in WSN. (2012) Procedia Technology 148 -162.

[3.] Magno, M, Benini, L, Giuffrida, R, Leonardi, S and Brunelli, D. A Portable Hybrid Hydrogen Fuel Cell-Battery Power Unit For Wireless Sensor Network. International Symposium on Power Electronics, electrical Drives, Automation and Motion. (2014), 07 August.

[4.] D. Rong, G. Lazaros, F. Carlo, and X. Ming. On Maximing Sensor Network Lifetime by Energy Balancing. IEEE transactions on Control of Network System, Vol 5, Issue 3. (2018). Pp. 1206-1218

[5.] Janis, T. Sergejs, and P. Dmirtjs S,Kshitij , Exploration of Possible Energy Source For Hybrid Power System of Indoor WSN. 5th IEEE Workshop on Advances in Information, Electronic and Electrical Engineering (AIEEE). . (2017), pp 1-5.

[6.] N.S. Octarina, F. Hamzah and M. Anwar. Solar Energy Harvesting For Wireless Sensor Network Node. International Symposium on Elctronics and Smart Device (ISESD). (2017). Pp: 30-33.

[7.] G. Werner-Allen, J. Johnson, M. Ruiz, J. Lees, and M. Welsh. Monioring Volcanic Eruption With A Wireless Sensor Network". EWSN. (2005) : 108-120.

[8.] Waltenegus, D., dan Cristian,P., "Fundamentals Of Wireless Sensor Networks", John Wiley & Sons,Ltd, 2010.

[9.] C. Park and P. H. Chou, "Ambimax: Efficient Autonomous Energy Harvesting System for Multiple Supply Wireless Sensor Nodes," in Proc. of the Third Annual IEEE Communications Society Conference on Sensor, Mesh and Ad Hoc Communications and Networks (SECON), Reston, VA, USA, Sep 25-28 2006, pp. 168–177.

[10.] E.Z. Amir, X. Liudong, M.V. Vinod, and S. Yun. Hybrid Wireless Sensor Network : A Reliability, Cost and Energy-Aware Approach. IET Wireless Sensor System. Vol. 6, Issue 2. (2016) pp. 42-48

[11] Wireless Sensor Network Architecture: Types, Working & Its Applications https://www.elprocus.com/architecture-of-wireless-sensor-network-and-applications/

[12] Fuel Cells https://users.encs.concordia.ca/~pillay/fuel-cells.html

Scheduling Optimization Using Genetic Algorithm

Faghanie Sugarizka[1 a)], Triwahju Hardianto[1 b)], Bambang Sujanarko[1 c)]

[1]*Electrical Engineering Study Program, Faculty of Engineering, Universitas Jember*

a) Corresponding author: faghanies2@gmail.com
b)triwahju@gmail.com
c)sujanarko.teknik@unej.ac.id

Abstract. Scheduling and transaction of electric utilities have a lot of uncertainties. These uncertainties can affect in the economy and environments. These uncertainties also must be managed properly using deregulation to increasing the electricity market competition. In this paper, the demand system, the required reserve, and the prices of purchased transactions in the future are considered as uncertainties. The integrated scheduling and transaction problem are formulated as an iteration programming problem for a power system. These formulas are then solved by using Genetic Algorithm to get optimized scheduling and economical condition. Based on the electrical system configuration, the results of these approaches are compared to the results of other approaches. The results of testing show that Genetic Algorithm method produced scheduling and transaction decisions that are sufficiently robust in dealing with the uncertainties.

Keywords: Genetic Algorithm, Power System, Scheduling, Between utilities

INTRODUCTION

Scheduling power systems and conducting transactions among electric utilities are essential. These routine activities are carried out every day by the utilities. The scheduling and the transactions are interrelated problems and are the optimization of various variables such as demand, reserves and transmission line capacity. There are also uncertainties in power connection, transactions, fuel prices, reserve units, etc. Uncertainty example is when there is an offer from a utility, it is necessary to determine whether to pursue an opportunity of transaction within fifteen minutes after the offer is received or not, because there may be a better offer at that time.[1]

Another example is fluctuations in demand system. The decisions of scheduling and transactions are commonly decided based on demand system predictions. In case there are changes in the demand, the decisions taken may not be economical anymore. The uncertainty effect can spread through time zone, significantly affecting economic schedules and transactions. The increasing pressure on competition in the utility industry has made this uncertainty increasingly important issue that must be managed properly. In this paper, we discuss how to schedule generators in several plants.[1]

Generator scheduling itself involves determining the time when start up and shut down, loading level and number of spinning reserves for each unit, during the scheduling period given. The schedule is affected by various constraints related to the system and the units. By using the genetic algorithm method, it is expected that scheduled generators on several plants can produce stable power and costs will be cheaper.[1]

MATHEMATICAL MODELING

The problem of generator scheduling can be expressed in a standard form as follows. For power systems with unit N, it is necessary to determine[2]:

- start and turn off time, and
- generation level

of all generating units at each time step, during the scheduling period specified by T, so that total start up, shutdown and operational costs are minimized subject to a set of power systems and unit constraints.[2]

The costs of fuel are a function of generator power output, P_i^t and for this analysis, quadratic cost functions are used, although GA formulations allow other cost functions to be used without difficulty. Its functions are[2]:

$$\alpha_i + \beta_i P_i^t + \gamma_i P_i^{t\,2}$$

The start-up cost depends on the number of hours the unit has been shut down before starting, and to model this factor, which is resulted by factory cooling, the exponential function is used. The equation for modeling this cost is in the form of:

$$\delta_i + \delta_i \left[1 - exp \left(\frac{-T_{off}}{\tau_i} \right) \right]$$

where T_{off} is unit down time. The constraints applied to the model in this paper are:

- the total power produced must meet the load demand,

- the unit loading rate must not violate the minimum and maximum loading limits permitted,

- available spinning reserves include the loss of the largest committed unit,

- the maximum generation capacity of each unit is limited by the ramp rate.

RESEARCH METHOD

The Genetic algorithm is divisible into 5 stage including population initialization, evaluation, selection, crossover, mutation, if these five stages have been passed and have reached an optimal value or not, if not then the process will return to the beginning but if it has reached the optimal value then the process will stop. Genetic algorithm flowcharts are as follows [3]:
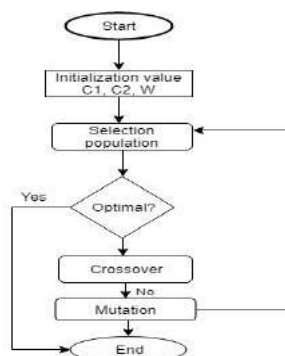
FIGURE 1. Flowchart Genetic Algorithm

GENETIC ALGORITHM

Definition

   In this part, the explanation of genetic algoritms (GA) is presented. The development of evolution theory is the base how the a computational algorithm works. This computational algorithm is then called the genetic algorithm used in order to find more natural aproach to solving the problems. There is still a problem in an application of how to attain the most optimal solution if there are many solutions offered. In this study, the research, firstly, discusses the basic theory of GA. Secondly, the instance of dealing with emerging cases is also shown in order to get better combination optimation. According to [4], in the field of computer science, a genetic algorithm (GA) is a higher level of a new approach to determining the best breakthrough of a larger class of evolutionary algorithms. In additon to that definition, GA is actually the most favourable method in terms of generating the best problem solving. It can depend on mutuation, crossover, and selection. The theory of Darwin's evolution was being a basic idea of a reseacher, John Holland, who first familiarized GA in 1960.

        In recent years, genetic algorithms have already been a popular one to be scientifically and technically studied by all experts. One of the applications is in power system. Many engineers are increasingly use this method in order to deal with some problems as follows. Firstly, GA is applied for distribution system loss minimisation. Secondly, it has already been implemented in load flow solution. The third problem that is economic dispatch has been tried to be solved by this method as well. Finally, it is also used in unit commitment.

   Genetic algorithms are based on models of genetic change in individual populations. Three basic elements of the models are as follows:

  • a 'fitness' measure that determines an individual's ability to affect future generations,

  • a selection and reproduction process which produces offspring for the next generation,

  • genetic operators which determine the genetic make-up of the offspring.

   A special feature of GA that makes it differ from other function optimization techniques is that the search for optimal solutions are resulted not from applying additional changes to a single structure (candidate solution), but from maintaining a population of solutions from which new structures are created using operator genetics[2].

 Genetic Algorithm (GA) for Optimization Functions

   The main control parameters of a GA are :

  ➢   the population size

  ➢   the selection population

  ➢   the cross-over rate

  ➢   the mutation rate

  ➢   the number of generations allowed for the evolution of the required structure.

GENETIC ALGORITHM FOR GENERATOR SCHEDULING

Schema encoding problem

The two overriding actions as a link a GA to the problem it is solving are :

•   The implementation of solve the problem solution to a chromosome representation.

•   An evaluation function that returns a measurement of worth for any chromosome in the context of the problem.

The success of the GA approach greatly depends on the problem mapping and the choice of the evaluation function.

Facing the scheduling problem of a generator is commonly found in electrical field. This can be seen as a close relation between cosy binary mapping and chromosome representation. As generally known, there are two states in how to represent the ON and OFF. Zero and one are used for OFF and ON, respectively. These can turn to on or off, in which the unit variable can be calculated. Hence, this variable can be utilised for generating capacity from computational process. In addition, a string is a result from completion candidate where the length of it would be the outcome of scheduling periods and generator numbers. After the limited loading of the generator is determined from the ramp level, the value of the cost function can be obtained from start-up function and minimum fee.

In this paper we will discuss how to schedule generators using genetic algorithms with various techniques including:

✓   Generate only a variable candidate solution by testing each proposed chromosome for feasibility, a very time-consuming process. This is similar to an enumerative procedure.

✓   Modify the genetic operator to fit the constraints. This is only possible for some constraints, otherwise representation can be too complex.

✓   Search for solutions, or parts of solution space, which violate constraints.

All three selected approach and obstacle are treated as penalty functions in an objective function combined with the initial cost function and fee operational.

GA function objective

Overall cost function to be minimised (OCF) is given by

OCF=start up cost (SCOST)

•   running cost (RCOST)

•   premature start penalty cost (PSTCOST)

•   premature shutdown penalty cost (PSDCOST)

•   failure to meet reserve penalty cost (FTRCOST)

The cost for each unit should be minimized in each time interval over the whole scheduling period.

Figures

In this paper explain the images and simulations for scheduling generators using the genetic algorithm method
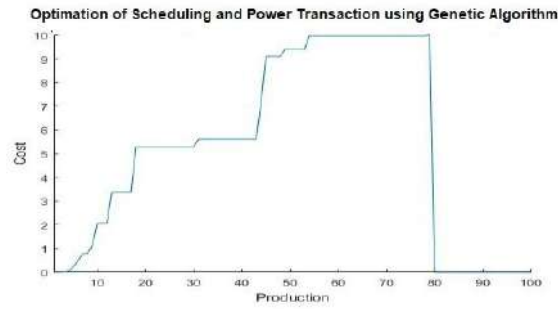
FIGURE 2. Genetic Algorithm For Generator Scheduling

Tables

In this paper shows the data table generator scheduling and comparison between ordinary generator scheduling and generator scheduling using genetic algorithms

Power Plant	PLN	GA
PLTU Gresik 1	2737 MW	1901 MW
PLTU Paiton	1786 MW	1403 MW
Muara Karang	1971 MW	1870 MW
PLTU Gresik 2	1371 MW	1000 MW
PLTU Gresik 3	441 MW	302 MW
Total Production (MW)	8306 MW	6476 MW
Total Cost (Rp)	648.565	565.812

TABLE 1. Comparison table between the PLN generator and the simulation generator with the Genetic Algorithm

SUMMARY

This paper discusses generator scheduling using genetic algorithms with generator start-up data at several plants which by using this method scheduling can produce stable power or voltage and cheaper prices and costs.

ACKNOWLEDGMENT

REFERENCES

[1]   P. B. Luh, "756 I E E E Transactions on Power Systems, Vol. 12, No. 2, May 1997," 1997. .

[2]   S. O. Orero and M. R. Irving, "A genetic algorithm for generator scheduling in power systems," *Int. J. Electr. Power Energy Syst.*, vol. 18, no. 1, p. 3, 1996.

[3]   A. Dastanpour, "Flowchart of genetic-algorithm." [Online]. Available: https://www.researchgate.net.

[4]   W. Wikipedia, "Genetic Algorithm." [Online]. Available: https://en.wikipedia.org/wiki/Genetic_algorithm.

[5]   A. J. Svoboda, Chung-Li Tseng, Chao-An Li, and R. B. Johnson, "Short-term resource scheduling with ramp constraints [power generation scheduling]," *IEEE Trans. Power Syst.*, vol. 12, no. 1, pp. 77–83, 1997.

[6]   C. E. Zoumas, A. G. Bakirtzis, J. B. Theocharis, and V. Petridis, "A genetic algorithm solution approach to the hydrothermal coordination problem," *IEEE Transactions on Power Systems*, 2004. .

[7]   H. Yan, B. Prasannan, and P. B. Luh, "Is I.E., Requirements an," *System*, 1995. .

[8]   S. Kumhar, M. Kumar, and M. Tech, "Generator Maintenance Scheduling Of Power System Using Hybrid Technique," 2016. .

[9]   Y. Yumbe, T. Hasegawa, and N. Furukawa, "Optimization method for inspection scheduling of power distribution facilities," *IEEE Trans. Power Deliv.*, vol. 28, no. 3, pp. 1558–1565, 2013.

[10]   H. Ariantara, S. Sarjiya, and S. Pramono Hadi, "The Solution for Optimal Power Flow (OPF) Method Using Differential Evolution Algorithm," *IJITEE (International Journal of Information Technology and Electrical Engineering)*, 2017. .

Optimization of Electric Power Factors Based on Fuzzy Logic Controls: Case Study at Nurul Jadid Islamic Boarding School

Ahmad Muhtadi,[1] Bambang Sujanarko[2], and Bambang Sri Kaloko[3]

Department of Electrical Engineering, University of Jember
[1]muhtadi1703@gmail.com, [2]bbsujanarko@yahoo.co.id, [3]kaloko@unej.ac.id

Abstract

This paper discusses about the optimizing electrical power using bank capacitors that are controlled using fuzzy logic. Bank capacitor is one of the electronic components built from a number of capacitors, where the function and purpose are to repair cos phi or also called the power factor, while fuzzy logic is an orientation of human thinking more flexibly used as a control control system. To prove the flexibility of fuzzy logic in the control system it will be done by applying the fuzzy logic algorithm on bank capacitors to be able to optimize the power factor.

Keywords power factor, fuzzy logic, capasitor bank

INTRODUCTION

power factor, PF, is the ratio of average power (P) to apparent power (S). Low power factor is caused by the number of inductive electrical equipment which results in the amount of losses that occur in the electrical system due to the large amount of current needed for reactive power. According to the previous journal, the power factor [1-2].

Fuzzy logic controllers have been applied to several systems by developing fuzzy logic control algorithms, Fuzzy Logic control systems that are used there are two inputs and one Fuzzy Logic Controller output. Where the two inputs are selected as "Error" and "Delta Error" while the output is "Duty cycle" That the output voltage is felt and compared to the reference voltage or set point. "Error" is the difference between the reference value and the actual value. Likewise "Delta Error" is the difference between the current error and the previous error [3]. The design and calculation of components for inductors has been carried out to ensure the converter operates in continuous conduction mode. Output evaluation is compared to the application of software using the MATLAB application. Fuzzy logic controls are implemented to get the power factor near unity, at reducing higher harmonics in the input current [4-5]. To overcome this problem several converter topologies and control schemes have been proposed in recent years. The previous paper proposed to study control techniques to improve the power factor converter and reduce total harmonic distortion in the input current by regulating the output voltage. This fuzzy logic control strategy is to increase power control factors. The proposed Fuzzy Logic control system is a two input one Fuzzy Logic Controller output [6].

Reactive power compensation in power distribution networks plays an important role in increasing the voltage and stability of the power system. Increased loading of the transmission line can sometimes cause voltage collapse due to lack of reactive power sent at load centers [7]. The conditions in the Nurul Jadid Islamic Boarding School at this time there are quite a lot of inductive loads in the form of electric machines that cause reactive power which will ultimately reduce the value of the power factor. The next result of this was an increase in electricity bills to be paid by Islamic boarding schools. Therefore, based on the problems stated above, it is necessary to improve the electric power factor in installations in Islamic boarding schools with electric power optimization. Besides improving the power factor, it is also hoped that the electricity bill from the State Electricity Enterprise.

RESEARCH METHODS

a. Stages of Research

The study begins with a literature study on the notion of power and power factors and their improvement. From the results of this study, the research objectives were formulated. Then the data needed is taken that is the electric power and the cost of electricity bills in one month. Based on these data it can be calculated the value of the power factor and the value of the capacitance needed for compensation so that the power factor can be corrected. The next step is to test Matlab / Simulink as well as control in optimizing.

b. Research sites

This research was conducted at the Nurul Jadid Islamic Boarding School in Karanganyar Village, Paiton District, Probolinggo Regency, East Java Province.

c. Variable Observation

Based on the variables obtained from previous studies, the variables observed and examined include the effects:

- Output variable:

  Qc : power compensated capacitors (kVAR)
  pf : power factor
- Input variable:

  P : active power (Watt)
  Q : reactive power (VAR)
  S : false power (VA)
  State Electricity Enterprise electricity bill

d. Data Collection and Analysis Techniques

Data collection techniques carried out to obtain the power factor (cos phi) in the form of electricity bills State Electricity Enterprise is using observation techniques. Preliminary data were obtained from the State Electricity Enterprise electricity bill for six months. Further data, after the Matlab / Simulink trial.

Data analyzed in the form of active power data, reactive power, apparent power, and nominal electricity bill in the form of fine cover must be paid. Data analysis was carried out by calculating the reactive power compensation needed by using the existing calculation method to obtain the value of the Matlab / Simulink test against the appropriate capacitor bank. All of these controllers are verified by Matlab / Simulink simulation through the use of a continuous time factory model and a discrete time controller [8].

RESULTS AND DISCUSSIONS

In this section we will provide research data and results via Simulink on the Matlab application. Following below are the research data, Simulink images and results.

a. Research data

Power and power factor measurements are performed when the condition does not use a capacitor to determine the reactive power required by the load. Power factor measurements are attempted during peak loads and measurements are made using cos phi meters measured in the distribution panel.

The following data is the measurement of power and power factors :

Table 1. Power & Cos φ Measurement Data

Time	kW	kVAR	kVA	Cos φ
30-31 July 2019				
03:00-04:00	593.995	370.36	700	0.85
05:00-06:30	340.612	294.08	450	0.76
06:30-07:00	315.313	246.13	400	0.79
08:00-11:00	478.701	361.73	600	0.80
12:00-15:00	440.489	32.35	550	0.80
16:00-17:30	361.431	268.08	450	0.80
18:00-22:00	361.694	345.22	500	0.72

b. Fuzzy Controller Structure

The first important step in the definition of a fuzzy controller is the selection of input variables. To improve operations, we need additional information about the power factor, namely active power and reactive power. This application enables a substantial increase in Simulink performance with gains in optimized power factors. Thus, in the proposed fuzzy controller we use two input variables and one output variable:
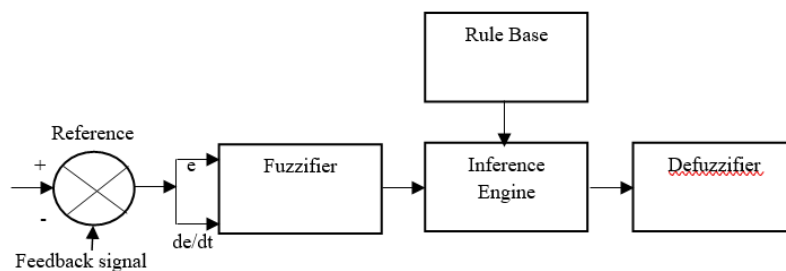
Fig. 1 Block diagram of typical fuzzy logic controller
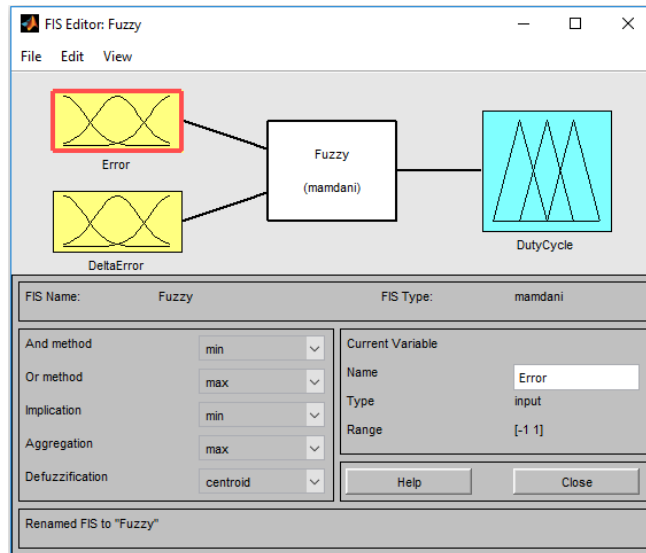
Fig. 2 FIS Editor
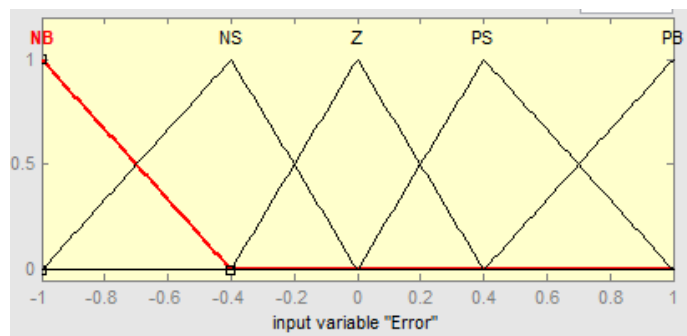
Fig. 3 Membership functions shapes for Error
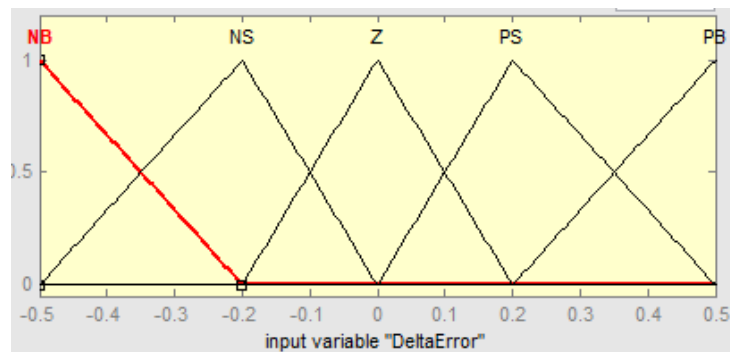
Fig. 4 Membership functions shapes for DeltaEror
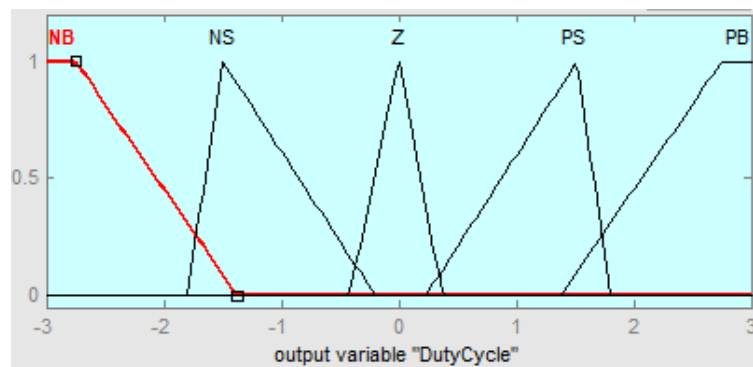
Fig. 5 Membership functions shapes for Duty Cycle
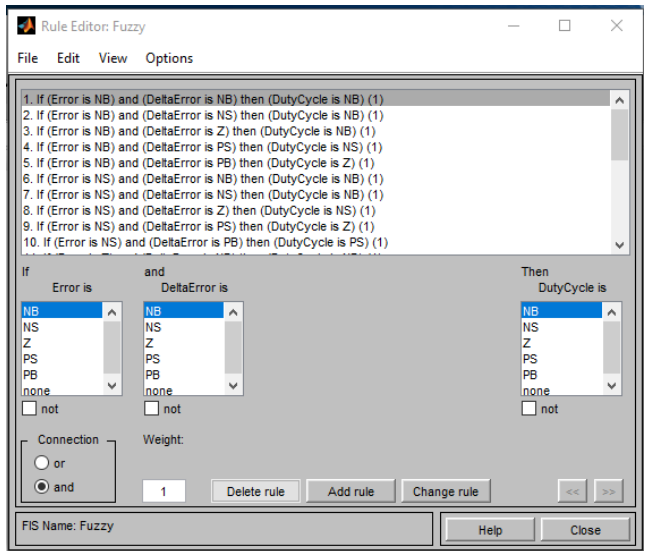
Fig. 6 Rule Editor
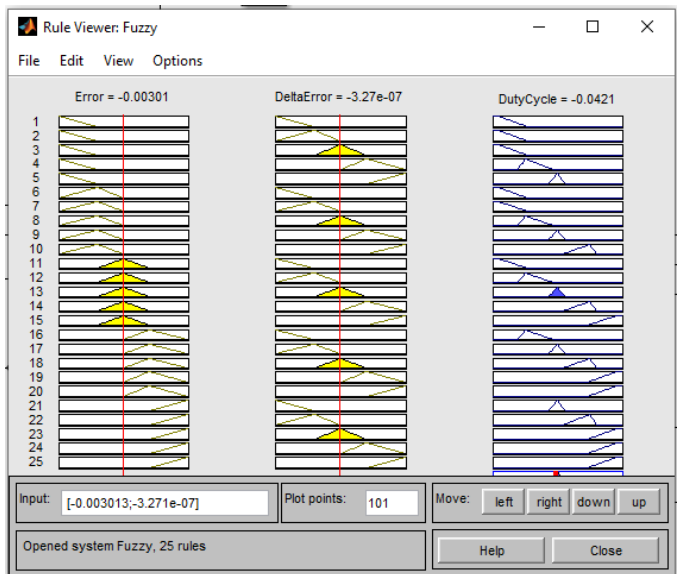
Fig. 7 Rule Viewer
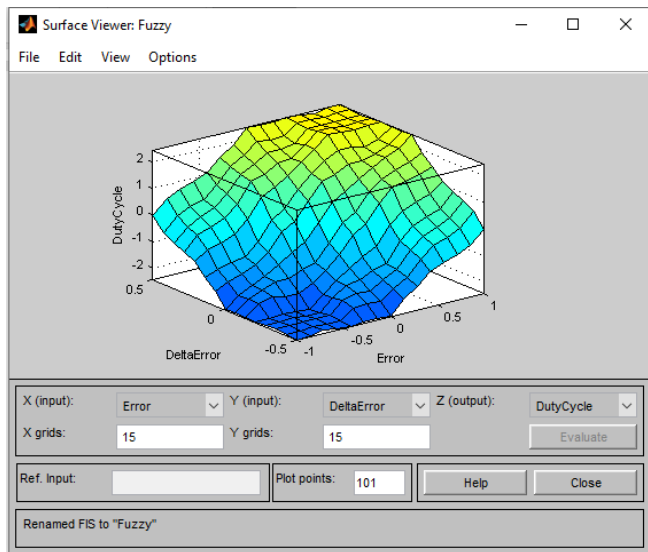
Fig. 8 Surface Viewer

c. Simulation Model and Results

Optimization power factor with fuzzy logic controls discussed in the previous session was validated using MATLAB / SIMULINK Software as shown in figures 9, 10 and 11.
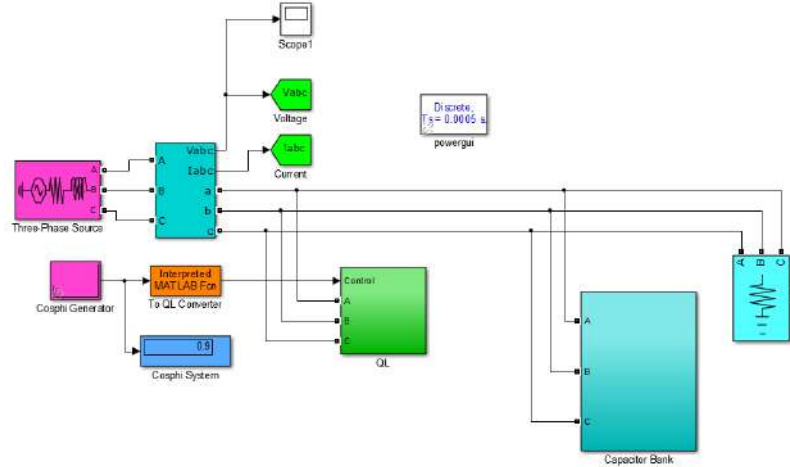
Fig. 9 Power Factor Optimization Simulation Circuit
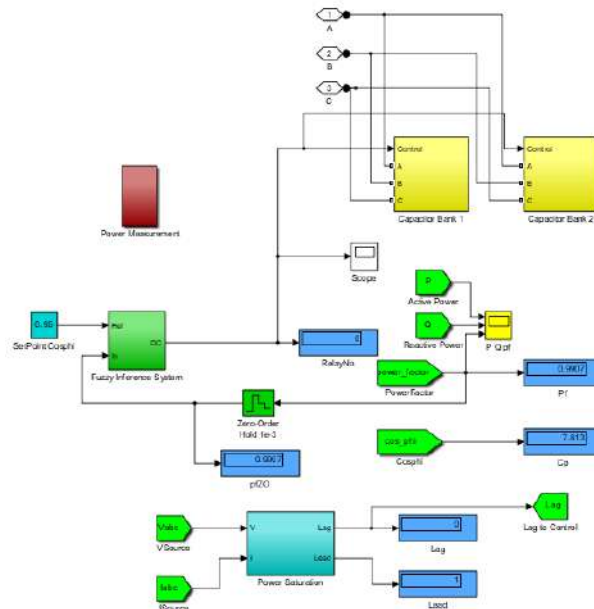
Fig. 10 Capacitor Bank Simulation Circuit
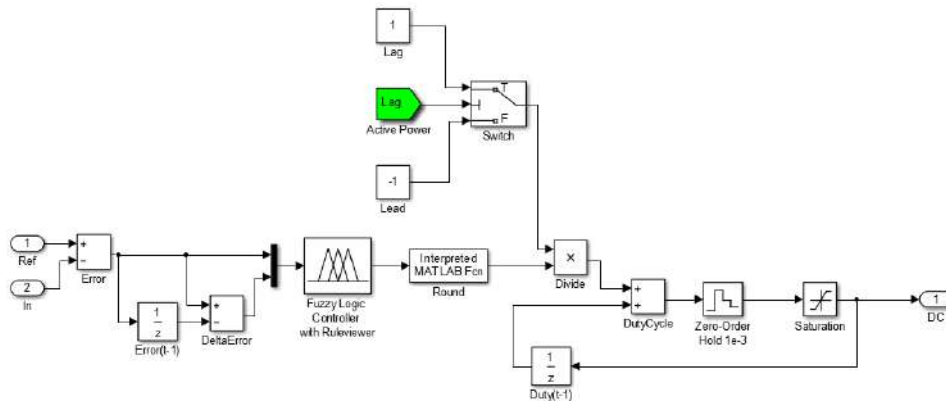
Fig. 11 Circuit Fuzzy logic controller simulation
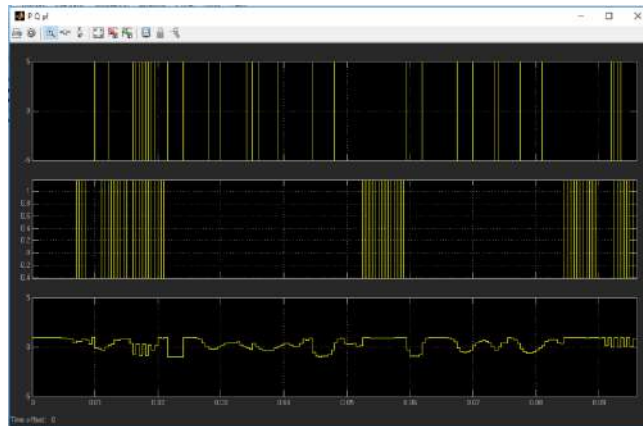
Fig. 12 Graph of simulation results

Table 2. Comparison of results before and after using Fuzzy Logic Controls

Research Measurement Data						Results Data	
Time	kW	kVAR	kVA	Cos φ	QC	pf	Cos φ
03:00-04:00	593.995	370.36	700	0.85	82.68	0.9907	0.95
05:00-06:30	340.612	294.08	450	0.76	129.11	0.9356	0.95
06:30-07:00	315.313	246.13	400	0.79	93.41	0.9601	0.95
08:00-11:00	478.701	361.73	600	0.80	129.88	0.9648	0.95
12:00-15:00	440.489	329.35	550	0.80	116.01	0.9677	0.95
16:00-17:30	361.431	268.08	450	0.80	93.03	0.968	0.95
18:00-22:00	361.694	345.22	500	0.72	170.04	0.907	0.95

CONCLUSION

Based on the results of the discussions and trials conducted, the following conclusions can be drawn:

1. At 03: 00-04: 00 the peak load of the power factor value is 0.9907 and at the lowest peak at 18: 00-22: 00 the power factor is 0.907

2. After the system power factor is improved by using fuzzy logic controls, the system's power factor has increased to 0.95. In all conditions

3. The application of the fuzzy logic control method to the optimization of power factors is more efficient and optimal in the use of electric power.

REFERENCES

[1] Zeynep Bala Duranay, Hanifi Guldemir, Servet Tuncer (2018). Fuzzy Logic Controlled Unity Power Factor Converter. *International Journal of Scientific & Engineering Research (IJSER), 9 (4).*

[2] A. Kessal, L. R. (2012). Power Factor Correction based on Fuzzy Logic Controller with Fixed Switching Frequency. *International Standard Serial Number (ISSN 1392 – 1215)*, 118.

[3] G. Bhanumanjari, O. Ranjitkumar (2015) A Fuzzy Logical Controlled New Power Factor Correction Technique Using Pfc Boost Converter. *International Journal Of Professional Engineering Studies (IJPRES) 4 (5),* 3.

[4] Moh Moh Myint Aung, Y. A. (2016). A Fuzzy Logic Approach for Improvement of Power Quality Using FC-TCR. *American Scientific Research Journal for Engineering, Technology, and Sciences (ASRJETS) , 26* (2), 239.

[5] VS Prasadarao K, Menikanta Sai Yarra, Sai Pramod Kumar Maddi. (2017). Comrative Analysis of Fuzzy and PI Controller Based Two Switch Buck-Boost Converter for Power Factor Correction. *International Journal of Applied Engineering Research (ISSN 0973-4562) 12 (1),* 297.

[6] P.Kripakaran, J. R. (2014). Power Factor Correction Using Fuzzy Logic Control. *IOSR Journal of Electrical and Electronics Engineering (IOSR-JEEE) , 9* (1), 11.

[7] Periyasamy, K. (2012). Power Factor Correction Based On Fuzzy Logic Controller With Average Current-Mode For DC-DC Boost Converter. *International Journal of Engineering Research and Applications (IJERA) , 2* (5), 771.

[8] Pranali V. Narayane, D. H. (2018). Power Factor Correction of a Single Phase AC to DC Interleaved Boost Converter using Fuzzy Logic Controller. *International Journal of Trend in Scientific Research and Development (IJTSRD) , 2* (4), 1884.

Optimization of the Operation and Maintenance Schedule of Power Plants Using Particle Swarm Optimization

Novangga Adi Mulyono[1], Bambang Sujanarko[2], Bambang Sri Kaloko[3]

Electrical Engineering, University Of Jember [1,2,3]

kobayakawaangga69@gmail.com[a], bbsujanarko@yahoo.co.id[b], kaloko@unej.ac.id[c]

Abstract. The more rapid progress in the field of electronics needs for electricity is also increasing. So that the electricity provider must optimize production of electric power to keep supply of electrical energy. To keep continuity of electricity supply, various types of power plants that form interconnections within the transmission network must always operate to produce electricity. But on the other hand, each power plant must too have time to not operate. That is the time to maintenance of main equipment. The purpose of maintenance that is no fatal damage to main equipment that can result in not operating for a long time. With the lack of power plant from the system, it can disrupt the stability of electrical energy to consumers. Scheduling operation and maintenance of a power plant is a routine work must be done. The importance of determining operation and maintenance schedule of a power plant is to maintain the stability of electricity to consumers. Scheduling becomes a complicated job because scheduling problems are combinatorials that have boundaries that must be fulfilled. In this study, an automatic scheduling model for operation and maintenance of electricity generation based on the Particle Swarm Optimization (PSO) algorithm was designed.

Keywords : Optimization, operating schedule, maintenance, particle swarm optimization

INTRODUCTION

The more rapid progress in the field of electronics, the need for electricity is also increasing. So that the electricity provider must also optimize the generation of electricity to maintain the supply of electrical energy continues to consumers. To ensure the continuity of production in a power plant, certainty is needed that the equipment or machinery used can operate properly. For this reason, a system of equipment with high reliability is needed (Simanjuntak, 2014).

But on the other hand, each power plant must also have time to not operate. That is the time to carry out maintenance of the main equipment. The purpose of the maintenance is so that there is no fatal damage to the main equipment that can result in not operating for a long period of time (Muslim, 2008). For that it is needed in the form of a schedule that can regulate the time for operation and maintenance of the power plant. Scheduling the operation and maintenance of a power plant is a routine work that must be done. The importance of determining the operation and maintenance schedule of a power plant is to maintain the stability of electricity to consumers.

In this study, a design scheduling and maintenance of an automatic power plant based on a particle swarm optimization algorithm was designed. PSO algorithm is an easy-to-understand optimization algorithm, quite simple and has proven performance that is reliable. The Particle Swarm Optimization (PSO) algorithm was introduced by Dr. Eberhart and Dr. Kennedy in 1995. The PSO algorithm is one of the optimization algorithms that mimic the processes that occur in the lives of bird and fish populations in survival (Haupt & Haupt, 2004). A similar research conducted by Anizar Indriani is the optimization of scheduling thermal power plants with dynamics programming. While the research that will be carried out by the author is to optimize the operating schedule and maintenance of the power plant using the Particle Swarm Optimization method. And as a case study, the author uses a diesel power plant.

MATHEMATICAL MODELLING

Min $f(x)$ where $X^{(B)} \leq X \leq X^{(A)}$, $X^{(B)}$ is the lower limit and $X^{(A)}$ is the upper limit of X. To calculate the position or coordinates of particles j at the iteration-i can use the formula as follows :

$$V_j(i) = V_j(i-1) + c_1 + r_1[P_{best,j} - x_j(i-1)] + c_2 r_2[G_{best} - x_j(i-1)]$$

$$J = 1,2, \dots, N$$

To calculate the position or particle coordinates j at iteration-i is the following formula:

$$X_j = X_j(i-1) + V_j(i):$$

$$J = 1,2, \dots, N$$

To evaluate the value of the objective function for each particle with the following formula :

$$f[X_1(i)], f[X_2(i)], \dots f[X_N(i)]$$

RESEARCH METHODS

The PSO algorithm is divided into 4 stages, namely initialization, evaluation, update and termination. If the four stages have been passed, a check on the results obtained has reached the optimal value or not, if not, the process will repeat itself until it gets optimal results. And if the process has reached the optimal value, the process will stop. The following flowchart of the PSO algorithm is as follows:
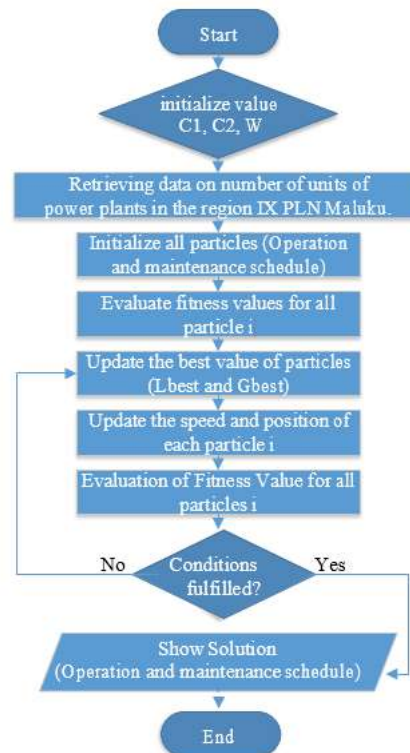
FIGURE 1. Flowchart of PSO algorithm

CASE STUDY

Case Description

The data collected is data from the PT. PLN (Persero) region IX Maluku unit and the Ambon North Maluku branch having 12 generating units. However, only 7 units operate and 5 units are totally damaged. So that it must use 15 rental generator units to sufficient the power needs of the load. The load data every week for 24 weeks and 22 generating units that supply power to the load are as follows:

TABEL 1. Capacity of Power Plant

Unit.	Capacity of Power Plant Unit (MW)	Unit.	Capacity of Power Plant Unit (MW)
1	10000	12	1800
2	6000	13	1000
3	6000	14	1000
4	6000	15	1000
5	6000	16	1000
6	3800	17	1000
7	3800	18	1000
8	3500	19	1000
9	2800	20	1000
10	2000	21	1000
11	2000	22	1000
Total power			**63700**
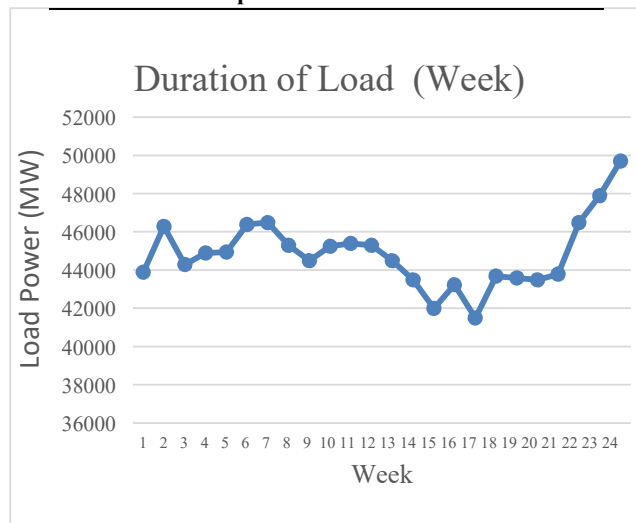
FIGURE 2. Duration of load

Results

In this section, the data in table 1 is simulated using the Matlab application by using equation 1 based on the method of optimizing particle crowds. From this data, 22 research units will be carried out research to produce the most optimal scheduling. The process of finding the most optimal value in determining the schedule is done with three experiments and using 100 iterations. So that by increasing the intensity of the experiment can approach the most optimal value. The experiments that have been carried out are as follows:

FIGURE 3. First experiment

In the second experiment using the same data has slightly different values. Where in the second experiment the curve is approach to 4.

FIGURE 4. Second experiment

And in the third experiment, the most optimal value is approach to 4.
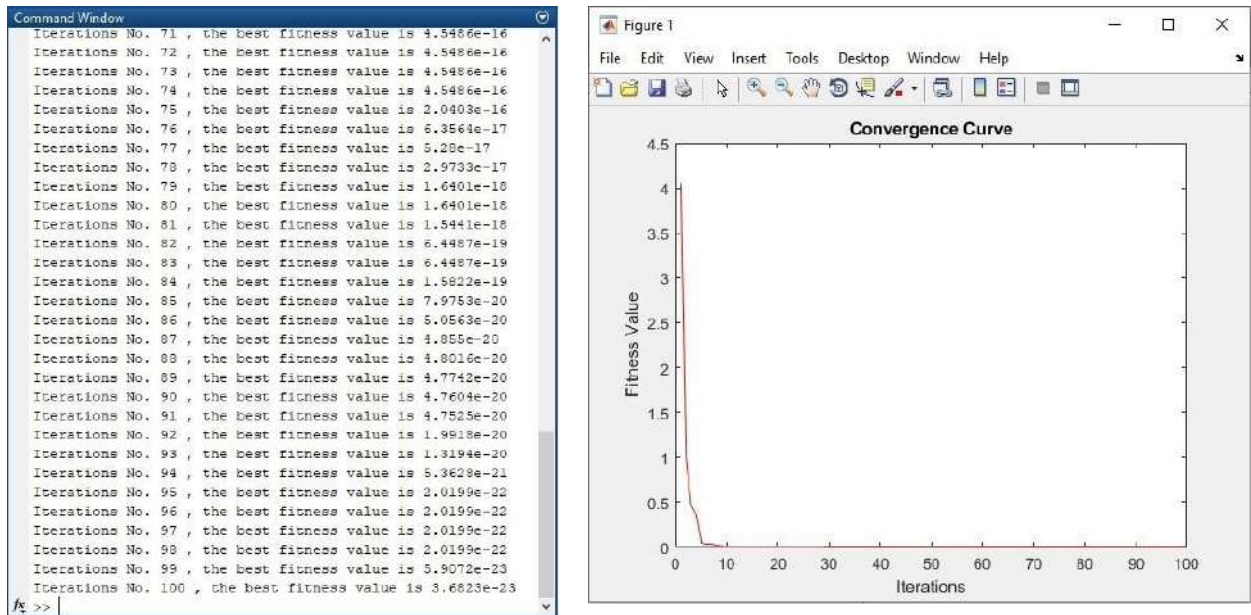
FIGURE 5. Third experiment

So that from the three experiments that have been carried out, the most optimal value in determining the operating schedule and maintenance of power plants is 4. So that in every generating unit within 24 days has 4 days to conduct maintenance. The most optimal combination of schedules and power generated from several combinations of each unit using the Particle Swarm Optimization method are as follows:

TABLE 2. Operation and maintenance schedule for diesel power plants with method of PSO

	Status Operation Unit																						Total Capacity (MW)
Unit	1	2	3	4	5	6	7	8	9	10	11	12	13	14	15	16	17	18	19	20	21	22	
Capacity / Weeks	10000	6000	6000	6000	6000	3800	3800	3500	2800	2000	2000	1800	1000	1000	1000	1000	1000	1000	1000	1000	1000	1000	
1	1	1	1	1	1	1	1	1	1	1	1	1	0	0	0	0	0	0	0	0	0	0	53700
2	1	1	1	0	1	1	1	1	1	1	1	1	0	0	0	0	1	1	1	1	1	1	53700
3	1	1	1	0	1	1	1	1	1	0	0	1	1	1	1	1	1	1	1	1	1	1	53700
4	1	1	0	1	1	0	1	1	1	1	1	1	1	1	1	1	1	1	1	1	1	1	53900
5	1	1	0	1	1	1	0	1	1	1	1	1	1	1	1	1	1	1	1	1	1	1	52900
6	1	0	1	1	1	1	1	0	1	1	1	0	1	1	1	1	1	1	1	1	1	1	52400
7	1	0	1	1	1	1	1	1	1	0	1	1	1	1	1	0	0	1	1	1	1	1	53700
8	1	1	1	1	0	1	1	1	0	1	1	0	1	1	1	1	1	1	1	1	1	1	53100
9	1	1	1	1	0	1	1	1	0	1	0	1	1	1	1	1	1	1	1	1	1	1	52900
10	0	1	1	1	1	1	1	1	1	1	1	1	1	1	1	1	1	1	1	1	1	1	53700
11	0	1	1	1	1	1	1	1	1	1	1	1	1	1	1	1	1	1	1	1	1	1	53700
12	1	1	1	1	1	0	1	1	1	0	1	1	1	1	1	1	1	0	0	0	0	0	53900
13	1	1	1	1	1	1	1	1	1	1	1	1	0	0	0	0	0	0	0	0	0	0	53700
14	1	1	1	0	1	1	1	1	1	1	1	1	0	0	0	0	1	1	1	1	1	1	53700
15	1	1	1	0	1	1	1	1	1	0	0	1	1	1	1	1	1	1	1	1	1	1	53700
16	1	1	0	1	1	0	1	1	1	1	1	1	1	1	1	1	1	1	1	1	1	1	53900
17	1	1	0	1	1	1	0	1	1	1	1	1	1	1	1	1	1	1	1	1	1	1	53900
18	1	0	1	1	1	1	1	0	1	1	1	0	1	1	1	1	1	1	1	1	1	1	52400
19	1	0	1	1	1	1	1	1	1	0	1	1	1	1	1	0	0	1	1	1	1	1	53700
20	1	1	1	1	0	1	1	1	0	1	1	0	1	1	1	1	1	1	1	1	1	1	53100
21	1	1	1	1	0	1	1	1	0	1	0	1	1	1	1	1	1	1	1	1	1	1	52900
22	0	1	1	1	1	1	1	1	1	1	1	1	1	1	1	1	1	1	1	1	1	1	53700
23	0	1	1	1	1	1	1	1	1	1	1	1	1	1	1	1	1	1	1	1	1	1	53700
24	1	1	1	1	1	0	1	1	1	0	1	1	1	1	1	1	1	0	0	0	0	0	53900
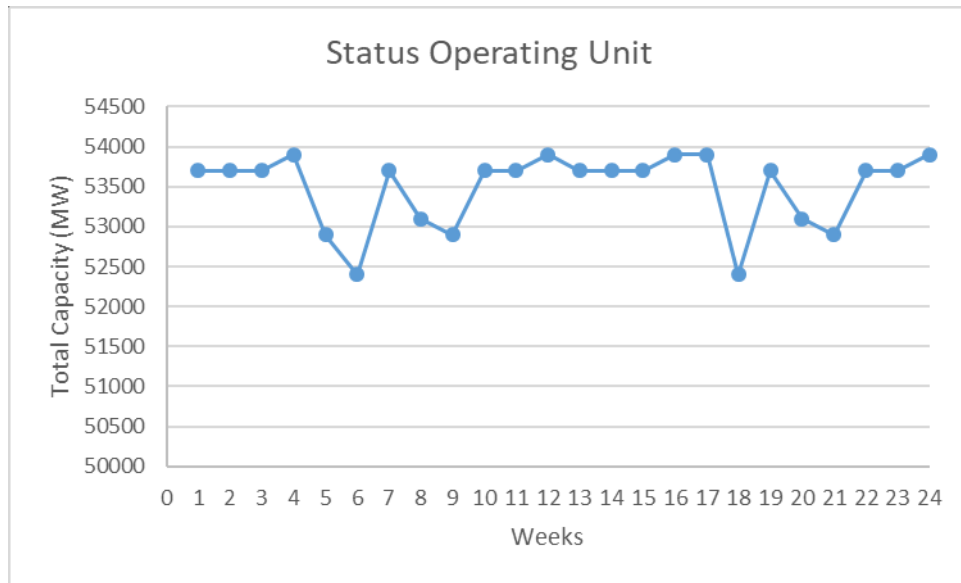
FIGURE 6. Status operating unit

CONCLUSION

The particle swarm optimization method is very efficient in determining the most optimal scheduling by considering several factors that constrain. Scheduling power plants for operation and maintenance using the particle swarm optimization method can maximize the performance and maintenance of a power plant. So that with regular maintenance with the existing schedule can maintain the quality of electricity and prevent damage resulting in disruption of electrical energy supply to consumers.

ACKNOWLEDGMENTS

REFERENCES

1. Dhanapal, M., & Lakshmi, K. (2013). Co-ordination of thermal unit system with wind energy system for scheduling problem in restructured power system. *2013 International Conference on Green High Performance Computing, ICGHPC 2013*.
2. Haupt, R. L., & Haupt, S. H. (2004). *Practical Genetic Algorithms.* Pennsylvania: Wiley Interscience.
3. Helseth, A., Fodstad, M., & Mo, B. (2018). Optimal hydropower maintenance scheduling in liberalized markets. *IEEE Transactions on Power Systems*, *33*(6), 6989–6998.
4. K.C, S., Laksminarayand, C., & Singh, M. K. (2016). Adaptive Particle Swarm Optimization For Best Schedule In Algorithmic - Level Synthesis. *ICCES*.
5. Kennedy, J., & Eberhart, C. R. (1995). Particle Swarm Optimization. *IEEE*.

6.   Latumahina, A., Wijono, & Suyono, H. (2015). Optimalisasi Penjadwalan, Perawatan dan Perbaikan Pembangkit PLTD 20 kV dengan Levelized Reserve Method. *EECCIS*.

7.   Muslim, H. S. (2008). *Teknik Pembangkit Tenaga Listrik.* Jakarta: Direktorat Pembinaan Sekolah Menengah Kejuruan.

8.   Shiau, F. (2011). A Hybrid Particle Swarm Optimization for A University Course Scheduling Problem With Flexible Preference. *Elsevier*, 235-248.

9.   Simanjuntak, O. T. (2014). *Studi Keandalan (Reliability) Pembangkit Listrik Tenaga Uap (Pltu) Labuhan Angin Sibolga.* Medan: Universitas Sumatera Utara.

10. Solichan, A., & Prasetyo, M. T. (2014). Optimasi Jadwal Operasi Dan Pemeliharaan Pembangkit Tenaga Listrik Menggunakan Metode Algoritma Genetik. *Simposium Nasional Teknologi Terapan*.

11. Wati, D. A., & Rochman, Y. A. (2013). Model Penjadwalan Matakuliah Secara Otomatis Berbasis Algoritma Particle Swarm Optimization (PSO). *Rekayasa Sistem Industri*, 22-31.

RSSI Measurement for IoT Smart Greenhouse System Based on Wireless Sensor Network for Control and Monitoring of Coffee Plants

Ike Fibriani [1,a)], Dedy Wahyu Herdiyanto [2,b)], Catur Suko Sarwono [3,c)] Muhammad Rizza [4,d)]

[1,2,3,4)]Electrical Engineering Department, University Of Jember, Kalimantan Street No. 37 Jember 68121

a) ikefibriani.teknik@unej.ac.id.
b) dedy.wahyu@unej.ac.id.
c) catursuko@gmail.com.
d) muhammadrizza1997@gmail.com.

Abstract. In agriculture, food, energy resources, transportation, and telecommunications aspects, technology has become the center of the direction of the development of modern life. One technique that is being developed called Wireless Sensor Network (WSN) that already exist and are widely used, and one of the most popular of wireless technology by using several nodes that are arranged in a collaborative network. By using WSN, data can be sent quickly and efficiently, and information can be monitored directly or in real time. In this research, WSN technology will be implemented in an intelligent greenhouse control system to improve the quality of coffee plants. Coffee plant cultivation in the greenhouse has the advantage of a more controlled microenvironment and uniformity of production on plants. This study focused on the development of smart greenhouses using the Wireless Sensor Network as a monitoring system combined with the Internet of Things (IoT) remote control to make greenhouse stay in ideal condition. The designed system has four central part, including node sensor, node coordinator, connection point, and server. Node sensors are used to monitor and provide data to the server. The data will be used as a reference for the server to decide the feedback action. Those parameters that must be maintained are the temperature (DHL11), light intensity (LDR), and soil moisture (YL-69) of the room. The sensor nodes placed on the greenhouse are connected with WSN technology to communicate using Xbee module between nodes. It will easier for the server pinpoint the node location. IoT additions are intended to facilitate checking plants, which is enough to use a smartphone without having to come to a greenhouse location, which is also expected to help coffee farmers to increase production more efficiently and can be monitored remotely. The server processes input data from sensor nodes and provide feedback on temperature, humidity, and light control through the closest sensor nodes. The results of this monitoring can be directly monitored and accessed on a smartphone. The system is also already been evaluated in RSSI and data error aspects. The RSSI data are obtained by comparing the calculation and monitoring the result of communication signal using XCTU. There are two conditions that observed, LOS and N-LOS. As for the result, the communication can be maintained in good condition around -67 dBm for LOS and -87 dBm for N-LOS with under 10% error rate.
Keywords: wireless, communication, sensor, network

INTRODUCTION

The development of an increasingly advanced era produces many technologies developed to facilitate human activities from technology in aspects of agriculture, food, energy resources, transportation, and telecommunications. The most rapidly developed one is telecommunications technology. Various countries are trying to create telecommunications technology that is faster and more efficient for suitable environments. Wireless sensor network technology is one of the techniques that popularly developed this day.

A Wireless sensor network (WSN) is a network of devices that have sensing, actuation, processing, and wireless communication capabilities [1, 7, 8]. The advantage of using WSN technology is that the data obtained can be sent quickly and efficiently, and information can be monitored directly or in real-time. It is utilizing more than one node as recipients who then gather at a node (coordinator) and forwarded to the server so that it can be monitored directly. Utilization of WSN technology is pervasive. In agriculture, WSN is used as an effective, efficient, and real-time monitoring medium. This method allows monitoring of changes in the condition of an object can be done appropriately and more efficiently.

This technology is also can be used in the agricultural field, which affects greenhouse design. The design of a greenhouse has a significant effect on the microenvironment inside. Greenhouse climate control can create the best environment for crops to grow, minimize the cost of production, and improve the quality of production [2]. Modern greenhouse, a combination of computers, sensors, wireless communications and other technologies, has been popularized over recent years, which typically represents a transformation from the traditional agriculture to the modern agricultural whose quality and yield are both higher [3]. It has been an advanced way in the field of agriculture production and acted as an important part of facility agriculture. One parameter of plant micro-environment is temperature. In the development of a smart greenhouse using the Wireless Sensor Network as a monitoring system to be made is a smart greenhouse using the Wireless Sensor Network with the addition of an Internet of Things (IoT) remote control. The IoT technology has experienced rapid growth, and is predicted to expand more in the near future. It is predicted that there will be more than 16 billion IoT connected devices in less than 4 years [4].

This research will focus on the design of a greenhouse for monitoring coffee plants using DHT 11, YL-69 modules, and also using an LDR sensor. The sensors are connected with WSN technology and IoT control so that the monitoring process becomes more efficient and can be monitored remotely. This system is applied to a greenhouse which is expected to be good or inadequate support for the growth of coffee plants. The results of this monitoring can be directly monitored and accessed on a smartphone.

After Introduction in Section I, the remaining of this paper written as follows: Section II present more detail research method. Section III presents the detail about system design and architecture. Section IV present the result of evaluation from this system. In addition, the last section, Section V, presents the conclusion from this system and future work that need to be applied.

RESEARCH METHOD

The research begins with the issue of monitoring systems effectively using Wireless Sensor Network technology. This system is intended to be applied as a monitoring of the growth of coffee plants in the greenhouse. In the planning stage, which is to complete all the tools needed to build this WSN system, then the design begins by making a prototype of the device. There are two nodes along with a sensor module as a reader that acts as a transceiver that sends sensor data to the primary node that acts as a receiver. The next step is to identify the data needed in the research to find out what data is needed.

Before carrying out real testing, the device needs to be tested in neutral to be able to find out if an error occurs in the system. After the system is ready, then testing and data retrieval can be done correctly as well as analyzing data from data that has been obtained. This analysis includes the RSSI (received signal strength indicator) value in the state of losses or losses, then the sensor data obtained is compared between the data obtained after transmission with the actual sensor data. RSSI is a parameter used by Wi-Fi transceivers to adapt its modulation and coding scheme so that the optimum data rate can be achieved [5, 6, 9].

Data collection includes RSSI, battery power, and sensor data from the device node. All three will be tested with distance variables and use two conditions, namely LOS and NLOS. RSSI will be compared between the data from calculations and data from measurements so that it can compare the error percent of the system used. Then the signal power also compares the calculation data and measurement data. In the sensor, data will compare the output value of the system with the value obtained from the measuring instrument to be able to calibrate the results of the measurement. The results can be analyzed using a graph so that it can be seen the performance of this system.

SYSTEM DESIGN

This system requires several stages of design to get data, from the configuration on XBee, configuration on the web as a server, and retrieval of data. In this configuration, Xbee has several roles, including as a node and also as a coordinator. The Xbee node functions to receive sensor data that has been installed, where this data is obtained from the DHT 11 sensor, the LDR sensor, and also the YL-69 sensor. Then the XBee coordinator acts as the receiver of data from the two nodes that have sensors installed to proceed to the server using the wifi module in the form of ESP8266.
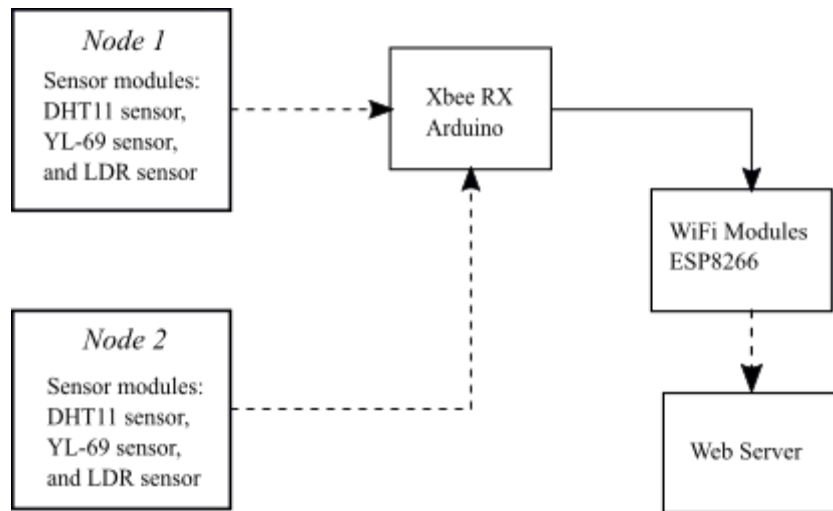
FIGURE 1. Configuration of greenhouse monitoring system

Figure 1 is the diagram of this system configuration. The block diagram consists of 4 parts. In the first part, there are node 1 and node 2, which contain DHT11 sensors, YL-69 sensors, and LDR sensors that have been installed on Arduino Uno as the microcontroller. The Xbee Pro (Tx) module acts as the sender of sensor data on the node. Data sent by these two nodes includes air temperature, light intensity, and soil moisture level of an object.
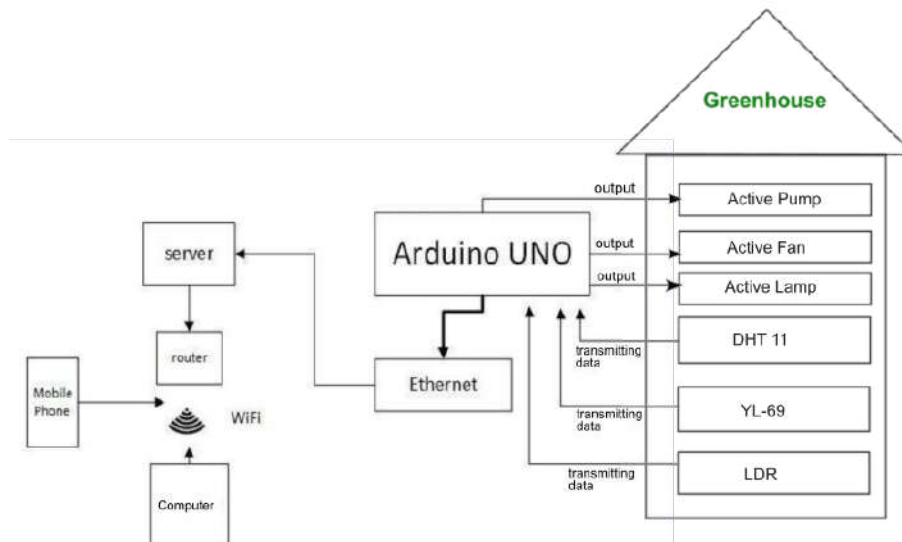
FIGURE 2. Greenhouse monitoring communication system design

On the receiver, the Xbee Pro (Rx) module has been installed, which is connected directly to Arduino Uno, which functions as a mini PC to manage the data obtained. Using the Wi-Fi module data then the data is sent to the web server in the form of thinkspeak, which on this website has been compatible with Arduino devices so that it makes it easy to upload sensor data. After connecting to this website, all sensor data results in the form of air temperature, light intensity, and soil moisture level can be seen in the form of graphs. The complete diagram of this network system are shown in figure 2

At the web configuration, this system uses the free server service https://thingspeak.com which supports Arduino. The ThingSpeak website display can be seen in figure 2.a. In thingspeak.com, the user will be directed to create a channel to display the sensor data that we get from Xbee. Then fill in the data, and the number of channels that will be created, the interface for the web is ready to use. The process of sending data from Xbee that has been connected to Arduino and also ISP8266 requires API keys. The data will be recorded in the Arduino program and sent automatically to this channel. The process of API keys configuration are shown in figure 2b.
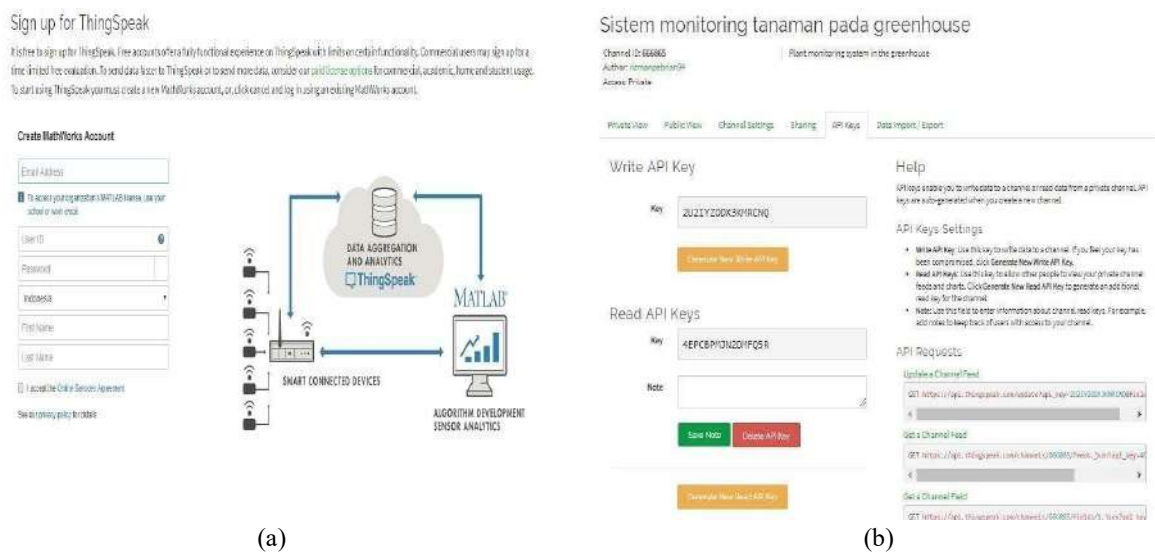
(a)   (b)

FIGURE 3. (a) ThingSpeak website, (b) API keys for connection

Figure 4.a is a flowchart of the entire system applied. After the process has started, then the initiation of input and output. Then read the existing sensor data that is the DHT11 sensor as a reader of temperature and humidity, the LDR sensor as a reader of light intensity and the YL-69 sensor as a reader of soil moisture levels. If the sensor readings occur an error, then the process will return to get the right data. If the data is correct, the next process sends data to Xbee. Then the data is continued on Arduino, which has been connected to the internet so that the data is directly uploaded on the web.

(a)   (b)
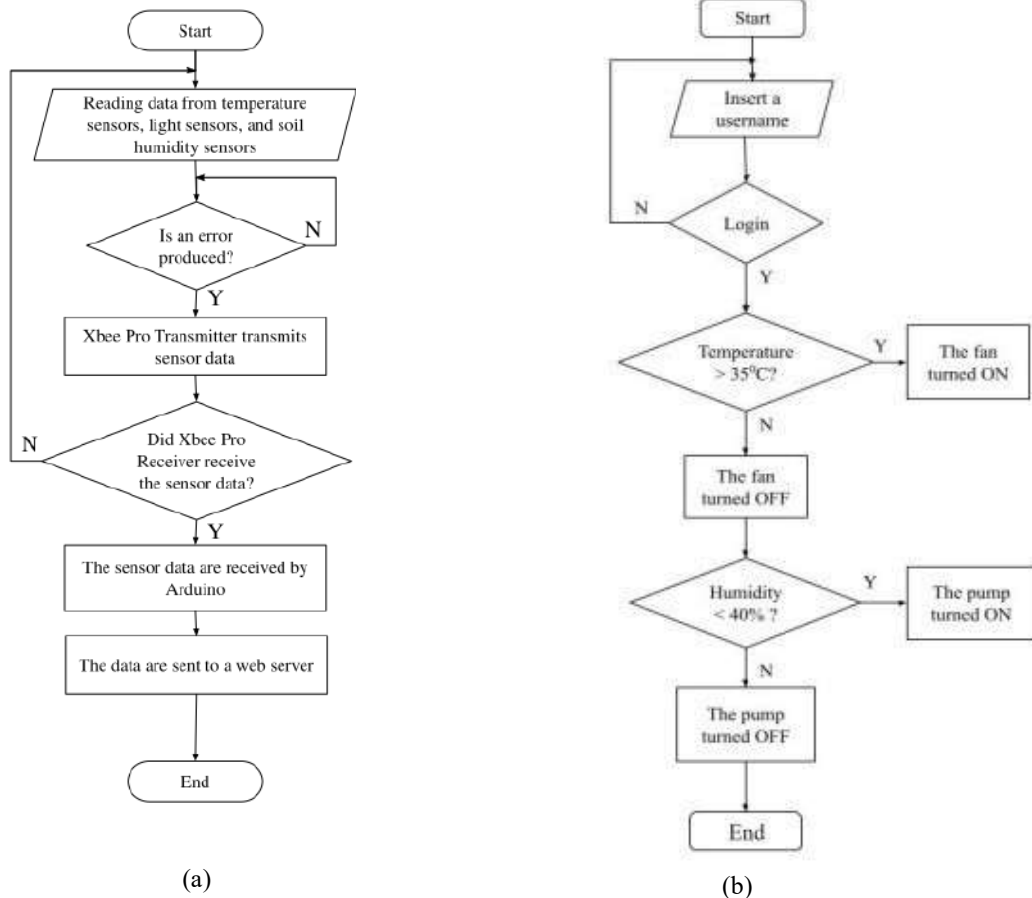
FIGURE 4. (a) Flowchart of monitoring system, (b) Flowchart of the applied temperature and humidity control

Figure 4.b is a flowchart of the applied temperature and humidity control system. After the process has started, then initialize the input and output. Then enter the username to be able to enter the application. If the username reads an error, the process will return to get the correct username. If the username is correct, then the next process is entered into the application. If the temperature is more than 35, the fan is ON. Otherwise, the fan is OFF. Then if the humidity is lower than the threshold, the pump is ON. Otherwise, the pump is OFF.

DISCUSSION AND RESULTS

This section explain the conducted tests to evaluate communication performance of the system based on RSSI. The RSSI test aims to find out the signal strength that can be received by the receiver from the transmitter. In systems using Xbee, the node acts as a transmitter and coordinator as a receiver. Data for RSSI is obtained by using XCTU software, where there are two conditions used, namely, NLOS and LOS.

In the NLOS conditions, the tests were carried out at a distance of 1 m, 2 m, 3 m, 4 m, 5 m, 6 m, 7 m, 8 m, 9 m, and 10 m. For testing LOS 10 m, 20 m, 30 m, 40 m, 50 m, 60 m, 70 m, 80 m, 90 m, and 100 m. The testing process is carried out using XCTU software when the sender communicates with the recipient with a change in the distance that has been determined and then compared with the calculation results. Then from the difference in measurements and calculations will get a value of percent error so that it can know the level of accuracy of RSSI data obtained from the experimental results.

NLOS Communication

The RSSI test from coordinator to node 1 and 2uses the sender's condition to transmit data to the receiver in real-time from a distance of 1 m to 10 m for NLOS and 10 m to 100 m for LOS conditions. The first test carried out with

the NLOS conditions obtained results in table 1. The value that is passed is the variation value of the change in the distance, which affects the signal strength. The coordinator part is used as a side to get the RSSI value. For this testing process, the reference RSSI value used for a distance of 1 m is -40 dBm.

In table 1 and 2, the results obtained from the RSSI test for NLOS conditions from node 1 and 2. The measurement value is obtained from XCTU software, and the calculation value is obtained from the results of the equation. Then the two values are compared to get an error value, so it can show the accuracy of the values obtained using this system.

Table 1. RSSI Node 1 value for N-LOS condition

No	Distance (m)	RSSI (dBm)		Error (%)
		Measurement	Calculation	
1	1	-56	-60	6,66
2	2	-58	- 66,02	12,14
3	3	-73	-69,54	4,97
4	4	-77	-72,04	6,88
5	5	-79	-73,97	6,80
6	6	-82	-75,56	8,52
7	7	-85	-76,90	10,53
8	8	-87	-78,06	11,45
9	9	-90	-79,08	13,80
10	10	-91	-80	13,75
	Average Error			9,55

The error value of the comparison of the two values shows the smallest error which is 6.66% in the first try, and the most significant error is in the ninth try at 13.80% and for an average error of 9.55%.

Table 2. RSSI Node 2 value for N-LOS condition

No	Distance (m)	RSSI (dBm)		Error (%)
		Measurement	Calculation	
1	1	-57	-60	5
2	2	-60	- 66,02	9,11
3	3	-68	-69,54	2,21
4	4	-72	-72,04	0,05
5	5	-77	-73,97	4,09
6	6	-79	-75,56	4,55
7	7	-81	-76,90	5,33
8	8	-85	-78,06	8,89
9	9	-88	-79,08	11,27
10	10	-90	-80	12,5
	Average Error			6,30

In testing node 2, the RSSI value obtained at the closest distance is -57 dBm and continues to decrease until at the farthest distance, it has an RSSI value of -90 dBm. The calculation value has a difference that varies with an average error value of 6.30%. The most significant error was found at a distance of 9 m that resulted in 11.27% error. Also, the smallest error was found at a distance of 4 m at 0.05%. It can be said to be inversely proportional. Testing this NLOS barrier type change can also affect the level of weakening of the RSSI value.

LOS Communication

The next test is the RSSI test with LOS conditions, with the same treatment that is by changing the distance as in testing under NLOS conditions. In this section, there is a difference that is the distance used is further, and between the transmitter and receiver, there is no obstacle whatsoever.

Table 3. RSSI Node 1 value for LOS condition

No	Distance (m)	RSSI (dBm) Measurement	RSSI (dBm) Calculation	Error (%)
1	10	-73	-80	9,58
2	20	-79	-86,02	8,88
3	30	-86	-89,54	4,11
4	40	-90	-92,04	2,26
5	50	-95	-93,97	1,08
6	60	-98	-95,56	2,48
7	70	Lost	-	-
8	80	Lost	-	-
9	90	Lost	-	-
10	100	Lost	-	-
		Average Error		4,73

Tables 3 and 4 show the results of this second test. With the closest distance of 10 meters and the furthest distance is 100 meters. From the test results, it can be seen that when at the closest distance, the RSSI value is -73 dBm and continues to decrease following the increasing distance. The furthest point that can be reached by the signal is at a distance of 60 meters with an RSSI value of -96 dBm. At longer distances at 70 meters to 100 meters, the connection between the transmitter and receiver cannot reach.

Table 4. RSSI Node 2 value for LOS condition

No	Distance (m)	RSSI (dBm) Measurement	RSSI (dBm) Calculation	Error (%)
1	10	-75	-80	6,66
2	20	-78	-86,02	10,28
3	30	-84	-89,54	6,59
4	40	-89	-92,04	3,41
5	50	-93	-93,97	1,04
6	60	-97	-95,56	1,48
7	70	Lost	-	-
8	80	Lost	-	-
9	90	Lost	-	-
10	100	Lost	-	-
		Average Error		4,91

In table 3, there is a decrease in the value of RSSI with increasing distance used. From these results, it can be said that the LOS condition has a longer transmission distance than the NLOS condition. Table 4 also shows that the influence of the farther distance reduces the value of the RSSI measurement. The closest distance is 10 meters with an RSSI value of -75 dBm and the farthest distance of transmission is 60 meters with an RSSI value of -97 dBm. At a distance of 70 meters, 80 meters, 90 meters, and 100 meters, the value of RSSI does not exist because the signal can no longer reach.

On the calculation value using equations, RSSI values are generated that are not much different from the measurement values using XCTU. It can also be seen that the smallest error value is at a distance of 50 m at 1.04% and for the most significant error at a distance of 20 m at 10.28%, so for an average of all error values of 4.91%.

CONCLUSION

The results of the study can also be known how the condition of NLOS and LOS is very influential on signal strength. Mainly by using the Xbee protocol can be seen with the NLOS condition at a distance of 3 meters the RSSI value of -73 dBm, but the LOS condition at a distance of 10 meters has an RSSI value of -73 dBm. So it can be concluded that the existence of obstacles between the coordinator and the node is very influential on signal quality

The next step for this research is to do packet loss evaluation and real field test to obtain more detailed result. The result will determine whether this system is ready to be implemented or not. There is also more room for improvement to use better hardware by using mini PC such as Raspberry Pi and better routing protocol. These two improvements can lead to green computing technology to get better energy efficiency.

REFERENCES

1. M.I.Jais, T.Sabapathy, M.Jusoh, P. Ehkan, L.Murukesan, I.Ismail, R.B. Ahmad. Received signal strength indication (RSSI) code assessment for wireless sensors network (WSN) deployed Raspberry-Pi. 2016 International Conference on Robotics, Automation and Sciences (ICORAS). Electronic ISBN: 978-1-5090-6205-8
2. Li Xiaofeng ; Qin Linlin ; Lu Linjian ; Wu Gang. Design and implementation of modern greenhouse remote monitoring system based on the Android system. 2015 34th Chinese Control Conference (CCC). Electronic ISBN: 978-9-8815-6389-7
3. Xijun Xing; Jiancheng Song; Lingyan Lin; Muqin Tian; Zhipeng Lei. Development of Intelligent Information Monitoring System in Greenhouse Based on Wireless Sensor Network. 2017 4th International Conference on Information Science and Control Engineering (ICISCE). Electronic ISBN: 978-1-5386-3013-6
4. Relecura. IoT - Internet of Things Technology Landscape and IP Commercialization Trends. 2017. [Online]. Available: https://relecura.com/reports/IoT_IP_Landscape_Commercialization_May2017.pdf. [Accessed: 12-Jul-2019]
5. Yoppy ; R. Harry Arjadi ; Henry Candra ; Haryo Dwi Prananto ; Tyas Ari Wahyu Wijanarko. RSSI Comparison of ESP8266 Modules. 2018 Electrical Power, Electronics, Communications, Controls and Informatics Seminar (EECCIS). Batu, East Java, Indonesia, Indonesia.
6. Andika, Ahmad Deny. 2013. Perancangan Sistem Pengukur Jarak Antara 2 Titik Wireless Xbee Pro Berdasarkan Nilai RSSI. Departemen Fisika Fakultas Matematika Dan Ilmu Pengetahuan Alam Universitas Sumatera Utara Medan
7. Ferdoush, Sheikh Mohammad. 2014. "A Low-Cost Wireless Sensor Network System Using Raspberry Pi And Arduino For Environmental Monitoring Applications". University Of North Texas.
8. Fuad, M. 2015. "Rancang Bangun Wireless Sensor Network Berbasis Protokol Zigbee dan GSM ntuk Sistem Pemantauan Polusi Udara". Sekolah Pascasarjana Institut Pertanian Bogor
9. Garnis Aishah, Suroso. 2017. "Pengkajian Kualitas Sinyal Dan Posisi Wifi Access Point Dengan Metode RSSI Di Gedung KPA Politeknik Negeri Sriwijaya". Politeknik Negeri Sriwijaya.

Design and Analysis of Rectenna Using the Cockroft-Walton Method with L Matching Impedance

Dodi Setiabudi[1,a)], Adelana Yogi Santosa[2,b)], Deschie Tri Aksara[3,c)],Alfredo Bayu Satriya[4,d)] Dedy Wahyu Herdiyanto[5,e)], Wahyu Muldayani[6,f)]

[1,2,3,4,5,6)]*Electrical Engineering Departement, University Of Jember*
Kalimantan Street No. 37 Jember 68121
[a)]dodi@unej.ac.id.
[b)]adelana1996@gmail.com.
[c)]deschie96@gmail.com.
[d)]alfredobayu.teknik@unej.ac.id.
[e)]dedy.wahyu@unej.ac.id.
[f)]wahyumuldayani.teknik@unej.ac.id.

Abstract. Electronic devices use a small DC (Direct Current) sources such as batteries with a limited lifetime. It is encouraging to produce new ideas and technologies that can be used from external sources which we commonly refer to as energy harvesters. Rectenna is a device that can be used to harvest electromagnetic waves, an antenna as a wave catcher and integrated with a rectifier or rectifier in the form of media to convert AC (alternating current) to DC voltage. Rectifiers consist of parallel series arrays between capacitors and diodes. High frequency and low level according to the special type of schotkky diode. Receiver antennas require large gain, one of which is a directional type antenna, which is a helical antenna spiral axial mode with a ground plane. To get a voltage greater than the input voltage, it is necessary to use Cockroft-Walton voltage multiplier rectifier which can create high voltage at low currents at a low cost. The proposed design and fabricated axial helix mode antennas have parameter values that have met the standard of working an antenna in general. The results of fabrication have GSM working frequency at 1900 MHz with return loss parameters of -20.3 dB and VSWR of 1.22. In designing the rectenna an antenna is needed that can work on GSM frequencies so that the frequency of 1900 MHz can be used on this device. While the analysis of the results of testing the DC voltage output of the two circuits shows different results, in general, the rectifier with matching impedance circuit produces a higher voltage than the rectifier without matching impedance. The output voltage is 85.3 mV with a distance of 100 m, 79.1 mV with a distance of 200 m, and 22.7 mV at a distance of 300 m, the rest of the rectenna cannot receive enough power level to be converted into DC voltage. The rectenna developing is very dependent on the effectiveness of power transfer from the antenna to the rectifier so that it also needs a topology matching type L matching impedance. The L matching impedance circuit produces a better DC voltage than without using a matching circuit. The results test prove that electromagnetic waves can be converted to DC with a value reaching +85.3 mV.

Keywords: Energy Harvesting, Rectenna, Voltage Multiplier, Cockroft-Walton, L Matching Impedance

INTRODUCTION

Today technology is advancing rapidly, especially in the telecommunications sector which shows significant changes. Both the hardware produced and the software contained in the electronic device. At present almost all electronic devices use a small DC (Direct Current) voltage [1]. The DC voltage source that we see and use most often is a battery, but in this case the battery has limited life time. On the other hand, the number of batteries that have reached life time causes pollution of the environment. This limited battery life has encouraged research to generate new ideas and technologies to drive wireless-based devices for an unlimited period of time or increase the time period [1]. Antennas are needed to convert electrical energy into electromagnetic energy in the receiver and transmitter parts also apply to the opposite of electromagentic energy converted to return to electrical energy [2,13].

The discussion included the design of axial mode helix antenna and 8x Cockcroft-Walton voltage multiplier system as wave surrender. The use of this method was chosen because of its ability to create high voltages at low currents and to double these voltages significantly at low cost [11]. The biggest advantage of this circuit is the voltage at each stage is equal to twice the peak input voltage in the rectifier half wave, while in the full wave rectifier is three times the input voltage [5].

The above axial helix mode antenna uses a copper wire wrapped around a PVC pipe (Polyvinyl Chloride) in a ground plane using aluminum plate material connected with a pigtail using a SMA connector [11,13]. Axial helix mode antenna in 3 dimensional geometry is presented with D, S, C, L as in Figure 1.
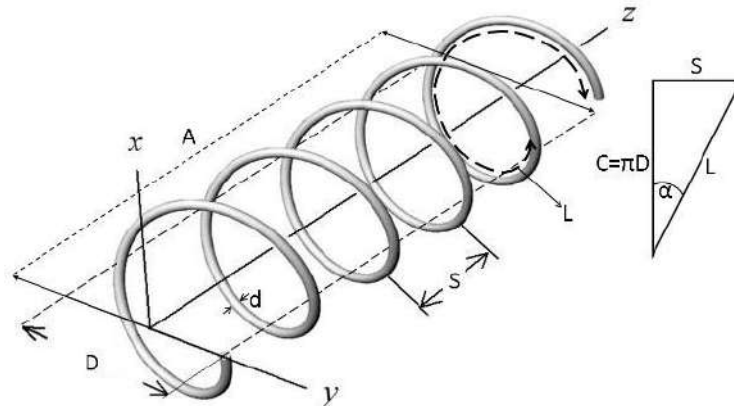
Figure 1. Axial Helix Mode Antenna

D as the circle diameter, S is the spacing between circles, A axial overall length, C around the circle, L length of wire in a circle, and α is pitch angle [10].

This Cockroft-Walton Rectifier series is a simple multiplier series popular with Cockroft and Walton. The disadvantage of this circuit is that the regulation of voltage is very bad, as the voltage drops very quickly as a function of the output current. [6,11]
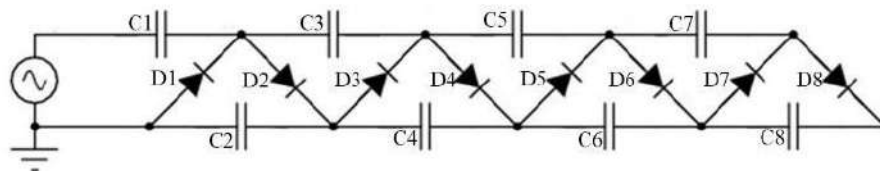
Figure 2. Cockroft-Walton Rectifier 8x

Voltage multiplier is the same as the double voltage of the two in maximizing power transfer can be implemented with passive components such as capacitors and inductors. [8]

Matching impedance is needed in RF circuit design to provide the possibility of maximum power transfer between source and load. In the impedance transmission line the load has a SWR (Standing Wave Ratio) equal to one, in order to transmit a certain amount of power without reflection. The L type matching circuit is a circuit that uses a capacitor and one inductor. Capacitors and inductors connected to form L are often used as circuit impedance matching components. As shown in figure 3 which is one of the various kinds of topology matching impedance circuits. [7]
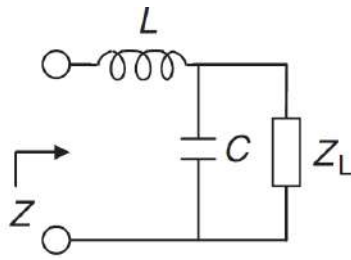
Figure 3. L Matching Impedance Circuit

RESEARCH METHOD

Figure 4 block diagram describes the flow of the design of the rectenna circuit obtained from the GSM signal. Rectifiers use the Cockroft-Walton method which is integrated with axial mode helix antennas, between rectifiers and antennas, there are L matching impedance circuits. After the core of the rectenna has been assembled with the appropriate specifications, the next experiment is to harvest the energy from the rectenna. Figures are presented center, as shown below and cited in the manuscript.
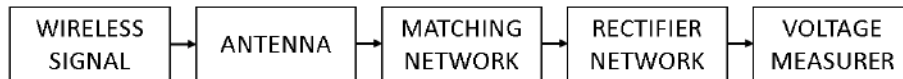
Figure 4. Block Diagram of the Project

Table 1. Specification Antenna Parameters

No.	Parameters	Value
1	Terminal Impedance	50 ohm
2	VSWR	< 2
3	Return Loss	$\leq$ -10 dB
4	Gain	$\geq$ 2 dBm

Table 2. Dimension of Designing Axial Helix Mode Antenna

No	Parameters	Variable	Dimention
1	Wavelength	λ	324,324 mm
2	Diameter of the helix antenna	D	103,326 mm
3	Around the helix antenna	C	324,324 mm
4	Pitch Angle	α	12°
5	Distance between turns	S	68,937 mm
6	Length	A	551,5 mm
7	Diameter ground plane	DGP	308,108 mm

Axial mode helix antenna is designed to work at the GSM frequency. In this study, it is expected to be able to give the desired results according to the specification and parameters table 1,2 and 3 dimension of designing axial helix mode antenna.
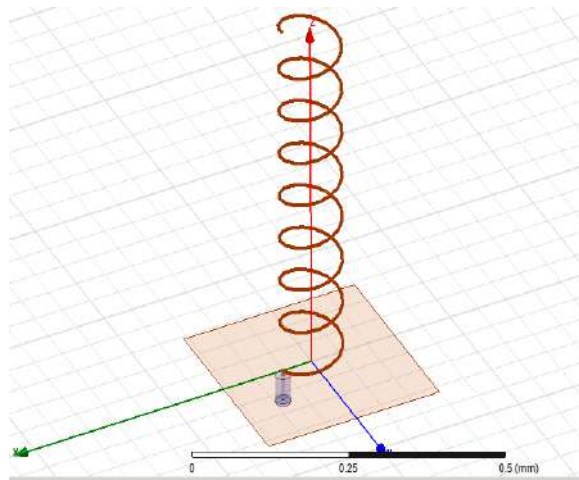
Figure 5. Axial Helix Mode Antenna Design

Table 3. Component Value Specifications Matching Series

No.	Parameters	Variable	Value
1	Q factor	Q	12,2
2	Capacitor	C_S	43,1 pF
3	Inductor	L_S	0.72 nH

Testing cockroft-walton rectifiers using 8 BAT 17-04 schottky type diodes with 330 nF capacitors compiled according to cockroft-walton rules using NI software Multisim v14.1 is shown in the following figure 6. In the picture marked yellow is a series of L matching impedance.
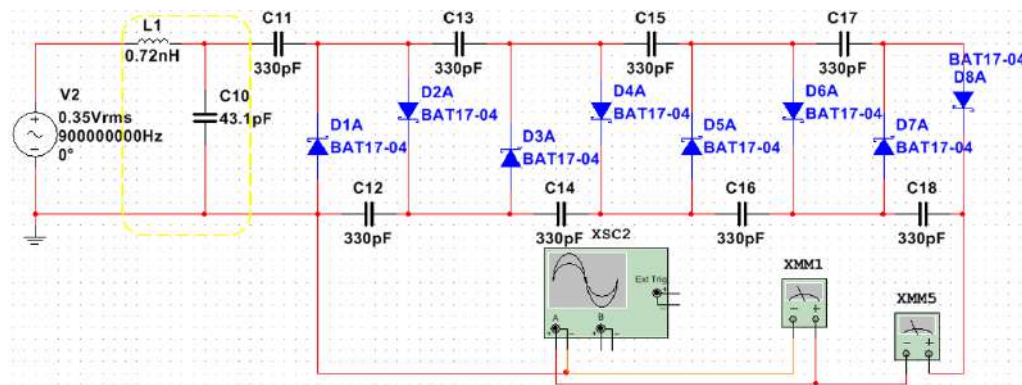
Figure 6. Rectifier Circuit with L Matching Impedance

RESULTS AND ANALYSIS

Hardware Fabrication

The fabrication process is carried out after the design process using HFSS v13 software with dimensions according to the design. The matching impedance of the antenna uses 81.08x4x0.2 mm copper plate, and the rectifier impedance uses 0.72 nH capacitors and 43.1 pF inductors. The axial mode helix antenna that has been fabricated can be seen in Figure 7 and rectifier in Figure 8.

Figure 7. Axial Helix Mode Antenna

Cockroft-Walton Rectifier uses dual mode jumpers so that in one series can be changed using matching circuits or not using matching circuits. In figure 8 is a rectifier connected to the L matching impedance circuit using 4 mini jumper series 2.54. Figure 9 uses 2 jumpers that directly pass through the matching circuit. The yellow box in the figure shows an L matching impedance circuit.
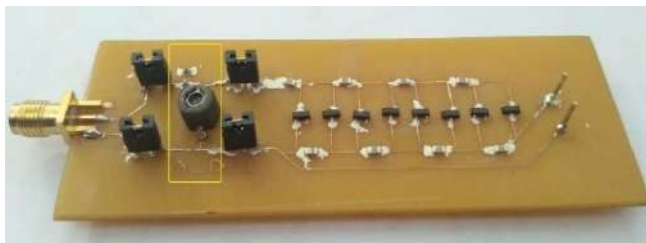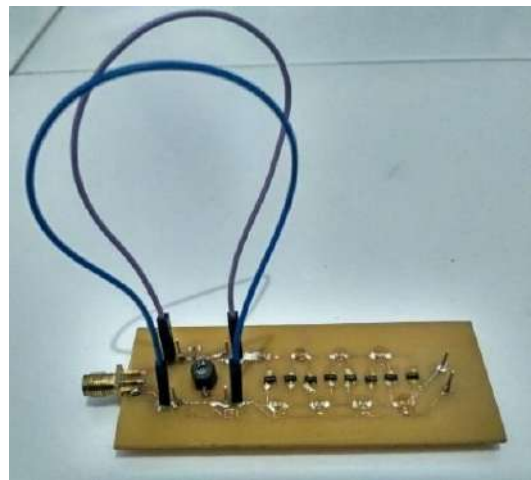
(a)   (b)

Figure 8. (a) Rectifier Cockroft-Walton with L matching Impedance, (b) Rectifier Cockroft-Walton without L matching Impedance

Antenna Analysis and Measurement

The results of measuring the axial antenna helix return loss parameters using the Spectrum Analyzer get the return loss value at the frequency of 1.90 GHz, namely -20.1 dB, can be seen in Figure 10.
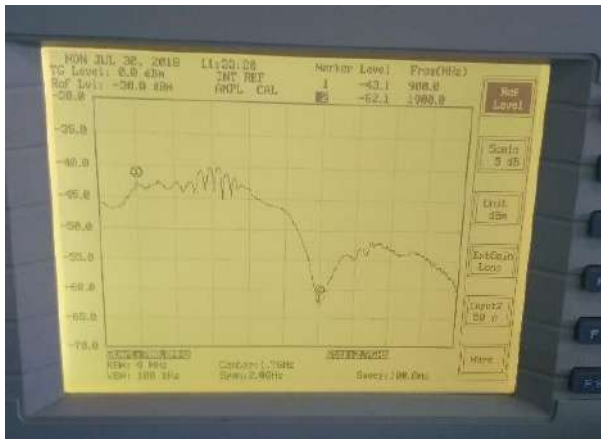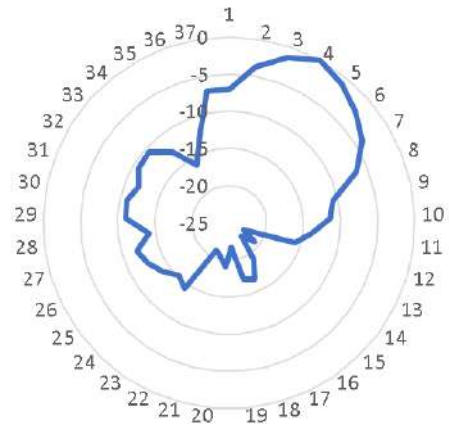
(a)	(b)

Figure 10. (a) Result of Measurement of Return Loss Antenna, (b) Antenna Radiation Pattern.

Generally there are significant changes with the simulation results influenced by many factors in the presence of a factor of mean square error (MSE) that occurs due to external influences. In the theory of tolerance in general it is often used in many cases without the existence of clear ideas on achievement factors and of course it is often necessary for designers to establish tolerance without the existence of a complete theory [4]. In this case it is well recognized that the occurrence of differences in resonance frequency is influenced by substrate or wire material which has a different thickness with the simulation results. Changes in the maximum value in resonant frequency occur in thicker substrate [3].

Implementation of Rectenna energy harvesting

The experiment was carried out with several distances from BTS to different rectenna instead of the different power levels from the source of electromagnetic waves. The distance from the measurement location to the BTS is determined using the Cell Tower Locator v1.27 software. The basis is to distinguish from the input of electromagnetic waves from high to low, for the farthest distance means the power level received is getting lower while the closest distance is the received power level the greater in dBm units. Tests are carried out at distances ranging from 100 m, 200 m, 300 m, 400 m, and 500 m. The output voltage results can be seen as in Tables 4 and Table 5.

Figure 12. Testing of Energy Harvesting Rectenna

Table 4. Data Results Data DC Voltage Measurement Rectenna with L Matching Impedance

No	Distance Ranging (m)	V DC (mV)
1	100	85,3
2	200	79,1
3	300	22,7
4	400	1
5	>500	0

Table 5. Data Results Data DC Voltage Measurement Rectenna without L Matching Impedance

No	Distance Ranging (m)	V DC (mV)
1	100	62,3
2	200	50,0
3	300	2,0
4	>400	0
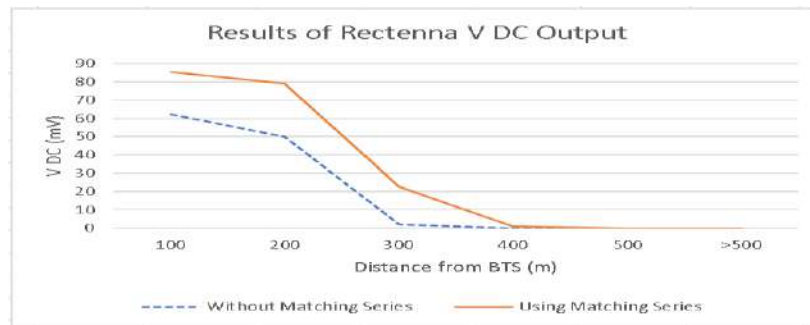
Figure 13. Graph of V DC Rectenna Results

CONCLUSION

In designing and fabricating axial helix mode antennas have parameter values that have met the standard of working an antenna in general. The results of fabrication have GSM working frequency at 1900 MHz with return loss parameters of -20.3 dB and VSWR of 1.22. In designing the rectenna an antenna is needed that can work on GSM frequencies so that the frequency of 1900 MHz can be used on this device.

While the analysis of the results of testing the DC voltage output of the two circuits shows different results, in general the rectifier with matching impedance circuit produces a higher voltage than the rectifier without matching impedance. The output voltage is 85.3 mV with a distance of 100 m, 79.1 mV with a distance of 200 m, and 22.7 mV at a distance of 300 m, the rest of the rectenna cannot receive enough power level to be converted into DC voltage.

REFERENCES

1. Lenin Anujin. *Design and Simulation of Energy Harvesting System Using GSM Signal*. International Journal of Latest Trends in Engineering and Technology (IJLTET). 2014. Vol 3, Issue 4.
2. Balanis, A. Constatiene. *Antenna Theory Analisis and Design*. Canada: Wiley Interscience. 2005.

3. Banerjee, Y. *Comparative Study of Resonant Frequency of Rectangular Microstrip Antenna*. Krishi Sanskriti Publications. Gauhati University. 2015.
4. Bracewell, R. N. *Tolerance Theory of Large Antennas*. IRE Tr. Ant. Prop., AP-9. 49. 1961.
5. Patel Akul P, Rathod Mulav. *Design, Simulation and Construction of Cockroft Walton Voltage Multiplier*. GRDJE. Department of Electrical Engineering S.V.I.T (VASAD). 2016. Vol 1, Issue 4.
6. Kuphaldt Tony R. *Lesson In Electric Circuits, Volume III - Semiconductors. Fifth Edition*. Open Book Project. 2009. (*Page 123 - 130*).
7. Bahl Inder J. *Fundamentals of RF and Microwave Transistor Amplifiers*. Canada: John Wiley & Sons, Inc., Publication. Hoboken, New Jersey. 2009. (*Page 149 - 153*).
8. Ho Dhin-Khan. *Dual-Band Rectenna for Ambient RF Energy Harvesting at GSM 900 MHz and 1800 Mhz*. IEEE. Hanoi: Hanoi University of Science & Technology (HUST), Vietnam. 2016.
9. American Radio Relay League (ARRL). *Antenna Book, 21th Edition*. The ARRL. Inc. 2007. ISBN:0-87259-987-6.
10. Kraus J. D. *Antennas. Second Edition*. Tata McGraw-Hill Publishing Company Limited. New Delhi. 2001. ISBN: 0-07-035422-7
11. Toudeskhi Arash. *Devolument of a New Cascade Voltage-Doubler for Voltage Multiplication*. Hindawi. Serdang: University Putra Malaysia, Malaysia. 2014. Vol 6
12. Cao Yanjie. *A 2.4GHz Circular Polarization Rectenna with Harmonic Suppression for Microwave Power Transmission*. IEEE. Baijing: Beijing University of Post and Telecomunication, China. 2016.
13. Setiabudi D., Wicaksono L. B. H. *Rancang Bangun Antena Helix Mode Axial dan Patch Meanderline DGS untuk Aplikasi LPWAN Berbasis IoT pada Daerah Rural.* Jurnal Rekayasa Elektrika (JRE). 2018. Vol 14, No 2.

Identification of Wood Types Based on Textures using Convolutional Neural Network (CNN) With Raspberry Pi

Bambang Kusriwanto[1]*, Khairul Anam[2], Bambang Sujanarko[3]

Electrical Engineering, University of Jember[123]

khairul@unej.ac.id

Abstract. The purpose of this study was to identify wood species based on texture by the CNN method using Raspberry pi. This research was conducted using 5 different types of wood. For each type of wood, 40 images are needed to identify it so that the desired wood is actually realized. Our experimental results show that the proposed method can increase recognition by up to 90%. So this study shows that the CNN and Raspberry pi methods are very accurate in distinguishing wood species. And this study only uses data sets of medium size, so further research is needed to use more methods of extracting features and types of wood.

Keywords: CNN, wood identification, Raspberry pi

INTRODUCTION

All types of wood have a different texture, strength, density, hardness, odor, and color. Texture is one of the important characteristics used in identifying objects in an image. Identification of types of wood has its own challenges. This is due to the diversity of wood species, the aging process and the phenomenon of damage that affects the appearance of wood material and sometimes even the structure of wood integrity [1].

Typically, experts identify wood species based on wood surface texture patterns (Menon et al. 1993). Experts who study wood surface texture carefully examine several important characteristics of wood such as arrangement of vessels or pores, wood parenchyma or soft tissue, parenchyma rays, fibers, phloem, latex traces and intercellular canals. For example, different wood species will have vessels of varying size, arrangement, number and density on their surface [2].

There are various kinds of wood texture that we can find out through the identification of various types of wood texture, one of which is by means of identification through wood texture. The method of identification of wood texture has been widely carried out by researchers, including identifying the type of wood through the results of the extraction of texture features using Gray Level Co-occurrence Matrix (GLCM), in research using the probabilistic neural network (PNN) method [1].

Identification of species from wood material is an important task. For example, in the construction industry, it is important to use certain types of wood because of their quality. the characteristics and properties of wood vary depending on different growth conditions and, most importantly, belonging to certain species. To choose the right material with suitable properties, it is necessary to identify wood species. Given that these tasks usually require human experts, automated information systems can increase efficiency and speed up the process [3]. Usually identification of wood species occurs according to the external characteristics of the tree, for example,

the shape of leaves or stems, as well as the smell of bark. However, when the tree undergoes processing and takes a board or wood form such identification becomes impossible. Thus, in this case one of the useful and unique characteristics left for each species is surface texture [4].

CNN is a type of algorithm that can learn the exact parameters of various image processing operations such as leveling, sharpening and edge detection for input images. CNN also has the ability to automatically study distinguishing filters to detect low-level structures such as edges and structures such as lumps and high-level objections such as faces, cats, dogs, cups, etc. [5].

Learning algorithms

Artificial neural network training is the process of adjusting the weights of connections between network neurons. on CNN, supervised learning is used, implying the use of training samples to compare network output with reference training sample values. Calculate errors and adjust the weight of the network connection to reduce the value of this error. In CNN, gradient descent or back propagation algorithm or modification is usually used. For fully connected and convolutional layers, the error value of the network output signal is as follows:

$$E(W) = \sum_{ik} (f_{ik} - y_{ik})^2$$

where E (w) is the error function of the network, fik is the value of the output signal from the neuron k from the network at the i-th sample submission from the training set, and yik is the expected value of the output signal from the kth neuron from the network when submitting the sample 3rd of the training sample.

Untuk lapisan sub-sampling, perhitungan kesalahan tidak dilakukan karena lapisan ini tidak berpartisipasi dalam pelatihan jaringan. Ketika menggunakan fungsi maksimum dalam lapisan sub-sampling (pemilihan nilai maksimum) proses kesalahan backpropagation terjadi sebagai berikut: kesalahan dari lapisan yang terletak setelah lapisan sub-sampling segera pindah ke lapisan convolutional yang terletak sebelum sub-sampel yang diberikan lapisan sampling. Ketika menggunakan fungsi yang melakukan perhitungan nilai rata-rata kesalahan, kesalahan dari lapisan jaringan, yang terletak setelah lapisan ini, dibagi dengan jumlah elemen lapisan sub-sampling dan ditransfer ke semua nilai lapisan konvolusional[6].

CONVOLUTIONAL NERVE NETWORK FOR OLD CLASSIFICATION

Convolutional neural networks are special architecture of artificial neural networks that mimic the features of the brain's visual cortex. They consist of several multidimensional layers and are designed for effective complex image recognition. For the first time such a model was proposed by Yann Lecun in 1989 and was intended for the recognition of handwritten symbols. The novelty of the model proposed by Lecun consists in introducing the multilayer perceptron convolution layer into the architecture where each neuron is only bound to a small area of neurons from the previous layer. This functionality makes it possible to detect primitive features of the original image, and at the next layer of the network receives more complex features so that it detects complex objects in the image.

Structure

Convolutional neural networks contain multidimensional layers as shown in Figure 8. The typical CNN layers are as follows :
• Input layer: image input.
• Convolution layer: all neurons in the layer, unlike the perceptron, are only connected to a portion of the neurons from the previous layer.
• Sampling layer (Pooling, Subsampling): choose the most significant features from the previous layer and significantly reduce the dimensions of the next layer of the network.
• Fully connected layer: a hidden layer of perceptron neural network type.
After the convolutional layer and the fully connected layer the neuron activation function can be used which changes the neuron signal and produces an output signal.

Proceedings of CCSE ASEAN 2019
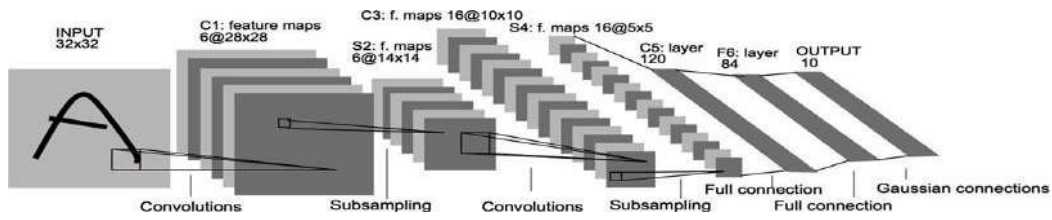
Figure 1. Example of the typical CNN architecture. Specifically, this is LeNet-5 CNN designed for digits recognition[5].

This journal explains the drawings and simulations for the identification of wood texture.
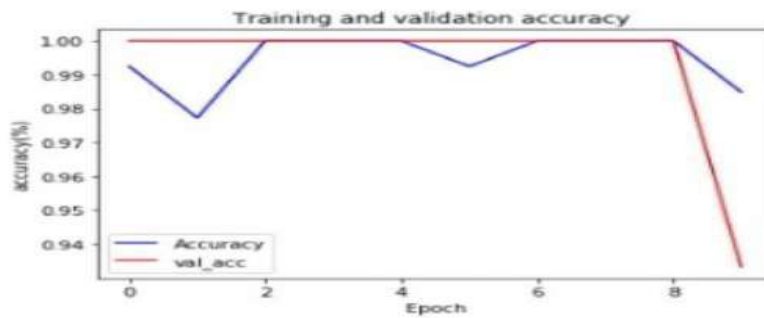
Figure 2. Training and validation accuracy

Table 1. Comp   using CNN

Wood species	ANN	CNN
Jati	73	**100**
Sengon	70	**99**
Total	**143**	**199**

CONCLUSION

In this study, we investigate the use of deep learning techniques to automatically identify wood species from five softwoods (teak, sengon, sono, acacia, mango). We built six CNN models and trained models for five species. Smartphone cameras are used to obtain macroscopic images of rough sawn surfaces from cross sections of soft wood.

REFERENCES

[1]   I. Amalia, "IDENTIFIKASI JENIS KAYU BERBASIS CITRA MENGGUNAKAN PROBABILISTIC NEURAL NETWORK (PNN)," vol. 14, no. 2, pp. 74–80, 2014.

[2]   I. Ibrahim, A. S. M. Khairuddin, H. Arof, R. Yusof, and E. Hanafi, "Statistical feature extraction method for wood species recognition system," Eur. J. Wood Wood Prod., vol. 76, no. 1, pp. 345–356, 2018.

[3]   M. C. Timar, L. Gurău, and M. Porojan, "Wood species identification, a challenge of scientific conservation," Int. J. Conserv. Sci., vol. 3, no. 1, pp. 11–22, 2012.

[4]   I. Ibrahim, A. S. M. Khairuddin, M. S. Abu Talip, H. Arof, and R. Yusof, "Tree species recognition system based on macroscopic image analysis," Wood Sci. Technol., vol. 51, no. 2, pp. 431–444, 2017.

[5]   D. Shustrov, "Species Identification of Wooden Material Using."

Smart Facial Detection as a Security System Using CCTV and CNN

Siti Nur'aini[1], Khairul Anam[2], Bambang Sujarnako[3]

[1,2,3] Department of Electrical Engineering, Faculty of Engineering, University of Jember

khairul@unej.ac.id

Abstract. Nowadays, CCTVs are only used to record the images or events around a certain area. If CCTV is equipped with intelligent capabilities that can recognize faces and suspicious motions and gives a certain alarm, CCTV can then be turned into a smart security system. This paper examines this object by utilizing computers and CNN. In the first step, some aspects of facial analyses from the application of large-scale face recognition/detection methods to wild images, emotional recognition, and micro-expression analysis are observed and classified. The second step is building an intelligent system using artificial intelligence to recognize faces and suspicious motions and generating the alarm. Finally, the last step is implementing the system using CCTV, computer, and CNN.
Keywords: CCTV, CNN, computers, face recognition.

INTRODUCTION

In solving someone's face, many methods that can be applied for, one of which is using Convolutional Neural Network (CNN). The Convolutional Neural Network that people usually know as CNN is part of Deep Learning. CNN is a learning process to find the best representation of the experiments ever tried. The basic data used is a collection of face photo data. Using the database process, the best results are obtained with a set level of achievement of 0%. If the testing data is carried out, it will receive as low as 0%. The face is one of the instruments that can be used for someone who has a face that is employed in an automatic system to support one's face [1]. Research on systems is more about control systems. This system is used to control the robot. Hence, it can control the images captured by CCTV cameras by taking pictures of faces. Seeing about facial problems, the writer came up with an idea to make a robot that can provide more sophisticated and accurate information to homeowners who install CCTV to get face images taken on CCTV recorders. This robot can easily move the information signal taken in the form of "red and yellow lights switching back and forth" for homeowners who install CCTV. The face pictures taken by homeowners give a red "flashing light" signal. An activated yellow light changes to alert detection. Face objects are described with various positions, expressions, moods, and so forth in order to be fixed based on two or three-dimensional face images.

Face Image Recognition System

Face recognition is a matter of visual pattern recognition. The face as a three-dimensional object is depicted with various kinds of illuminations, poses, and expressions to be identified based on the two-dimensional image of the face. A facial recognition system generally consists of four stages as follows [1]:
1. Face detection (localization)
2. Face alignment
3. Feature extraction
4. Matching
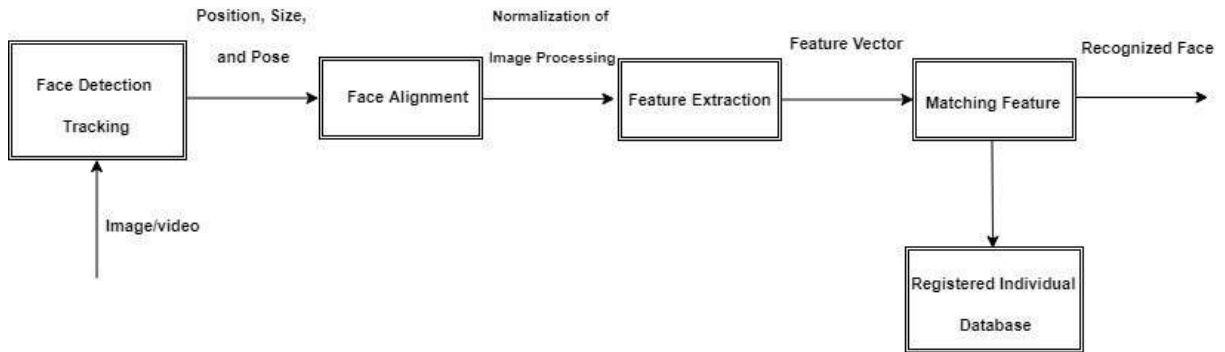
Figure 1. Face Recognition flowchart [1]

Pre-processing Stage

Localization and normalization are pre-processing stages before facial recognition (facial feature extraction and matching) is carried out. Face detection separates the face area from the background. In the case of video, detected faces need to be tracked using the face tracking component. Face detection provides a rough estimate of the location and scale of each detected face. Face alignment (normalization) is aimed at achieving more accurate localization and face normalization. Face components, such as the eye, nose, mouth, and outline of the face, are placed based on location points. The input of face image is normalized by paying attention to geometric properties (size, pose, expression, etc.), using transformation or geometry formation. The face is usually further normalized with regard to photometric properties (illumination and greyscale). [1]

Feature Extraction Stage

After the face is normalized geometrically and photometrically, the extraction from the normalized face image provides effective information that is useful for distinguishing faces from different people while paying attention to geometric and photometric variations. [1]

Matching Stage

For face matching, feature vectors extracted from normalized face input are matched with faces that have been registered in the database, producing output in the form of face identities when a match is found with certainty or otherwise indicating an unrecognized face. The results of facial recognition are very dependent on the features extracted to represent facial patterns and the classification method used to distinguish faces. Therefore, localization and facial normalization are the basis for extracting effective features. [1]

Design of CCTV Camera Robot Work Design

At the bottom of the robot devoted to CCTV media only, face detection can be implemented on the device that uses a camera. However, this research only focuses on CCTV because people have the most devices around. This

research will also be more useful if this research is implemented on the media. For example, CCTV can detect the face of someone who is committing a crime. Consequently, the face detection can be analysed the identity of the perpetrator. Testing still uses a webcam because it is more flexible and it still uses CNN. This image processing aims to find the face of the image of a moving object that has been captured. Afterwards, the image is processed by separating the image from the background, so that only the part considered to be skin is displayed while the non-skin part will be discoloured. Then from the target pursuing by CCTV cameras, the mechanical design of the driving motor is needed. The movement of the motor is a way to change the position of the CCTV camera to obtain the target.
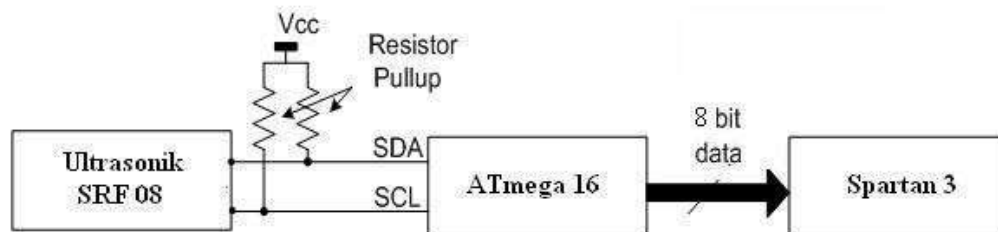
Figure 2. Ultrasonic sensor circuit diagram [4]

The face detection and obstacle avoidance algorithms in this system are as follows:
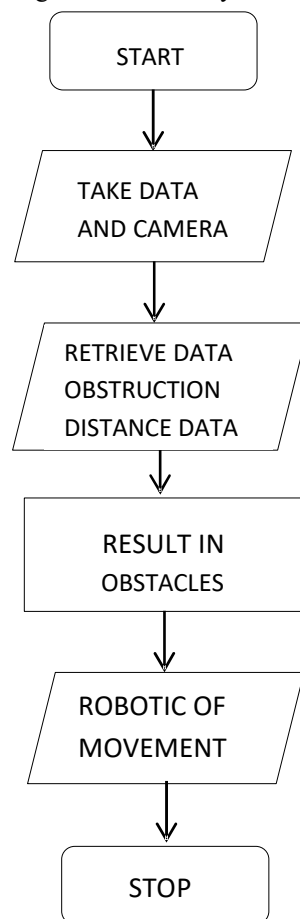
Figure 3. System Algorithm [4]

BASIC THEORY

Convolutional Neural Network (CNN) is the development of the Multilayer Perceptron (MLP) which is designed to process two-dimensional data. CNN is included in the type of Deep Neural Network because of the high network depth. Moreover, it is also because of being widely applied to image data. CNN can also consider each pixel to be an independent feature resulting in unfavourable output. [2] Since extraction is done in the frequency domain, the image is transformed into a two-dimensional Fourier:[1]

$$I(k, l) = \frac{1}{\sqrt{MN}} \sum_{m-0}^{M-1} \sum_{n-0}^{N-1} I \quad (m, n) e^{-j2\pi(k\frac{m}{M} + i\frac{n}{N})}$$

This is trial and evaluation accuracy of CNN method with incognito variations
In this scenario, a trial is performed using different input images to obtain results in the form of an accuracy ratio. Variations to be made include variations in beard and moustache, variations in glasses, variations in headgear/ hat, variations in lips/eyebrows/nose, variations in skin wrinkles, and variations in the mixture.

Table 1. Experiments using phase features [1]

Incognito Type	Accuracy ratio based on experiments
Variation of beard and mustache	82 % of 55 trial
Variations in glasses	70 % of 25 trial
Variation of headgear/hat	80 % of 30 trial
Lip/eyebrow/nose variations	71,6 % of 50 trial
Variations in skin wrinkles	80 % of 25 trial
Mixed variations	72 % of 50 trial

Table 2. Experiments without using phase feature [1]

Incognito Type	Accuracy ratio based on experiments
Variation of beard and mustache	22 % of 55 trial
Variations in glasses	15 % of 25 trial
Variation of headgear/hat	23,24 % of 30 trial
Lip/eyebrow/nose variations	10 % of 50 trial
Variations in skin wrinkles	25 % of 25 trial
Mixed variations	12 % of 50 trial
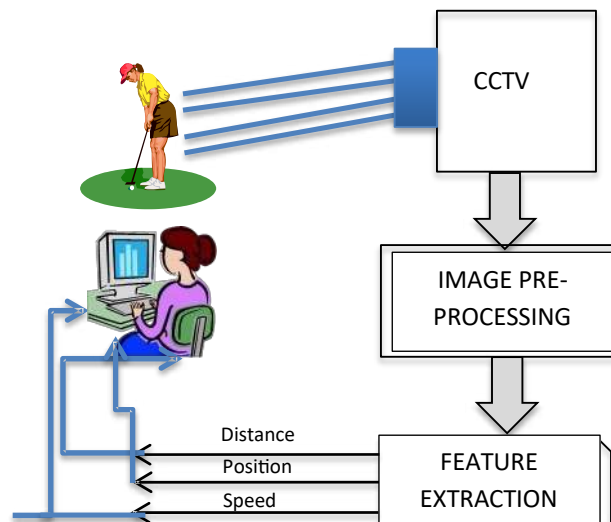
Figure 4. System Diagram Blocks

CONCLUSION

According to the table above it can be concluded that the recognition of human faces using phase features is better than devoid of using phase features. Therefore, this research strongly emphasizes the extraction of phase features in the input image both the image to be detected and the image in the database. The features used as the core of this introduction lie in the eye, nose, and mouth. Consequently, when the area is closed or subject to change, the accuracy of the CNN method will diminish in value. The best performance of the method in writing this journal is on variations of beard/moustache, headgear/hat, and skin wrinkle. For the rest, it shows less good performance. This is because there are only a few areas on the face that change and the rest of the face contributes to the correct recognition.

REFERENCES

[1]   P. Yogiswari and R. Soelaiman, "PENGENALAN CITRA PENYAMARAN WAJAH," pp. 1–9.

[2]   I. W. S. E. P, A. Y. Wijaya, and R. Soelaiman, "Klasifikasi Citra Menggunakan Convolutional Neural Network (Cnn) pada Caltech 101," vol. 5, no. 1, 2016.

[3]   W. S. Pambudi and D. Purwanto, "Implementasi Metode Anfis untuk Menghindari Dynamic Obstacle di Area Koridor pada Three Wheels Omni-Directional Mobile Robot," no. February 2015, 2011.

[4]   T. Pustaka, "ROBOT PENDETEKSI WAJAH DAN PENGHINDARAN HALANGAN," pp. 1–5, 2004.

Preparation of Magnetic Chitosan/Coffee Residue Composites and Their Application in Adsorption of Dyes

Meta Fitri Rizkiana[1,a)], Bekti Palupi[1], Ari Susanti[1], Rizki Fitria Darmayanti[1], Boy Arief Fachri[1]

[1]*Department of Chemical Engineering, University of Jember, Jalan Kalimantan No. 37, Tegalboto, Jember 68121 Indonesia*

a) Corresponding author: metafitririzkiana@unej.ac.id

Abstract. The excessive use of chemical substances has contributed to environmental pollution. Organic and inorganic wastes, as a result of rapid industrialization and urbanization, have led to an enormous water pollution problem. Trace amounts of any of these water contaminants are significant hazard on the environment and human beings. The discovery of synthetic dyes displaced the protagonist natural dyes due to their low production cost, better resistance against the environment, and brightness. The textile industry and other industries such as paper, plastic, cosmetics are the primary customers of synthetic dyes. Most of these synthetic dyes are stable (due to their complex aromatic structures), toxic, non-biodegradable. Dye compounds are difficult to decompose and dangerous if the aquatic system is exposed in a large concentration. Trace amounts of synthetic dyes can be recognized easily in the aquatic system and reduce the photosynthetic activity of the marine ecosystem by preventing the penetration of light and oxygen. Researchers have attempted to develop a separation method for removing various pollutants and improve the quality of discharged wastewater. One of the methods is magnetic separation or separation technology employing magnetic adsorbents. Magnetic separation provides convenient tools for treating wastewater treatment against traditional separation methods such as filtration or sedimentation. Magnetic carriers can easily be separated from a mixture or medium by applying an external magnetic field. Preparation of magnetic carriers from non-magnetic precursors has been successfully carried out using a simple procedure. Magnetic microparticles were entrapped in chitosan and coffee residue. Magnetic chitosan/coffee residue composites (MCCC) have been developed and exhibit good sorption behavior towards synthetic dyes in aqueous solution. The MCCC has shown promising tools for dyes removal in wastewater. The MCCC was characterized by Fourier-Transform Infrared Spectroscopy, UV-visible spectrophotometer. The results indicated that the adsorption behavior was influenced by type of dyes, the mass ratio of chitosan and coffee residue.

Keywords *magnetic separation, dyes removal, chitosan, coffee residue, MCCC (magnetic chitosan/coffee residue composites), adsorption*

INTRODUCTION

Batik is a typical Indonesian handicraft as a result of dyeing cloth. Batik forms specific patterns and well-known for high artistic value. The process of making batik has been divided into several processes, i.e. the formation of patterns, dyeing, fixation, and *pelorodan* [1]. The methods of dyeing batik have been an influence on the quality of batik. The coloring of batik using synthetic dyes has been widely used in the batik industry because of their numerous advantages over natural dyes. More stable and uniform results encourage industry to use artificial dyes. High demand for batik production has led water pollution caused by batik industrial waste containing synthetic dyes. Advance technology for the separation and purification of batik industrial waste before being discharged into the environment is necessary.

The technology of separation and purification of a chemical is necessary in various lines of life. One of the most interesting and developed techniques is magnetic separation. Magnetic carriers can easily be separated from a mixture or medium by applying an external magnetic field. Some applications have utilized magnetic separation technology such as industrial waste treatment, immobilization of enzymes and microbial cells, drug delivery, and adsorption [2].

Nanoparticles or microparticles magnetic have attracted the interest of many researchers in various fields including nanotechnology, biotechnology, pharmacy, and environmental technology. Chemical procedures such as coprecipitation, sol-gel synthesis, sonochemical reactions, hydrothermal reactions, hydrolysis, thermolysis, electrospray, and microwaves have been used for the synthesis of magnetic particles [3].

Materials that respond to external magnetic fields can be classified as smart materials or responsive materials. Magnetic particles can be selectively separated from the mixture by the influence of external magnetic fields or magnetic separators. These properties were very beneficial for biological applications because the majority of biological materials composed of diamagnetic properties. These diamagnetic properties allow the mixture to experience selective separation [4]. The synthesis of magnetic carriers from non-magnetic precursors has been successfully carried out by Safarik et al. Safarik [3] used simple procedures and have been applied to various inorganic, organic, and biological precursors. The bond strength between iron oxide magnetite particles and non-magnetic precursor surfaces occur if there is a balance between van der Waals forces, electrostatic and hydrophobic interactions between magnetic particles and non-magnetic substrates.

The advantages of magnetic carriers from inorganic material precursors are thermal stability, resistance to solvents and microbes, easy fabrication, and durable. However, the functional groups of inorganic materials are limited for selective separation [5]. Natural polymers and synthetic polymers such as calcium alginate, polystyrene, polyacrylamide, polyvinyl alcohol, nitrocellulose, polyvinyl butyral [6] have been used as non-magnetic precursors.

Chitosan is a polyaminosaccharide with many advantages (biodegradable, biocompatible, hydrophilic, polycation). Chitosan has been produced from the chitin deacetylation reaction. The use of chitosan for various applications is based on the characteristics of chitosan which are unique, available, and affordable [8]. Chitosan as a non-magnetic precursor was synthesized by Denkbas et al [5]. Spherical, non-porous chitosan micromagnetic had been observed from the results of SEM (Scanning Electron Microscope). The magnetic nanoparticles of Fe_3O_4 and chitosan with a diameter of 25 nm in the form of spheres were successfully synthesized by the hydrothermal methods and peroxide as oxidizers [9]. Chitosan magnetic nanocomposite with an amine functional group has been used to remove metal ions from wastewater. The interaction between chitosan magnetic nanocomposite and metal ions is reversible so that it allows nanocomposites to be recycled [10].

Coffee grounds as waste from the food industry commonly used as animal feed and compost, but the majority of coffee grounds has been burned and producing dangerous carbon dioxide (greenhouse gases). Researchers have utilized coffee grounds to build new technologies. Coffee grounds have been recycled into something more useful. Food industry waste such as coffee grounds have been used as a cheap adsorbent for removal of heavy metals from waste water. Magnetic modification of coffee grounds is very potential in the magnetic separation technique [11]. In this study, two precursors of chitosan and coffee grounds will be used for synthesis bio-magnetic adsorbent. Bio-magnetic adsorbent will be used for dyes removal in batik industrial waste. The effect of mass ratio between two precursors in the ability of bio-magnetic adsorbent in the adsorption of dyes was examined.

MATERIALS AND METHODS

Materials

Spent coffee grounds were obtained locally. This material was dried at 105 °C. Chitosan was extracted from shrimp shell. Magnetite microparticles were obtained locally. Sodium hydroxide, acetic acid, methanol were obtained from Merck. Batik industrial waste was prepared by diluting synthetic batik dyes (remazol yellow) and water.

Fabrication of Bio-Magnetic Adsorbent

A total of 2.5 grams of chitosan were dissolved in 100 ml of acetic acid (1% v / v). 2.5 grams of coffee grounds were dissolved in methanol 20 ml, then 5 grams of magnetite were added and stirred using a shaker for 2 hours until homogeneous. After being evenly mixed, the mixtures were added drop by drop into 30 ml sodium hydroxide 1 M to convert the dissolved bio-magnetic into ferrogel [12]. The resulting solid were washed with water and methanol to remove the remaining impurities, then bio-magnetic adsorbent was dried 60°C in the oven for 2 hours.

Dye Removal Test

Batik industrial waste could be prepared from diluting batik synthetic dyes remazol yellow with water. Each dye was dissolved in water with a concentration of 0.01 mg / ml which was then referred to dye stock. The methods were adjusted to Safarik et al [11]. 30 mg of bio-magnetic adsorbent with various concentrations was dissolved in 3 ml of demineralized water in a test bottle. Batik industrial waste or dye stock of 7 ml was added until the total volume becomes 10 ml. The solution was mixed using a shaker for 3 hours at room temperature; then the solution was left to stand until the solvent changes color. Bio-magnetic adsorbent at the mass ratio of chitosan and coffee grounds which produces the best removal performance were tested using various dyes (remazol blue and red).

Fourier-Transform Infrared Spectroscopy

The following characterization aims to identify functional groups between chitosan, magnetite, and bio-magnetic adsorbent. The synthesis process was successfully carried out if we can identify different functional groups between chitosan, magnetite, and bio-magnetic adsorbent. FTIR spectras were recorded with KBr discs in the range of 4000 - 400 cm^{-1}.

Ultraviolet-Visible Spectroscopy

This characterization aims to determine the adsorption of dyes by bio-magnetic adsorbent. Batik waste with certain concentrations were tested at various wavelengths to find out the maximum wavelength of the dye. Batik waste before and after addition of bio-magnetic adsorbent were tested for its absorbance at a maximum wavelength. Spectrophotometric results showed the performance of bio-magnetic adsorbent in the dyes removal.

RESULTS AND DISCUSSIONS

Chitosan, coffee grounds, and magnetite solutions were mixed with a certain mass ratio. The mass ratio between chitosan, coffee grounds, magnetite in grams can be presented in Table 1 below. Magnetite microparticles were trapped in a chitosan and coffee grounds ferrogel matrix. Bio-magnetic adsorbent was fabricated from non-magnetic precursors chitosan and coffee grounds.

Table 1. Mass Ratio Chitosan : Coffee Grounds : Magnetite

Mass Ratio Chitosa: Coffee Grounds : Magnetite	Samples
1,5 : 3,5 : 5	ACC15
2,5 : 2,5 : 5	ACC25
3,5 : 1,5 : 5	ACC35
5 : 0 : 5	AC50

The bio-magnetic adsorbent was evaluated by holding the magnet close to bio-magnetic adsorbent. Chitosan and coffee grounds are non-magnetic materials. After magnetite microparticles were introduced to matrix, bio-magnetic adsorbent from chitosan and coffee grounds precursors were attracted to magnets as shown in Figure 1. Coffee grounds has a porous surface structure, have large surface area and good adsorption capacity.
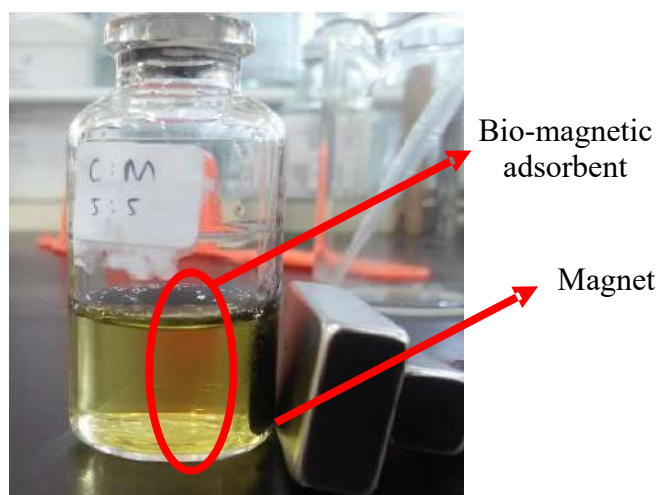
FIGURE 1.. Bio-magnetic adsorbent can be pulled by magnet

Fourier-Transform Infrared Spectroscopy Results

The bonding mechanism were observed from FTIR characterization. FTIR spectra of magnetite, chitosan and bio-magnetic adsorbent were shown in Figure 2. The peak at wave number 3400 cm^{-1} on the curves b and c showed the presence of –OH groups. Whereas, the peak at wave number 572 cm^{-1} in curves a and c showed the presence of Fe-O groups. The new peak at wave number 1735 cm^{-1} on the curve c showed the presence of C = O esters which were analyzed from chlorogenic acid and caffeine [13]. The absorbance characteristics of chitosan at wave number 1589 cm^{-1} showed bending vibration of N-H group. Wave number 1390 cm^{-1} showed stretching of the -C-O group from primary alcohol in the chitosan structure [9]. The results of FTIR characterization indicated that bio-magnetic adsorbent from chitosan and coffee grounds was successfully synthesized. The surface of magnetite or iron oxide which is negatively charged has a high affinity for chitosan which is positively charged so that chitosan can coat the surface of iron oxide using electrostatic bonds.
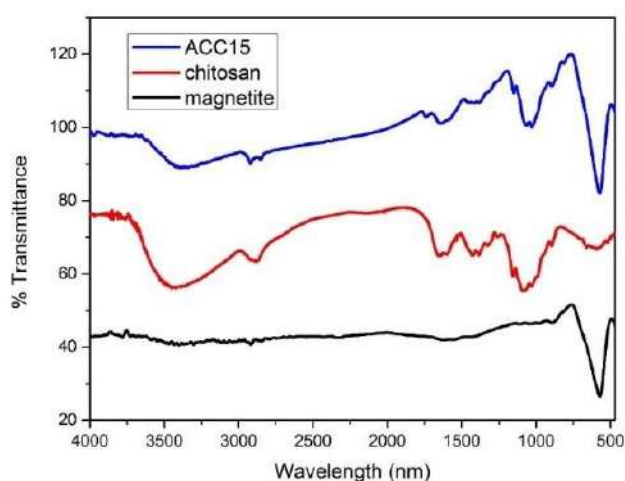
Figure 2. FTIR Results

Dye Removal

Bio-magnetic adsorbent was tested on the performance of dye adsorption. The synthetic dyes was remazol yellow. The coloring agent used for the adsorption performance test is dissolved in water. The results of dyes adsorption can be observed by UV-visible spectrophotometry in Figure 3. The dye solution showed maximum absorbance at a wavelength

of 417 nm. Addition of bio-magnetic adsorbent to the dye solution sample caused the solution slightly clear. The absorbance measured at the same wavelength showed the decrease in absorbance. The results indicate that the dye has been adsorbed by bio-magnetic adsorbent. The maximum decreasing absorbance occurred in the sample ACC35 by 64%.
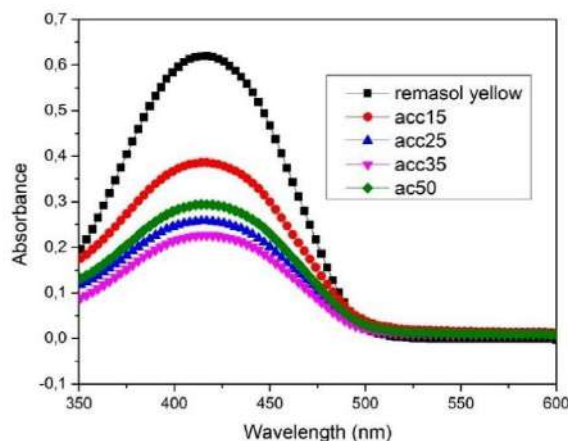
Figure 3. UV-visible Spectrophotometry Results
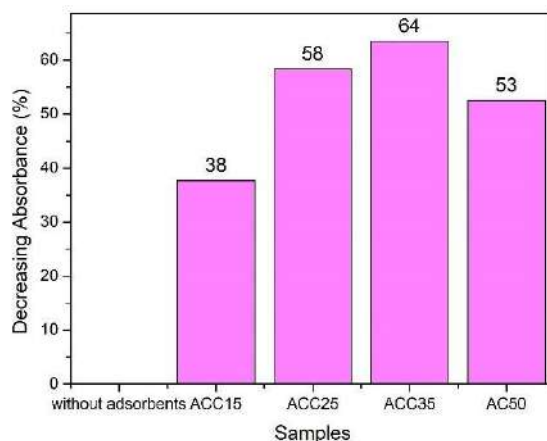
Figure 4. Decreasing Absorbance in %

CONCLUSION

The fabrication of bio-magnetic adsorbent has been successfully carried out using an easy and simple synthesis method. Bio-magnetic adsorbent have ability to adsorb dye. In this study, the results demonstrate that chitosan and spent coffee grounds can be transformed into a magnetic form. Bio-magnetic adsorbents have potential for dyes removal in batik industrial waste. It can be proven from the change in color of the dye solution and decreasing absorbance in the analysis of UV-visible spectrophotometry. The maximum decreasing absorbance occurs in the ACC35 sample by 64%. To maximize the dyes removal, for future project, decreasing size to nanoparticle can be considered.

ACKNOWLEDGEMENTS

REFERENCES

[1] Pujilestari, Titiek. (2017). *Optimasi pencelupan kain batik katun dengan pewarna alam tingi dan indigofera. Dinamika Kerajinan dan Batik*, Vol.34, No.1, 53-62.

[2] Safarik, I. Safarikova, M., Forsythe, S.J. (1995). A review : The application of magnetic separations in applied microbiology. Journal of Applied Bacteriology, 78, 575-585. doi: 10.1111/j.1365-2672.1995.tb03102.x.

[3] Safarik, I. *et al*. (2014). Mechanochemical synthesis of magnetically responsive materials from non-magnetic precursors. Material Letters, 126, 202-206. doi: 10.1016/j.matlet.2014.04.045.

[4] Safarik, I. Safarikova, M. (2009). Magnetic nano- and microparticles in biotechnology. Chemical Papers, 63 (5), 497-505. doi: 10.2478/s11696-009-0054-2.

[5] Denkbas, E.B. Kilicay, E. Birlikseven, C. Ozturk, E. (2002). Magnetic chitosan microspheres: preparation and characterization. Reactive and Functional Polymers, 50, 225-232. doi: 10.1016/S1381-5148(01)00115-8.

[6] Tanyolac, D. Ozdural, A.R. (2000). A new low cost magnetic material : magnetic polyvinylbutyral microbeads. Reactive and Functional Polymers, 43, 279-286. doi: 10.1016/S1381-5148(99)00054-1.

[7] Tanyolac, D. Ozdural, A.R. (2000). Preparation of low-cost magnetic nitrocellulose microbeads. Reactive and Functional Polymers, 45, 235-242. doi: 10.1016/S1381-5148(00)00037-7.

[8] Rinaudo, M. (2006). Chitin and chitosan : properties and application. Progress in Polymer Science, 31, 603-632. doi: 10.1016/j.progpolymsci.2006.06.001.

[9] Li, Gui-yin. *et al*. (2008). Preparations and properties of magnetic Fe_3O_4-chitosan nanoparticles. Journal of Alloys and Compounds, 466, 451-456. doi: 10.1016/j.jallcom.2007.11.100.

[10] Liu, Xiaowang. *et al*. (2009). Magnetic chitosan nanocomposites : a useful recyclable tool for heavy metal ion removal. Langmuir, 25, 3-8. doi: 10.1021/la802754t.

[11] Safarik, I. Horska, K. Svobodova, B. Safarikova, M. (2012). Magnetically modified spent coffee grounds for dyes removal. European Food Research and Technology, 234, 345-350. doi: 10.1007/s00217-011-1641-3.

[12] Ainiyah, Sidratu. (2017). Imobilisasi selulase dan xylanase pada magnetic kitosan untuk produksi gula reduksi. Repository ITS.

[13] Ribeiro JS, Salva TJ, Ferreira MMC. (2010). Chemometric studies for quality control of processed Brazilian coffees using drifts. J Food Qual 33: 212– 227.

[14] Al-Kdasi, A. Idris, A. Saed, K. Guan, C.T. (2005). Treatment of textile wastewater by advanced oxidation process – a review. Global Nest: the Int. J. Vol 6, No 3, pp 222-230.

[15] Galanakis, Charis M. (2017). Handbook of coffee processing by-products. London: Academic Press, Elsevier.

[16] Kumar, Majeti R.V. (2000). A review of chitin and chitosan applications. Reactive and Functional Polymers, 46, 1-27. doi: 10.1016/S1381-5148(00)00038-9.

[17] Purwanti, Ani. (2014). Evaluasi Proses Pengolahan Limbah Kulit Udang untuk Meningkatkan Mutu Kitosan yang Dihasilkan. Jurnal Teknologi, Vol.7, No.1, 83-90.

[18] Reddy, D.H.K. Lee, S.M. Application of magnetic chitosan composites for the removal of toxic metal and dyes from aqueous solution. Advances in Colloid and Interface Science, 201-202, 68-93. doi: 10.1016/j.cis.2013.10.002.

[19] Riyanto, dkk. (1997). Katalog Batik Indonesia. Yogyakarta: Departemen Perindustrian dan Perdagangan RI Badan Penelitian dan Pengembangan Industri dan Perdagangan.

[20] Shen, Chensi. *et al*. (2011). Fast and highly efficient removal of dyes under alkaline conditions using magnetic chitosan-Fe(III) hydrogel. Water Research, 45, 5200-5210. doi: 10.1016/j.watres.2011.07.018.

[21] Suprihatin, Hasti. (2014). Kandungan organik limbah cair industri batik jenis Sidoarjo dan alternatif pengolahannya. Pusat Penelitian Lingkungan Hidup Universitas Riau.

[22] Susanto, Sewan. (1973). Seni Kerajinan Batik Indonesia. Jakarta: Balai Penelitian Batik dan Kerajinan, Lembaga Penelitian dan Pendidikan Industri, Departemen Perindustrian R. I.

[23] Vakili, M. et al. (2014). Application of chitosan and its derivatives as adsorbents for dye removal from water and wastewater: A review. Carbohydrate Polymers, 113, 115-130.

[24] Agustina, S., Swantara, Suartha. (2015). Isolasi Kitin, Karakterisasi, dan Sintesis Kitosan dari Kulit Udang. Jurnal Kimia, 9(2), 271-278.

[25] Kadam, A., Lee, D.S. (2015). Glutaraldehyde cross-linked magnetic chitosan nanocomposites: Reduction precipitation synthesis, characterization, and application for removal of hazardous textile dyes. Bioresources Technology. doi: 10.1016/j.biortech.2015.06.148.

[26] Pospiskova, K., Safarik. (2013). Low-cost, easy-to-prepare magnetic chitosan microparticles for enzymes immobilization. Carbohydrate Polymers, 96, 545-548.

[27] Wulandari, Ika O., Sabarudin, A., Santjojo. (2016). Pembuatan Nanopartikel Kitosan-Fe3O4 secara Kopresipitasi Ex-Situ menggunakan TPP/Sulfat sebagai Crosslinker dan Karakterisasinya menggunakan XRD. Natural B, Vol. 3, No.3.

[28] El-Reash, A.Y.G., Otto, M., Kenawy, I.M., Ouf, A.M. (2011). Adsorption of Cr(VI) and As(V) ions by modified magnetic chitosan chelating resin. International Journal of Biological Macromolecules, 49, 513-522.

[29] El-Reash, A.Y.G. (2016). Magnetic Chitosan Modified with Cysteine-Glutaraldehyde as Adsorbents for Removal of Heavy Metal from Water. Environmental Chemical Engineering, Volume 4, Issue 4, Part A, 3835-3847.

[30] Hosseini, F., Sadighian, S. Monfared, H., Mahmoodi N. (2016). Dye removal and kinetics of adsorption by magnetic chitosan nanoparticles. Desalination and Water Treatment. Vol. 57, Issues 51, 24378-24386.

Efficacy of Carbonized and Caustic Pre-Treated Brewers' Spent Grains (BSG) as Sorbent for Diesel Oil and Coconut Oil

Roxanne Kathlyn O. Alivio, Nika A. Bungabong, Syra Jean R. Cos and May V. Tampus[1, a)]

[1]*Department of Chemical Engineering, University of San Carlos, Nasipit, Talamban 6000 Cebu City, Philippines*

[a)]Corresponding author: mvtampus@usc.edu.ph

Abstract. Brewing craft beer is becoming a current worldwide trend. The Philippines is one of the countries that produce craft beer. A major by-product in craft beer brewing is brewers' spent grains (BSG). BSG is a lignocellulosic agro-industrial residue that possesses a porous structure and has low density. These attributes are considered favorable characteristics of a good oil sorbent. Meanwhile, oil spills in the sea and in water bodies is a pressing environmental concern. The use of a natural sorbent in oil spills as an alternative to synthetic ones is being explored by many researchers. This study investigated the effect of carbonization and caustic pretreatments of BSG on its ability to sorb diesel oil (DO) and coconut oil (CO). Sorption experiments were carried out in static oil and in oil/water sorbates. A substitute ocean water (SOW) was used in oil/water sorbates. Oil sorption capacity (OSC), oil retention, and water uptake were evaluated. In sorption with oil sorbate, carbonized BSG has an OSC of 3.39 g diesel oil (DO)/g sorbent and 2.54 g coconut oil (CO)/g sorbent in both oil sorbates, improving OSC of untreated BSG by 74.0% and 25.5%, respectively. Meanwhile, a much greater improvement resulted from caustic pretreatment with OSCs of 10.28 CO/g sorbent and 5.76 g DO/g sorbent. For the case of oil/water sorbates, the OSC values of both carbonized BSG (BSG-CR) and caustic pre-treated BSG (BSG-CU) were slightly reduced since water would compete in going in to the interstitial spaces of the sorbents. The hydrophilic properties of BSG, being a lignocellulosic material is evident in its higher water uptake in substitute ocean water (SOW) sorbate of 3.43 g SOW/g sorbent compared to its OSC. This high water uptake was reduced in BSG-CR by 98 % in both DO-SOW and CO-SOW sorbates. For BSG-CU, a decrease of water uptake was also observed (88-90 % reduction) in both DO-SOW and CO-SOW sorbates. After a draining time of 2 hours, 76-91 % of oil sorbed remained in BSG-CR while a slightly lesser value of 72-80 % remained in BSG-CU. In this work, carbonization and caustic pre-treatment were found to have significant influence on the efficacy of BSG as sorbent for DO and CO in terms oil sorption capacity, oil retention capacity, and water uptake.

INTRODUCTION

Oil spill pollution is one of the most serious threats that our marine ecosystem is facing. In fact, there is now a higher risk of oil spillage in marine areas worldwide during oil exploration, transportation, and storage due to high oil demand [1]. From 1974 to 2014, three hundred large scale oil spills have already been recorded worldwide based on >10,000 barrels lost from shipping vessels [2]. From 1980 to 2013, twenty maritime disasters have also occurred in the Philippine waters which may have caused oil to be spilled [3].

Diesel oil and coconut oil are considered to be significant contributors of environmental contaminants caused by oil spills. In the Philippines, diesel oil comprises 41 % of the total demand for crude oil which comes largely from the transportation sector [4]. Oil spilled into the sea results in the formation of water-soluble acids. They are highly toxic to marine organisms. [5,6,7] On another note, coconut oil is a major export product of the Philippines. Its export was forecasted to increase up to 8.8 x 10⁵ tons in market year 17/18 [8]. The transportation of large quantities of the oil could increase the risk of spills during loading, unloading, and shipping accidents. One undesirable effect is oxygen depletion caused by the slightly odorous oil slick across the water's surface[9]. Macro-quantities of the oil in water bodies have been found to be harmful to birds which can get oiled and some aquatic organisms which may die from asphyxiation[9,10, 11, 12].

The need to find cheaper means of treating oil spills led to the use of sorbents. They are predominantly attractive due to their ability to turn oil contaminants into semi solid or solid phase. They are used to recover liquids either by adsorption, absorption or a combination of both [13,14]. An ideal oil spill sorbent must possess the following properties: hydrophobicity and oleophilicity, low water uptake, high oil sorption capacity, good oil retention capacity over time, biodegradability, reusability, and ease of oil recovery from the sorbents [15–17].

A wide variety of sorbent materials were the subject of research [18–20]. For years, synthetic polymers like polypropylene and polyurethane have proven to be effective sorbent materials for spilled oil worldwide. But, they both non-biodegradable and non-renewable. Ultimately they become a source of environmental problem themselves [2]. Meanwhile, inorganic mineral products like diatomite, perlite, and vermiculite are abundant in nature but are found to have low oil sorption capacity and buoyancy [21,22]. Natural sorbents are now on trend since they are environmentally friendly, have densities closer to that of synthetic polymers and relatively cheap [23]. Sources of these sorbents are agro-industrial or agricultural by-products, residues, and wastes – sugarcane bagasse [24–27], rice husk [28], wheat straw [26], milkweed [17], vegetable fibers [5,23], coco peat powder [29], and peat moss [19,30]

Sorption experiments can be performed in either static or dynamic conditions. Raw and coated brown cardboards were used as sorbent in both oil and oil/water sorbates [31]. Another study performed sorption experiments in a static condition using both oil and oil/water sorbates [28, 32]. Diesel oil and corn oil were used.

Brewers' spent grains (BSG) is an underexploited agro-industrial residue of the brewing industry. It represents 85% of the total generated by-products [33]. The increasing interest of beer consumers worldwide to craft their own beer drove the development of microbreweries resulting to an increased generation of BSG which can be potentially used as an oil sorbent. BSG is composed mostly of cellulose, hemicellulose, lignin, and proteins. The amounts of cellulose and hemicellulose vary and are in the range of 16.8-25.4 %, and 15.18-28.40 %, respectively. [34–37] They are hydrophilic and are strongly polar [38]. The lignin content in BSG, on the other hand, ranges from 11.9-27.8 %, which contains hydrophobic functional groups [39]. High lignin leads to high hydrophobicity which contributes to a high oil sorption capacity of sorbents. Lignocellulosic materials are proven to sorb oil but they are generally hydrophilic [25,40]. Sorbed water occupies their interstitial spaces and impedes oil sorption. Thus, they need to be pre-treated in order to improve their hydrophobic property and surface characteristics.

Carbonization is involves heating the sample in the absence of oxygen. Its aim is to enrich the carbon content of the material and develop a pore structure in the carbon matrix [41]. It also increases the pore volume and surface area of the material. Analysis of the sorption properties and scanning electron microscope (SEM) micrographs of carbonized pith bagasse showed that carbonization contributes largely on the pore development of the material and decreases its water uptake. This enhances its potential use as sorbent material in oil spill clean-up [27].

Caustic treatment can be done in order to improve the hydrophobicity of BSG. It removes some parts of the hemicellulose and lignin which makes the BSG fibers cleaner and hydrophobic [42]. The application of fast caustic treatment produced a BSG with an increased contact angle of 107° [35]. Another work showed that Na^+ was able to widen the pores in between the lattice planes and penetrate into them [43].

In this work, carbonized BSG and caustic pre-treated BSG were used as sorbents in oil and oil/water sorbates. Dried BSG was used as control. Their efficacy as oil sorbents was investigated. This can be assessed from the data of the oil sorption capacity, oil retention capacity, and water uptake of the sorbents from the sorption experiments. The contact time, appropriate sorbent loading, and draining time of the sorbents were determined prior to the main sorption experiments. Moreover, the sorbents were characterized by proximate analysis, bulk density, and field emission scanning electron microscopy (FESEM) prior to use in sorption experiments.

MATERIALS AND METHODS

Materials and Chemicals

Wet brewers' spent grains (BSG) freshly withdrawn from the malting step were acquired from a local microbrewery plant in Mandaue City, Cebu. Coconut oil used was Sun Valley Cooking Oil. Diesel oil used was Shell V-power Nitro+ Diesel. Chemical reagents used were (%w/w): magnesium chloride hexahydrate ($MgCl_2 \cdot 6H_2O$, Scharlau, Barcelona, Spain, 99.0%); potassium hydrogen phthalate ($C_8H_5KO_4$, 99.95-100.05%), sodium hydroxide (NaOH, 97.5-100.05%), anhydrous calcium chloride ($CaCl_2$, 93.0 %), strontium chloride hexahydrate ($SrCl_2 \cdot 6H_2O$, 98.5%), potassium bromide (KBr, 98.0%), potassium chloride (KCl, 99.8%) sodium bicarbonate ($NaHCO_3$, 99.7%), boric acid (H_3BO_3, 99.5%), and sodium chloride (NaCl, 99.9%) (Ajax Finechem, NSW, Australia). A technical grade NaOH (98%) (Ajax Finechem, NSW, Australia) was used for the caustic treatment of BSG.

Collection, Storage and Preparation of Brewers' Spent Grains

The collected wet BSG samples were washed with tap water several times until the water turned light brown and then with distilled water once. These samples were temporarily stored at 0 °C. Samples for characterization and sorption experiments were dried at 105 °C to reach a moisture content of <10 %w/w and stored in a desiccator for further characterization and use.

Dried BSG samples were milled (Wiley Mill, Thomas Scientific, USA), sieved (Intertest Benelux, Italy) and size classified (Endecotts Ltd., England). Samples that were retained on the 850, 425 and 250 μm-screens were used for the sorption experiments. Particle size of the samples was determined from the FESEM images of the particle. Their diameter was measured using the ImageJ® software application.

BSG samples have a particles size (μm) of 900-1300, 420-430, and 690-830 for the untreated (BSG-DR), carbonized (BSG-CR), and caustic treated (BSG-CU) samples, respectively.

Carbonization and Caustic Pre-treatment of Brewers' Spent Grains

Carbonization conditions and procedure of BSG were adopted from Mohamed Hussein et al. [13] and Conag et al [44], respectively. Pre-dried and pre-weighed empty 100-mL crucibles were filled with ~20 g (80% of their capacity) with the dried BSG. The heating rate used was 10 ºC/min. Average mass yield of the carbonized sorbents is 42.94%.

Caustic treatment of BSG was done according to the method by Pires et al. [35]. The sample was soaked in standardized 0.7582 ± 0.0040 M aqueous NaOH solution in a ratio of 1:15 (g sample: mL solution) at 70 ºC for 20 min with manual stirring every 5 min. After the treatment, the samples were repeatedly washed with distilled water until the pH is within 7.0-7.4. They were then dried at 105.2 ± 1.09 °C to reach a moisture content of <10%. Average mass yield of the caustic treated sorbents was $18.53 \pm 0.67\%$.

Characterization of the Dried and Pre-treated BSG Sample

Loose and tapped bulk density of the BSG sorbent samples were determined according to ASTM D7481-18 standard test methods for determining loose and tapped bulk densities of powders [45]. Proximate analysis for the determination of moisture, volatile matter (VM), ash (Ash) and fixed carbon (FC) content of the BSG was done according to ASTM D1762 – 84 standard method for chemical analysis of wood charcoal [46].

Surface morphology of the sorbents was examined using a FESEM (ZEISS Sigma 500 VP Field Emission Scanning Electron Microscope, Jena, Germany). Prior to the analysis, the samples were sputter-coated twice with gold (Quorum Q150R S Rotary Pumped Coater) in an argon atmosphere using a current of 20 mA for 60 s. The coated samples were analyzed at high vacuum (4.89×10^{-7} mbar) using three magnifications – 25X, 64-200X and 8000X.

Preparation of Substitute Ocean Water

The preparation of substitute ocean water (SOW) for the determination of the oil sorption capacity, oil retention capacity and water uptake of BSG was done according to the method described in ASTM D1141-98 [47]. Prior to use, the SOW was added with standardized 0.1 N NaOH solution until it reached a pH of 8.2. It was freshly prepared every run.

Characterization of Coconut Oil and Diesel Oil

The density of the diesel oil (DO) and coconut oil (CO) was measured using a liquid densitometer model Kern EW150-3M (Kern Instruments, Germany). Meanwhile viscosity was determined using a 10-inch long glass falling ball viscometer (Gilmont Instruments, USA). A 1-inch diameter stainless steel (type 316) ball was used. Temperature of the samples was maintained at 26 ºC. The viscosity of the oil was calculated using

$$\mu_{ss} = K \bullet (\rho_t - \rho) \bullet t \tag{1}$$

where μ_{SS} is the viscosity of the oil in centipoises (cP), ρ_t is the density of the stainless-steel ball (8.02 g/mL), ρ is the density of the oil at the specified temperature (g/mL) t is the time of descent in min and K is the viscosity constant which is 3.3 cP·mL/g-min. Determinations were done in triplicates.

Oil Sorption Experiments

The oil sorption experiments were done according to the method described in ASTM F726-12 standard test method for sorbent performance of adsorbents and ASTM F716-09 standard test methods for sorbent performance of absorbents [48,49,50]. The method used was that for Type II sorbents. The sorbents used were BSG-DR, BSG-CR and BSG-CU. The sorbates used were DO, CO, SOW, DO-SOW mixture and CO-SOW mixture. Oil sorption experiments under static conditions were conducted at 26 ºC. Experiments were done in triplicates.

A test cell (20 x 20 x 10 cm^3) made of ordinary glass was used. Mesh baskets (30 x 30 cm^2) made of organza cloth (180 μm mesh size) were sewn on a stainless-steel wire. The test cell was filled with 2 L of sorbate for the oil system and the SOW system, respectively while 175 g oil and 1.75 L SOW were used for the oil-water system. A measured amount the sorbent was placed on the mesh basket and immersed into the test cell for sorption. After sorption, the mesh basket with the sorbent was removed from the test cell and allowed to drain for 30 ± 3 s. The amount of oil sorbed, OS (g oil/ g sorbent) was then determined using (2). Experiments were done in triplicates.

$$OS = \frac{S_1 - MB_0 + BSG_0 - W}{BSG_0} = \frac{O}{BSG_0} \tag{2}$$

where S_1 is the mass of the mesh basket containing the sorbent after sorption, MB_0 is the mass of the mesh basket (g), BSG_0 is the mass of the sorbent (g), W is the amount of water sorbed (g) and O is the amount of oil sorbed (g). It must be noted that W is equal to zero in CO and DO sorbates. W can be found from the water uptake experiment.

Determination of Equilibrium Sorption Time

Equilibrium sorption time experiments were adopted from the work of Wang et al. [28]. Sorption times used were 0.15, 0.50, 0.45, 1, 3, 5, 10, 20, 40, 60, 90 and 120 min. Sorbent load (4 g) and sorbate volume (2 L) were kept constant. A plot of the OS versus time was made in order to determine the equilibrium sorption time t_e. This is the time at which the sorbent can no longer sorb any more of the sorbate. The t_e was taken to be the point at which the line started to plateau. The t_e was used as basis for the determination of OSC, WUC and ORC.

Determination of Oil Sorption Capacity

The experiment to determine the oil sorption capacity (OSC) was done in similar manner as that of the t_e except that the amount of sorbent was varied while the time was fixed at 60 min. The amounts of sorbent used were 4.04 ± 0.05, 7.01 ± 0.06 and 9.98 ± 0.17 g. A plot of the OS versus BSG_0 was established in order to find OSC. The OSC is the maximum amount of oil that the sorbent is able to sorb expressed in g oil sorbed/ g sorbent. It is the point at which there was no observed increase in the plot of OS versus BSG_0.

Determination of Water Uptake (WU)

Water uptake may occur in sorption involving oil-water mixtures (DO-SOW and CO-SOW). Water uptake experiments were done by air-drying (Philips Essential Care BHD006/00) the mesh basket containing the sorbent after sorption. The change in weight was measured every 10 min until a weight difference of 0.01 g between S_1 and S_2 was reached. The WU (g water/g sorbent) was calculated using

$$WU = \frac{S_1 - S_2}{BSG_0} = \frac{W}{BSG_0} \tag{3}$$

where S_1 is the weight of the mesh basket containing the sorbent after sorption (g), BSG_0 is the amount of sorbent (g), O is the amount of oil sorbed, S_2 is the sum of the sorbent before sorption and the amount of oil sorbed and W is the amount of water sorbed.

Determination of Oil Retention Capacity (ORC)

The determination of ORC was performed according to the method described by Chai et al. [32] wherein after sorption, the mesh basket containing the sorbent was hung on an empty test cell and allowed to drain at various times (1, 3, 5, 10, 20, 40, 60, 90, and 120 min) over a 20.32-cm diameter aluminum container. W and O were calculated. The data gathered was that of the mass of oil retained on the sorbent for each draining time. From the plot of oil retained (g oil/g sorbent) versus time (min), the ORC of the sorbent was determined.
The ORC is the point where there was no observed change in the amount of oil retained (g) with time.

Statistical Analysis

Statistical analysis was done using MS Excel 2016 data analysis tool. The two-way ANOVA was carried out to determine whether statistically significant differences are present in the responses resulting from different times and pretreatments applied.

RESULTS AND DISCUSSION

Oil sorption is affected by several factors including: (1) the properties of the sorbent used such as the density, surface morphology, porosity, and the surface area; (2) sorbent dosage; (3) contact time; (4) temperature and; (5) certain functional groups found in the sorbent [16,51]. In this study, the efficacy of carbonized and caustic pre-treated BSG was investigated.

Characteristics of Carbonized and Caustic Pre-treated BSG Sorbents

Caustic pre-treatment of the BSG significantly altered the bulk density of the BSG. The highest loose bulk density (g/cm^3) was obtained from BSG-DR (0.34 ± 0.00), followed by BSG-CR (0.22 ± 0.01), and BSG-CU (0.09 ± 0.01). The same trend was observed for the tapped bulk density (g/cm^3) of BSG-DR (0.41 ± 0.04), BSG-CR (0.27 ± 0.01), and BSG-CU (0.11 ± 0.01).

Proximate analysis of the samples was evaluated on a % dry weight basis. The BSG-DR has a moisture content of 6.88 ± 0.03 % which is close to the reported literature value (7.0 %) [51]. Meanwhile, BSG-CR has a higher FC (57.77 ± 0.52 %) and a lower VM (31.97 ± 0.60 %) than the BSG-DR (FC 13.16 ± 0.34 % and VM 76.87 ± 0.35 %). The FC and VM values of BSG-DR are 13.16 ± 0.34 % and 76.87 ± 0.35 %, respectively. Literature report similar results (FC 18.9 % and VM 77.1 %) [52]. The high VM content and low FC of BSG-DR would explain the low yield obtained after carbonization where ~58 % of its VM was released. The BSG-CU has the lowest FC (10.45 ± 0.20 %) and highest VM (79.42 ± 0.09 %). All BSG samples has low ash content (BSG-DR 3.10 ± 0.02, BSG-CR 7.12 ± 0.12 %, 4.34 ± 0.11 % for BSG-DR, BSG-CR, and BSG-CU, respectively). In this study, ash content of BSG-DR is still within the range found in literature (BSG-DR 3.15 – 4.0%) [51,52].

FESEM analysis showed that BSG-CR samples have rougher and more pronounced porous structure than BSG-DR. The same observations were made by Vlaev et al. [40] on carbonized rice husks. Meanwhile, BSG-CU samples have a lamellar structure.

Characteristics of Coconut Oil and Diesel Oil

The determination of the properties of oils used in the experiment was also essential to determine the appropriate draining time for the determination of equilibrium time sorption experiment. Coconut oil and diesel oil used in this work are classified as medium oil and light oil, respectively [49]. The density (g/mL) of CO and DO are 0.9285 ± 0.0017 and 0.8315 ± 0.0013, respectively. The viscosity (cP) of CO and DO are 42.9108 ± 0.1767 and 3.9126 ± 0.1107, respectively. These results are in agreement with the studies by Abdullah et al. [53] and Ali et al. [54].

Effect of Pre-treatment on the Efficacy of BSG as Oil Sorbent

Effect of Pre-treatment on Oil Sorption Capacity

Oil sorption experiments were done by submerging the samples in diesel oil (DO), diesel oil – substitute ocean water (DO-SOW), coconut oil (CO) and coconut oil – substitute ocean water (CO-SOW) systems. The oil sorbed (OS (g oil/ g sorbent) by BSG-DR, BSG-CR, and BSG-CU at varying sorbent loading in CO and CO-SOW is shown.
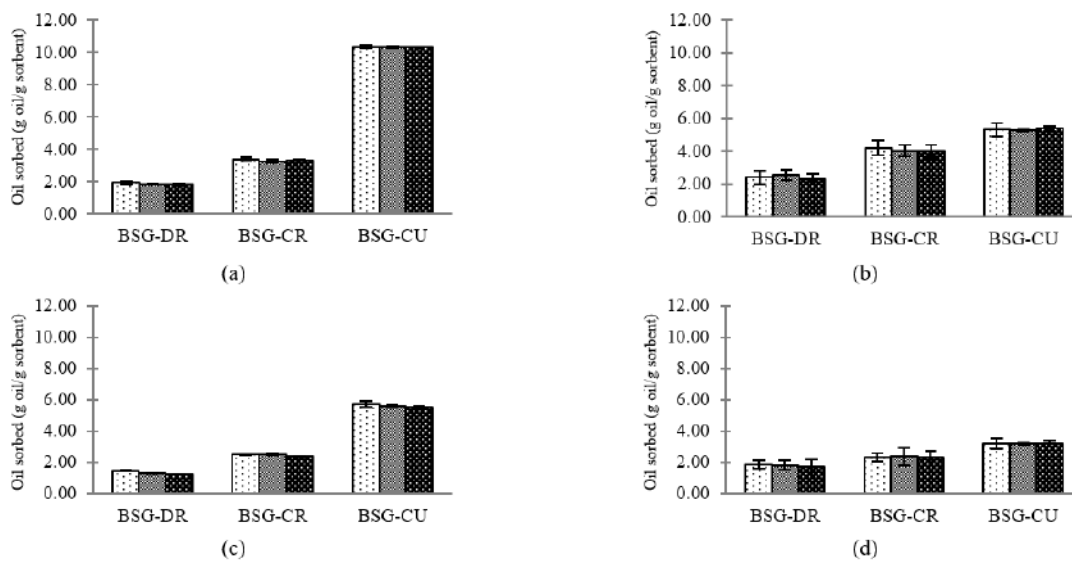
FIGURE 1. Oil sorbed (OS) for (a) CO, (b) CO – SOW, (c) DO and (d) DO – SOW of different BSG sorbents at a contact time of 60 min and at 26 °C and sorbent loading of ▨ 4 grams, ▨ 7 grams, and ▧ 10 grams

It can be observed that in all sorbate systems, the OS values do not change as mass is increased (Figure 1). The OSC of the sorbents was determined from these data. Shown in Figure 2 are the OSC of the BSG sorbents.
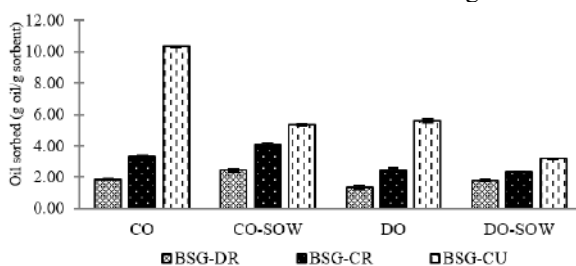
FIGURE 2. Oil sorption capacity (OSC) of BSG in different sorbates at 20 min contact time, 26°C and 4 g sorbent load

The OSC values of BSG-DR and BSG-CR in CO and CO-SOW sorbates are comparable. In these sorbates, BSG-CU has the highest OSC. The OSC of BSG-CU for CO is greater than that for CO-SOW. The same trends were observed for the DO and DO-SOW sorbates. But OSC values of BSG sorbents in DO and SO-SOW are lower than those for CO and CO-SOW. Based on the data of OSC, sorbent bulk density and density of CO and DO, BSG belong to low-capacity oil spill sorbent [55].

The OSC of a solid sorbent depends on its surface area and pores [56]. BSG is fibrous and porous making it an ideal sorption material. For such material, the controlling mechanisms are usually adsorption and capillary action. These mechanisms are influenced by fiber properties, sorbent pore structure, oil properties, and the interaction between the sorbent and oil which can in turn affect the OSC [57]. Carbonization and caustic treatment of BSG affected these factors. But the latter has a more advantageous effect on OSC.

In this study, BSG-CU exhibited a lamellar structure. From the FESEM analysis of the sorbent, it is observed that the surface of BSG-CU appears to be more ridged as compared to the smooth surface of the BSG-DR. The presence of Na^+ during caustic treatment may have widened the pores between the lattice planes and created an ordered planar structure [58]. This structure provides more area for attachment of the sorbate [59] which may have caused the increase in OSC [51,60].

Oil properties which include density and viscosity may also affect oil sorption. Less dense and less viscous oil may easily sorb through the sample [61]. From the results, CO (medium oil) has higher density and viscosity than DO (light oil). In this work, BSG sorbents have higher OSC for CO than for DO which does not confer with literature.

Interaction between the sorbent and the oil is affected by the pretreatment of the sorbent. Reduction of particle size increases the surface area of the sorbent.   Carbonization increases the pore volume and surface area of the sorbent by enriching the carbon content and developing initial pore structure in the carbon [41,62,63]. Caustic treatment enhances the hydrophobic property of BSG made evident by the increase in contact angle from 69.10 ˚ to 107 ˚ [35].

Effect of Pre-treatment on Oil Retention Capacity (ORC)

Sorbents for oil spill must have good retaining ability so that the oil sorbed is still retained during its transport away from the affected site. Oil retention of the different BSG sorbent in CO and DO is shown in Figure 3. Similar oil retention trends were found for sorbates in CO-SOW and in DO-SOW.
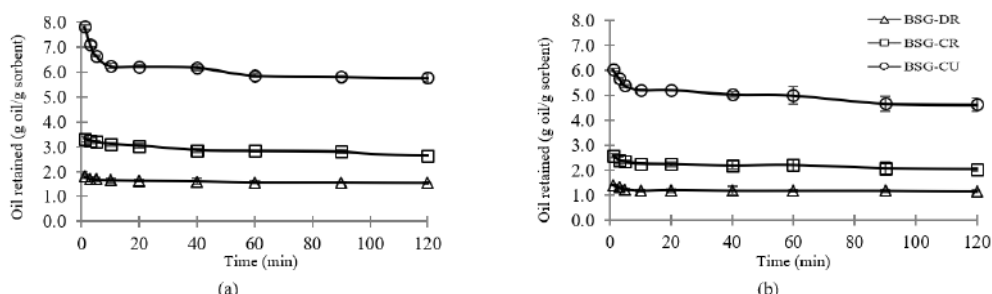
FIGURE 3. Oil retention (OR) of different BSG sorbents in oil sorbates (a) CO and (b) DO at 26 °C and 4 g sorbent load

TABLE 1. Oil Retention Capacity (ORC) and % Retention of BSG Sorbents at 120 min Draining Time of, 26 °C and 4 g Sorbent Load

Oil Sorbates	BSG-DR			BSG-CR			BSG-CU		
	OR_i (g oil/g sorbent)*	ORC (g oil/g sorbent)	% Retention	OR_i (g oil/g sorbent)	ORC (g oil/g sorbent)	% Retention	OR_i (g oil/g sorbent)	ORC (g oil/g sorbent)	% Retention
CO	1.80 ± 0.08	1.55 ± 0.06	86.02	3.31 ± 0.10	2.63 ± 0.02	79.48	7.81 ± 0.09	5.76 ± 0.15	73.81
DO	1.40 ± 0.02	1.15 ± 0.06	81.80	2.57 ± 0.09	2.03 ± 0.08	79.04	6.02 ± 0.06	4.62 ± 0.26	76.80
CO-SOW	2.34 ± 0.27	2.03 ± 0.32	86.98	3.88 ± 0.32	3.13 ± 0.07	80.59	7.30 ± 0.23	5.69 ± 0.18	77.91
DO-SOW	2.08 ± 0.42	1.73 ± 0.08	83.23	3.21 ± 0.31	1.87 ± 0.24	80.84	5.67 ± 0.36	4.34 ± 0.47	76.49

*Oil retained at draining time of 1 minute

The ORC of BSG sorbents and their % retention are presented in Table 1. Results suggest that a sorbent with the fastest initial sorption rate had the least oil retaining ability. This implies that a sorbent with higher porosity, BSG-CR and BSG-CU, does not retain oil better. This trend is similar to that of the study done by Wei et al. [64]. The nonwoven polypropylene sorbent with the higher porosity had higher initial oil sorbed, but poor OR.

BSG-CU has the highest ORC but with the lowest % retention. BSG-DR has the highest % retention among the BSG sorbents. From the study of Chai et al. [32], the % retention of DO in the raw pomelo peel sorbent was 77%. In this study, the amount of DO retained from BSG-DR is higher (87%) than the reported literature value.

Effect of Pre-treatment on Water Uptake

Not all weight gain by the BSG in CO-SOW and DO-SOW refers to oil sorbed, since water is also incorporated into its porous structure and fibers. The water uptake (WU) of BSG sorbents immersed in SOW and CO-SOW as a function of sorption time is shown in Figure 4. WU of BSG sorbents in CO-SOW and DO-SOW exhibit similar trends.
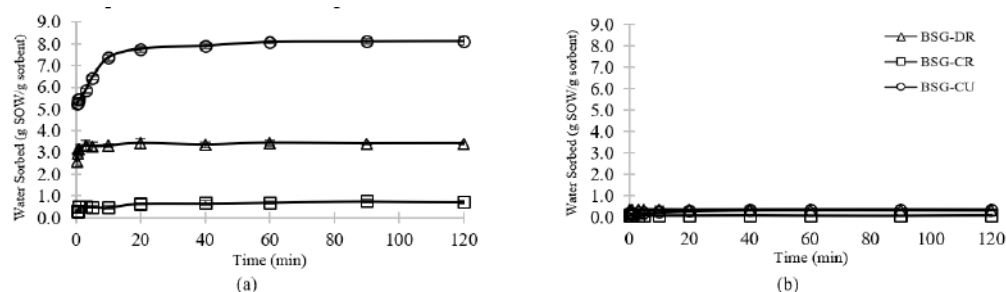
FIGURE 4. Water uptake (WU) of BSG sorbents in (a) SOW and (b) CO-SOW at 26 °C and 4 g sorbent load

Results reveal that caustic pre-treatment enhanced the ability of BSG to sorb SOW. BSG-DR, BSG-CR, and BSG-CU have WU (g SOW/g sorbent) of 3.43, 0.70, and 8.08, respectively. In CO-SOW, the WU of BSG-DR, BSG-CR, and BSG-CU are 0.32, 0.07, and 0.34, respectively. In DO-SOW, the WU of BSG-DR, BSG-CR, and BSG-CU are 0.36, 0.10, and 0.41, respectively. The water sorbed in BSG-CR for all sorbate was considerably negligible. It can be supposed that there was much lower contact in BSG-CR with the sorbate.

Proceedings of CCSE ASEAN 2019

CONCLUSION AND RECOMMENDATIONS

Brewers' spent grains (BSG) possess some of the necessary characteristics that a good sorbent must have such as low density and a porous structure. But its efficacy as an oil sorbent can be enhanced with carbonization and caustic pre-treatment. Under the conditions employed in this study, BSG-CU as sorbent for CO has the highest OSC while a lower OSC was obtained for DO. Caustic pre-treatment enhanced OSC for CO by 454 % and by 319 % DO. Carbonization enhanced the efficacy of the BSG to sorb oil to a lower degree. OSC of BSG-CR for CO and DO was improved by 79 % and 86 %, respectively.

For the case of CO-SOW and DO-SOW, the OSC values of BSG-CU were reduced due to water uptake. The hydrophilic properties of BSG is evident in its high WU of 3.43 g SOW/g sorbent. This WU was reduced in BSG-CR by 80 % in SOW, 98% in CO-SOW, and in 97% DO-SOW. On the other hand, it was increased in BSG-CU to 136 % in SOW, and decreased by 91 % in CO-SOW, and by 97 % in DO-SOW. After a draining time of two hours, 76-81 % of oil was retained in BSG-CR while a slightly lesser value of 74-78 % remained in BSG-CU. Although BSG-DR has the highest % oil retention (82-87%) among the BSG sorbents but it has the lowest ORC (1-2 g oil/g sorbent).

Future works may consider quantification of its hydrophobic properties through contact angle and surface area measurement to further support findings. Investigation of the surface functional groups by Fourier Transform Infrared Spectroscopy (FTIR) can also be done to further learn about surface chemistry. Surface tension analysis of the sorbates can also be done. It is also useful to study the reusability of BSG as sorbent. In cases where recovery is difficult, used BSG sorbent can always be utilized for biomass energy recovery. The calorific value of BSG can be quantified after sorption as this would determine its potential as fuel, thus leaving no secondary waste to the environment.

ACKNOWLEDGMENTS

REFERENCES

1. Department of Energy, Oil supply/demand report 2017, https://www.doe.gov.ph/downstream-oil.
2. R. Pagnucco and M. L. Phillips, J. Environ. Manage. **225**, 10–16 (2018).
3. ABS-CBN News. Maritime disasters in the Philippines. ABS-CBN News 2015. http://news.abs-cbn.com/nation/regions/07/02/15/list-maritime-disasters-philippines (accessed August 1, 2018).
4. Department of Energy. Power supply and demand highlights (January-June 2017) **15** (2017).
5. R. A. Alimen and M. C. D. Alimen, Iamure Int. J. Mar. Ecol. **1** (2013).
6. T. R. Annunciado, T. H. D. Sydenstricker and S. C., Amico, Mar. Pollut. Bull. **50**, 1340–46 (2005).
7. M. Hussein, Is. Ib. Sawsan and A. A. Razik, Glob. Nest. J. **4**, 440–48 (2009).
8. USDA Gain Report. Philippine oilseeds and products situation and outlook. USDA Foreign Agric. Serv. 1–**13 (**2017).
9. S. M. Mudge. Spill Sci. Technol. Bull., **2**, 187–91 (1995).
10. M. A. Salgado. "The effects of vegetable oil contamination on mussels," Ph.D. thesis, University of Wales, 1995.
11. R. W. McKelvey, I. Robertson and P. E. Whitehead, Mar. Pollut. Bull. **11**, 169–71 (1980).
12. D. J. Russell and B. A. Carlson, Pacific Sci. **32**, 1–15 (1978).
13. M. Hussein, Is. Ib. Sawsan, and A. A. Razik, Glob. Nest. J. **4**, 440–8, (2009).
14. S. S. Banerjee, Chemosphere **64** (6),1026–31 (2006).
15. R. Frost, O. Carmody, Y. Xi and S. Kokot, Surf. Sci. **9**, 2066–76 (2007).
16. A. Ifelebuegu and A. Johnson, Crit. Rev. Environ. Sci. Technol. **47**, 964–1001 (2017).
17. G. Thilagavathi, C. Karan and D. Das, J. Environ. Manage. **219**, 340–49 (2018).
18. H. Li, L. Liu and F. Yang, Procedia Environ. Sci. **18**, 528–33 (2013).
19. P. Narayanan, A. Ravirajan, A. Umasankaran, D. G. Prakash and P. S. Kumar, J. Ind. Eng. Chem. **63**,1–11 (2018).
20. Y. Zhang, S. Yang, J. Q. Wu, T. Q. Yuan and R. C. Sun, Materials (Basel) **6**, 6733–6747 (2014).
21. H. Liu and B. Y., ACS Sustain. Chem. Eng. **5**, 49–66 (2016).
22. S. T. Nguyen, J. Feng, N. T. Le, A. T. T. Le, N. Hoang, V. B. C. Tan, et al., J. Ind. Eng. Chem. Res. **1**, 18386−18391 (2013).
23. S. C. Amico, Rev. Mater. **15**, 386–95 (2010).
24. A. Bayat, S. F. Aghamiri, A. Moheb and G. R. Vakili-nezhaad, Chem. Eng. Technol. **28**, 1525–1528 (2005).
25. P. C. Brandão, T. C. Souza, C. A. Ferreira, C. E. Hori and L. L. Romanielo, J. Hazard. Mater. **175**, 1106–1112 (2010).
26. N. Dashti, N. Ali, M. Khanafer and S. S. Radwan, Environ. Pollut. **227**, 468–75 (2017).
27. M. Hussein, A. A. Amer and Is. Ib. Sawsan, J. Anal. Appl. Pyrolysis **82**, 205–211 (2008).
28. Z.Wang, J. P. Barford, C. W. Hui and G. McKay, Chem. Eng. J. **281**, 961–969 (2015).
29. L. Yang L., X. Li, Y. Zhang and C. Lu, Ind. Crops Prod. **101**, 1–10 (2017).
30. V. R. Olga, V. I. Darina, A. I. Alexander and A.O. Alexandra, Procedia Chem. **10**, 145–50 (2014).
31. Bayik G. and A. Altin, J. Clean Prod. **196**, 1052–64 (2018).
32. W. Chai, X. Liu, J. Zou, X. Zhang, B. Li and T. Yin, Carbohydr. Polym. **132**, 245–251 (2015).
33. Mussatto S. I. and I. C. Roberto, J. Chem. Technol. Biotechnol. **81**, 268–274 (2006).
34. S.Aliyu and M. Bala,African J. Biotechnol. **10**, 324–331 (2013).
35. E. J. Pires, H. A. Ruiz, J.A. Teixeira and A.A. Vicente, J. Agric. Food Chem. **60**, 5994–5999 (2012).
36. S. I. Mussatto, G. Dragone and I. C. Roberto, J. Cereal Sci. **43**, 1–14 (2006).
37. Mussatto S. I. and I. C.Roberto, Process Biochem. **43**, 540–546 (2008).
38. A. Oushabi, S. Sair, F. Oudrhiri Hassani, Y. Abboud, O. Tanane and A. El Bouari, South African J. Chem. Eng. **23**, 116–123 (2017).

39. H. Djati Utomo, P. Ru Yi, S. Zhonghuan, N. Li Hui and L. Zheng Bang, Environ. Nat. Resour. Res. **6**, 35 (2015).
40. L. Vlaev, P. Petkov, A. Dimitrov and S. Genieva, J. Taiwan Inst. Chem. Eng. **42**, 957–64 (2011).
41. C. Li Lee, P. San H`ng, T. Paridah, K. Ling Chin, P. San Khoo, R. Ahmad Raja, et al, Asian J. Sci. Res. **10**, 24–33 (2016).
42. M. Mamunur Rashid, S. A. Samad, M. A. Gafur, M. Rakibul Qadir and A. M. S. Chowdhury Effect of reinforcement of hydrophobic grade banana bark fiber on the physicomechanical properties of isotactic polypropylene. Int. J. Polym. Sci. **2016**, 1–8 (2016).
43. M. J. John and R. D. Anandjiwala, Polym. Compos. **29**, 187–207 (2008).
44. A. T. Conag, J. E. R. Villahermosa, L. K. Cabatingan and A.W. Go, Energy Sustain. Dev. **42**, 160–169 (2018).
45. ASTM International. ASTM D7481-18 Standard Test Methods for Determining Loose and Tapped Bulk Densities of Powders using a Graduated Cylinder. ASTM 2018.
46. ASTM International. ASTM D1762 – 84 Standard method for chemical analysis of wood charcoal. Am. Soc. Test. Mater., 1990, p. 292–3.
47. ASTM. Standard practice for the preparation of substitute ocean water, **98,** 98–100 (2003).
48. Bazargan A, Tan J, McKay G. Standardization of Oil Sorbent Performance Testing. J. Test. Eval., **43**, 20140227 (2015).
49. ASTM International. Standard Test Method for Sorbent Performance of Adsorbents **94**, 5–6 (2014).
50. ASTM International. ASTM F716 - 09 Standard Test Methods for Sorbent Performance of Absorbents (2009).
51. R. Wahi, L. A. Chuah, T. S. Y. Choong, Z. Ngaini and M. M. Nourouzi, Sep. Purif. Technol. **113**, 51–63 (2013).
52. V. Pérez, J. M. Murillo, R. Bados, L. S. Esteban, R. Ramos and J. M. Sánchez, "Preparation and gasification of brewers' spent grains", presented in the 5th *International Conference on Sustainable Solid Waste*, June 21-24, 2017, Athens, Greece.
53. M. A. Abdullah, A. U. Rahmah and Z. Man, J. Hazard. Mater. **177**, 683–691 (2010).
54. N. Ali, M. El-Harbawi, A. A. Jabal and C.Y. Yin, Environ. Technol. **33**, 481–486 (2012).
55. M. Z. Iqbal and A.A. Abdala, Envi. Sci. Pollut. Res. **20**, 3271–3279 (2013).
56. B. Lee, J. S. Han and Rowell R.M., "Oil Sorption by Lignocellulosic Fibers," in *Kenaf Properties Processing and Products*, Ag & Bio Engineering (Mississippi State University, Mississippi, USA, 1999), p. 423–433.
57. H. Zhu, S. Qiu, W. Jiang, D. Wu and C. Zhang, Envi. Sci. Technol. **45**(10), 4527-4531 (2011).
58. K. L. Iroba, "Effect of pretreatment on the breakdown of lignocellulosic matrix in barley straw as feedstock for biofuel production," Ph. D. Thesis, University of Saskatchewan, 2014.
59. H. Choi and R. Cloud, Environ. Sci. Technol. **26**, 772–776 (1992).
60. C. Wong, T. McGowan, S. G., Bajwa and D.S. Bajwa, BioRes. **11** (3), 6452–6463 (2016).
61. M.A. Abdullah, A. U. Rahmah and Z. Man, J. Hazard. Mater. **177**, 683–91 (2010).
62. J.S. Aznar, KTH Chem. Sci. Eng. **66**, 7 (2011).
63. J. Landon, X. Giao, A, Omosebi, and K. Liu, "Structure and Surface-Modified Carbon Xerogel Electrodes for Capacitive Deionization," in *Submicron Porous Materials*, edited by P. Bettotti, (Springer International Publishing AG, Cham, Switzerland, 2017), pp. 1–24.
64. Q. F. Wei, R. R. Mather, A. F. Fotheringham and R.D. Yang, Mar. Pollut. Bull. **46**, 780–783 (2003).

Variation of Cocopeat Ash Catalyst Composition and Transesterification Time against the Quality of Biodiesel from Fish Oil Canning Waste

Siti Diah Ayu Febriani[1], Saiful Anwar[2] Prisca Amalia Nofitasari[3], Mochamad Irwan Nari[4]

[1,2,3,4] Politeknik Negeri Jember
[1]siti_diah@polije.ac.id

ABSTRACT

Biodiesel is one of the environmentally alternative to diesel fuel for diesel engines. The process of biodiesel synthesis is generally still done conventionally using a homogeneous catalyst that is not environmental friendly. So it is necessary to substitute such a heterogeneous catalyst that can be obtained from sources that are in the environment around us. Biodiesel used in this research is the result of oil based biodiesel waste fish cannery by using heterogeneous catalysts in the form of cocopeat ash. This research was conducted at the laboratory of renewable energy engineering at the end of March 2019. This research was designed using RAL or Completely Randomized Design with 2 factorials with 4 repetitions with first factor is catalyst composition 3%, 5%, 7% w/v and second factor is reaction time length 60 minutes and 120 minutes. The material used in this study is the oil from fish canning waste from Muncar Banyuwangi, coconut fiber (cocopeat), phenolphthalein, methanol (100%), ethanol (97%), H2SO4 (98%), distilled water, NaOH, KOH and acetic acid. While the tools used in this activity are analytic, erlenmeyer, picnometer, titration glass, measuring cup, heater, burette, statif, pipette, spatula, magnetic stirrer, thermometer, stationery, calcination tool, fine filter paper, separating funnel, oven, cup and sieve. The result of the research showed that the purification process of fish canning factory waste is carried out using 2 stages, namely degumming and neutralization, the change of density, viscosity, acidity and FFA value in fish oil before and after purification. The highest yield obtained from A3B2 treatment is catalyst composition of 7% and time of 2 hours with the value of rendemen of 81%. From the test results as for some parameters that meet the standard SNI-04-7182-2015, among others, density value of 876.3 kg / m³, flash point of 160ºC, iodine number of 16.36 gr / 100gr and calorific value of 47.47 Mj / kg.

Keywords: biodiesel, catalyst composition, reaction time length

INTRODUCTION

In Indonesia, one of the oils which has the greatest potential, especially as biodiesel raw material, that is fish waste in Muncar, Banyuwangi, East Java. The use of biodiesel made from fish is very beneficial, especially for villages in Muncar because it can reduce waste in the village and can be used as an alternative fuel. However, because the FFA value in fish oil is still very high, it is necessary to study the purification and characterization of fish oil when used as raw material for biodiesel. Making biodiesel which tends to run slowly so that a catalyst is needed. This catalyst serves to reduce the activation energy of the reaction so that the reaction can take place more quickly. Catalysts that are in the same phase (liquid) with their reactants are called homogeneous catalysts. While catalysts that are in different phases with their reactants (which can be solids, liquids which cannot be mixed or gas) are called heterogeneous catalysts [1]

Biodiesel synthesis process is generally still done conventionally using a homogeneous catalyst that is not environmentally friendly. So the need for substitution such as heterogeneous catalysts that can be obtained from sources that are in our surroundings, such as cocopeat.

According to [2], cocopeat is a coconut fiber which contains the dominant K and Cl elements. Due to the high content of potassium (K), this material is suitable for use as a natural catalyst in the manufacture of biodiesel. From the testing of coconut coir ash (ASK), the composition of compound in the form of K was obtained at 18.21%. So that through this research an assessment of the process of making biodiesel made from raw material from fish canning plant waste with natural catalysts of cocopeat ash with the aim of obtaining a high biodiesel yield, an efficient process and in accordance with SNI-04-7182-2015 biodiesel standards as diesel engine fuel.

METHOD

Research site was at the Renewable Energy Engineering Laboratory, Politeknik Negeri Jember. The materials used in this study were oil from fish canning plant waste originating from Muncar Banyuwangi, coconut coir (cocopeat), phenolphthalein, methanol (100%), ethanol (97%), H_2SO_4 (98%), aquades, NaOH, KOH and acetic acid. While the tools used in this activity are analytical balance, erlenmeyer, pycnometer, beaker glass titration tool, measuring cup, heater, burette, stative, pipette, spatula, magnetic stirrer, thermometer, stationery, calcination tool, fine filter paper, separator funnel, oven, saucer and sifter.

RESEARCH PROCEDURE
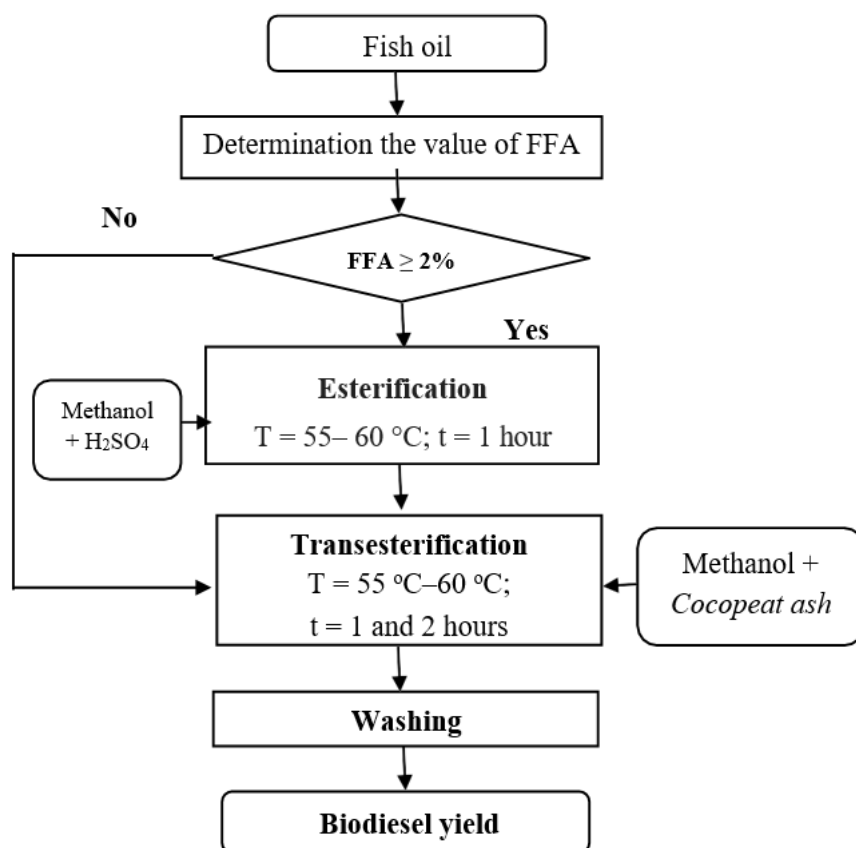
Figure 1. Flow Chart of Biodiesel Process

PRETREATMENT FISH OIL

Pretreatment of fish oil is divided into 2 stages, namely degumming and neutralization stage. Degumming is a process for removing dissolved substances in fish oil. This process begins by mixing fish oil at 80 ° C with water at 60 °C as much as 20% v/v oil and then mixing it using a magnetic stirrer at a speed of 400 rpm for 15 minutes. After 15 minutes, the separation was carried out using a separator until the oil formed three layers, namely oil, water and gum, and then the oil was separated from the other two layers. Furthermore, water is added again at 60°C and shaken. This step is carried out until the water pH of the laundry is neutral. Neutralization phase here aims to eliminate free fatty acids found in fish oil. Neutralization was carried out by giving 4.12 M NaOH to the oil that had been heated at 70°C and stirred for 2 minutes. Then transferred to a separating funnel and added 70°C of water as much as 10% v/v oil. Soap and water are separated from oil after 3 layers have formed in the separating funnel. States that to calculate ml NaOH [3], the following equation is used:

$$\text{ml NaOH} = \frac{\text{Acid Number x 40 x Oil(ml)X 1.3 x } \rho \text{ x 10}}{\text{56 x 1000 x 16.7}} \tag{1}$$

CHARACTERIZATION OF FISH OIL AFTER PRETREATMENT

After the oil has performed the pretreatment stage, the physico-chemical characteristics that must be known are the same as the initial oil characterization including free fatty acid levels using AOAC, the density of the picnometer method using ASTM D1298, acid number using AOAC and viscosity the otswald method using ASTM445.

CATALYST PREPARATION
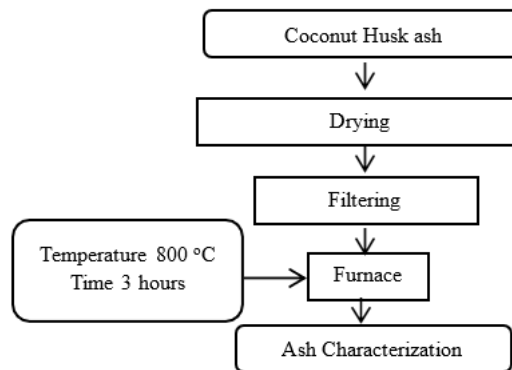
Figure 2. Flow Chart Catalyst Preparation

RESEARCH PARAMETERS

After washing, the characteristics of biodiesel yield are then carried out using several parameters. Some parameters observed include:

1. Biodiesel Yield
   The calculation of biodiesel yield is carried out using the following formula:

$$Yield\ (\%) \ = \frac{Biodiesel\ after\ washing\ process\ (g)}{Fish\ oil\ mass\ (g)} \times 100\% \qquad (2)$$

2. Biodiesel Characteristics According to SNI 7182: 2015
   The parameters to be used are based on the character of biodiesel according to SNI 7182: 2015.

RESULTS AND DISCUSSION

Preliminary Research

Preliminary research was conducted with the aim of determining the value of the composition of the fish oil catalyst from fish canning plant waste that will be used in the main research to get the best biodiesel yield. Fish oil that will be used as many as 5 samples with a variation of the K2O catalyst composition of 3%, 4%, 5%, 6% and 7% w / v with the best transesterification reaction time of 60 minutes [3].

After initial characteristics, the fish oil pretreatment / purification process is carried out. The results of the characterization of oil from fish canning plant waste before and after purification are as follows

Table 1. Characterization of Oil from Fish Canning Waste Before and After Purification

Parameter	Oil before purification	Oil after purification
FFA (%)	8.4	6.5
Acid Number (mg KOH/gr)	33.7	26.3
Density (kg/m^3)	698	700
Viscosity (Cps)	35	45

Table 1 shows the decrease and increase in parameter values in fish oil before and after refining. The decrease occurred in the value of free fatty acid / FFA values and acid numbers of 6.56% and 26.33% from the initial values of 8.4% and 33.72%. The decrease in these two parameters occurs because of the addition of a base namely NaOH in the neutralization process thereby reducing the acidity of the fish oil. Conversely an increase in density and viscosity values after purification is equal to 700 kg / m3 and 45 cps from an initial value of 698 kg / m3 and 35 cps. This clear increase in viscosity is due to the use of a method that involves the amount of water in the purification process, causing the viscosity value to increase. Other factors that influence the increase in viscosity include pressure, temperature, presence of other substances, size, molecular weight, and intermolecular strength.

DETERMINATION OF THE NUMBER OF CATALYSTS IN THE MAIN RESEARCH

Determination of the amount of catalyst is known by conducting preliminary research. The results of preliminary research conducted later will become a reference for the main research. Preliminary research conducted using fish oil as many as 5 samples with a sample volume of 100 ml. Variations in composition used include 3%, 4%, 5%, 6% and 7% w / v with the best transesterification reaction time of 60 minutes [4]. The following is a graph of the results of preliminary research as follows:
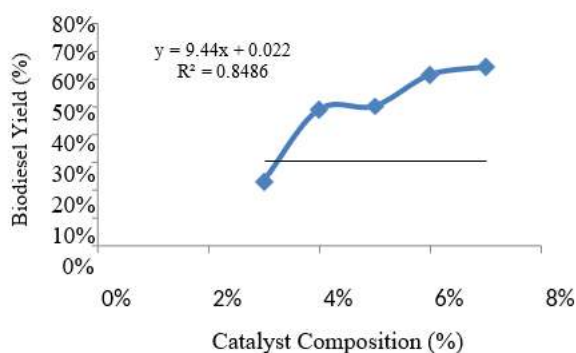
Figure 3. Chart of Results of Preliminary Research Results

Figure 3 shows the relationship between catalyst composition and biodiesel yield which is directly proportional. This shows that the greater the catalyst composition used, the greater the yield produced. The highest yield was produced on biodiesel with a catalyst composition of 7% which is not much different from the composition of the catalyst 6%, namely 61% and 64%. As for the lowest yield produced in the composition of the catalyst 3% with a yield of 23%. From the graph above it can also be seen the determination value that is equal to 0.8486, which means the relationship between the two factors is good because the value is close to $R2 = 1$.

Based on these results, it was determined the level of catalyst composition to be used was 3%, 5% and 7% with a length of time of transesterification of 60 minutes and 120 minutes. Determination of the amount of catalyst is obtained by looking at the results of the yield closest to the results of preliminary research that has been done.

BIODIESEL YIELD

The yield is a comparison of the quantity of biodiesel divided by the initial oil. According to [3], the factors that influence the value of the yield of a biodiesel in the transesterification reaction are the type of catalyst, reaction time, molar ratio between triglycerides and alcohol, water content, soap content and free fatty acid content. The samples that will be calculated for the yield are: A1B1 (3% catalyst composition and 1 hour reaction time), A2B1 (5% catalyst composition and 1 hour reaction time), A3B1 (7% catalyst composition and reaction time 1 hour), A1B2 (3% catalyst composition and 2 hours reaction time), A2B2 (5% catalyst composition and 2 hours reaction time) and A3B2 (7% catalyst composition and 2% reaction time).

The graph of the relationship between the different treatment of the catalyst composition to the length of transesterification is presented as follows.
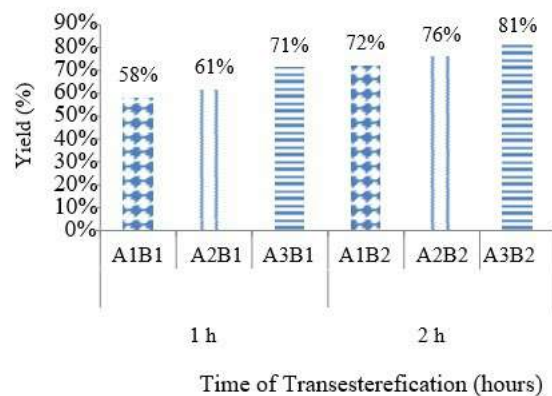
Figure 4. Catalyst relationship with Yield

Based on (Figure 4) it can be seen that there is a relationship between catalyst composition and length of reaction time. The more catalyst composition and reaction time in the transesterification process, the greater the yield produced. This is because the longer the reaction time in the transesterification process the longer the catalyst and methanol will mix, causing the solution to be very homogeneous.

The highest yield obtained was obtained from the interaction of two treatments, 2 hours reaction time and 7% catalyst composition, which was 81%. While the lowest yield produced by the two treatments was 58% with a reaction time of 1 hour and 3% catalyst composition. This proves that the length of time and composition of the catalyst affect the increasing value of the yield of biodiesel. The data obtained were then analyzed using variance (ANOVA) using the F test with a confidence level of 95% and 99%.

Because the reaction time and catalyst composition values have a very significant effect on ANOVA variance, further testing of these interactions is needed. In further testing, the difference between the average pair of treatments was carried out using the DMRT (Duncan Multiple Range Test) test. Based on the DMRT test, it shows that the highest yield of biodiesel is made from fish canning plant waste obtained in the treatment time reaction time of 2 hours and catalyst composition of 7%.

From the analysis results above it can be seen that there is no significant difference in the treatment of A1B1 (reaction time is 1 hour, catalyst composition is 3%) and A2B1 (reaction time is 1 hour, catalyst composition is 5%). Decision making based on further testing is on the A3B2 treatment, which is the treatment time of the reaction time of 2 hours and the catalyst composition of 7% with a mean yield of 81.02% due to its effect which has a very significant effect on the yield of biodiesel yield.

BIODIESEL CHARACTERIZATION

In this study a biodiesel characterization test was carried out on the A3B2 treatment with a reaction time of 2 hours and a 7% catalyst composition. The biodiesel quality parameters to be tested include density testing, viscosity, flash point, acid number, water content, iodine number, saponification number, cetane number and heat value. The following test results will be explained as follows.

Table 2. Comparison of Biodiesel Waste from Fish and Canning Plants SNI Biodiesel Standards 04-7182-2015

Parameters	Biodiesel Waste from Fish Canning Plants	Biodiesel Standards
Density in 40ºC(kg/m3)	876.3	840-890
Kinematic Viscosity in 40ºC(cps)	11.2431	2.3-6.0
Setana Number	42.75	min.51
Flash Point (ºC)	160	min. 100
Water and sediment (%-vol)	0.06	max. 0.05
Acid Number (mg-KOH/g)	0.59	max. 0.5
Iodium Number (%-massa)	16.36	max. 115
Heating Value (MJ/kg)	47.47	min. 40

Density or density is the amount of a substance per unit volume. The higher the density, the higher the mass of each volume. This density is also closely related to the heating value and power produced by a diesel engine per unit volume of fuel [5]. The value of biodiesel density of fish canning plant waste is 876.3 kg/m^3. This increase in density is possible due to the influence of the remaining catalyst that is not completely wasted during the washing process takes place, causing the density to increase.

Viscosity is a property used to determine the nature of fluid resistance to flow. High viscosity generally forms a thick fluid and makes it difficult to fog on a diesel engine. The value of viscosity in biodiesel from fish canning plant waste does not meet SNI 04-7182-2015 (2.3-6.0 cSt) requirements, which is 11.2431 cSt. According to [5] biodiesel which has a viscosity value that exceeds the provisions of the conditions will produce an incomplete combustion reaction thereby increasing wear and exhaust emissions.

The flash point is the lowest temperature point where the fuel will form steam and ignite by itself when reacting with air and triggered by fire. From the research that has been done, the flash point value from biodiesel from fish

canning plant waste is 160 ℃. This value meets the requirements of SNI 04-7182-2015 (Min 100 ℃) so that biodiesel is easy to handle and safe to store.

Acid number is an important indicator in biodiesel. The lower the acid number, the less free fatty acids contained in biodiesel [6]. The value of this acid number shows that the biodiesel from the waste of the fish canning plant does not meet the SNI 04-7182-2015 standard (max 0.5 mg-KOH / g) of 0.59 mg-KOH / g. According to [3] high levels of fatty acids in biodiesel cause soot to appear in the injector engine and cause corrosion in the engine.

The maximum limit of the presence of water in biodiesel according to the requirements of SNI 04-7182-2015 is a maximum of 0.05%, while the water content of biodiesel in fish oil is 0.06%. This water content value indicates that the biodiesel waste from fish canning plant does not meet the standards. This is because there is residual water in the biodiesel washing process itself.

Iodine number is a number that indicates the level of unsaturation of the constituent bidiesel compounds. The more unsaturated compounds in biodiesel the higher the price of iodine produced and the lower the CO_2 flue gas produced [6]. The maximum limit of iodine prices according to the standard is a maximum of 115% and the iodine value in fish oil biodiesel is 16.36 g/100g. From the results of these tests indicate that the value of biodiesel iod waste from fish canning plants meet biodiesel standards.

The saponification function is to determine the value of cetane numbers in biodiesel. The value of this saponification number is not listed in the SNI standard. The high number of saponification in biodiesel from fish canning plant waste is 41.79 mg / g. According Nurdini

[2] states that the longer the transesterification reaction causes more complete conversion, so that the fatty acids and the number of saponification decreases.

The high setana number causes biodiesel to ignite easily in the combustion cylinder and does not accumulate at relatively low temperatures [5]. From the approach taken, it was produced the index value of cetana waste from fish canning plant at 42.75 and it can be said that it does not meet the SNI 04-7182-2015 biodiesel standard which is a maximum of 51

The heating value or commonly known as heating value is the amount of heat energy released per unit mass of fuel. The maximum limit of the calorific value according to American HHV value is USA No. 2 Distillate (Diesel) of 40 Mj / Kg. The equation used to calculate the calorific value is to use the approach made by [2] using the iodine value and saponification approach. From the calculation results, the calorific value of the biodiesel waste from the fish canning plant was 47.47 Mj/kg. So the heat value of biodiesel is said to meet the standard.

CONCLUSION

From the results of the research conducted, conclusions can be drawn including:

1. The process of purifying fish canning plant waste is carried out using 2 stages, namely degumming and neutralization. From the purification results it was found that there was an increase in the value of the density and viscosity parameters and conversely a decrease in the value of the FFA and acid number. There is a decrease in value due to the addition of bases in the purification process while there is an increase in viscosity due to the use of water in the purification process.
2. The use of cocopeat ash catalyst as biodiesel catalyst produced the best yield of 81%, namely in the treatment of A3B2 by using a 7% catalyst composition and 2 hours. The more catalyst composition and reaction time in the transesterification process, the greater the yield produced.
3. From the results of tests carried out, as for some biodiesel standards of fish canning plant waste that meet SNI-04-7182-2015, among others, the density value is 876.3 kg / m3, flash point is 160oC, iodine number is 16.36 gr / 100gr and heat value of 47.47 MJ / kg.

REFERENCES

1. Helwani, Z., M.R. Othman, N. Aziz dan W. J. N. Fernando. *Solid Heterogeneous Catalysts For Transesterification Of Triglycerides With Methanol*: *A Review*. (Elvesier, 2009), Pp. 1-10.
2. Nurdini, D. A. ''Design Process of Making Biodiesel from used Cooking Oil with Natural Cocopeat Ash Catalyst''. Thesis. Faculty of Agricultural technology, Institut Teknologi Bandung. 2008
3. Syarif, M. ''Calcium Carbide Residue (CCR) as a catalyst for Heterogeneous Bases in the Kesambi Oil Transesterification Reaction (Schleichera Oleosa L)''. Thesis. Politeknik Negeri Jember. 2016.
4. Astutik, F. E. M. ''Use of Banana Stem as a Heterogeneous Catalyst in the Transesterification of Used Cooking Oil Reactions in the Biodiesel Production Process'' Thesis. Politeknik Negeri Jember. 2014.
5. Prihandana R., Hendroko R. dan Nuramin M. *Cheap Biodiesel Overcomes Pollution and Scarcity of Fuel*. PT. Agromedia Pustaka, Jakarta, 2006.
6. Padil, S. Wahyuningsih, dan A. Awaluddin. *Making Biodiesel from Coconut Oil through Methanolysis Reaction Using a CaCO3 catalyst which is incanded. (Natur Indonesia Journal, 2010)*. Pp.27-32.
7. Demirbas, A. *Fuel properties and calculation of higher heating values of vegetable oils*. *(Elsevier,* 1998). Pp. 9–10.

Characterization of Sugar Cane Fiber of Genetic Engineering Product for Biodegradable Materials

Rahma Rei Sakura[1, a)] and Bambang Sugiharto[2, b)]

[1]Mechanical Engineering Department, University of Jember, Jember, Indonesia
[2]Biology Department, University of Jember, Jember, Indonesia

[a)]Corresponding author: rahmareisakura@unej.ac.id
[b)]sugiharto.fmipa@unej.ac.id

Abstract. Sugar cane (Saccharum officinarum L.) is one type of agricultural plant with abundant biomass production in Indonesia. However, the production of sugar cane still not sufficient, so the Indonesian Sugar Plantation Research Center develops new types of sugar cane and has 70 varieties. This encourages researchers in Indonesia to continue to assemble new varieties of sugar cane plants with biotechnology, which is referred to as GM crops. In previous studies, three types of PRG sugar cane have been produced by overexpressing two genes, namely the SoSPS1 and SoSUT1 genes. Overexpression of these genes to increase the content of sucrose in sugarcane. The purpose of this study to determine the effect of overexpression of the SoSPS1 and SoSUT1 genes in fiber structure of sugarcane. In addition, this study also aimed to identify the thermal properties of GM sugar cane fiber for environmentally friendly technology applications. The research method will be carried out by extracting fiber on sugarcane stems. PRG sugar cane fiber is dried and partly carried out the carburization process, which is the carbonation process in the fiber. Then the material characterization test was carried out using SEM, FTIR, and XRD tests. The results obtained characterization test that gene overexpression in sugarcane has an influence on the formation of sugarcane fiber structure. A significant impact was shown on sugar cane PRG-D5. The carburization process in sugar cane PRG has a significant impact on the structure, chemical properties, and crystallinity. Homogeneous structure formation will form a good chemical and morphological characteristics.

KEYWORDS: PRG Sugar Cane, Sugar Cane Fiber, Green Material, PRG Sugar Cane Characterization.

INTRODUCTION

Indonesia is a country that has abundant agricultural and plantation products. The Indonesian Sugar Research and Development Center (P3GI) states that it has more than 70 varieties of sugarcane. Indonesia produces sugarcane amounted to 2,497,997 tons (Directorate General of Plantations). However, the production of sugar from sugar cane in Indonesia is still not sufficient. So, it is necessary to assemble new sugar cane varieties to produce high sugar. The increasing variety of sugar cane in Indonesia has caused researchers to develop innovations and technologies by increasing the added value of the sugar cane industry and the by-product industry of sugar cane.

Sugar cane (Saccharum officinarum L.) is the largest industrial plant in the world and will develop in more than 100 countries (White et al., 2011). Although this is intended primarily for the development of sugar production, at present, the main focus is to create sustainable energy. In addition, lignocellulosic biomass such as sugar cane can be the basis of a biorefinery with a wide range of appropriate products (Moncada et al., 2012).

The main components formed from sugarcane are sucrose, fiber, and water, with a percentage of 12%, 15%, and 70% (Anon., 2017). Other components found in sugarcane plants are simple sugars (glucose and fructose), inorganic

materials, nitrogenous substances, latex, wax, and organic acids (Chen and Chou, 1993). The chemical composition of bagasse fiber is shown in the table below.

TABLE 1. The chemical composition of bagasse fiber

Cellulose	Hemicellulose	Lignin	Protein	Latex and Wax	Ash	Sucrose	Silica	Glucose	Reference
50	25	25							Huang *et al.* 2012, Xu *et al.* 2010
40	24,4	15	1,8	0,6	5	14		1,4	Vazquez *et al*. 1999
40-43	28-30	9-11	8-9	2-2,5	5-6				Ramaraj 2007
46	24,5	19,5		3,5	2,4		2		Mulinari *et al*. 2009a
69,4	21,1	4,4		5,5	0,6				Habibi *et al*. 2008
41,8	28	21,8							Bilba *et al*. 2003
55,2	16,8	25,3			1,1				Trindade *et al*. 2005
56	6	29			7				Maldas and Kokta 1991
36,32	24,7	18,14							Vilay *et al*. 2008

The dried sugar cane stems (bagasse) have main fibers, namely cellulose, hemicellulose, and lignin (Paturau, 1989). Cellulose is glucopolysaccharide which has the general formula $C_6H_{10}O_5$ and the main constituents of plant tissue. Hemicellulose is a polysaccharide consisting of different sugars, but xylose is currently the most dominant. Lignin is an amorphous structure with complex phenolic polymers that are cross-linked with hemicellulose. At present, sugar cane plants have been assembled with GM products (high yield) through biotechnology. PRG sugar cane assembly is done through overexpression of SoSPS1 and SoSUT1 genes, to increase the sucrose sugar content.

In cotton plants, it is known that genetic engineering overexpression of SPS genes can cause physical and chemical properties of fiber that are better than the parent plants (non-GM crops). That is because the synthesis of sucrose in cotton is used fully to improve the quality of fiber in cotton. Haigler et.al., (2007) states that overexpression of the spinach SPS gene in cotton correlates with high fiber quality under controlled environmental conditions. Whereas in the PRG sugar cane plant, overexpression of SoSPS1 and SoSUT1 some of the sucrose produced can be used to improve the process of fiber synthesis.

In this study, an analysis of the GM sugarcane bagasse fibers will be analyzed by overexpressing two genes, namely the SoSPS1 and SoSUT1 genes. The resulting data will be compared with non-PRG bagasse fiber to see the effect of gene overexpression. Sugarcane bagasse fibers used in the form of particles will be analyzed the formation of structures and characterization of the thermal properties. The results obtained can be used in biodegradable materials.

MATERIALS AND METHODS

Materials

The raw material in the form of Wild Type bagasse, PRG-SP3 cane, PRG-SU2 cane, and PRG-D5 cane. Sugarcane bagasse is taken from the sugarcane stems with position 3-10 segments upwards. There are four types of samples materials obtained. The four types of samples are separated into two parts, namely without treatment and treatment. The sample was treated without grinding process then sieving with 50 Mesh particle size. As for the treatment sample, the carburization process was carried out at a temperature of 600 oC and held for 60 minutes to

form activated carbon material. Activated carbon obtained, grinding process then sieving with 50 Mesh particle size.

Materials Characterization Testing

Test samples produced with variations in the treatment and type of bagasse amounted to 96 test samples. The test sample is tested to obtain the formation of the structure and thermal properties of each sample. There are several tests, namely Differential Scanning Calorimetry (DSC), Scanning Electron Microscope (SEM), Fourier Transform Infrared Spectroscopy (FTIR), and X-Ray Powder Diffraction (XRD).

The results of testing the samples obtained then analyzed the characterization of the material. The analysis includes analysis of the chemical composition, analysis of phase changes, analysis of thermal properties, and morphological analysis of the formation of the test material. The results of the report will be described in the form of tables and graphs to facilitate analysis.

The conclusion is the effect of overexpression of two genes, namely the SoSPS1 and SoSUT1 genes in the formation of the PRG sugar cane fiber structure. The effect of the carburization process on the formation of the structure and thermal properties in the PRG sugar cane fiber.

RESULTS AND DISCUSSION

Characteristics of Sugar Cane Transgenic

In this study, there are four types of Genetically Modified Product (PRG) sugarcane, namely Wild Type sugar cane, PRG-SP3 sugar cane, PRG-SU2 sugar cane, and PRG-D5 cane. Wild type sugarcane is a parent sugar cane plant which is then overexpressed by two genes, namely the SoSPS1 and SoSUT1 genes. Sugarcane plants produce sucrose in the leaves which are then taken to the stem. The sucrose product is stored in sugarcane stems which is partly used for the synthesis of other plant parts. Genetically engineered sugarcane products are designed to increase sucrose yield in the leaves through the process of photosynthesis named PRG-SU2. While the results of the synthesis process of other plant parts get results in the form of increased biomass on sugarcane stems called PRG-SP3. PRG-D5 cane is a sugar cane plant with overexpression of two genes, namely an increase in sucrose yield and an increase in biomass.

Collecting sugarcane stems and squeezing sugar cane juice is done within one day. Sugarcane bagasse (bagasse) from the squeeze is dried in direct sunlight within one week. Bagasse that has been dried is grinding using a cutting tool (blender) until the bagasse becomes 50 Mesh particles size.

| (a) | (b) | (c) | (d) |

FIGURE 1. Sugar Cane bagasse that has been dried (a) Wild type, (b) PRG-SP3, (c) PRG-SU2, (d) PRG-D5.

Figure 1 shows that PRG-SP3 is the highest mass of sugarcane bagasse. This happens because not all sucrose

carried by sucrose transporters is stored on sugarcane stems. Some sucrose is used for the synthesis of other plant parts.

|(a)|(b)|(c)|(d)|

FIGURE 2. Sugar Cane bagasse that has been a grind with 50 Mesh particle size (a) Wild type, (b) PRG-SP3, (c) PRG-SU2, (d) PRG-D5.

|(a)|(b)|(c)|(d)|
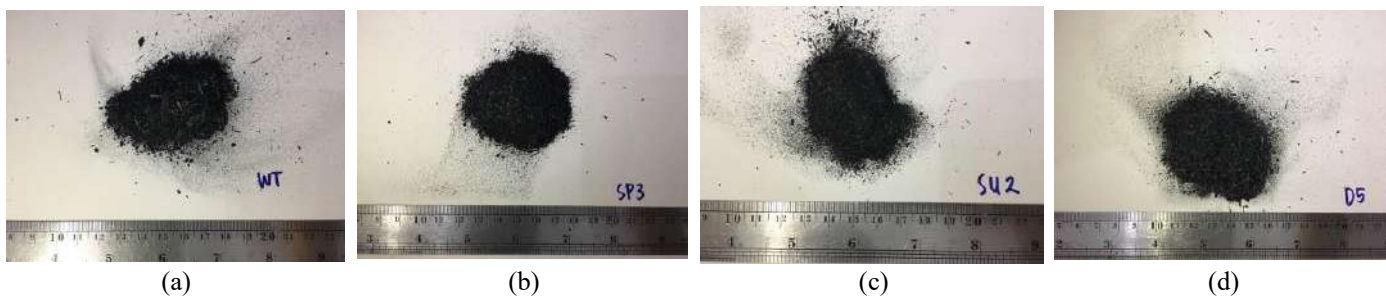
FIGURE 3. Sugar Cane bagasse that has been carburized T = 600 ºC with 50 Mesh particle size (a) Wild type, (b) PRG-SP3, (c) PRG-SU2, (d) PRG-D5.

Figure 3 shows that the bagasse fiber which has been carried out by drying process with direct sun exposure within one week. The picture shown does not look significant difference because the same particle size is 50 Mesh. Figure 4.3 shows that the results of the carburization process with a temperature of 600 oC, get perfect results. This is caused by the bagasse fiber (bagasse) which is treated not to be ash in the form of particulate fibers and carried out at high temperatures.

The carburization process must be carried out under vacuum, and it is ensured that no air enters the gaps in the container. If the carburization process is not vacuumed, the bagasse fiber powder will turn to ash because it is carried out at high temperatures. Bagasse fiber powder of genetically modified products is then subjected to characterization testing. The characterization test consists of DSC, SEM, FTIR, and XRD. DSC testing is done to measure weight loss with the intention to predict the effect of heating on the characteristics of the resulting powder. SEM testing is done to see the morphology and crystals formed in the bagasse fiber powder both without treatment or treatment. FTIR testing was carried out to know the chemical composition contained in the bagasse fiber powder while XRD testing to know the phase changes that occur in the bagasse fiber powder.

Fourier Transform Infrared Spectroscopy (FTIR)

FTIR testing is a test using infrared spectroscopy equipped with Fourier transforms to detect and analyze the results of the spectrum. This test shows that the peak of the graph is at source 400 - 4000 cm^{-1}.
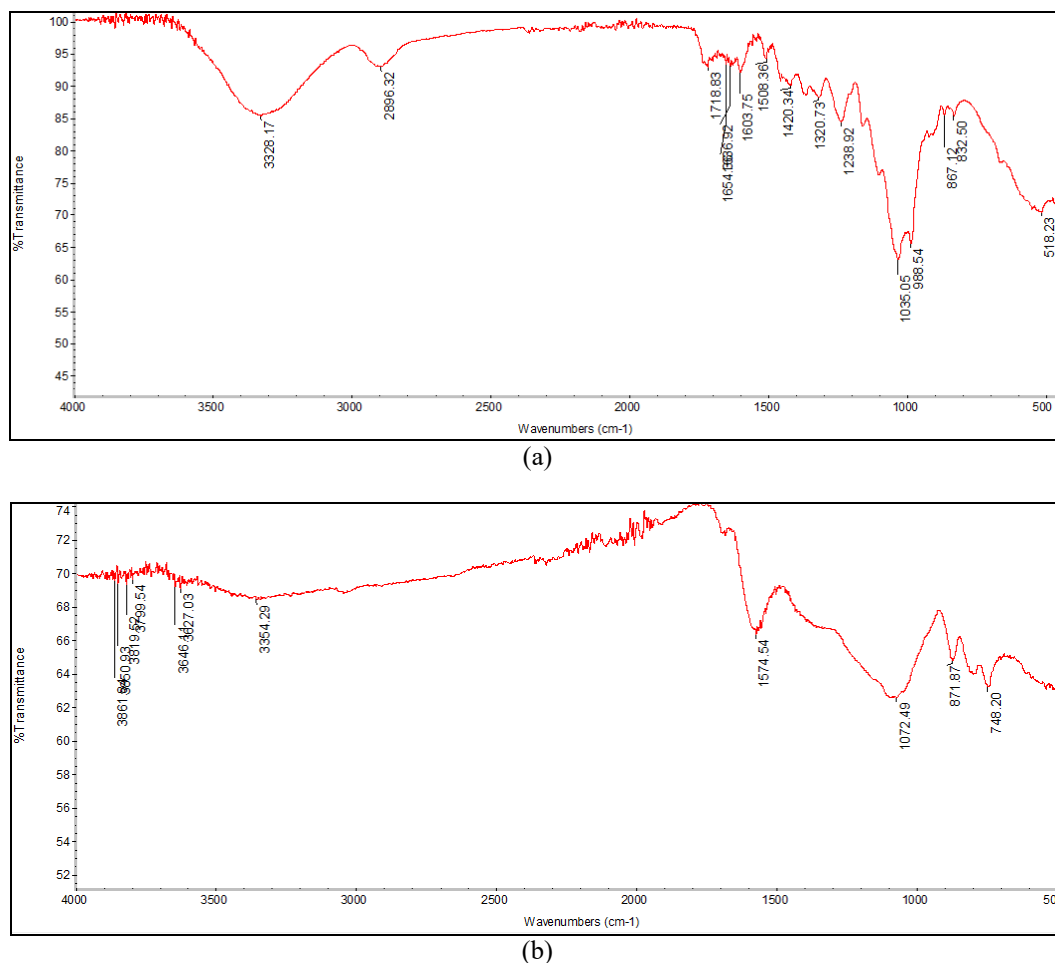
FIGURE 4. FTIR test result (a) PRG-D5 without treatment, (b) PRG-D5 with treatment T = 600 °C

Figure 4 shows that there are differences in the results of D5 sugar cane testing without and with heat treatment. The results of D5 sugar cane testing without treatment showed that there were several peaks, including 1034.83, 2915.53, and 3331.85. Peak 1034.83 is defined as an alcohol functional group that has a chemical bond between carbon and oxygen, and lignin and cellulose are detected. The peak of 2915.53 is defined as the alkanes functional group, which has the chemical bond of carbon with hydrogen and is identify by lignin and cellulose. While the peak 3331.85 has an alcohol functional group with chemical bonds of oxygen with hydrogen, and there are lignin and cellulose.

D5 sugar cane testing with a treatment of T = 600 °C has several peaks, namely 1088.51, 1574.37, 3379.71 and 3627.03. The peak of 1088.51 was defined as an alcohol functional group, has chemical bonds of carbon and oxygen, and there are lignin and cellulose. The peak of 1574.37 was defined as a cyclic alkene functional group that has the chemical bond of carbon with carbon, and only cellulose exists. The peak 3379.71 was defined as an alcohol functional group with chemical bonds of oxygen and hydrogen, and there are lignin and cellulose. While peak 3627.03 was defined as a functional group of alcohols that have chemical bonds of oxygen with hydrogen, and there are lignin and cellulose.

X-Ray Powder Diffraction (XRD)

XRD testing has the aim to determine the phase contained in the material. The XRD test results are further analyzed to determine the characteristics of each peak, such as the phase or compound of the material, its crystalline level, and the crystal plane.
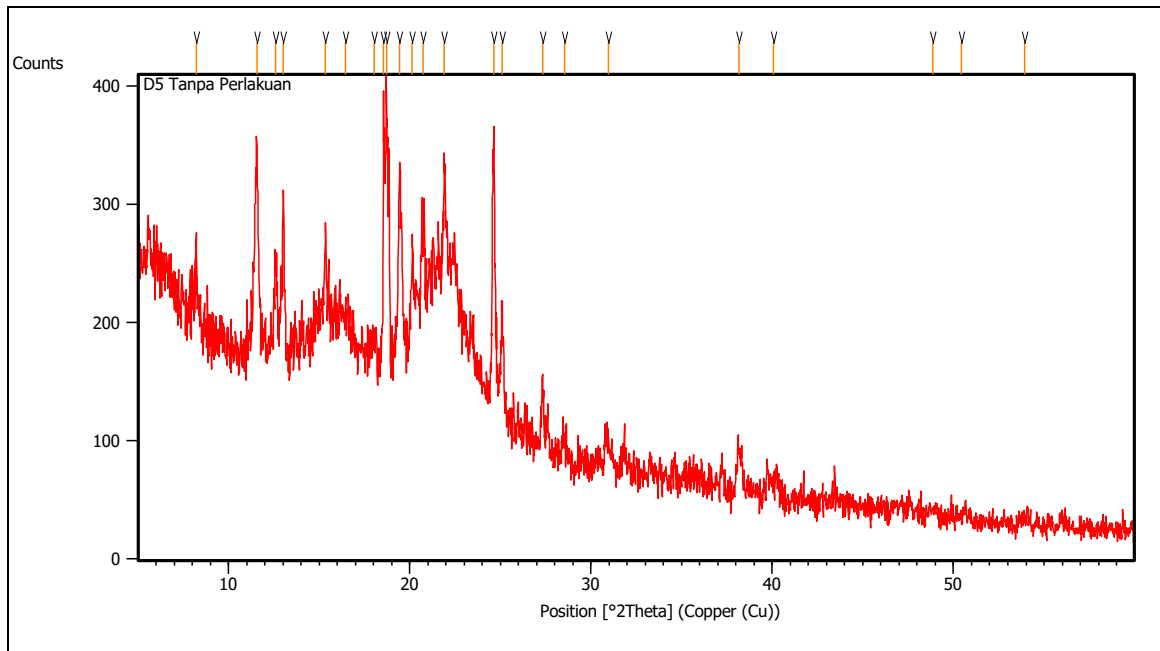
(a)
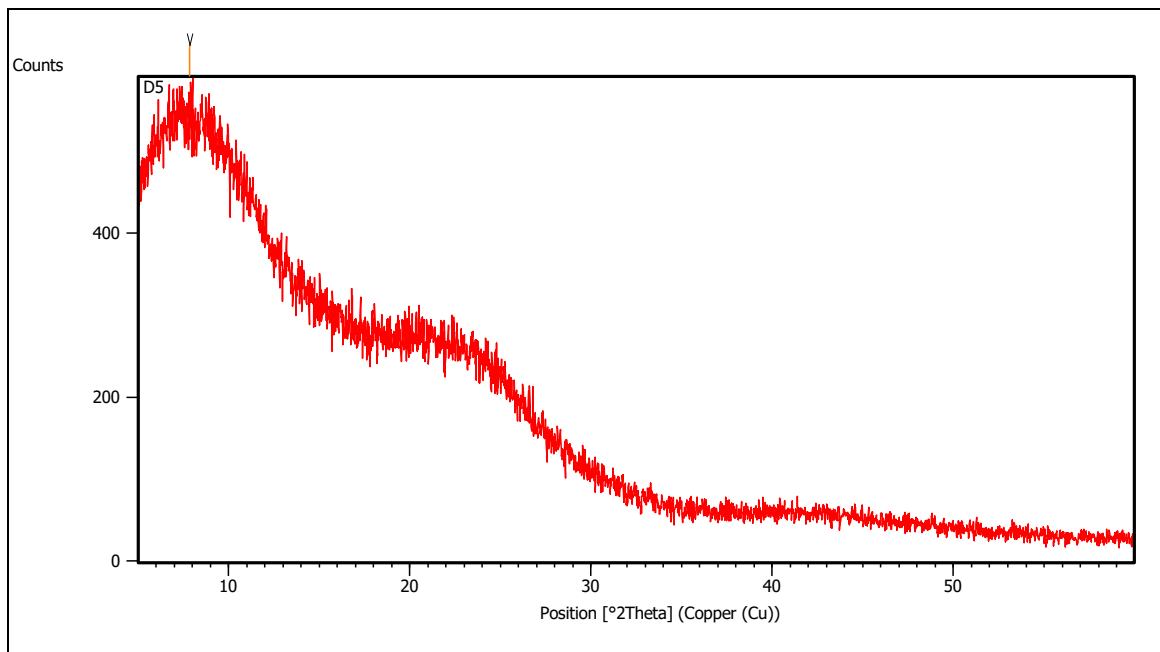
(b)

FIGURE 5. XRD test result (a) PRG-D5 without treatment, (b) PRG-D5 with treatment T = 600 °C

XRD test results of sugar cane PRG-D5 showed that sugar cane PRG-D5 without treatment had many peaks. This shows that the crystal structure of sugarcane that has no treatment is amorphous.

TABLE 2. Peak list XRD testing of PRG-D5 without treatment

Pos. [°2Th.]	Height [cts]	FWHM Left [°2Th.]	d-spacing [Å]	Rel. Int. [%]
18.5443	261.74	0.0502	4.78474	99.96
24.6256	261.85	0.0502	3.61521	100.00

The table above shows that there are two peaks with the highest intensity at position two thetas is 18.5443 and 24.6256.

Sugar Cane PRG-D5 with heat treatment has the highest peak with an intensity of 83.28.

TABLE 3. Peak list XRD testing of PRG-D5 with treatment

Pos. [°2Th.]	Height [cts]	FWHM Left [°2Th.]	d-spacing [Å]	Rel. Int. [%]
7.8443	83.28	0.0900	11.26158	100.00

The table above shows that the highest intensity at position two thetas is 7.8443.

Scanning Elektron Microscope (SEM)

SEM testing is done to determine the morphology of the material. In SEM testing is carried out with magnifications between 500 - 3000x. Morphological picture of WT sugar cane without treatment and with treatment.

(a)   (b)
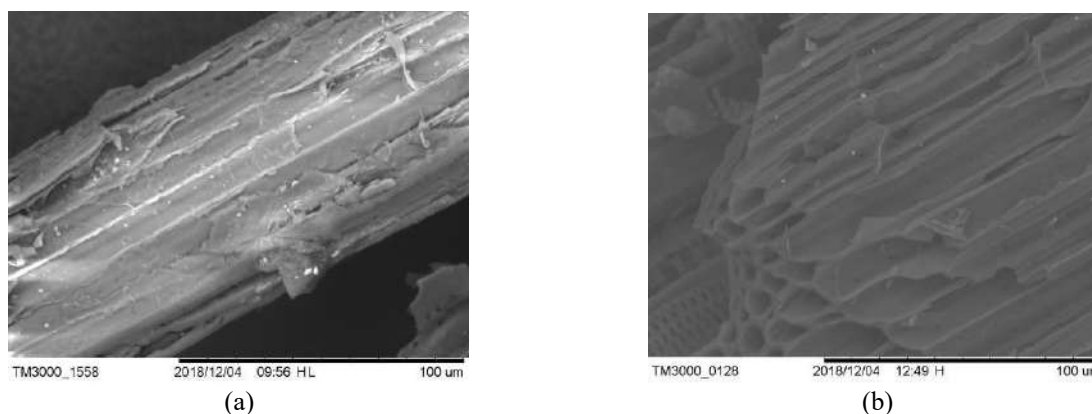
FIGURE 6. SEM test results of sugarcane WT (a) without treatment, 1000x magnification, (b) with treatment T = 600 ºC, 1000x magnification

Figure 6 (a) shows that WT sugarcane without treatment has a morphology that still contains lignin, cellulose, and hemicellulose. Whereas Figure 6 (b) shows that WT cane which has been treated has a more regular morphology and only cellulose. This is caused by heating at high temperatures which will cause the structure of lignin and hemicellulose to degrade. The direction of fiber morphology shows that the direction of the fiber is homogeneous. Homogeneous fiber direction causes sugarcane to have strength towards the fiber.

CONCLUSION

Overexpression of genes in sugarcane has an influence on the formation of sugarcane fiber structure. Significant influence was shown on sugar cane PRG-D5. The carburization process in sugar cane PRG has a significant influence on its structure, chemical properties, and crystallinity. The results obtained indicate that the formation of homogeneous structures will form a better chemical and morphological characteristics.

ACKNOWLEDGMENTS

REFERENCES

1. Anon., 2007. Annual Report, 2006. Mauritius Sugar Industry Research Institute, pp. 87–90.
2. Bismarck A, Mishra S, Lampke T. Plant fibers as reinforcement for green composites. In: Mohanty AK, Misra M, Drzal LT, editors. Natural fibers, biopolymers, and biocomposites. USA: CRC; 2005. p. 37–108.
3. Bledzki AK, Zhang W, Chate A. Natural-fibre-reinforced polyurethane microfoams. Compos Sci Technol 2001;61:2405–11.
4. Chen, J.C.P., Chou, C.C., 1993. Cane Sugar Handbook – A Manual for Cane Sugar Manufacturers and Their Chemists, 12th ed. John Wiley and Sons, Inc.
5. Direktorat Jendral Perkebunan, 2015.
6. Drochytka R, Zach J, Korjenic A, Hroudova J. Improving the energy efficiency in buildings while reducing the waste using autoclaved aerated concrete made from power industry waste. Energy Build 2013;58:319–23.
7. Lalonde, S., E. Boles, H. Hellmann, L. Barker, J.W. Patrick, W.B. Frommer, and J.M. Ward (1999) The dual function of sugar carriers: transport and sugar sensing. Plant Cell 11:707-726.
8. Miswar, B. Sugiharto, J. Soedarsono dan S. Moeljopawiro (2005) Transformasi gen sucrosephosphate synthase (SoSPS1) tebu (*Saccharum officinarum* L.) untuk meningkatkan sintesis sukrosa pada daun tembakau (Nicotiana tabacum L.). Berkala Ilmiah BIOLOGI 4(5):337-347.
9. Miswar, B. Sugiharto, J. Soedarsono dan S. Moeljopawiro (2007) Transformasi gen sucrosephosphate synthase (SoSPS1) menggunakan Agrobacterium tumefaciens untuk meningkatkan sintesis sukrosa pada tanaman tebu (Sacharum officinarum). Jurnal Berkala Penelitian HAYATI. 12 (2): 137-144.
10. Moncada, J., El-Halwagi, M.M., Cardona, C.A., 2012. Techno-economic anal-ysis for a sugarcane biorefinery: Colombian case. Bioresour. Technol., http://dx.doi.org/10.1016/j.biortech.2012.08.137.
11. Mufitdhah, N., R. Rafika, W.T. Widodo, F.H. Prasetyo, B. Sugiharto, (2015) Different Contribution of Sucrose Phosphate Synthase and Sucrose Transporter Protein for Sucrose Accumulation in Transgenic Sugarcane Stem. CDAST: Jember University.
12. Paturau, J.M., 1989. By-products of the Cane Sugar Industry, An Introduction to Their Industrial Utilization, 3rd ed. Elsevier Publishing Co, Amsterdam, pp. 37–42.
13. Pusat Penelitian Perkebunan Gula Indonesia.
14. Ramesh M, Palanikumar K, Reddy KH. Mechanical property evaluation of sisal–jute–glass fiber reinforced polyester composites. Compos Part B-Eng 2013;48:1–9.
15. Rashdi AAA, Sapuan SM, Ahmad MMHM, Khalina A. Combined effects of water absorption due to water immersion, soil buried and natural weather on mechanical properties of kenaf fiber unsaturated polyester composites (KFUPC). Int J Mach Manuf Eng 2010;5:11–7.
16. Shah D. Developing plant fiber composites for structural applications by optimizing composite parameters: a critical review. J Mat Sci 2013;48(18):6083–107.
17. Singh, G.B., and S. Solomon. (1995) Sugarcane: agro-industrial alternatives. New Delhi: Oxford & IBH Publishing Co. Pvt. Ltd.
18. Sugiharto, B., Sumadi, H. Sasakibara, and T. Sugiyama (1997a) Differential expression of two genes for sucrose-phosphate synthase in sugarcane: Molecular cloning of the cDNAs and comparative analysis of gene expression. Plant Cell Physiol 38:961-965.
19. Sugiharto, B., S. Suhastuti, and H. Sakakibara (2001) Expression of sugarcane sucrose phosphate synthase isoenzyme in Escherichia coli and their characterizations. The Second Indonesian Biotechnology Conference. KBI-Yogyakarta, PA-7.
20. White, J.E., Catallo, W.J., Legendre, B.L., 2011. Biomass pyrolysis kinetics: a comparative critical review with relevant agricultural residue case studies. J. Anal. Appl. Pyrolysis 91, 1–33.

Metal Oxide as Soluble Nano Catalyst on Biodiesel: a Review

Setyo Pambudi[1], Nasrul Ilminnafik[2, a)] Boy Arief Fachri[3, b)]

[1]*Mechanical Engineering, Universitas Jember-68121 Jember, Indonesia*
[2]*Department of Mechanical Engineering, Universitas Jember-68121 Jember, Indonesia*
[3]*Department of Chemical Engineering, Universitas Jember-68121 Jember, Indonesia*

[a)]setyopmbd@gmail.com
[b)]nasrul.teknik@unej.ac.id
[c)]fachri.teknik@unej.ac.id

Abstract. Recently nanoparticles of metal oxide developed as soluble nano additive in liquid fuels to improve fuel quality. One application of nano metal oxide particles is an additive to biodiesel. Biodiesel is an alternative fuel that can reduce dependence on fossil fuels. Pure biodiesel has a relatively lower calorific value compared to fossil fuels. Low calorific value results in increased brake specific fuel consumption. Moreover, biodiesel has a higher density and viscosity compared to fossil fuel. The content of carbon monoxide (CO), unburned hydrocarbons (HC) and nitrogen oxide (NOx) in exhaust gases with biodiesel is higher than fossil fuels. Metal oxide nanoparticles are added to biodiesel between 6 to 80 nm with concentrations about 50 to 500 ppm. Addition of metal oxide nanoparticles to biodiesel can improve brake thermal efficiency, reduce brake specific fuel consumption, carbon monoxide (CO), unburned hydrocarbons (HC), nitrogen oxide (NOx) and improve carbon dioxide (CO_2) emission due to the catalytic effect of metal oxide nanoparticles. Metal oxide performs as an oxidation catalyst which diminishes the activation temperature of carbon combustion and enhances the hydrocarbon oxidation promoting a complete combustion. Nanoparticles that are often used in various studies are nickel(II) oxide (NiO), cerium(IV) oxide (CeO_2), titanium oxide (TiO_2), zinc oxide (ZnO), aluminum oxide (Al_2O_3),and silicon dioxide (SiO_2). This review paper describes the progress and development of nano metal oxide applications as additives for biodiesel. The discussion in this paper is divided into 3 main topics, they are the effects of nanoparticles on the biodiesel properties, engine working, and emission appearance.

Keywords: nanoparticles, catalytic effect, biodiesel, engine performance, fuel consumption, exhaust gases

INTRODUCTION

World energy needs still depend on fossil fuel. One of the fuel that continues to experience increased consumption is liquid fuel. Liquid fuel consumption in the world is estimated rises from 95 million to 113 million barrels per day (MBPD) in the period 2015 to 2040.

This increase in liquid fuel consumption occurs in the industrial and transportation sectors [1]. Bioenergy is promoted as a substitute to reduce dependence on non-renewable fuels (fossils) and to reduce greenhouse gas emissions. Bio energy is a non-fossil fuel produced from growth and growth of animals (biological). Utilization of bio energy currently reaches 50 EJ / year, or about 10% of global energy needs. The potential for major global bio energy techniques in 2050 is estimated at 160-270EJ / year [2]. One of the many bioenergy developed today is biodiesel.

Biodiesel is an alternative fuel for ignition compression engines that are environmentally friendly. Biodiesel has better properties than petrodiesel because it is made from renewable materials, biodegradable, sulfur-free and aromatic, and non-toxic [3]. Biodiesel or Fatty Acid Methyl Esters (FAME) can be made from a variety of vegetable oils or animal oils [4][5]. The raw material for vegetable oil or animal oil used to produce biodiesel is known as

triacylglyceride (TAGs) or often called triglycerides. In general, the process of biodiesel production is known as the transesterification process. The process of tranesterification is the reaction between triglycerides and alcohol with the help of a catalyst to produce fatty acid alkyl esters. The by-product of transesterification is glycerin, also called glycerol. The most commonly used alcohol is methanol [6].

The use of biodiesel in the compression ignition engine can reduce smoke opacity but increase Brake Spesific Fuel Consumption (BSFC) [7]. The increase in fuel consumption is due to the smaller heating value of biodiesel compared to petrodiesel, so to get the same power output requires more fuel consumption [8]. In addition, the use of biodiesel also reduces Brake Thermal Efficiency (BTE). In biodiesel flue gases, hydrocarbons that do not ignite (HC), Carbon Monoxide (CO) are found to be lower with petrodiesel fuel [9]. However Nitrogen Oxide (NOx) contained in the flue gas increased significantly when using biodiesel compared to petrodiesel [10][11][12][13]. Biodiesel consists of five main long carbon chains, they are FAME: methyl palmitate (MP, C17H34O2, C16: 0) and methyl stearate (MS, C19H38O2, C18: 0) as saturated FAME, methyl oleate (MO, C19H36O2, C18: 1), methyl stearate (MS, C19H38O2, C18: 0) as saturated FAME, methyl oleate (MO, C19H36O2, C18: 1), methyl linoleate (ML, C19H34O2, C18: 0) 2) and methyl linolenic (MLE, C17H32O2, C18: 3) as unsaturated FAME [14]. Biodiesel has an oxygen content that is bound to suppress the formation of soot particles which results in reduced radiant heat transfer thereby increasing the reaction temperature and NOx formation [15].

Catalytic combustion is widely used in various fields, especially in the use of fossil fuels that are efficient and low in pollutants. Catalytic combustion can increase efficiency and reduce NOx pollutant emissions [16]. Catalytic combustion is also often used in small scale combustion. The addition of a catalyst can increase the stability limit so that the fire is more easily stable despite being in a very small space and far from stoichiometric Air Fuel Ratio (AFR) [17][18][19]. In internal combustion engines it is not practical to add catalyst in the combustion chamber. To improve performance and improve internal combustion engine emissions, the catalyst is directly mixed in liquid fuel. The catalyst added in nano-sized liquid fuels so that metal catalysts can dissolve and mix in liquid fuels. Catalysts in liquid fuels are often referred to as nano additives [20].

Nano metal oxide is often used to improve performance and improve biodiesel exhaust gases. From the background above, this paper aims to provide an overview of several things including: 1. The use of nano metal oxide as a soluble nano catalyst. 2. Effects of soluble nano catalyst on biodiesel properties. 3. Effects of soluble nano catalyst on biodiesel performance. 3. Effects of soluble nano catalyst on biodiesel exhaust gases. This paper is a narrative review by comparing several studies to find conclusions and match them with existing theories.

PRESENT STATE OF THE ART: NANO METAL OXIDES

Metal oxide belongs to an important group of engineered nanoparticles, besides being used in liquid metal additives, nano metal oxide is widely used in cosmetics and sunscreens, coatings and textiles that clean themselves. Other applications include its use as an air fuel and battery processing agent and newer car catalytic converters [21]. Ultrasound is used to mix biodiesel with nano metal oxide.
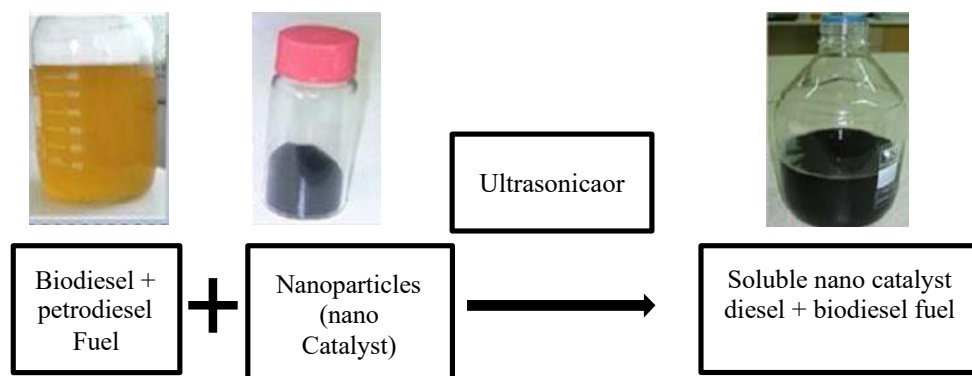
Figure 1. soluble nanocatalyst mixed with using an ultrasonicator [22]

To characterize nano metal oxide, several methods can be used, among others, by using Scanning Electron Microscope (SEM), X-ray Diffraction (XRD), and Transmission electron microscopy (TEM). From TEM and SEM images it can be seen the average particle size of nano metal oxide. The size of the nano metal oxide is certainly no

bigger than the diesel engine fuel injector nozzle hole. So that nanoparticles do not inhibit the rate of fuel flow into the combustion chamber [23]. Figure 2 is the results of SEM and TEM of TiO $_2$ nanoparticles.
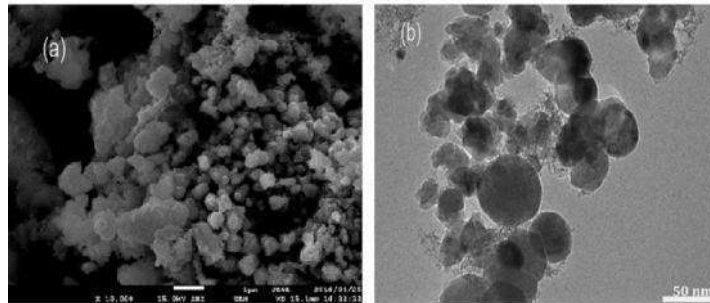
Figure 2. SEM (a) and TEM (b) image of TiO$_2$ nanoparticles [23]

X-ray Diffraction (XRD) is used to confirm that nanoparticles are nano metal oxides. Figure 3 XRD results from NiO nanoparticles, where Ni-O particle patterns are found in the range of 20 ° -80 ° [24].
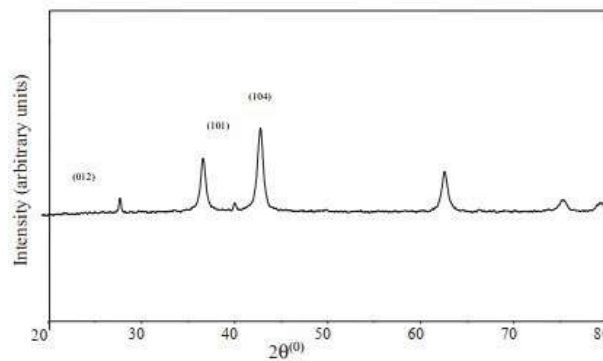
Figure 3. XRD of NiO [24]

FUEL PROPERTIES

The nano metal oxides used as soluble nano additives in biodiesel are 6 to 60 nm in size with a concentration of 10 to 300 ppm. The parameters measured in biodiesel that have been added or not yet added by nanoparticles are density, viscosity, calorivic value and centane number with ASTM D7467 standard. Various combinations of concentration and particle size that have been used as biodiesel additives in various studies are shown in table 1.

Table 1. Summary of fuel properties of biodiesel with soluble additive nano metal oxide

Biodiesel	Nano metal oxide	Size (nm)	Concentrations (ppm)	Density	Viscosity	Flash point	Calorific value	Cetane number	Ref.
J. Curcas	Al$_2$O$_3$	Mean: 51	0	895	5.25	85	38.88	53	[25]
			25	896	5.31	84	39.22	54	
			50	897	5.35	82	39.53	56	
J. Curcas 20% + Diesel 70% + Ethanol 10%	Al$_2$O$_3$		25	837.2 (20 ^{0}C)	2.57	22	39.137	54	[26]
Palm	γ Al$_2$O$_3$	6 - 12	0		4.8	130	38.49	51	[27]
			25		4.76	160	38.52	55	
			50		4.74	168	38.56	59	
			75		4.73	172	38.582	62	
			100		4.73	180	38.59	63	
Rubber seed B20	Al$_2$O$_3$		10		4.1		42000		[28]
			20		4.2		41000		
			30		4.2		41000		

Feedstock	Nanoparticle	Concentration	Density	Viscosity	Flash point	Calorific value	Cetane number	Ref
mustard	TiO_2	100		4.34		37.854	54	[29]
		200		4.38		37.652	57	
C. inophyllum B20	TiO_2	40	844.5	3.72		41.935	53.94	[30]
Canola B20	TiO_2	0	915	4.8			42	[31]
		300	840	3.4			56	
C. inophyllum	TiO_2	0	868.6	4.72	122	38	52	[32]
		50	869.2	4.73	123	37.12	53	
		100	870.4	4.75	124	37.54	55	
Algae	TiO_2 SiO_2	0	0.816 (gm/cc)	3.12	60.49	40.422	47	[33]
		50	817	3.03	62.45	42.6	48	
		100	817	3.01	63.61	44	48	
C. inophyllum	TiO_2	0	815	3.1		43	45	[34]
		100	870	5.1		38	52	
	TiO_2 + Ethanox	100	902	4.7		38	56	
		200	904	4.6		39	58	
		300	910	4.8		39.2	59	

Generally, the increase of the concentration of nanoparticles is proportional to the increase of the density of biodiesel [25][34]. But in other studies, the density is not so affected by the amount of nano particle concentration in biodiesel [27]

Likewise with viscosity, the higher the concentration of nanoparticles, the higher the viscosity on biodiesel [25] [28][29][32][34]. However, other studies state that the higher the concentration of nanoparticles, the lower the viscosity of biodiesel [27][31][35].

Flash points in the study [25] decreased with increasing concentration of nanoparticles. Whereas other research states that the higher the concentration of nanoparticles, the flash point is increasing [27][32][33].

At calorific value, the higher the concentration of nanoparticles, the higher the heat value of biodiesel [25][27][27]. While other studies state that the higher the concentration of nanoparticles, the lower the heating value of biodiesel.

Of the ten studies that have been reviewed, the Cetane number has consistency. The higher the concentration of nanoparticles, the higher the biodiesel cetane number [25][27][29][31][32][35][34]. From all references reviewed, the addition of nanoparticles does not significantly affect the density, viscosity, and flash point values, but the cetane number has a relationship with the addition of nanoparticles. The higher the concentration of nanoparticles, the higher the value of biodiesel cetane number.

ENGINE PERFORMANCE

Brake specific fuel consumption (BSFC)

Brake specific fuel consumption (BSFC) is a comprehensive measurement of fuel consumption in the combustion chamber that presents simultaneously the vehicle's fuel consumed and power produced in a certain time expressed in gr/ kWh unit. In fact, fuel consumption has a higher value than an ideal combustion [36]. Nano cerium oxides (CeO2) particles can reduce brake specific fuel consumption (BSFC) on biodiesel rice bran. Biodiesel 20% and petrodiesel 80% (B20), Biodiesel B20 + CeO2 50ppm, Biodiesel B20 + CeO2 100 ppm were tested using 1 cylinder diesel engine test equipment. Biodiesel without the addition of CeO2 nanoparticles has a higher brake specific fuel consumption (BSFC) value compared to biodiesel with CeO2 nanoparticles [37]. Other research states that the addition of cerium oxide on amide-functionalized multiwall carbon nanotubes (MWCNT) 30, 60, 90ppm to biodiesel of used cooking oil biodiesel 5% (B5) and biodiesel 20% (B20) can reduce BSFC by 0.42%, 0.84% and 3.09% on B5 biodiesel, and 0.34 %, 1.49%, and 4.51% in B20 biodiesel.

Nano CeO_2 supplies oxygen molecules in a chain reaction initiating the burning of hydrocarbon and the uncomplete burned carbon. Burning more fuel in the cylinder produces more energy. Additionally, CeO2 nano prevents the deposition of non-polar components in the cylinder wall and burns residual carbon. Nano catalysts in fuels produce

millions of nano clusters that explode to decompose and destroy deposits and prevent the formation of deposits in the cylinder walls [36].

EMISSION CHARACTERISTIC

Diesel engines have exhaust gas emission parameters comprising carbon monoxide (CO), nitrogen oxide (NOx), and hydrocarbons (HC).

Nitrogen oxides (NOx)

Nitrogen oxide is formed due to the presence of nitrogen in the air. Nitrogen reacts with oxygen during the combustion process. Which affects the amount of NOx content in exhaust gas emissions, among others, combustion temperature, combustion activation energy, and the equivalent ratio in combustion [38]. Biodiesel exhaust gas emissions, containing more NOx compared to petrodiesel due to biodiesel containing oxygen so that the combustion of biodiesel involves more oxygen content and causes the combustion temperature to increase. So the NOx in the exhaust gas increases [39].

The metal oxides in biodiesel escalate the local oxygen content in combustion and extend the duration of diffusion controlled combustion resulting in increased NOx emissions [40] using the additive Al2O3 biodiesel ziziphus B25 the higher the concentration of nanoparticles, the higher the NOx in the flue gas, which is 0 ppm = 3,148 g/ kWh, 25 ppm = 3,456 g/ kWh, and 3,729 g/ kWh. However, other studies have revealed that the higher the concentration of nanoparticles, the lower the NOx concentration in flue gas [25] using AL2O3 and biodiesel jatropha B100 [41] TiO2 Mahua B100 [23] TiO2 Mustard B100 [42] Al2O3 cashew. They are of the opinion that, however, from the whole NOx biodiesel research with additive nano metal oxide there is still more compared to petrodiesel.

Carbon monoxides (CO)

The formation of CO emissions is due to the lack of oxygen in combustion, uneven mixing of air and fuel, and lack of combustion processes. From several references that have been reviewed, CO emissions decrease along with the addition of nanoparticles to biodiesel or a mixture of biodiesel and petrodiesel. With the addition of 200 ppm TiO2 nanoparticles to neat mahua biodiesel oil (BD100) can reduce CO emissions by 9.3% in peak brake power [41]. Zizipus jujube biodiesel methyl ester blended fuel (ZJME25) and nano particle AL2O3 by 25ppm at full load can reduce CO by 22.66% [40]. Cashew nut sell BD100 biodiesel can reduce CO emissions by 57.70% compared to petro diesel. The addition of AL2O3 to BD100 biodiesel cashew nut can reduce CO emissions by 62.29% when compared to petro diesel and can reduce by 10.85% when compared to BD100 biodiesel cashew nut without AL2O3 [42].

Nano metal oxide particles as additives on biodiesel can reduce CO emissions due to the active catalytic effect on metal oxides. The catalytic effect on nano metal oxide increases the rate of mixing of fuel with air during the combustion process, so that the catalyst activity reduces the formation of CO and converts it to CO2[41].

Hydrocarbon (HC)

Hydrocarbon (HC) is formed due to incomplete fuel combustion. Along with increasing power in diesel engines hydrocarbon (HC) emissions will also increase because more fuel injection is needed to maintain a constant speed at high power. Insufficient oxygen content in incomplete combustion can result in increased amounts of hydrocarbon (HC) in the flue gas [43].

The oxygen content in biodiesel contributes to HC oxidation thereby reducing the HC content in the flue gas. Adding nano metal oxides can also escalate the oxygen content in biodiesel. The addition of Al2O3 nano metal oxide to *Zizipus jujube* biodiesel methyl ester blended fuel (ZJME25) can reduce HC emissions by 25% at 25ppm and up to 36.11% at 50ppm addition compared without using nano metal oxide [40]. Cashew nut sell BD100 biodiesel can reduce HC in exhaust emissions by 20.83% compared to petrodiesel. And with the addition of nano Al2O3 to biodiesel biodiesel BD100 can reduce HC content in exhaust gas by 27.08% compared to petrodiesel.

SUMMARY

This review provides an overview of the development of the use of nano metal oxide as a soluble nano catalyst in biodiesel. The conclusions of the above review are the following:

1. From all references reviewed, the addition of nanoparticles does not significantly affect the density, viscosity, and flash point values, but the cetane number has a relationship with the addition of nanoparticles. The higher the concentration of nanoparticles, the higher the value of biodiesel cetane number.

2. The addition of nano metal oxide can reduce the brake specific fuel consumption (BSFC) of biodiesel because nano metal oxide contains oxygen molecules which can oxidize hydrocarbons and carbon monoxide. More fuel burned causes the energy produced is also greater and decreases fuel consumption.

3. The addition of nano metal oxide to biodiesel and its mixture did not significantly influence NOx, but CO and HC dropped significantly due to the catalytic effect of nano metal oxide on combustion in the combustion chamber.

REFERENCES

[1]   Goncalves, E. G., & Lorenzi, H. Morfologia Vegetal. 2007

[2]   H. Haberl, T. Beringer, S. C. Bhattacharya, K. H. Erb, and M. Hoogwijk, "The global technical potential of bio-energy in 2050 considering sustainability constraints," *Curr. Opin. Environ. Sustain.*, vol. 2, no. 5–6, pp. 394–403, 2010.

[3]   A. Demirbas, "Biodiesel production from vegetable oils via catalytic and non-catalytic supercritical methanol transesterification methods," *Prog. Energy Combust. Sci.*, vol. 31, no. 5–6, pp. 466–487, 2005.

[4]   H. Fukuda, A. Kond, and H. Noda, "Fukuda-H._2001_Biodiesel-fuel-production-by-transesterification-of-oils.pdf," vol. 92, no. 5, 2001.

[5]   J. Van Gerpen, "Biodiesel processing and production," *Fuel Process. Technol.*, vol. 86, no. 10, pp. 1097–1107, 2005.

[6]   S. K. Hoekman and C. Robbins, "Review of the effects of biodiesel on NOx emissions," *Fuel Process. Technol.*, vol. 96, pp. 237–249, 2012.

[7]   O. Özener, L. Yüksek, A. T. Ergenç, and M. Özkan, "Effects of soybean biodiesel on a DI diesel engine performance, emission and combustion characteristics," *Fuel*, vol. 115, no. 10, pp. 875–883, 2014.

[8]   S. M. A. Rahman, H. H. Masjuki, M. A. Kalam, M. J. Abedin, A. Sanjid, and H. Sajjad, "Production of palm and Calophyllum inophyllum based biodiesel and investigation of blend performance and exhaust emission in an unmodified diesel engine at high idling conditions," *Energy Convers. Manag.*, vol. 76, pp. 362–367, 2013.

[9]   B. S. Chauhan, N. Kumar, and H. M. Cho, "A study on the performance and emission of a diesel engine fueled with Jatropha biodiesel oil and its blends," *Energy*, vol. 37, no. 1, pp. 616–622, 2011.

[10]   H. Raheman and S. V Ghadge, "Performance of compression ignition engine with mahua (Madhuca indica) biodiesel," vol. 86, pp. 2568–2573, 2007.

[11]   A. Dhar, R. Kevin, and A. Kumar, "Production of biodiesel from high-FFA neem oil and its performance , emission and combustion characterization in a single cylinder DICI engine," *Fuel Process. Technol.*, vol. 97, pp. 118–129, 2012.

[12]   B. Ashok, K. Nanthagopal, and D. S. Vignesh, "Calophyllum inophyllum methyl ester biodiesel blend as an alternate fuel for diesel engine applications," *Alexandria Eng. J.*, 2017.

[13]   H. G. How, H. H. Masjuki, M. A. Kalam, Y. H. Teoh, and H. G. Chuah, "E ff ect of Calophyllum Inophyllum biodiesel-diesel blends on combustion , performance , exhaust particulate matter and gaseous emissions in a multi- cylinder diesel engine," *Fuel*, vol. 227, no. October 2017, pp. 154–164, 2018.

[14]   O. Herbinet, W. J. Pitz, and C. K. Westbrook, "Combustion and Flame 154 (2008) 507-528 Detailed chemical kinetic oxidation mechanism for a biodiesel surrogate," vol. 154, pp. 507–528, 2008.

[15]   K. Varatharajan and M. Cheralathan, "Influence of fuel properties and composition on NO x emissions from biodiesel powered diesel engines: A review," *Renew. Sustain. Energy Rev.*, vol. 16, no. 6, pp. 3702–3710, 2012.

[16]   Z. Gong, W. Wenfei, Z. Zhao, and B. Li, "Combination of catalytic combustion and catalytic denitration on semi-coke with Fe2O3 and CeO2," *Catal. Today*, vol. 318, no. 2010, pp. 59–65, 2018.

[17] T. A. Wierzbicki, I. C. Lee, and A. K. Gupta, "Combustion of propane with Pt and Rh catalysts in a meso-scale heat recirculating combustor," *Appl. Energy*, vol. 130, pp. 350–356, 2014.

[18] P. Taylor, B. Zhong, F. Yang, and Q. Yang, "Combustion Science and Technology Catalytic Combustion of n-C 4 H 10 and DME in Swiss-Roll Combustor with Porous Ceramics," no. October 2014, pp. 37–41.

[19] Y. Wang *et al.*, "Combustion of hydrogen-air in micro combustors with catalytic Pt layer," *Energy Convers. Manag.*, vol. 51, no. 6, pp. 1127–1133, 2010.

[20] D. T. Wickham, R. Cook, S. De Voss, J. R. Engel, and J. Nabity, "SOLUBLE NANO-CATALYSTS FOR HIGH PERFORMANCE FUELS ∗ Introduction . Combustion Enhancement," vol. 27, no. 6, pp. 552–561, 2006.

[21] T. Puzyn *et al.*, "Using nano-QSAR to predict the cytotoxicity of metal oxide nanoparticles," *Nat. Nanotechnol.*, vol. 6, no. 3, pp. 175–178, 2011.

[22] G. Najafi, "Diesel engine combustion characteristics using nano-particles in biodiesel-diesel blends," *Fuel*, vol. 212, no. January, pp. 668–678, 2018.

[23] D. Yuvarajan, M. Dinesh Babu, N. BeemKumar, and P. Amith Kishore, "Experimental investigation on the influence of titanium dioxide nanofluid on emission pattern of biodiesel in a diesel engine," *Atmos. Pollut. Res.*, vol. 9, no. 1, pp. 47–52, 2018.

[24] P. C. Srinidhi, A. Madhusudhan, and S. V Channapattana, "E ff ect of NiO nanoparticles on performance and emission characteristics at various injection timings using biodiesel-diesel blends," *Fuel*, vol. 235, no. March 2018, pp. 185–193, 2019.

[25] J. S. B. R. B. Anand, "The influence of nano additive blended biodiesel fuels on the working characteristics of a diesel engine," pp. 257–264, 2013.

[26] H. Venu and V. Madhavan, "Effect of Al2O3nanoparticles in biodiesel-diesel-ethanol blends at various injection strategies: Performance, combustion and emission characteristics," *Fuel*, vol. 186, pp. 176–189, 2016.

[27] R. L. Krupakaran, T. Hariprasasd, A. Gopalakrishna, and P. Babu, "The performance and exhaust emissions investigation of a diesel engine using γ-Al2O3 nanoparticle additives to biodiesel," *Carbon Manag.*, vol. 7, no. 3–4, pp. 233–241, 2016.

[28] S. Mahalingam and S. Ganesan, "Effect of nano-fuel additive on performance and emission characteristics of the diesel engine using biodiesel blends with diesel fuel," *Int. J. Ambient Energy*, vol. 0, no. 0, pp. 1–6, 2018.

[29] D. Yuvarajan, M. D. Babu, N. Beemkumar, and P. A. Kishore, "Experimental investigation on the in fl uence of titanium dioxide nano fl uid on emission pattern of biodiesel in a diesel engine," *Atmos. Pollut. Res.*, no. x, pp. 1–6, 2017.

[30] A. Praveen, G. L. N. Rao, and B. Balakrishna, "Performance and emission characteristics of a diesel engine using Calophyllum Inophyllum biodiesel blends with TiO 2 nanoadditives and EGR," *Egypt. J. Pet.*, 2017.

[31] S. Nithya, S. Manigandan, P. Gunasekar, J. Devipriya, and W. S. R. Saravanan, "The Effect of engine emission on canola biodiesel blends with TiO 2," vol. 0750, no. December, 2017.

[32] K. Nanthagopal, B. Ashok, A. Tamilarasu, A. Johny, and A. Mohan, "Influence on the effect of zinc oxide and titanium dioxide nanoparticles as an additive with Calophyllum inophyllum methyl ester in a CI engine," *Energy Convers. Manag.*, vol. 146, pp. 8–19, 2017.

[33] S. Karthikeyan and A. Prathima, "Environmental effect of CI engine using microalgae methyl ester with doped nano additives," *Transp. Res. Part D*, vol. 50, pp. 385–396, 2017.

[34] P. Gunasekar, S. Manigandan, N. Ilangovan, S. Nithya, and J. Devipriya, "Effect of TiO2 and nozzle geometry on diesel emissions fueled with biodiesel blends," *Int. J. Ambient Energy*, vol. 0, no. 0, pp. 1–19, 2017.

[35] S. Karthikeyan and A. Prathima, "Environmental Effects Environmental effect of CeO 2 nanoadditive on biodiesel," vol. 7036, no. November, 2016.

[36] M. Mirzajanzadeh, M. Tabatabaei, M. Ardjmand, and A. Rashidi, "A novel soluble nano-catalysts in diesel – biodiesel fuel blends to improve diesel engines performance and reduce exhaust emissions," *FUEL*, vol. 139, no. x, pp. 374–382, 2015.

[37] S. Karthikeyan, A. Elango, and A. Prathima, "The effect of cerium oxide additive on the performance and emission characteristics of a CI engine operated with rice bran biodiesel and its blends," *Int. J. Green Energy*, vol. 13, no. 3, pp. 267–273, 2016.

[38] M. Mofijur, H. H. Masjuki, M. A. Kalam, and A. E. Atabani, "Evaluation of biodiesel blending, engine performance and emissions characteristics of Jatropha curcas methyl ester: Malaysian perspective," *Energy*,

vol. 55, pp. 879–887, 2013.

[39] G. Tüccar, E. Tosun, T. Özgür, and K. Aydin, "Diesel engine emissions and performance from blends of citrus sinensis biodiesel and diesel fuel," *Fuel*, vol. 132, pp. 7–11, 2014.

[40] C. S. Aalam, C. G. Saravanan, and M. Kannan, "Experimental investigations on a CRDI system assisted diesel engine fuelled with aluminium oxide nanoparticles blended biodiesel," *Alexandria Eng. J.*, vol. 54, no. 3, pp. 351–358, 2015.

[41] A. K. Pandian, R. B. B. Ramakrishnan, and Y. Devarajan, "Emission analysis on the effect of nanoparticles on neat biodiesel in unmodified diesel engine," *Environ. Sci. Pollut. Res.*, vol. 24, no. 29, pp. 23273–23278, 2017.

[42] S. Radhakrishnan, D. B. Munuswamy, Y. Devarajan, T. Arunkumar, and A. Mahalingam, "Effect of nanoparticle on emission and performance characteristics of a diesel engine fueled with cashew nut shell biodiesel," *Energy Sources, Part A Recover. Util. Environ. Eff.*, vol. 40, no. 20, pp. 2485–2493, 2018.

[43] M. Annamalai *et al.*, "An assessment on performance, combustion and emission behavior of a diesel engine powered by ceria nanoparticle blended emulsified biofuel," *Energy Convers. Manag.*, vol. 123, pp. 372–380, 2016.

Reinforcement Modeling of Building Beams Using Glass Fiber Reinforced Polymer (GFRP) Due to Building Function Changes in Jember

Maudy Anggie Permata Putri[1,a)], Winda Tri Wahyuningtyas[2,b)], Dwi Nurtanto[3,c)]

[1,2,3]*Civil Engineering Departement, Engineering Faculty, Jember University*

[a)]maudyanggiepp97@gmail.com
[b)]windatri.teknik@unej.ac.id
[c)]dwinurtanto.teknik@unej.ac.id

Abstract. One of effort to increase the space in the building is by adding a floor up. Additions to the upper floors can be done on limited land. However, the addition of the floor causes the ring balk function change becomes the floor beam function. Changing the function of the ring balk becomes floor beam makes the load received by the beam increase. The different types of dead loads and live loads received cause the beam reinforcement is needed. One of the reinforcement methods that can be done is by using Fiber Reinforced Polymer (FRP) material. The advantages of Fiber Reinforced Polymer (FRP) materials are lighter, have high tensile strength, not corrosion, easy to install, and easily formed. In this case, Glass Fiber Reinforced Polymer (GFRP) material is selected. This material is one type of FRP with cheaper price compared to other FRP types. Coating ring balk with GFRP aims to allow the ring balk as a floor beam function without having to destroy it as a whole. So, this case does not interfere with ongoing activities in that building. This study was conducted by modeling a 3 floors into 6 floors building with concrete roof using structure analysis program. The 35/40 ring balk will be function as a main beam on the 4[h] floor assuming a size of 45/60 with an additional beam of 40/50 to be able to withstand the load given. The results of the maximum moment (Mu = 20845.75 kgm) on the 4th floor main beam are a reference to determine the GFRP needed for reinforcement. Reinforcement is done by coating the beams with 1 mm of GFRP as much as 3 layers on 3 sides of the beam. Based on the analysis carried out it produces øMn (=21893.2861 kgm) > Mu (= 20845.75 kgm). Deflection which calculated composite is 3.63 mm.

INTRODUCTION

In the initial planning of a building, structural elements are designed to firmly withstand dead loads and live loads according to the planned analysis. Changing the function of the ringbalk becomes floor beam makes the load received by the beam increase. The type of load received by the beam is certainly greater than the original load. Based on these problems, innovations in reinforcement on beam structural elements can be carried out using lightweight materials such as Glass Fiber Reinforced Polymer (GFRP). According to Parmo and Taufikurrahman (2013), the advantages of Fiber Reinforced Polymer (FRP) materials are lighter, have high tensile strength, are not corrosion, easy to install, and are easily formed. In addition, another advantage of reinforcement using Glass Fiber Reinforced Polymer (GFRP) is to coat the beam and do not need to destroy the beam as a whole. This certainly does not interfere with the ongoing activities in the building. This study aims to determine the modeling of the change in ringbalk function into floor beams on the structure of the building and GFRP needed to reinforce the ringbalk so that it can be the floor beam function.

METHOD

This study uses the Teacher Training and Education Faculty H Building of Jember University, located on Jalan Kalimantan No. 37, Jember. The building is a 3-story building that will be added to the modeling until the ringbalk is not able to withstand the load given. The secondary data obtained includes the compressive strength of concrete (= 20.75 MPa), steel tensile strength (= 320 MPa), the ringbalk dimension (= 35 cm x 40 cm).

Research Flow Chart

Analysis and modeling on the part of the building beam will be presented through the flow diagram on **Figure 1** as follows.
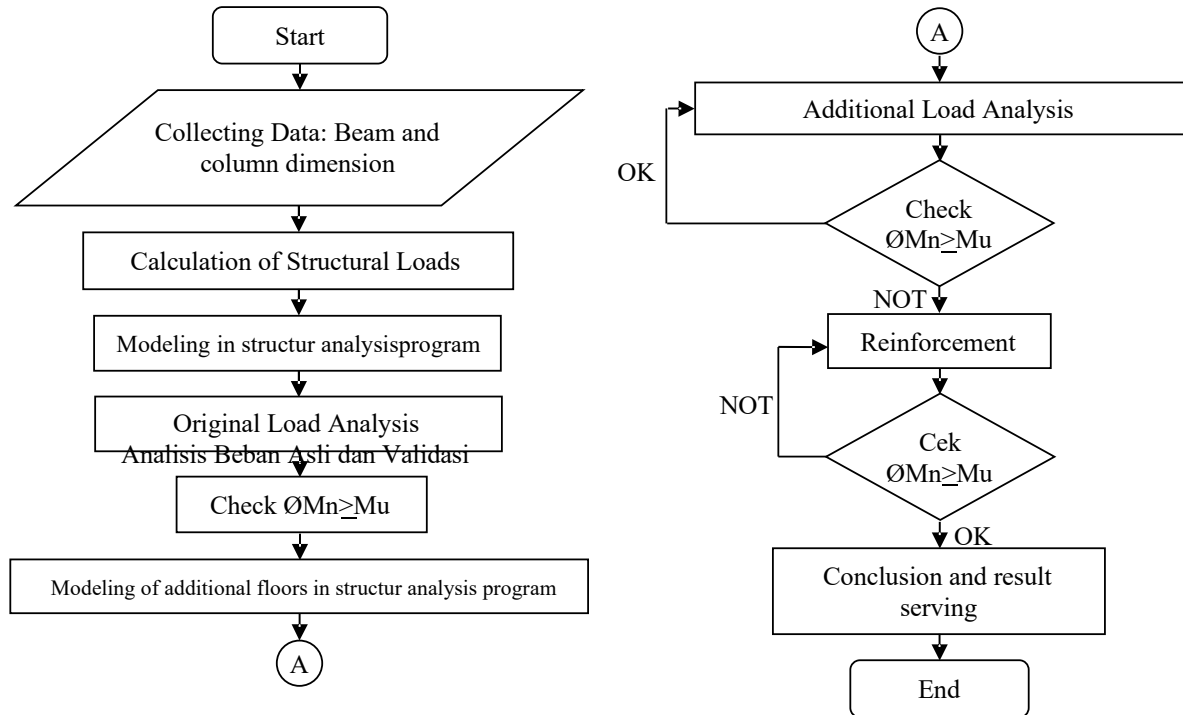
Figure 1. Research Flow Chart

DISCUSSION

Loading on the initial structure of the 3-story building

The loading is carried out using the envelope method, then checking the capacity of the ringbalk structure components using the structure analysis program. In **Figure 2**, the result of checking the capacity of the structure produces green, so the building structure falls into the safe category.
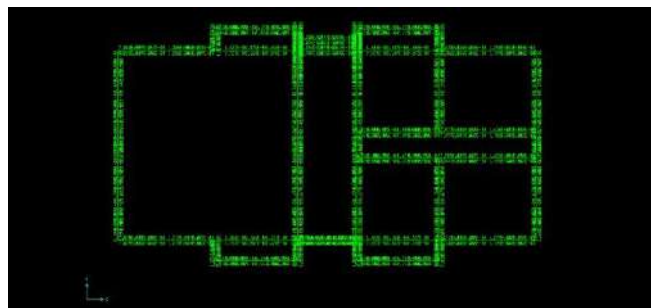
Figure 2. The result of checking the capacity of the ringbalk structure components

New floor beam dimension planning

In order to be able to function as a floor, additional beams need to be done. The beam dimensions on the 4 th floor are calculated based on the preliminary design which results in the dimensions of the beam of 40/50, the reference beam of 45/60 and the column of 70/70. The placement of the beam is marked in orange in **Figure 3** below.
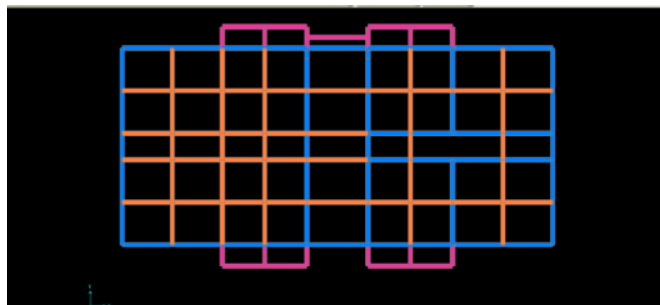
Figure 3. Additional beam

After checking the capacity in structure analysis program, **Figure 4** shows the green color of the 45/60 beam structure and 40/50 additional beam, so that it can be categorized in a decent or safe condition.
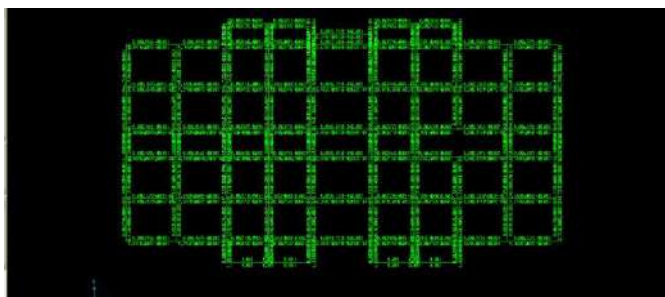
Figure 4. The result of checking the capacity of the 4 th floor beam structure components

Table 1. Moment and Shear of the Beam

	Initial Ringbalk of 3-story building	Main beam of 4th floor as a reference
Dimension (cm)	35/40	45/60
Moment (kgm)	4560.13	20845.75
Shear (kg)	6356.99	15616.04

Strengthening on Ringbalk Using GFRP

Strengthening using the E-Glass Woven Roving will be carried out on the ringbalk so that it can be function as a 4th floor beam which refers to ACI 440.2R-17.
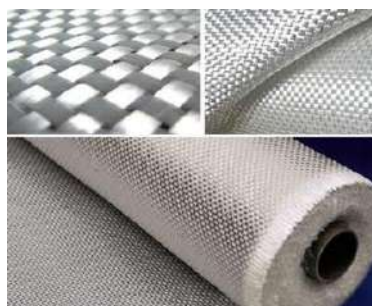
Figure 5. E-Glass Woven Roving [14]

Table 2. Beams Before Reinforcement Data

Parameter	Amount	Unit
Compressive strength of concrete (f'c)	20.75	MPa
Tensile strength of steel (fy)	320	MPa
Width of beam (b)	350	mm
Height of beam (h)	400	mm
Diameter of circular section (D)	16	mm
Concrete coat thick (ts)	25	mm
Enviromental reduction factor (Ce)	0.75	
GFRP ultimate tensile strength (f_{fu}*)	2680	MPa
Strain level of GFRP (ε_{fu}*)	0.045	
Elastic modulus of GFRP (E_f)	72000	MPa
Thick of GFRP (t_f)	1	mm
Elastic modulus of steel (E_s)	200000	MPa
Elastic modulus of concrete (E_c)	21409.519	MPa
Mu of 45/60 beam (planning moment)	20845.75	kgm

Table 3. Calculation of beam bending after strengthening by GFRP

Parameter	Amount	Unit
Area of circular section (As)	1408	mm^2
Distance of circular section center to the concrete side (d')	33	mm
Effective height of beam (d)	367	mm
Ratio of nonprestressed reinforcement (ρs)	0.011	
Width of GFRP (Wf)	350	mm
Amount of GFRP layer (n)	3	lapis
Cross-sectional area of GFRP (Af)	1050	mm^2
Design ultimate tensile strength of GFRP (ffu = Ce x ffu*)	2010	MPa
Design rupture strength of GFRP (Ɛfu = Ce x Ɛfu*)	0.034	
GFRP reinforcement ratio (ρf)	0.008	
Stiffness with GFRP (k)	0,4	
Ratio of area of circular section to beam cross-sectional area (ρg)	0.01006	
β₁ (f'c ≤ 30 MPa)	0.85	
M_{DL}	134946600	Nmm
Icr	613199433.7	mm^4
Strain level at installation of GFRP (ε_{bi})	0.0026	
Debonding strain of GFRP (ε_{fd})	0.004	
Effective strain level of GFRP (ε_{fe})	0.0033	

Strain level of concrete (ε_c)	0.003	
Strain level of steel (ε_s)	0.0052	
Stress in steel reinforcement (fs)	320	MPa
Effective stress in GFRP (ffe)	237.9721	MPa
Maximum strain of concrete corresponding to f'c ($\varepsilon'c$)	0.0016	
Stress factor β_1	0.924	
Stress factor α_1	0.7746	
Depth of neutral axis (c)	134.7566	mm
Flexural component strength Mns	137304321.1	Nmm
Flexural component strength Mnf	84391690.46	Nmm
Net tensile strain (εt)	0.0016	
ψf (*3-side "U-wrap"*)	0.85	

The flexural strength produced by reinforcing beams uses the GFRP as follows.

$$\emptyset M_n = \emptyset [M_{ns} + \psi_f \times M_{nf}] + \emptyset M_{n \text{ initial of ringbalk}}$$
$$= 0.65 [137304321.1 + 0.85 \times 84391690.46] + 0.75 (110744858)$$
$$= 218932861 \text{ Nmm}$$
$$= 21893.2861 \text{ kgm} \geq M_u = 20845.75 \text{ kgm} \tag{1}$$

The deflection that occurred in the beam after reinforced using GFRP was equal to 3.63 mm < permit deflection (= 11.111 mm). While the shear strength produced is $\emptyset Vn$ (= 6196337.584 kg) > Vu (= 15616.04 kg).
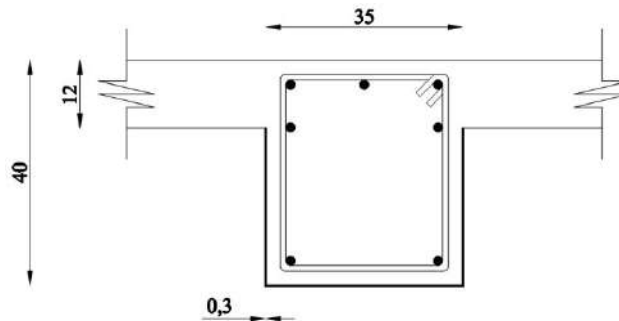
Figure 7. Beam sketch that have been coated by GFRP

CONCLUSION

Based on the results of Reinforcement Modeling of Building Beams Using Glass Fiber Reinforced Polymer (GFRP) Due to Building Function Changes in Jember, it can be conclude as follows.

1) This study was conducted by modeling 3 floors into 6 floors building with concrete roof using structure analysis program. The 35/40 ringbalk will function as a main beam on the 4th floor assuming a size of 45/60 with an additional beam of 40/50 to be able to withstand the load given. The results of the maximum moment (Mu = 20845.75 kgm) on the 4th floor main beam are a reference to determine the GFRP needed for reinforcement.

2) Strengthening is done by coating the beams with 1 mm of GFRP as much as 3 layers on 3 sides of the beam. Based on the analysis carried out it produces øMn (=21893.2861 kgm) > Mu (= 20845.75 kgm).

SUGGESTION

Based on the evaluations of Reinforcement Modeling of Building Beams Using Glass Fiber Reinforced Polymer (GFRP) Due to Building Function Changes in Jember, there are several suggestions that need to be considered, namely:

1) To apply reinforcement to other components of the building structures, such as columns and plates.
2) To analyze the type of collapse due to the connection that occurs between the beam and the addition of GFRP
3) To strengthen building structures with laboratory tests.
4) To analyze the connections that occur between beams.

REFERENCES

1. ACI Committe 440. (2017). *ACI 440.2R-17: Guide for the Design and Construction of Externally Bonded FRP Systems for Strengthening Concrete Structures*. American Concrete Institute, Farmington Hills

2. Badan Standardisasi Nasional. (2012). *SNI 1726 – 2012: Tata Cara Perencanaan Ketahanan Gempa untuk Struktur Bangunan Gedung dan Non-Gedung*. Badan Standardisasi Nasional, Jakarta

3. Badan Standardisasi Nasional. (2013). *SNI 1727 – 2013: Bebam Minimum untuk Perancangan Bangunan Gedung dan Struktur Lain*. Badan Standardisasi Nasional, Jakarta

4. Badan Standardisasi Nasional. (2013). *SNI 2847 – 2013: Persyaratan Beton Struktural untuk Bangunan Gedung*. Badan Standardisasi Nasional, Jakarta

5. Boen, T. (2009). *Cara Memperbaiki Bangunan Sederhana yang Rusak Akibat Gempa Bumi*. Australia–Indonesia Facility for Disaster Reduction, Jakarta

6. Ginardi, I. P. (2014). "Perbandingan Kekuatan Lentur Balok Beton Bertulang dengan Menggunakan Perkuatan CFRP dan GFRP". Jurnal Mahasiswa Jurusan Teknik Sipil 1 (2), 1-8.

7. Hermanto, E. dan F. Kistiyani. (2006). "Kegagalan Bangunan dari Sisi Industri Konstruksi". Media Komunikasi Teknik Sipil 14 (1), 51-52.

8. Kaontole, J. T., M. D. J. Sumajouw, dan R. S. Windah. (2015). "Evaluasi Kapasitas Kolom Beton Bertulang yang Diperkuat dengan Metode *Concrete Jacketing*". Jurnal Sipil Statik 3 (3), 167-174.

9. Kiswono, B. dan E. Jayanto. (2017). "Studi Perbaikan Balok Beton Bertulang Menggunakan Glass Fiber Reinforced Polymer (GFRP) untuk Meningkatkan Kekuatan Tarik pada Bending Momen". Agregat 2 (2), 159-165.

10. Nugraini, S. (2017). Skripsi: Analisis Pemodelan Kegagalan Struktur dan *Retrofitting* pada Bagian Kolom Gedung 8 Lantai. Program Studi S1 Teknik Sipil Universitas Jember, Jember.

11. Nurlina, S., H. Suseno, M. T. Hidayat, dan I. M. Y. Pratama. (2016). "Perbandingan Daktilitas Balok Beton Bertulang dengan Menggunakan Perkuatan CFRP dan GFRP". Rekayasa Sipil 10 (1), 62-68.

12. Parmo dan Taufikurrahman. (2013). "Perbaikan Kekuatan dan Daktilitas Balok Beton Bertulang Menggunakan *Glass Fiber Reinforced Polymer* (GFRP) *Strips*". Jurnal Ilmu-Ilmu Teknik 10 (3), 63-70.

13. Sudarsana, K. dan A. A. Gede Sutapa. (2007). "Perkuatan Kolom Bulat Beton Bertulang dengan Lapis *Glass Fiber Reinforced Polymer* (GFRP)". Jurnal Ilmiah Teknik Sipil 11 (1), 1-9.

14. Jiahe Taizo Glass Fiber Co, Ltd. Woven Roving http://www.jhblxw.com.cn/eng/product/18_54

Biogeotechnical – Environmental Remediation using Natural Grown Philippine Bamboo Species for Soil Slope Stabilization

*Cesario A. Bacosa Jr.[1, 2], Marnie B. Giduquio [1], Michael E. Loretero [1]

[1]School of Engineering, University of San Carlos, Cebu City, Philippines , [2]Western Philippines University, Palawan, Philippines.

[1,2] *bacosao81976@yahoo.com ,   [1] mbgiduquio@gmail.com , [1] mloretero@yahoo.com

ABSTRACT

This paper presents the importance of plant root systems to the stability of slopes, particularly on engineered cut slopes. The locally grown plant of study is the selected common Philippine bamboo species such as Kawayan Tinik *(Bambusa Blumeana Schultes),* Bayog *(Dendrocalamus Merrillianus Elmer),* Kawayan Kiling *(Bambusa Vulgaris Schrader) a*nd Patong *(Dendrocalamus Asper Schultes)*. It is native to tropical and temperate Asia and the Pacific Islands that grows widely, abundantly in the moist areas, riverbanks and sloppy areas in the Philippines. The study determined the effects of roots strength of the Philippine bamboo species on soil properties and soil slope factor of stability. This study used the single group design of experimental research which attempts to establish cause-and-effect relationship with the alleged cause manipulated. The material used in the study was composed of plant roots sample from the slope areas. Likewise, the study used the standard tools and equipment to determine the properties of soil. The material selection and preparation were in accordance of the standard requirements of the American society of testing materials with three (3) sets of samples in each stratified site. The following were the detailed research procedures; (1) Site visit and exploration (2) Collection of Sample, (3) Plant Physical properties analysis, (4). Root strength test., (5) Analyses the result of the laboratory test and see how effective does the sample used for slope protection, and (7) Comparison of the strength of   other plant tensile strength to bamboo roots tensile strength. The results revealed that roots of Philippine Bamboo species make the soil stable and developed high internal friction, cohesion, develops high strength preventing immediate erosion and landslide. The void spaces between the soil particles filled up by bamboo roots systems and the result arguably, implies that the higher the plant age, the higher the plant diameter and height, thus the higher pull out resistance. A higher level of plant diversity generally associated with natural regeneration, may increase slope stability that offered by monospecific and single age plantings. The use of Philippine Bamboo species such as Kawayan Tinik *(Bambusa Blumeana Schultes*), Bayog *(Dendrocalamus Merrillianus Elmer)*, Kawayan Killing (*Bambusa Vulgaris Schrader)* and Patong *(Dendrocalamus Asper Schultes)* as vegetation in cut slope, hillslope, and riverbanks can minimize and prevent erosion and shallow landslides.

Keywords: Bioengineering, Root Strength, Vegetation, Landslide, Slope Stabilization, Biotechnical, Geotechnical- Environmental Remediation.

INTRODUCTION

The importance of plant root systems to the stability of slopes has received considerable attention in recent years particularly on engineered cut slopes; this is bioengineering for slope stabilization. Roots can influence slope Stability through hydrological and mechanical factors.

[1] Soil-bioengineering has been mostly used in controlling erosion, but it has also been shown to be successful in stabilization of slopes against shallows failures. [2] The root systems can contribute an additional component to the shearing resistance. Roots help stabilize hill slopes by reinforcing soil shear strength. To evaluate the effect of roots on slope stability, information about the number of roots and their strength should be known affected in a major way [3]. The positive effect of roots on soil stability depends both on the tensile strength of the individual roots [10] and on the spatial distribution of the root ass in the soil the roots,[4] Plants are very much vital and have an important role in natural built environment that will be used in slope stabilization.[5]

Forest vegetation, especially tree roots, helps stabilize slope by reinforcing soil shear strength. The roots increase the shear strength of soil by transmitting developed shear stress to tension strength. The additional strength created by roots is defined as the growing cohesion, which increases with vertical stress and area occupied by the roots. Roots can be influence slope stability through hydrological and mechanical factors. To evaluate the effect of tree roots on slope stability, information about the number of roots and their strength should be known. [Greenwood, J.; Norris, J. & Wint, J. 2004].

Tree roots, helps stabilized hill slopes by reinforcing soil shear strength. To evaluate the effect of tree roots on slope stability, information about the number of roots and their strength should be known affected in a major way.Vegetation may be used in slope protection to prevent or reduce erosion from precipitation, surface runoff, and internal seepage or piping. In this instance, the vegetation using various types of bamboo may replace one or more layers of granular filter materials which would be placed on the slope in conventional application. The plant is the one of the most common weeds that grow widely and abundantly throughout the tropics, especially in the moist areas, and can be found in Palawan ocean Islands [6].

Bamboo is found in abundance been used fully to its extent although it is considered as natural engineering material [6]. The bamboo is grown in various continents of the world (Table 1). The Asia–Pacific bamboo region is the largest bamboo growing area in the world [7, 8]. Asia has large area of bamboo is occupied by six countries viz. India, China, Indonesia, Philippines, Myanmar, Vietnam and others. Globally among sympodial and monopodial, sympodial type of bamboo dominates major part [9].

Table 1: Bamboo regions along with countries [9].

Bamboo region	Countries
1. Asia–Pacific	China, India, Burma, Thailand, Bangladesh, Cambodia, Vietnam, Japan, Indonesia, Malaysia, Philippines, Korea and Sri Lanka
2. American bamboo Region (Latin America, South America and North America)	Mexico, Guatemala, Costa Rica, Nicaragua, Honduras, Columbia, Venezuela and Brazil
3. African bamboo region	Mozambique, Eastern Sudan
4. European countries	England, France, Germany, Italy, Belgium, Holland. United States and Canada have introduced a large number of bamboo species from Asian and Latin American bamboo producing countries

In the Philippines and in the rest of South and Southeast Asia, the versatility of bamboo is apparent from its many uses as containers, ornaments, toys, food supplements, musical instruments, structural components, and various industrial items (Tamolang et al., 1980). Other uses for example, bamboo leaf ash stabilization on lateritic soil in highway construction **(Amu & Adetuberu, 2010),** ethnobotanical uses **(Sharma and Borthakur,2008)** and many more.

Of the 62 bamboo species which are shown in (Table 2), 21 are endemic or native Philippine bamboos. Thirteen are climbers and eight are erect. The rest are introduced and a few of them, introduced in prehistoric times [10 – 13]. The commercially important bamboos which are usually used in construction, furniture, basketry and decorative articles are shown in (Table 3). The current commercial bamboos can be increased to 15 species, especially those with thick culm walls and big-diameter culms which include *Bambusa bambos* (L.) Voss, *B. oldhamii* Munro, *B. utilis* Lin, *Dendrocalamus latiflorus* Munro D., *giganteus* Munro, and *Guadua angustifolia* Kunth [14 -18]. It cannot grow in the shade. It prefers moistsoil. Synonyms: Arundarbor bitung (Schultes.) Kuntze Arundo aspera (Schult.f.) Oken Arundo piscatoria Lour. Bambusa as.

Figure 1 *Dendrocalamus Asper Schultes*   **Figure 2.***Dendrocalamus Merrillianus Elmer*

Figure 3. *Bambusa Blumeana Schultes*   **Figure 4. *Bambusa Vulgaris Schrader***

The main objective of this study to describe the bamboo root strength capacity , root   Tensile strength, root Shear strength, root pull out strength and its effects to slope soil Moisture content, Liquid limit, Plastic limit, Cohesion, angle of internal friction, and Factor of safety of the slope areas.

METHODOLOGY

This study used the single group design of experimental research which attempts to establish cause-and-effect relationship with the alleged cause manipulated. The material used in the study was composed of plant roots sample from the slope areas. Likewise, the study used the

standard tools and equipment to determine the properties of soil.The material selection and preparation was in accordance of the standard requirements of the American society of testing materials (ASTM), (AASHTO) and the bureau of research and standards (BRS).The materials used were stratified taken from slope areas there were nine (9) samples each stratified area. This study used the standard procedure of materials selection and testing of the three (3) sets of samples in each stratified site. The said laboratory procedure was derived from the engineering manual for materials testing and laboratory. The following were the detailed research procedures; (1) Site visit and exploration (2) Collection of Sample, (3) Plant Physical properties analysis, (4). Root strength test., (5) Analyses the result of the laboratory test and see how effective does the sample used for slope protection, and (7) Comparison of the strength of vetiver grass and other plant tensile strength to bamboo roots tensile strength. In considering tree and plant anchorage and resistance of the roots to failure, root tensile strength was a factor. Root tensile strength averages for plants and trees by vary species.

RESULTS AND DISCUSSION

3.1Bamboo roots strength.

Tensile strength is resistance of a material to breaking under tension. the resistance of a material to breaking under tensionThe root strength of *Dendrocalamus merrillianos E.* roots ranging from 9988.948 kPa to 3745.856 kPa and the load (g) ranging from 3000g to 1200g.The root strength of *Bambusa vulgaris S.* roots ranging from 12763.656 kPa to 4682.320 kPa and the load (g) ranging from 2300g to 1500g, the root strength of *Dendrocalaus asper S.* roots ranging from 13873.539 kPa to 6555.247 kPa and the load (g) ranging from 2500g to 1800g.The results reveal the root test of *Dendrocalamus merrillianos E., Dendrocalamus asper S., and Bambusa vulgaris S.* has a tensile strength of 9988.948 kPa, 12763.656 kPa, and 13873.539 kPa. This implies the root test to hold soil and rock and prevent immediate erosion. The roots that penetrate to the soil and slope materials is considered as one solution to minimize and prevent erosion.The Bamboo *root* strength and the root effect to hold soil and rocks and prevent immediate erosion. The Shear strength of the obtained soil without roots ranges from 0.34 to 0.97 [kPa], its mean shear strength was 0.58 kPa while soil with bamboo roots shear strength ranges from 4.2 to 14.4 [kPa], its mean shear strength was 8.2 [kPa]. The pull-out strength of Bamboo roots averaged from 1376.67 to 1814.97 [KN]. The pull-out strength means the force that would have to be applied to roots anchorage. And holding capacity.

Table 2 . Plants root Tensile strength [9] compared to Bamboo root tensile strength.

Botanical name	Common Name	Tensile Strength (MPa)	Average (MPa)
Salix spp	Willow	9-36	22.5
Populus spp	Poplars	5-38	21.5
Alnus spp	Alders	4-74	39
Pseudotsuga spp	Douglas fir	19-61	38.5
Acer sacharium	Silver maple	15-30	22.5
Tsuga heterophylia	Western Hemlock	27	27
Vaccinum spp	Huckleberry	16	16
Hordeum vulgare	Barley Grass	15-31	23

Vetiveria Zizaniodes	Vetiver Grass	40-120	80
Melastoma Clavarei H. Vaniot	Malatungaw		81.53
Melastoma Malabathricum sp.	Amomocil	130.71	81.48
*Dendrocalamus Asper Schultes.	**Patong**	**56.18 – 138.73**	**86.43**
*Dendrocalamus Merrillianos Elmer.	**Bayog**	**37.48 – 99.88**	**57.07**
*Bambusa Vulgaris Schrad.	**Kawayan Tiring**	**46.82 – 127.43**	**89.55**

* Newly added plant

In table 1, the Bamboo *root* tensile strength was compared to other plant and it was found out that that 89.55 mPa average tensile strength of bamboos is higher compared to all other plants [10].

3.3 Soil properties with Bamboo roots

The Soil moisture content is the quantity of water contained in soil with bamboo roots Ranges from 22.22% to 23.21%, its mean moisture content were 22.55% while the soil without roots ranges from 20% to 27.77%. This plants absorbed water to lessen the saturation that causes Landslide and slope failures. The Liquid Limit is the moisture content at which soil to begin to behave as a liquid material and begins to flow. The obtained results shows that the soil with Bamboo roots ranges from 90.81% to 32.87%, its mean liquid limit was 23.2% while the sample without roots *bamboo roots* ranges from 11.46% to 22.97%,it has a low potential for swelling that usually causes slope failures. The Plastic limit obtained from soil Bamboo roots ranges from 28.57% to 50%, while sample without bamboo roots ranges from 33.33% to 40%, its mean plastic limit changes from medium to high of soil transitions between brittle and plastic behavior. The root of Bamboo roots *affects* the soil classification on which presence of the Bamboo roots *changed* type of soil to another type of the soil.

The cohesion of the obtained soil without bamboo roots ranges from 0.462771 kPa to 1.567453 kPa, while with Bamboo roots soil sample ranges from 1.340594 kPa to 5.512018 kPa, this shows that roots makes the soil become more cohesive. The soil angle of internal friction is improved when there is an interaction between soil and roots of the Bamboo roots.

3.4 Soil Slope Factor of Stability and safety.

The table 3 below shows the factor of stability of without roots of Bamboo roots is 0.15 which means the slope areas is highly susceptible and the factor of safety with the roots Bamboos *is* 0.903, thus the slope areas is marginally stable. Therefore, the Bamboo stabilizes the soil slope.

Table 3 .Soil Slope Factor of Stability Analysis stability *with and without bamboo roots.*

Factor of Stability	Bottom of the Slope	Middle of the slope	Top of the Slope	Mean	Factor of Stability
Factor of safety with Bamboo roots	1.02	1.08	0.98	1.03	Marginally stable
Factor of safety without Bamboo roots	0.05	0.13	0.18	0.15	Highly susceptible

The Table 4 shows the value F value within rows of 4.4314 is greater than F critical of 2.60299, and the value F value between columns of 2.8848 is greater than F critical of 2.60289 tested at 0.05 level of significance, then null hypothesis is rejected. The study revealed that there is

significant difference between on the slope stability factors of   with bamboo and soil without bamboo roots

Table 4. Comparison of slope Factor of stability *with and with Bamboo roots.*

Source of variation	SS	df	MS	F -Value	F critical (0.05)	Remarks
Bamboo species	899608.1	5	179922	4.4314	2.60299	Significant
Bamboo roots tensile strength	585624.5	5	117125	2.8848	2.60289	significant
Error	1015025	25	40601			
Total	2500258	35				

The table reveals that the bamboo species has significant difference roots strength when used as slope stabilizers also the bamboo roots tensile strength has significant difference   factor of stability when used as slope stabilizers. This implies that bamboo root systems is good soil and slope stabilizers.

CONCLUSION

Based on findings, the following were drawn:

Bamboos is native to plant of most common weed that grow widely and abundantly throughout the in Palawan and abundantly found in the hill slopes and cut slopes.

Base on the data gathered, Bamboo has a high pull out strength, the shear strength is effective and capable to hold soil and rocks penetrated to the soil at the certain depth to prevent slope failure and erosion [10].

The soil sample with roots of Bamboos has a small amount of water presence compare to soil sample without roots. This indicates that the roots of bamboos increase water content of the soil sample decrease, soil has a capacity changes its shapes without altering its volume, the soil plastic limit changed, and soil type changed.

The soil with *Bamboos* has a high cohesion, thus, difficult to break apart. However, cohesion of soil changes significant depending on the presence of water.   The   stability   and bearing capacity of soil with *Bamboos*   Depends primarily on the interactions between particles and the Bamboo roots improves the soil cohesion. This implies that the roots of *bamboo roots* improve the factor of stability of the soil slope and   good stabilizer of soil slope or cut slope area. The bamboos *were* an effective and efficient slope stabilizer and can prevent shallow landslides.

.

RECOMMENDATION

After a careful study and analysis of the findings of this study, the following suggestions and recommendations were drawn for considerations. In reducing landslide risk several factors should to be taken into account.

1) Study further higher level of plant diversity generally associated with natural regeneration, may increase slope stability above that offered by monospecific and single age plantings.
2) The use of bamboos *as* vegetation in cut slope and hill slope to minimize and prevent erosion[10].
3) Further study is recommended on Bamboos *as* slope and road cut slopes stabilizers and other parameters not cited in this study.

REFERENCES

[1]   Waldron and Dakessian , 1981; Schmidts et al., 2001; Fournierf et al., 2006), *Significance of tree roots decomposition for shallow landslide*

[2] Genet, Marie et al, "*The Influence of the Cellulose Content on Tensile Strength in Tree   Roots*" From http://link.Springer.com/article/10.1007%2Fs11104-005-
8768 (February 17, 2017)

[3] Mattia, C,; Bishetti, G. & Gentile, F., (2005) *'Biotechnical characteristics of root systems of typical Mediterranean species'* , Plant and soil

[4] Greenwood, J,Norris, J,Wint, 2004) '*Assessing the contribution of vegetation to slope   stability*', proceeding of the institution of the Civil Engineers.

  [5] Wong W. *Melastoma malabathricum: Too Beautiful to Be Called a Weed*. Singapore: Green Culture; 2008.

[6] Sean Regg P. Salcedo, (2015), *Tree root strength of meslatoma malabathricum as vegetation to minimize landslide.* (Undergraduate Thesis) Holy Trinity University, PuertoPrincesa City.

[7] Meyer K. *Revision of the Southeast Asian genus Melastoma (Melastomataceae) Blumea*: Journal of Plant Taxonomy and Plant Geography. 2001;46(2):351–398.

[8] Van Valkenberg JLCH, Bunyapraphatsara N. *Melastoma malabathricum* L. In: van Valkenburg JLCH, Bunyapraphatsara N, editors. *Plant Resources of South-East Asia No. 12(2): Medicinal and Poisonous Plants 2*. Leiden, The Netherlands: Backhuys; 2001. pp. 365–366.

[9] Hengchaovanich, D., Nilaweera, N., 1998. *An assessment of strength properties of vetiver grass roots in relation to slope stabilization*. In: Proceedings of the First International Conference on Vetiver. Office of the Royal Development Projects Board, Bangkok, pp. 153–158.

[10] Junie Mark P. Somera ,(2016). *Study of Roots Strength Capacity of Malatungaw Plant (Melastoma Malabathricum Sp.) For Slope Stability*. (Undergraduate Thesis) Western Philippines University, Aborlan, Palawan.

[11]Greenwood, J.; Norris, J. & Wint, J. 2004, ' Assessing the contribution of the vegetation to slope stability', Proceedings of the Institution of Civil Engineers, vol. 157, no. 4, pp. 199-207.

[12]Mattia, C.; Bishetti, G. & Gentile, F. 2005, Biotechnical characteristics of root system of typical Mediterranean species, Plant and Soil, vol. 278, no.1, pp 23-32

Performance Improvement of MPPT Solar Panel Control Using Fuzzy Logic Method

Moh. Khotib[1,a)] Bambang Sujanarko.[2,b)] Bambang Sri Kaloko[3,c)]

[1,2,3]*Electrical Engineering, University of Jember*

[a)]Corresponding author: moh.khotib@gmail.com
b)sujanarko.teknik@unej.ac.id
c)kaloko@unej.ac.id

Abstract. Solar power (PV) system is currently widely used because it is relatively cheap, easier in installation, and also environmentally friendly. However, PV system has some weakness such as an output voltage which depends on weather conditions and ambient temperature. It becomes a serious problem that should be solved in PV system. Usually this problem is solved using Maximum Power Point Tracker (MPPT). In this paper, MPPT will be designed and discussed in order to keep small losses using a simple design of converter. This MMPT design is based on Fuzzy logic. Basically, the principle of MPPT based on fuzzy logic controller is to get current and voltage, so that PV system has minimum power losses. To achieve it, the duty cycle value is used to adjust the angle of ignition switch of MOSFET on the converter. The proposed method was shown through simulation performed by using MATLAB software. Simulation results show that the system is able to improve the PV power extraction efficiency significantly by approximately 98% of PV's power.

Keywords: MPPT, PV, fuzzy logic

INTRODUCTION

The development of technology in this era is experiencing very rapid progress, so that the need for electrical energy has increased significantly [1]. Many power plants are starting to switch from old models that use fossil materials that absolutely experience a reduction in availability. In addition, this energy cannot be renewed. According to current issues, a lot of energy undergoes crisis and global warming is often discussed. Hence, in this occasion the research will be focused on photovoltaic (PV) since this cannot lead to pollution.

The solar power system (PV) is currently widely used by the general public because a number of factors that support it such as relatively cheap prices, quite easy installation, and also environmentally safe [2]. Yet, there are still weaknesses in the PV system when operated. Those are such as the dependence on weather conditions and the problems of ambient temperature in the process of using PV [3].

Those problems lead to the unreal output of energy generated by PV so that various voltages are found because of environmental condition and changing weather. This will certainly breed trouble in order to determine maximum/expected value from voltage produced. Therefore, the researcher plan to add maximum power point tracking (MPPT) system equipped with optimization of fuzzy logic in that PV system [4]. This is aimed at automatically obtaining voltage value that can be evaluated using fuzzy logic optimization.

In this study the author will try to simulate a PV model with optimization of fuzzy logic to obtain varying load values such as resistivity, inductiveness, and capacitance by using Simulink Matlab with the purpose of simulation as similar as possible to real conditions. We know with PV systems in real conditions consists of solar cells, BOOST converter, controller. The burden in this case usually uses batteries, but in this study, the author will try to replace

with other loads such as motors and resistors. Subsequently, the author compares the output powerbecause, in studies that have been done before, no one has tried to use the different load variations on the MPPT PV system with the fuzzy method.

MATHEMATICAL MODELLING

Basically, PV consists of P-N layers (Positive-Negative) which are arranged in a thin layer of semiconductor. In electromagnetic radiation PV solar energy can directly be converted into electricity [5] and photovoltaic effects to achieve higher voltages and currents. Several cells are used and arranged in series and parallel but the manufacture must be as needed [6]. PV cells can be indicated by a simple equivalent circuit shown in Figure 1. In this figure the circuit resistance (R_s) represents the loss of the interval due to the current flow, while the shunt resistance (R_{sh}) corresponds to the ground leakage and is usually ignored.
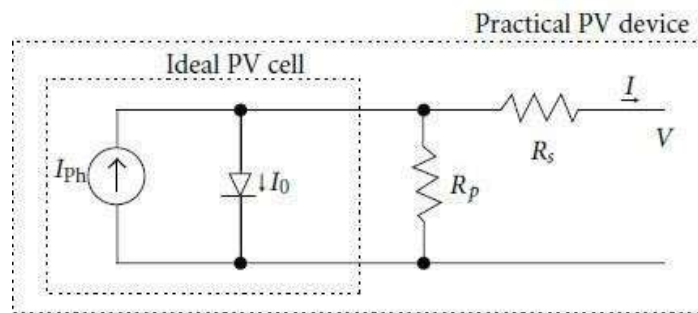
FIGURE 1. PV cell sequential circuit

Solar radiation will be output as well as temperature and wind power, the author uses matlab or simulink, and can be seen in figure 2. Then the net current PV is the difference between the photo current (I_{Ph}) and the diode current (I_d) like this formula..

$$I = I_{Ph} - I_P = I_{Ph} - I_P \left(\exp \frac{e(V + IR_S)}{mkT_C} \right) - 1 \qquad (1)$$

Where :

M = Idealization Factors
K = Boltzmann Gas Constant
Tc = Absolute Cell Temperature
E = Electronic Costs
V = Voltage Worn Disel
1o = Dark Saturated Flow
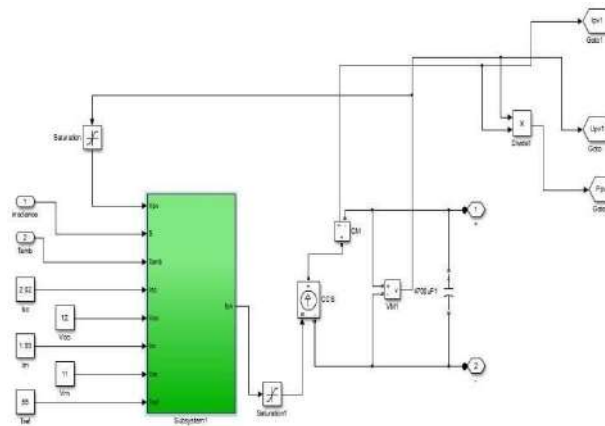
FIGURE 2. Sub System Circuits of Solar Cells in Matlab Simulink
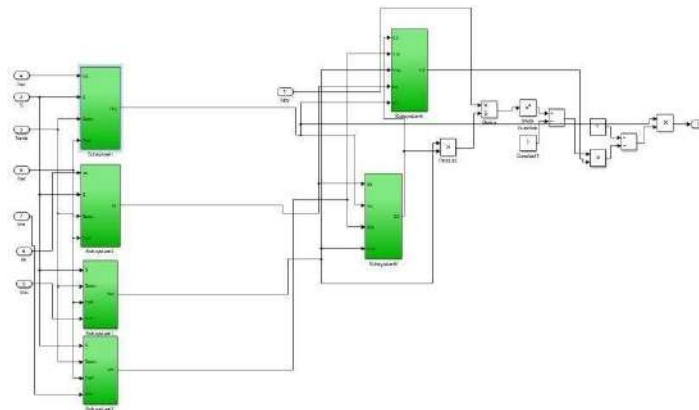
FIGURE 3. **Circuit of Solar Cell Sub System in Matlab Simulink**

In the picture above it is explained that to get a good output, the PV system must be operated at the maximum point of MPPT. And as for the voltage or output varies, because temperature and insulation affect the output. So that the MMPT system is needed to get results that do not disappoint[7].
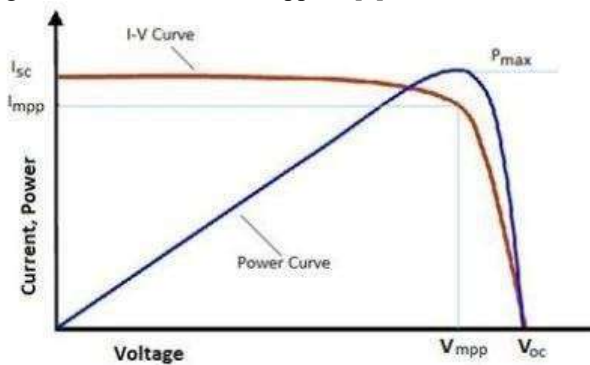
FIGURE 5. PV curve - IV solar cells

PV has many different characteristics. One point on the V-I or V-P curve, called the Maximum Power Point (MPP), where the entire PV system operates at its maximum and produces the best power. This can be found with the help of MPPT (Maximum Power Point Trackers) [7]. PV systems using MPPT controllers with fuzzy logic controls have been shown in Figure 6.
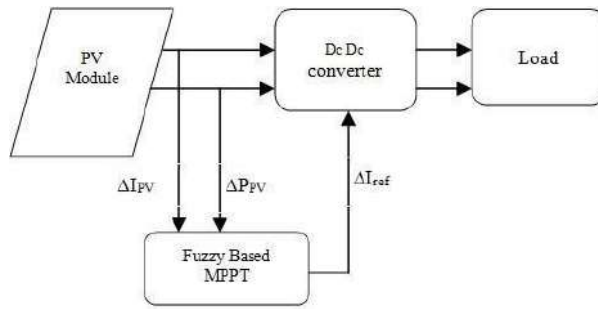
FIGURE 6. Block diagram of PV + MMPT with Fuzzy controls.

RESEARCH METHODS

In this system the author uses fuzzy logic aims to regulate and control the output of the controller. Information can be seen from Figure 7.
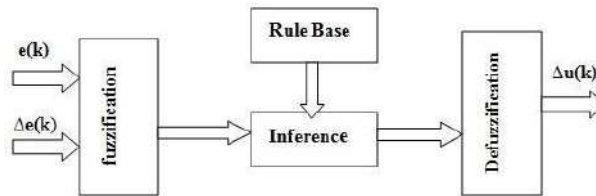
FIGURE 7. Fuzzy logic block diagram

There are two entries for controller error e (k) and error changes Δe (k). The Fuzzification block changes the firm input (0 and 1) to fuzzy input. Rules are formed in the basic rules and are applied in inference blocks. Defuzzification converts fuzzy output into a firm output. Fuzzy inference is done using the Mamdani method and defuzzification uses the center of gravity to calculate this FLC output which is a change in the duty cycle.

The input to the Fuzzy controller is a change in the PV array Power (pPpv) and changes in the current of the PV array (ΔIpv) which corresponds to the two intensity of the sampling time. Both inputs are processed by Fuzzy controller and the output of Fuzzy controller is incremental reference current ((Ireff). This output is given to the Dc-Dc power converter. The first input variable (refPref) for fuzzy logic controllers is divided into seven Fuzzy circuits: PB (Positive Big), PM (Positive Medium), PS (Positive Small), ZZ (Zero), NS (Negative Small), NM (Medium Negative) and NB (Large Negative). The second input variable (pIpv) for fuzzy logic controllers is divided into 3 Fuzzy sets: N (Negative), Z (Zero) and P (Positive). Only one output variable (pIpv) is divided into 7 Fuzzy sets: PB (Positive Big), PM (Positive Medium), PS (Positive Small), ZZ (Zero), NB (Big Negative), NM (Negative Medium) and NS (Small negatives). Rules are formed as shown in table 1. The Input and output membership function is shown respectively in Figures 8, 9 and 10

Table 1. Rule Base

ΔP_{PV} ΔI_{PV}	PB	PM	PS	ZZ	NS	NM	NB
P	PB	PM	PS	PS	NS	NM	NB
Z	PB	PM	PS	ZZ	NS	NM	NB
N	NB	NM	NS	NS	PS	PM	PB
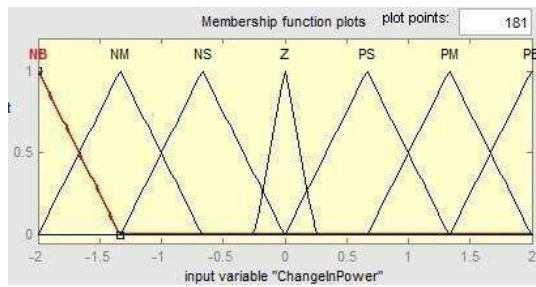
FIGURE 8. Membership function-change in Power input
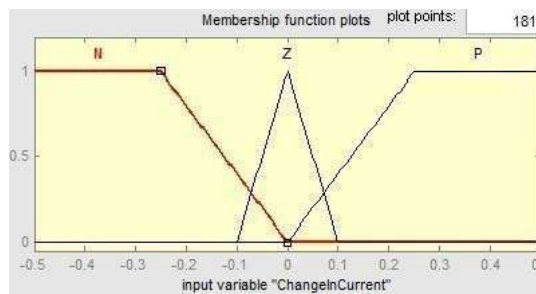
FIGURE 9. Membership functions changes in input
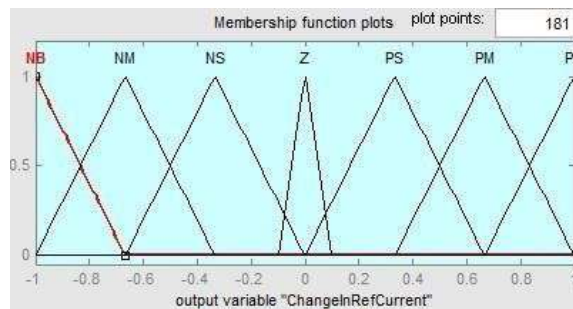
FIGURE 10. Membership function-changes in reference output

RESULTS AND DISCUSSION

MPPT Fuzzy Logic Control model with load variations to be studied has been modeled on Simulink Matlab as shown in figure 11.
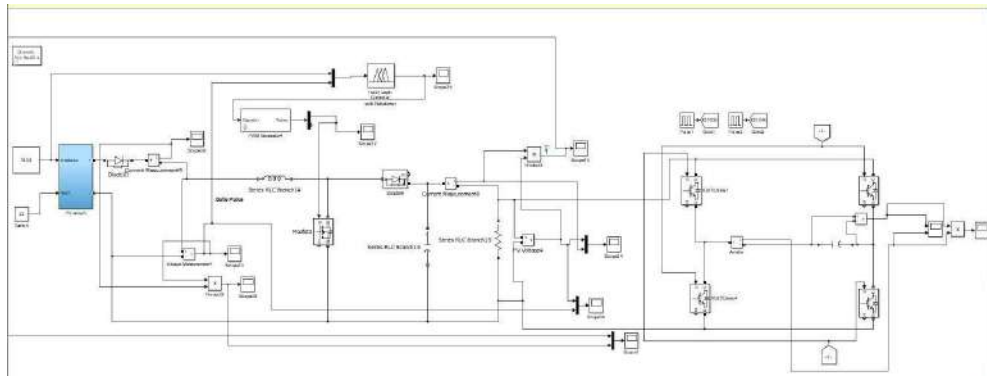
FIGURE 11. MPPT-based fuzzy logic control to be studied

In the MPPT-based fuzzy logic control model the different load variations will be applied to be examined in order to determine its efficiency.
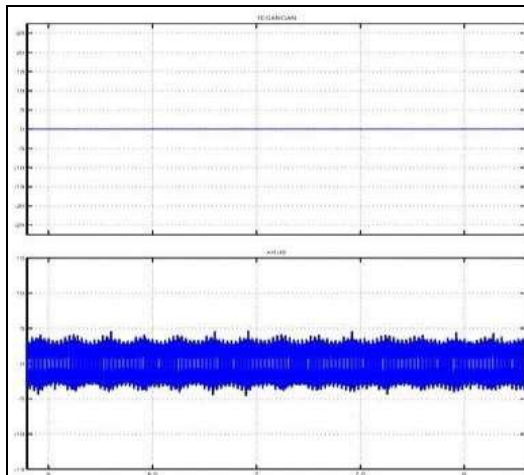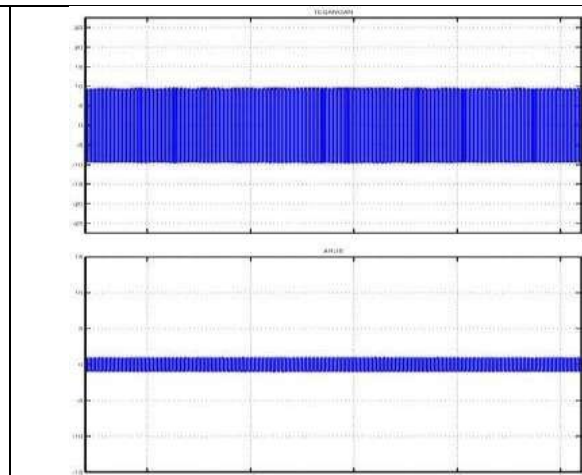
FIGURE 12. Capasitive	**FIGURE 13.** Resistive
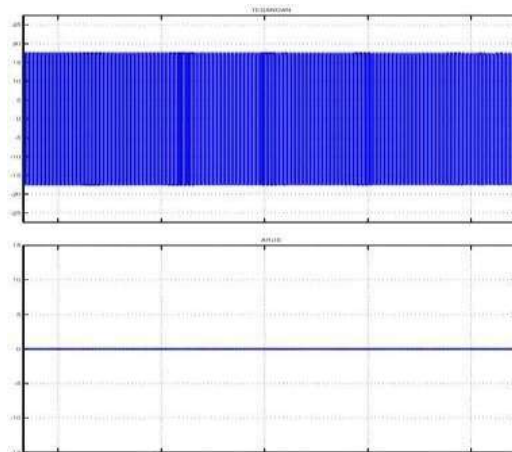
FIGURE 14. Inductive

CONCLUSION

After doing Simulink experiments on Matlab R2013a, by entering data 500, 1000, and 1500 Ohms for each Resistor, Capacitive, and Inductive, it turns out that it produces different voltage and current wave data, so we can choose among the best three.

ACKNOWLEDGMENTS

REFERENCES

1. M. Fannakh, M. L. Ehafyani, and S. Zouggar, "Hardware implementation of the fuzzy logic MPPT in an Arduino card using a Simulink support package for PV application," *IET Renew. Power Gener.*, vol. 13, no. 3, pp. 510–518, 2019.

2. A. Al Nabulsi, R. Dhaouadi, and S. Member, "Nabulsi, Dhaouadi, Member - 2011 - Efficiency Optimization of a DSP-Based Standalone PV System using Fuzzy Logic and Dual-MPPT Control- annotated.pdf," vol. 8, no. 3, pp. 1–12, 2012.

3. N. Priyadarshi, S. Padmanaban, M. S. Bhaskar, F. Blaabjerg, and A. Sharma, "Fuzzy SVPWM-based inverter control realisation of grid integrated photovoltaicwind system with fuzzy particle swarm optimisation maximum power point tracking algorithm for a grid-connected PV/wind power generation system: Hardware implementation," *IET Electr. Power Appl.*, vol. 12, no. 7, pp. 962–971, 2018.

4. P. K. Ray, S. R. Das, and A. Mohanty, "Fuzzy-controller-designed-pv-based custom power device for power quality enhancement," *IEEE Trans. Energy Convers.*, vol. 34, no. 1, pp. 405–414, 2019.

5. M. A. Abdourraziq, S. Abdourraziq, and M. Maaroufi, "Efficiency optimization of a microcontroller-based PV system employing a single sensor fuzzy logic controller," *IET Power Electron.*, vol. 11, no. 3, 2018.

6. B. N. Alajmi, K. H. Ahmed, S. J. Finney, and B. W. Williams, "A maximum power point tracking technique for partially shaded photovoltaic systems in microgrids," *IEEE Trans. Ind. Electron.*, vol. 60, no. 4, pp. 1596–1606, 2013.

7. K. S. Tey, S. Mekhilef, and S. Member, "Pauta_Ejercicio_1_2009_02.pdf," vol. 61, no. 10, pp. 5384–5392, 2014.

Remote Monitoring and Control of Photovoltaic System Using Short Message Service and Arduino Uno

Rizqi Afif[1, a)] Triwahju Hardianto[2, b)] Bambang Sujanarko [3, c)]

[1,2,3]*Electrical Engineering, University of Jember*

[a)]rizqiafif21@gmail.com
[b)]triwahju@gmail.com
[c)]sujanarko.teknik@unej.ac.id

Abstract. In the modern era, all people use electronic equipment and then all people need electrical energy. Electrical energy is a major requirement of developing a civilization, and renewable energy is a wise choice as sources of electric energy. One of the most widely used renewable energy systems is Photovoltaic. However In remote area, the need for monitoring PV system is crucial to ensure stable PV power delivery. This paper describes a remote monitoring and control design for PV in remote area. The monitoring system is equipped with voltage sensor, current sensor, temperature sensor and irradiation sensor and build based on Arduino Uno and using Short Message Service (SMS). Real time clock chip is used for real time recording.

Keywords: Remote, monitoring, control, SMS, Arduino Uno.

INTRODUCTION

In the modern era, electrical energy is a major requirement. electricity is generally produced from fossil energy, so that it is possible to make fossil energy reserves increasingly thinning. Therefore, the use of renewable energy as a producer of electrical energy needs to be done, one of which is photovoltaic energy. Solar power generation is an alternative power plant that is widely developed, solar panels (solar panels) as a type of renewable electricity generation in the future will increasingly have an important role as a substitute for fossil energy or renewable energy.

Utilization of renewable energy has a very important role in meeting energy needs. The potential of solar energy as a renewable energy source is widely available in nature. Therefore the development of solar energy potential as an alternative source of renewable and pollution-free energy becomes an urgent need for all humanity. Development and utilization must be done both in the form of research in the laboratory and its application in the form of appropriate technology that can be directly utilized by the community.

The development of renewable energy, including solar energy, has now become an alternative in the supply of electricity, especially in remote locations that are not covered by the PLN electricity network. The construction of solar energy power plants using photovoltaic systems (PV) in hard-to-reach areas provides benefits to the community that have a positive impact on improving economic conditions, social and cultural.

The design of PV monitoring devices and systems in remote areas requires a tool to monitor the performance of the PV system and maintain the sustainability of the generating unit. To meet the needs of remote monitoring, a device and monitoring system must be installed so that the unit can monitor at that location. And the monitoring data is expected to be accessed or known quickly and easily by using mobile phones or handphones that are often used daily.

Researchers have conducted many studies discussing various electrical energy monitoring applications. in the development of a monitoring system designed to be monitored locally, remotely using a GSM modem as data transmission [1], web-based internet network [2], [3], [4], and web-scada implementation to monitor and control solar-wind hybrid plants remotely via the internet network. And this research still uses a serial communication cable network and Local Area Network (LAN) [5].

IoT-based monitoring and control applications, among others, were developed to control equipment on smart home [6] and monitoring the status of the electricity distribution network [7] based on IoT technology. Meanwhile, some literature discusses the generic architecture of IoT for smart cities [8] and for embedded equipment [9]. The monitoring system uses an internet network that requires a signal that must be stable and strong so that the data transmission gets good and fast results, however, if the system is used in remote locations or remote villages that lack a stable and strong signal it will have problems in receiving and sending the information. With this, a system that can still be used even though the signal network is lacking and unstable is developed, which is using the SMS (Short Message Service) system.

In this study, a wireless node based on SMS gateway for monitoring electrical power and parameters generated in the PV system were designed. The design of a monitoring system that was developed using an arduino uno-based SMS will help monitor the plant in the remote area, by the parties concerned, even though not at the location of the plant can monitor it regularly. The results of the monitoring of electrical energy are sent via SMS wirelessly using mobile or cellular network access.

RESEARCH METHODS

In the discussion this section includes hardware design in the form of sensor devices and wireless sensor nodes, software design, and testing of devices that have been made.

System design

The design of this remote control and monitoring can be seen in Figs. 1. In general, the design of the remote control and monitoring system consists of the following parts.
1. Sensor modules, including DC voltage sensors and DC currents at the panel output, and DC voltage sensors and DC currents at the battery output output.
2. Wireless node, consisting of signal conditioning and data processing devices, SMS for SMS sending communication, power supply circuit, and load remote control.
3. SMS gateway, in the form of an SMS module with access to sending and receiving SMS using the GSM SIM module 800L.
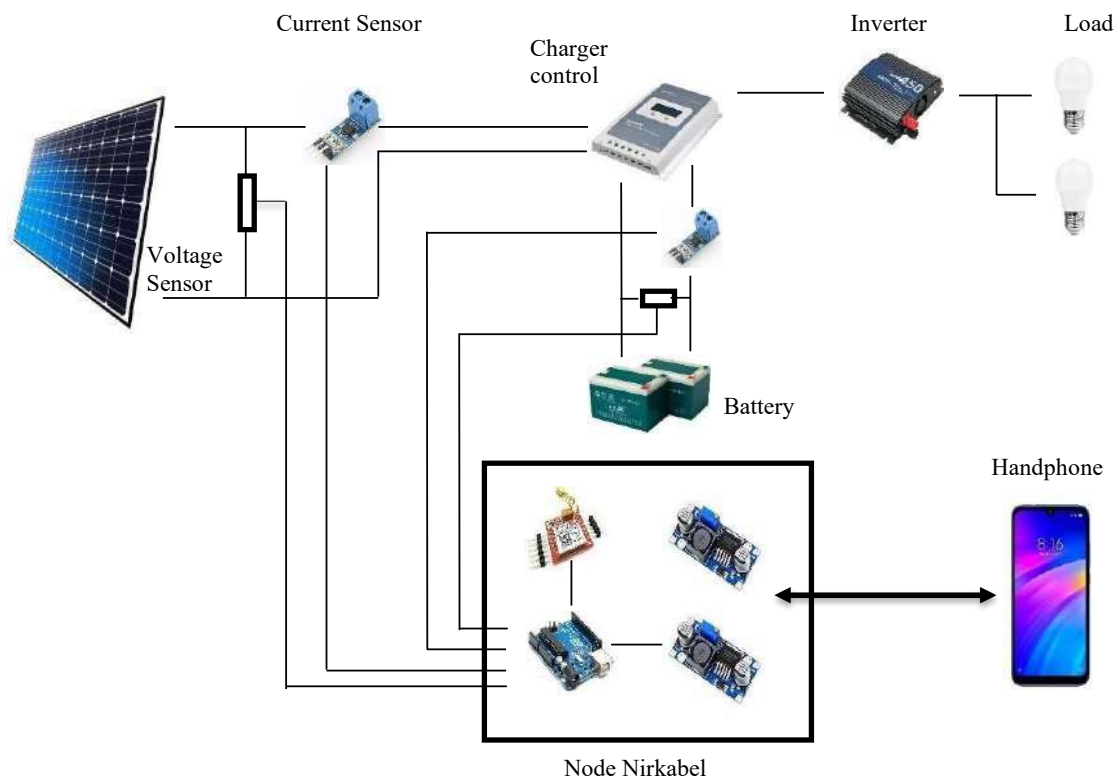
FIGURE 1. Designing a remote control system and monitoring the electrical power and environmental parameters of the PV system using an Arduino Uno-based SMS

TABLE 1. Specification of monitoring system

PV system nominal voltage	24 V DC
PV current sensor	ACS 712 30A *unidirectional hall effect current sensor*
Data processing	Arduino Uno
SMS getway	GSM 800L
Wireless node power supply	24 V to 5 V DC - DC converter

Voltage Sensor

In the voltage sensor used the basic principle of using a voltage divider circuit such as Figure 2 with the sensor output voltage is formulated as in (1).

$$V_0 = V_I \cdot \left(\frac{R_2}{R_1 + R_2} \right) \tag{1}$$

In the voltage divider circuit is used to reduce the PV voltage to a lower voltage with a maximum value of the output voltage is 5 volts. And this voltage divider circuit is used at the output of the battery which serves to reduce the output voltage of the battery to 5 volts. The specified voltage value is the maximum voltage limit required by Arduino to be able to read the output voltage.

Current Sensor

The current measurement itself uses the ACS712 sensor which is an unidirectional current sensor with the ability to read currents up to 30A. The current sensor circuit is shown in figure 3.
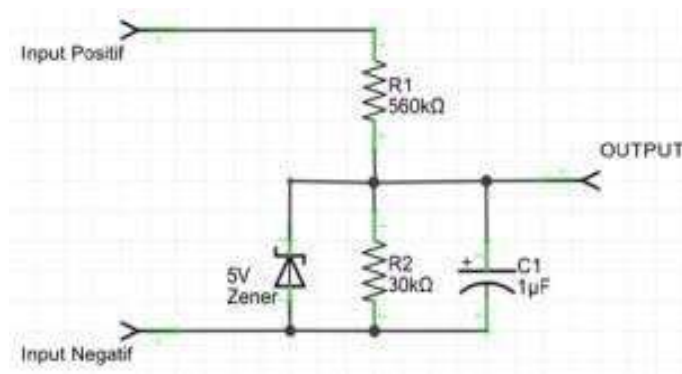
FIGURE 2. Voltage sensor circuit
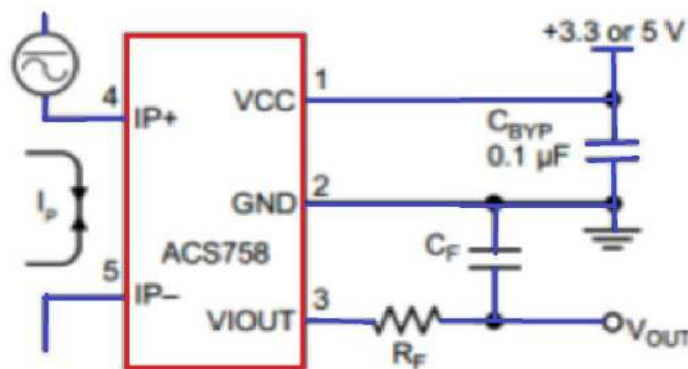
FIGURE 3. Current sensor circuit [12]

Wireless Node Design

The developed wireless node is a board that integrates the data processing section (Arduino Uno) with the GSM 800l module to receive and send data in the form of SMS (Short Message Service). At the node there are inputs and outputs for Arduino in reading sensors. This node supplies power from the system battery via a DC-DC converter for the needs of the Arduino 5V power supply and sensors, and AMS1117 regulator ICs for the 3.3v 800L GSM module power supply. Serial communication between Arduino and the 800L GSM module uses two lines that are connected through a circuit.

Software Design

The software design is developed and installed on the wireless node so that the wireless node is able to measure the magnitude of the parameters being monitored, processing measurement results, and sending measurement data to the 800L GSM module. The picture below shows the software design flow chart that was made.
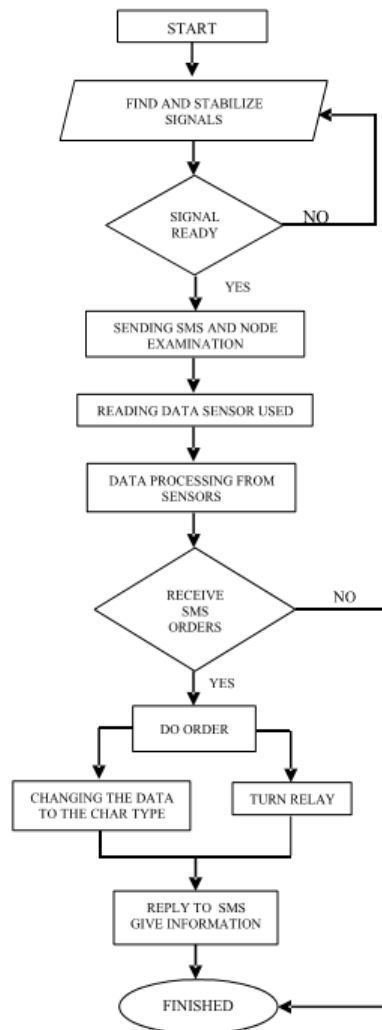
FIGURE 4. Software design flowchart

For logging, data processing, and appearance and data access functions through the 800L GSM module, the GSM module is used to be used as an SMS receiver and sender. Applications that can be carried out include collecting sensor data in real time and sending SMS to the user's mobile phone, storing measured data, analyzing and visualizing data, alarm functions, and scheduling.

RESULTS

Implementation of the Design

The design of the monitoring system is implemented and tested on a 50 Wp PV system at the Electrical Engineering Conversion Laboratory of Electrical Engineering UNEJ. Figure 8 shows the wireless sensor node device that was developed. While the block diagram of the installation of wireless nodes and sensors on this system is shown in Figure 5.
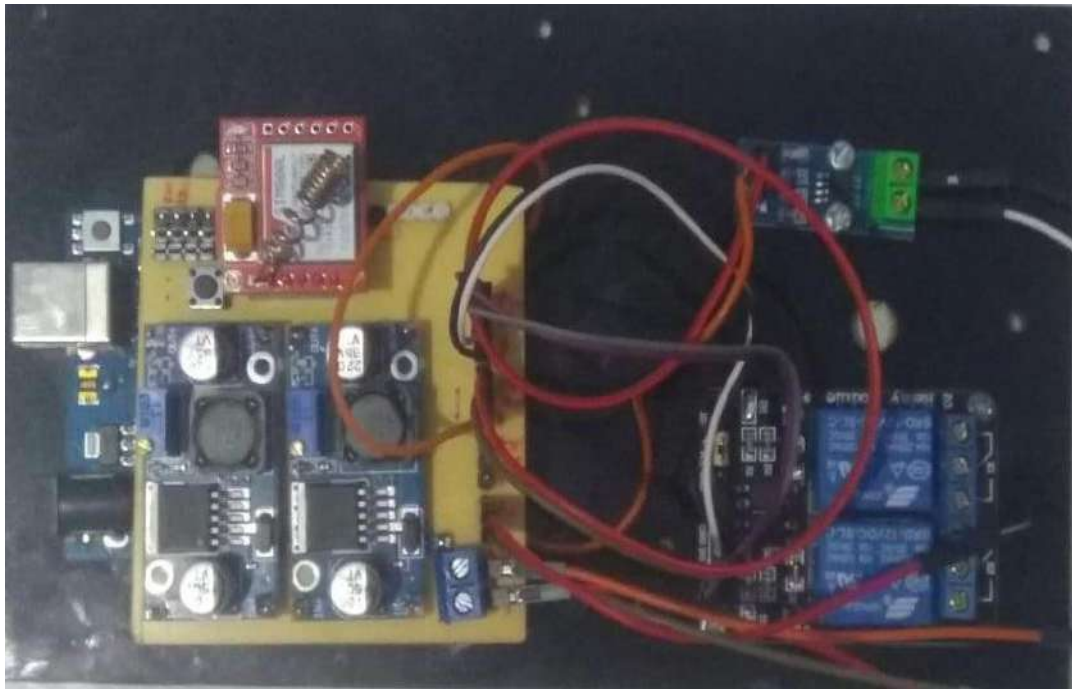
FIGURE 5. Wireless sensor node device.

Current Sensor Testing

Current sensor testing is done by measuring the current sensor output voltage and comparing the value of the results of processing by the node with the measured value measured with a DC clampmeter. Table IV presents the results of the current sensor test.

TABLE 2. Flow sensor testing results

Rated Current Measurement (A)	Data Processing Results by Node (A)	*Error (%)*
0	0	0
1.02	1.06	4
1.51	1.57	6
2.04	2.12	8
3.45	3.55	10
4.61	4.54	7
6.23	6.18	5

The test results show that the current sensor device works well with a very small percent error, which indicates that the largest percent error is 10% and the smallest is 0%.

Voltage Sensor Testing

Testing this voltage sensor hardware simulates the change in voltage in a photovoltaic system using a variable DC power supply. The power supply voltage varies from 0 to 30 V. The results of the test are presented in the table below.

TABLE 3. Test results of voltage sensors

Rated Power Supply Voltage (V)	Node Reading Voltage (V)	*Error* (%)
0	0	0
5.01	4.89	12
10	9.98	2
15	15.12	12
20.01	19.85	16
25	25.05	5
30	30.03	3
35.01	34.94	6
40	40.04	4

The test results show that the current sensor device is made to work well with a very small percent error, which indicates that the largest percent error is 16% and the smallest is 0%.

Wireless Node Testing

Wireless node testing includes hardware and software testing. Hardware testing is done by checking the board that has been made, in the form of connectivity testing, power supply, and the wireless node reference voltage value. Software testing is done through.

Analysis and Discussion

The entire monitoring system design that was made was tested on a 50 Wp PV system in the Energy Conversion Laboratory and Electric Power Systems at the Department of Electrical Engineering, University of Jember. Observations were made to test the performance of the monitoring system. Observation data for 24 hours on 07 August 2019 from 00.00 WIB until 24.00 WIB shown in FIG. 6 and Fig. 7. Data is taken in cloudy and sunny weather conditions. The monitored photovoltaic system output data includes PV current, PV voltage, PV module electrical power, battery current, battery voltage, and battery output power. The current value and PV power are proportional to solar radiation as shown in the monitoring data. The current value and PV power are proportional to solar radiation as shown in the monitoring data. The design of the time interval for sending monitoring data is every 60 minutes. Table 5 shows the delivery time data of the monitoring system monitoring results. The average interval of sending monitoring data to the server is 75 seconds depending on the signal captured by the module. The test results show the system is able to receive, process and transmit monitoring data reliably.

The figure 8 show SMS commands sent to the divice to carry out certain commands. However the ordered SMS has been determined by the program that has been set, if it's not in accordance with the SMS set command then the tool will not execute the command and will not reply and provide any information. The tool can also control remotely to turn on two relays that can be connected directly with lights or household appliances that can make it easier to control remotely. In tjis tool is still limited to only two relays, but can be added a few more relays, so that it can control ousehold appliances remotely such as home lights, water pumps and others.
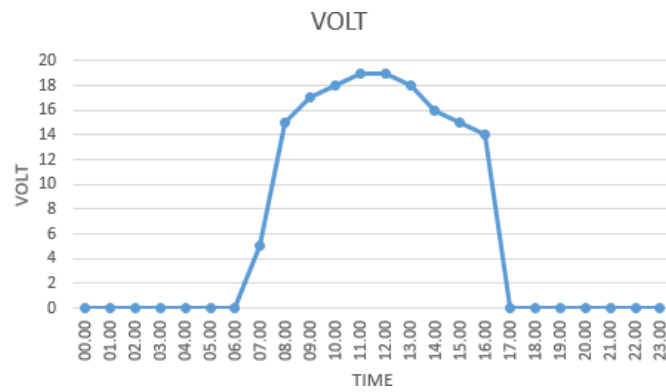
FIGURE 6. Graph of PV output voltage
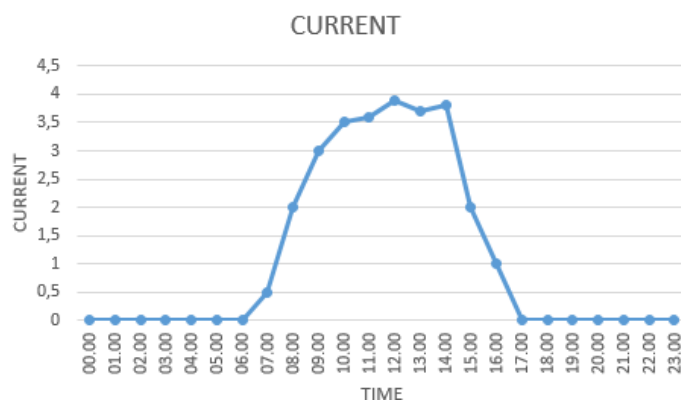
FIGURE 7. Graph of PV output current

FIGURE 8. SMS commands to the tool and information from the tool

TABLE 4. Monitoring system monitoring time

Design time intervals for processing orders to sending information	1 minute 25 seconds
The average time interval between processing orders and sending information	1 minute 5 seconds
Minimum processing time for orders to dispatch information	60 second
The maximum time from processing an order to sending information	2 minute

TABLE 5. Battery charging

Time	Battery Charging Voltage (V)	Battery Charging Current (A)
07.00	5	0
08.00	14	1.7
09.00	16	2.4
10.00	18	2.7
11.00	19	3.2
12.00	19	3.5
13.00	18	3.3
14.00	16	2.7
15.00	15	0

In table 5 describes the battery charging to charge the battery from low to full conditions takes 6.15 hours. Charging current fluctuates due to cloudy weather so that the average current is 1.95 A and the charging voltage ranges from 5 V to 19 V. After the battery is fully charged, the charging current shows 0 A indicating that no current has flowed into the battery and the battery voltage has become 15 V.

CONCLUSION

This paper presents the design of a wireless monitoring system for monitoring electrical energy and controlling controls on Arduino uno-based photovoltaic systems using SMS. The design includes wireless node hardware and software to process monitoring data and send data to mobile phones via SMS, wireless monitoring via a GSM module. The prototype design that was developed was tested on a laboratory scale to find out the function of the monitoring system. Based on the test results, it is known that the monitoring system can work well displaying measurement data in real time via SMS.

The node device can read and process sensor output data with a small error rate, as well as send monitoring data to mobile phones with an average of very short periods of time, and transmission will be interrupted when the signal from the card used is interrupted.

ACKNOWLEDGMENTS

REFERENCES

1.   Winasis., Nugraha, A. W. W., Rosyadi, I & Nugroho, F. S. T. (2016). *Desain Sistem Monitoring Sistem Photovoltaic Berbasis Internet of Things. JNTETI. 5 (4) : 328.*

2. Zahran Mohamed, Atia Yousry, Al-Husein Abdullah, El-Sayed Ihab, LabVIEW Based Monitoring System Applied for PV Power Station, Proceedings of the 12th WSEAS International Conference on Automatic Control, Modelling & Simulation, 2010.
3. Shariff, F, , Rahim, N.A., Ping, H.W. 2013. Photovoltaic remote monitoring system based on GSM, IEEE Conference on Clean Energy and Technology (CEAT). Page(s): 379 - 383.
4. Li Wang, Kuo-Hua Liu. 2007 Implementation of a Web-Based Real-Time Monitoring and Control System for a Hybrid Wind-PV-Battery Renewable Energy System, International Conference on Intelligent Systems Applications to Power Systems (ISAP). Page(s): 1 - 6.
5. Kopacz Cs., Spataru S., Sera D, Kerekes. 2014. Remote and Centralized Monitoring of PV Power Plants. International Conference on Optimization of Electrical and Electronic Equipment OPTIM.
6. Iskandar Dadang, Santosa P. Insap. 2013.Sistem Informasi Gardu Induk dan Gardu Distribusi Berbasis Web. Jurnal Nasional Teknik Elektro dan Teknologi Informasi (JNTETI), 2 (2).
7. Soetedjo Aryuanto, Nakhoda Yusuf Ismail, Lomi Abraham, Farhan. 2014 Web-SCADA for Monitoring and Controlling Hybrid Wind-PV Power System, TELKOMNIKA. 12 (2): 305-314.
8. Li Wang, Kuo-Hua Liu. 2007. Implementation of a Web-Based Real-Time Monitoring and Control System for a Hybrid Wind-PV-Battery Renewable Energy System, International Conference on Intelligent Systems Applications to Power Systems (ISAP). Page(s): 1 – 6.
9. Qing-Hai Ou, Wang Zheng, Zhen Yan, Li Xiang-Zhen. 2013. Status Monitoring and Early Warning System for Power Distribution Network Based on IoT Technology. 3rd International Conference on Computer Science and Network Technology (ICCSNT). Page(s): 641 - 645.
10. Ganchev, I., Zhanlin Ji, O'Droma, M. 2014. A generic IoT Architecture For Smart Cities. Irish Signals & Systems Conference 2014 and 2014 China-Ireland International Conference on Information and Communications Technologies (ISSC 2014/CIICT 2014).
11. Yashiro, T., Kobayashi, S., Koshizuka, N., Sakamura, K. 2013. An Internet of Things (IoT) Architecture For Embedded Appliances. Humanitarian Technology Conferen3ce (R10-HTC). IEEE Region 10; Page(s): 314 - 319.
12. ACS758 datasheet, Pinout ,application circuits Thermally Enhanced, Fully Integrated, Hall Effect-Based Linear Current Sensor With 100 μΩ Current Conductor http://www.datasheetdir.com/ACS758+Current-Sensor

Design of Flood Detection Using Telemetry System Based on Xbee Pro Wireless

Satriyo Budi Utomo [a], Januar Fery Irawan [b], Sumardi, Joko S.,
Kristianta, Fathur R.S

Faculty of Engineering, University of Jember, Indonesia

[a] satryo.budiutomo@yahoo.com
[b] Corresponding author: januar_ir@yahoo.com

Abstract. In the rainy season, Indonesia have some areas hit by floods every year,it causes huge losses for some citizens. We can used the designed tool of flood detection using telemetry system based wireless Xbee PRO, it's a tool that cangivea warningto citizenswhen flood happens. The sensor weused are Ping ultrasonic sensors. Thefrequencyemittedis 42.076 to 47.9542KHz. While themaximumdistance that can be detectedis 3meters. The wireless Xbee PRO maximum distance for the outdoor area is 380 meters. The highest value for packet loss when we gaveobstacleis76.67% which isat a distance of150 meters, while the lowest packet loss is53.3% when the distance is 75 meters. If the water level rises above 2.5 meters then the sirene will be ringing, it is the signal telling that the situation is a danger. Every data detected will be displayed using the interface which is delphiin the form of graphs and stored in the database. Delphi interface will also sound an alarm when the water level exceeds 2.5meters.

INTRODUCTION

Indonesia is a country with great natural potential based on geographic and geological conditions. However, this has made Indonesia a disaster-prone country. To reduce the impact of disasters, information and communication technology has a lot of potential, especially in the socialization of disaster management, predicting disaster, assisting in making decisions related to disasters, disseminating warnings of disasters to the community, and managing victims of disasters when the disaster itself has already occurred.

Flood disasters are events that often occur in the last few years. Almost every year this disaster struck in several cities in East Java. Floods generally occur because the existing waterways are not able to accommodate the overflow of water, in a relatively flat area and near the watershed. In the rainy season, several regions in Indonesia are often flooded each year causing huge losses to residents affected by the flood and the government. Damage occurred

everywhere both the structure and infrastructure suffered a lot of damage, the victims fell even not a few who died because of the disaster. Flooding does not only occur in large cities that are very densely populated, even small cities with moderate populations are also frequently hit by flooding.

Flooding may be happened whenever, so it can not be identified when there will be a flood because of the sudden arrival. For the reasons above, it is necessary to design a flood detection device that can detect floods from a distance in real time so that the signs of flooding can be known as early as possible in order to reduce and minimize the losses that occur and can avoid the public from the dangers of flooding that can dying. Areas that are usually affected by floods during the rainy season, one of which is Jember Regency, although the flooding that occurred was not as severe as in the capital, but even though it was not severe flooding was still a danger that harms and endangers humans.

Very rapid technological developments provide many benefits including fast delivery of information so that any information can be monitored in real time or at that time, it is done to obtain accurate information. Wireless is one of the communication techniques to convey information using radio waves to replace cables connecting computers with networks, so that computers can communicate with networks more effectively and efficiently and with adequate speed. These advantages are very supportive of using wireless as a medium used to access information in real time.

Previous research conducted by Suprato, (2010) with the title of River Water Advance Telemetry System using GSM Modem Based on AVR ATmega 32 Microcontroller to get signs of flooding as early as possible accurately but there are still some shortcomings such as sending data using SMS so that the data cannot be known in real time, using sensors that are vulnerable to damage if exposed to water, and many other shortcomings. The deficiencies and background above give the writer an idea to choose the title "Designing Flood Detection Devices Using XBeePRO Wireless Telemetry System" with the aim of perfecting the tool from previous studies.

LITERATURE REVIEW

This study applied a flood detection tool developed from previous research [7]. The detector used a sensor, while for the sending it uses the ATmega 8 microcontroller, and the communication media uses XBeePRO wireless. The tool's working system is if the water is at a height of 2.5 meters then the siren will live (on). Telemetry is the process of measuring the parameters of an object (objects, spaces, natural conditions) whose measurement results are sent to other places through the process of sending data either using cable or without using cable (wireless). The word telemetry comes from the Greek language, tele means distance while metron means measurement. In telemetry terms are defined as an engineering field that utilizes instruments to measure heat, radiation, altitude, speed or other properties and transmit measurement data to recipients who are physically far away, outside the reach of the observer or user. Media delivery by telemetry system using cable or without using a cable (wireless), then the data can be used directly or need to be analyzed. In general the telemetry system consists of six supporting parts, namely measuring objects sensors, transmitters, transmission lines, receivers and displays. [3]. Wireless communication (wireless) as a medium of communication on computer networks is very popular and has become commonplace at this time. Thus the process of exchanging data will be easier and less complicated. In its development, wireless communication is also used for communication between microcontrollers and this has made data communication between microcontrollers much easier.

Xbee Proo is one of the wireless technology allowing one or more equipment to communicate without a physical connection, that is, without the need for a network or cable equipment as shown in figure 1. Wireless technology uses radio frequency transmission as a tool for sending data, while cable technology uses cables. Wireless technology ranges from complex systems such as Wireless Local Area Networks (WLANs) and cellular phones to simple equipment such as wireless headphones, wireless microphones and other equipment that does not process or store information. Wireless Local Area Network (WLAN) is the relationship between one computer with a computer and / or other peripherals using a little cable. The computer network uses radio waves as a data transmission medium. Information (data) is transferred from one computer to another using radio waves. WLAN is often referred to as a

Wireless Network or Wireless Network. It also includes infrared equipment such as remote controls, wireless computer keyboards and mice, and wireless hi-fi stereo headsets, all of which require a direct line of sight between the transmitter and receiver to make the connection (Janner Simamarta, 2014).

Packet Loss, a parameter that describes a condition that shows the total number of packets lost, can occur due to collision and congestion on the network and this affects all applications because retransmission will reduce overall network efficiency even though there is enough bandwidth available for applications the. Generally, network devices have a buffer to hold the data received. If there is a long enough congestion, the buffer will be full, and new data will not be received.

Some of the causes of packet loss are:
1. Congestion, caused by excessive queues in the network
2. Working nodes exceed the buffer capacity
3. Memory is limited to nodes
4. Policing or control of the network to ensure that the amount of traffic that flows according to the amount of bandwidth. If the amount of traffic flowing in the network exceeds the available bandwidth capacity, policing control will get rid of excess traffic.
5. Noise or commonly called noise is an interference signal that is acoustic (sound), electrically, or electronically that is present in a system (electrical / electronic circuit) in the form of noise that is not the desired signal.

Sources of noise can be grouped into three categories:
1. Intrinsic sources of noise arising from random fluctuations in a physical system such as thermal and shot noise.
2. Sources of man-made noise such as motors, switches, digital electronics.
3. Noise due to natural disturbances such as lightning and sunspots.

Packet loss calculation is done by comparing the data sent by the computer minus the data received by the computer, then calculated into the percentage of data lost with equation number 1.

$$Packet\ loss\% = \frac{|DT-DD|}{DT} \times 100\% \qquad (1)$$

Where, DT = Packet Data Sent and DD = Data Packet Received

(a)   (b)
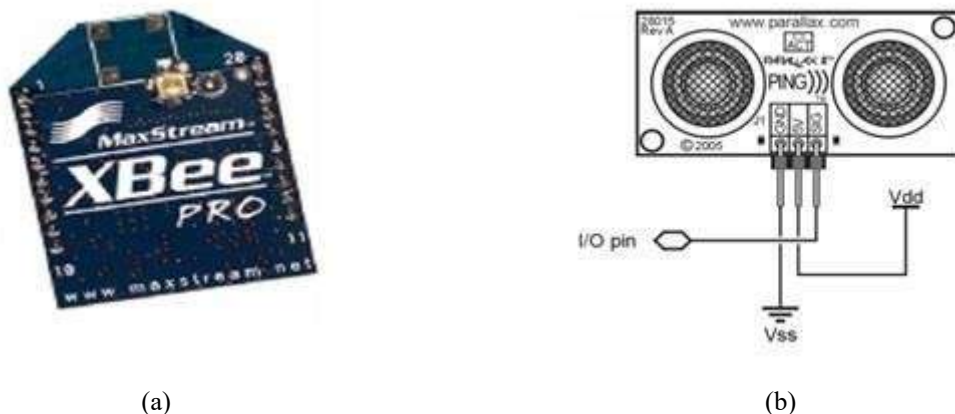
FIGURE 1. Transmitter and Sensor Components of Detector [8] (a) Xbee Pro b) Ping Sensor

Ping sensor is an ultrasonic sensor that can detect the distance of an object by emitting ultrasonic waves and then detect the reflection. With this sensor the river water level can be detected. On the Ping module))) there are 3 pins that are used for powersupply (+ 5V), ground and signal paths. Figure 2 below is a parallax ping sensor image.In this parallax ping sensor, the ultrasonic transmitter has a signal frequency of 50 KHz to be used as a temporary sound wave and will only emit waves when there is a trigger pulse from the microcontroller (high pulse for 5us). This wave will be emitted for 200uS and propagates at a speed of 344,424m / sec (or 1cm every 29,034us), when it hits the wave object it is reflected back to the ping sensor. While waiting for the reflection, the ping sensor generates a pulse. This pulse will stop (low) when the sound of the reflection is detected by the ping sensor. Therefore the pulse width can represent the distance between the ping sensor and the object.

Then the microcontroller measures the pulse width and converts it in the form of distance with the following calculation:

$$Distance = (Pulse\ Width\ /\ 29{,}034us)\ /\ 2\ (cm) .... (1)$$

or

$$Distance = (Pulse\ Width\ x\ 0.034442)\ /\ 2\ (cm) ....(2)$$

The error rate of the difference between the sensor reading and the actual reading can be determined by the formula:

$$Error\% = (|\ HT\text{-}HP\ |)\ /\ HT \times 100\% ....(3)$$

Where, HT = Theory Price (actual value) and HP = Practice Price (sensor measurement value)

RESEARCH METODOLOGY

Telemetry system of flood detection equipment consists of 6 supporting parts namely sensor measuring objects, detection devices, data processors, transmission lines, data receivers and displays. The object measured is the water level using the ping sensor as a detector. Microcontroller functions as a processor and converter of digital data into water level data. Wireless transmitter is used to transmit data from the microcontroller to the computer. Wireless receiver is used to receive data from a wireless transmitter. The computer functions to process digital data received from the microcontroller. Delphi software as a digital data viewer that will be converted into graphics in realtime.

```
+------------------+     +------------------+     +------------------+
| Ultrasonic Sensor|---->|  Microcontroler  |---->|    Wireless      |
|       Ping       |     |                  |     |   Transmitter    |
+------------------+     +------------------+     +------------------+
                                                          |
                                                          v
+------------------+     +------------------+     +------------------+
| Delphi Software  |<----|    Computer      |<----| Wireless Receiver|
+------------------+     +------------------+     +------------------+
```
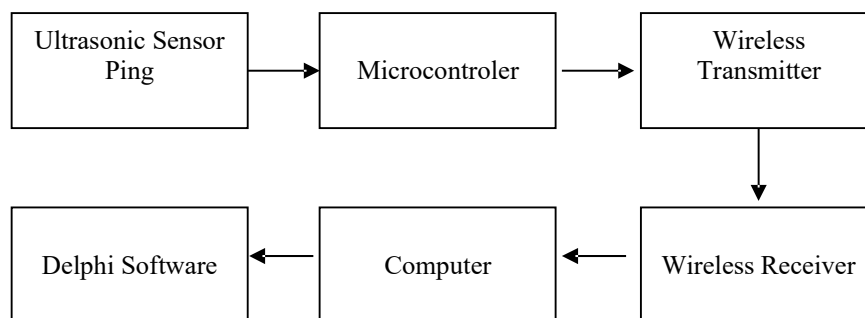
FIGURE 2. Telemetry System Chart of Flood Detection Devices

Block Diagram Tool

The tool that will be made, the tool is planned to be divided into six sections as indicated in figure 3.
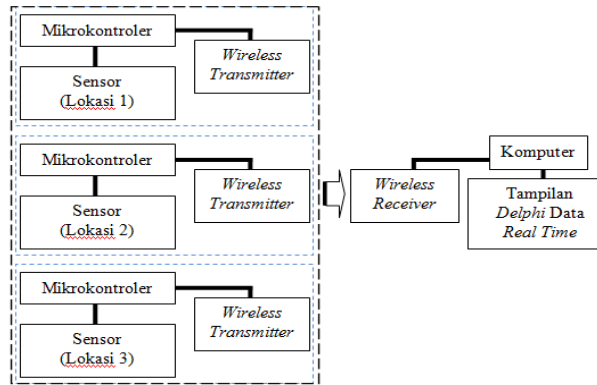
FIGURE 3. Tool Diagram Block

The function of each part is as follows:
  a. The sensor will detect the water level in a river where the output of this sensor is digital data.
  b. Microcontroller functions as a processor and converter of digital data into water level data.
  c. Wireless transmitter is used to transmit data from the microcontroller to the computer.
  d. Wireless receivers are used to receive data from a wireless transmitter.
  e. The computer functions to process digital data received from the microcontroller.
  f. SoftwareDelphi as a digital data viewer that will be converted into graphics in real time.

Wireless Work Design

The wireless work system is the wireless receiver broadcasts to the wireless sender. After the broadcast is received by the wireless sender, for example the wireless receiver sends broadcast character 1 then the one sending data is wireless sender 1. Furthermore, if the wireless receiver is broadcasting character 2 then the one sending data is wireless sender 2, and so on like that. Here shows the topology used is topology (star), centralized control, all clients must go through the center that distributes the data to all the nodes or clients that they choose. The central node is called the primary station / server while the others are called the secondary station / client server.
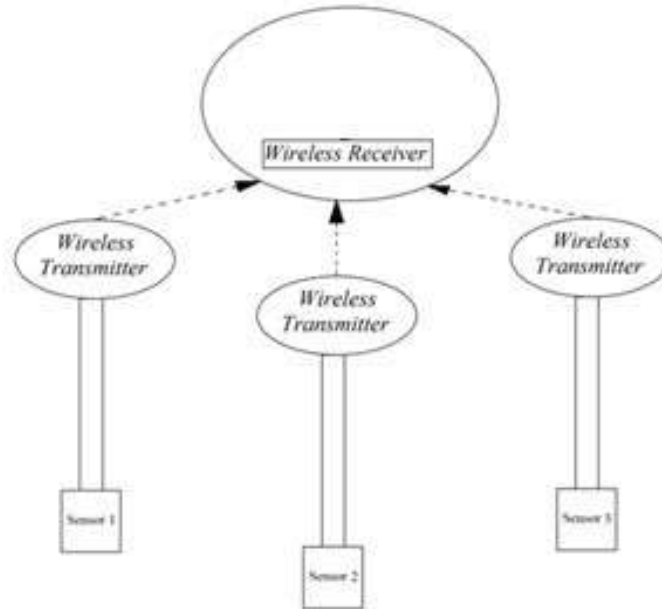
FIGURE 4. Wireless Work Design

RESULTS AND DISCUSSIONS

In this discussion, explained the results of research and testing in accordance with predetermined parameters. Starting with sensor frequency testing, sensor testing, wireless testing, data transmission testing, packet loss testing, and Delphi software testing. Table 1 below is a table of sensor frequency test results.

Sensor Testing Results Data

In testing this transmitter, it will measure the frequency emitted by the sensor, by testing using a frequency counter. The distance referred to here is the distance between the device and the frequency counter. This test is done by taking data randomly using a length measuring instrument. The first test results on the sensor transmitter, the frequency produced when the distance of 2.52 meters is equal to 42.076 KHz, after that the second test is conducted with a distance of 2.54 meters the frequency increases to 42.4902 KHz. The third test with a distance of 2.57 meters produces a frequency of 42.847 KHz. The fourth test with a distance of 2.75 meters produces a frequency that is equal to 45.8494 KHz. The fifth test has an increase in the frequency value that is equal to 47,9542 KHz with 2.79 meters distance. The sixth test obtained a frequency of 47.4956 with a distance of 2.84 meters, and the last of the seven frequencies amounted to 47.9542 KHz with a distance of 2.87 meters. Figure 6 below is a graph of sensor test results.

TABLE 1. Frequency Sensors

Number	Distance (m)	Frequency Test Results (KHz)
1	2.52	42.076
2	2.54	42.4902
3	2.57	42.847
4	2.75	45.8494
5	2.79	46.5451
6	2.84	47.4956
7	2.87	47.9542

.
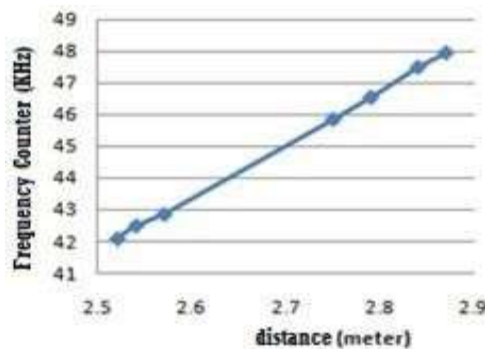
FIGURE 6. Frequency Sensor Graph

By looking at the graph above, it indicates that the emitted frequency is in accordance with what is desired to be transmitted to the receiver. In the datasheet, the maximum frequency of the ping sensor is 50 KHz. Here you can see the farther the distance, the greater the frequency of the sensor produced. This frequency testing uses a frequency counter. The frequency emitted by wirelees cannot be measured, because it is in accordance with the datasheet of XBee PRO itself, the frequency is 2.4 GHz, while the frequency counter has a maximum limit of 1.3 GHz.

Wireless Testing Results

Wireless test results in outdoor conditions and measured in an area that has many trees where the receiver is placed 30 cm above the ground. The test is carried out without the use of additional antennas and the position of the wireless transmitter is no higher than 2.5 meters. Here the wireless testing is done with a difference of 10 meters, the results of the data show when the distance 210 - 380 meters the experiment was carried out successfully. This shows that wireless communication is very good. The maximum distance of Xbee PRO used to be able to send and receive data in areas full of trees is 380 meters. If the distance between the transmitter and receiver exceeds 380 meters, the data sent will not reach the receiver or be lost.

In the actual datasheet, the distance for outdoor itself is 120 meters to 3.2 km, but for long distances you can add an antenna as a signal amplifier for example wire whip, UFL, or RPSMA antennas. The factor that causes data to be sent does not arrive or is lost is packet loss (packet loss) will occur if the transmission has an error (error). Disconnection often occurs, because it is not always within the coverage area. Limited communication bandwidth. Limited and varied range of mobile node capabilities. Can also noise or what is commonly called noise is an interference signal that is acoustic and electric.

Packet Loss Test Results

Based on the packet loss graphic image, it can be seen that wireless communication using XBee PRO with a barrier that is not going well here can be observed at a distance of less than 150 meters with a packet loss value of 76.67%. This figure shows that the data sent is not well received by the computer. However, at a distance of 125 meters the value of packet loss has decreased, the data sent by 25, while only 8 received by the computer so that at that distance has a packet loss of 68%. At a distance of 100 meters, the difference in data received by the computer with the data sent has decreased packet loss, with a packet loss of 65%. The average value of packet loss using a barrier that is equal to 64.4%, it shows that the value of packet loss can be categorized as very bad because it already exceeds 25%. This indicates that wireless communication using XBee PRO with a barrier is not optimal for distances of 150 meters or more. So, the farther away with the computer, the greater the value of packet loss.
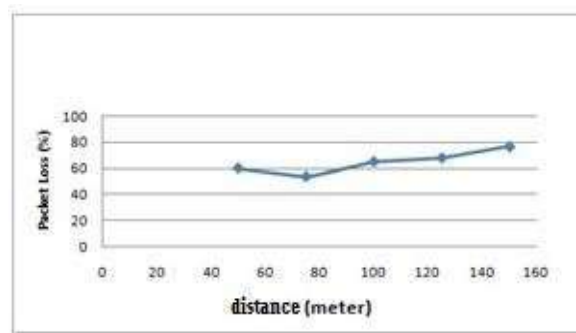
FIGURE 7. Packet Loss Graph with Barriers

In the measurement of packet loss there are several factors that influence it, including wall, barrier trees, noise or noise, limited bandwidth and distance. The greater the bandwidth, the longer the transmission distance. The amount of traffic flowing in the network exceeds the existing bandwidth capacity, policing control will get rid of the excess of existing traffic.

CONCLUSIONS

After planning and making the system, then testing and analysis are carried out. The frequency produced by the Ping sensor has range from 42.076 KHz to 47.9542 KHz. Maximum distance of XBee PRO to be able to work in an area full of trees (Outdoor) reaches 380 meters. The average value of packet loss with a barrier that is equal to 64.4%,

with the highest packet loss value is 76.67% that is at a distance of 150 meters, while the lowest packet loss is 53.3% at a distance of 75 meters.

ACKNOWLEDGMENTS

REFERENCES

1. R. Rahmat, M. Syahputra, and M. Lydia, "Real Time Monitoring System for Water Pollution in Lake Toba," in 2016 International Conference on Informatics and Computing (ICIC), Mataram, 2016, pp. 383-388.
2. S. Ponomarev and T. Atkison, "Industrial Control System Network Intrusion Detection by Telemetry Analysis," IEEE Transactions on Dependable and Secure Computing, vol. 13, no. 2, pp. 252-260, March 2016.
3. M. Satrio, A. A. Rafsanjani and R. R. T. Sadewo G. Nugroho, "Avionic system design Unmanned Aerial Vehicle for disaster area monitoring," in 015 International Conference on Advanced Mechatronics, Intelligent Manufacture, and Industrial Automation (ICAMIMIA), Surabaya, 2015, pp. 198-201.
4. J. Tristancho, C. Barrado, S. P. Mansilla, and E. Pastor, "A telemetry modeling for intelligent UAV monitoring," in 2009 IEEE/AIAA 28th Digital Avionics Systems Conference, Orlando, 2009, pp. 7.C.1-1-7.C.1-4.
5. K. L. Chen, Y. R. Chen, Y. P. Tsai, and N. Chen, "A Novel Wireless Multifunctional Electronic Current Transformer Based on ZigBee-Based Communication," IEEE Transactions on Smart Grid, vol. 8, no. 4, pp. 1888-1897, July 2017.
6.   L. H. Wang, T. Y. Chen, K. H. Lin, Q. Fang, and S. Y. Lee, "Implementation of a Wireless ECG Acquisition SoC for IEEE 802.15.4 (ZigBee) Applications," IEEE Journal of Biomedical and Health Informatics, vol. 19, no. 1, pp. 247-255, January2015.
7. J. C. Chou et al., "Wireless Sensing Systemfor Flexible Arrayed Potentiometric Sensor Based on XBee Module," IEEE Sensors Journal, vol. 16, no. 14, pp. 5588-5595, July 2016.
8. XBee 1mW Chip Antenna - Series 1 https://www.kr4.us/xbee-1mw-chip-antenna-series-1-802-15-4.html

Study of The Effect of Size Fractions on Gold Cyanidation Process

Siti Aminah[1,a)] and Fadila Rahmana[1,b)]

[1]Faculty of Engineering, University of Jember, JL. Kalimantan 37 Jember, Indonesia

[a)] Corresponding author: lilu.amin@yahoo.com
[b]fadila.rahmana@gmail.com

Abstract. Significant researches have been carried out to increase gold extraction efficiency in the leaching process, such as by optimizing cyanide concentration and dissolved oxygen concentration in the cyanidation process, selective leaching of gold from oxide ores with ammonia-cyanide solution, and addition of wood-extract biopolymer in the cyanidation process. The as-received ore sample was crushed, blended, ground and sieved, to obtain sample with a determined size fraction (P_{80} -200#). The chemical and mineral composition of the ore were analyzed using mineragraphy analysis, X-ray diffraction (XRD), X-ray fluorescence (XRF) and fire assay. A series of cyanidation process by bottle-roll tests. The highest gold extraction percentage (83.87%) in the cyanidation process when ore with size fraction of -400# was used. Using ore with size fraction of -200#, gold extraction percentage of 74.4% was obtained.

Keywords: gold, ores, cyanidation

INTRODUCTION

Gold is a precious metal that is widely used and has an important role in human life. Gold belongs to the group of precious metals because of its presence on earth which is rare and has certain specific properties. Gold can be found in the form of minerals where gold is the dominant precious metal, such as metals (*native*), *electrum*, *calaverite*, *sylvanite*e and minerals where gold is a minor element, such as *arsenopyrite*, *pyrite*, *chalcopyrite*, and others. Based on its ease of extraction, gold ore is classified as *free-milling* gold ore, complex gold ore and refractory gold ore. *Free-milling gold ore* can be processed with conventional cyanidation methods with a size that is not too smooth. For complex gold ore, it will require consumption of more leachate reagents during the cyanidation process while refractory gold ore requires *pre-treatment* before leaching.

The gold extraction method which is still widely used for the exploitation of gold for the mining industry scale is the cyanidation method and the amalgamation method (Hiskey, 1985 and Lee, 1994). In the amalgamation method, the use of mercury can have a negative impact on the environment, which can pollute the environment directly (Steele et al., 2000). The cyanidation method has several advantages including a relatively high percent extraction for *free-milling* ore, and requires lower consumption of reagents than using other reagents such as thiourea and thiosulfate. This cyanidation method can also be used to extract gold in a wide fraction of ore size range, from coarse to fine. Some factors that can affect the extraction performance using the cyanidation process is the concentration of the cyanide

reagent used, the duration of the cyanidation process, solute of oxygen concentration, percent solids, ore particle size fraction, the pH of solute, and the intensity of stirring.

One factor that affects the percent of gold extraction is the particle size fraction of gold ore used. The particle size used during the cyanidation process must match the size of the presence of gold and will also be influenced by associated minerals in the gold ore. In this study, there will be 5 variations of size fractions so that it will be known at what particle size, gold can be extracted more.

MATERIAL AND RESEARCH METHODS

The research was conducted to study the effect of gold ore size fraction on the percent of gold extraction in the cyanidation process. Ore samples were *as received* dried in the oven for 24 hours to remove the water content in the ore. Preparation starts with crushing all ores using *jaw crusher*, *roll crusher* and grinding to obtain ore sizes P $_{80\ \text{-}200\ \#.}$ All ores are mixed and homogenized using a *rotary splitter.* At various sizes so that the sample packets of the ore are homogeneous and ready to be used for further research. These ore packages will be used for the characterization and cyanidation process.

The following is the procedure for ore sample preparation:
1. The ore sample is dried in a oven 105^0C for 24 hours.
2. Dried ore is reduced in size using a *laboratory jaw crusher, roll crusher* and crushed *with a ball mill* to have a fraction of size $P_{80\ \text{-}200\ \#\ (74\ \text{microns})}$. Then sifting is done.
3. Blending the ore to produce a sample composite that will be used in subsequent experiments.
4. Ore samples are then sampled using a *rotary splitter* so that representative ore sample packs are produced.
5. Ore that has been prepared is analyzed for its Au and Ag content by *fire* assay and ICP.

(a)	(b)
(c)	(d)

FIGURE 1. instrument used for ore size reduction and sampling (a) Jaw Crusher, (b) Roll Crusher, (c) Grinding, and (d) Rotary Splitter.

Ore characterization is carried out on ore samples to identify the type and nature of the ore that will be used for research. Mineragraphic analysis of the polish is done to determine the location and size of gold in the ore and mineral followers. Analysis of the composition of chemical elements in the ore was carried out with *X-Ray Fluorescence* (XRF) and *Fire Assay*. Identification of the dominant mineral types contained in the ore is done by *X-Ray Diffraction* (XRD) analysis.

Procedures Preg-Robbing Test

Samples measuring 75 µm P80 inserted into the beaker 500 mL. Furthermore, a solution containing 2 gr / L NaCN was prepared with a pH of 10.5-11. The cyanide solution was reacted with AuCLgold standard solution 4- 50 ppm to obtain a gold cyanide solution with gold concentrations of 1.3 and 5 ppm, respectively. This solution is then stirred for 30 minutes to complete the conversion from $AuCL_4$ to Au $(CN)_{2-}$.

A total of 100 grams of sample were reacted with 200 mL of cyanide-gold solution with 0, 1, 3 and 5 ppm concentrations, respectively. Samples were agitated for 24 hours with sampling times of 15, 30, 60, 120 and 1440 minutes. Then the preg-robbing potential is calculated using the following equation:

$$\%PRB = (1-m) \times 100\% \tag{1}$$

where %PRB is the potential *preg-robbing* and m is the gradient of the distribution curve between the concentration of gold added to the concentration of gold in the solution . *Preg-robbing tests* performed are shown in Figure 2.

(a)

FIGURE 2. Experiments for determining the nature preg-robbing ore.

After the characterization of the samples was completed, a series of cyanidation and CIL experiments were carried out at the Hydro and Electrometallurgical Laboratory, Metallurgical Engineering Study Program, FTTM-ITB. The cyanidation experiment was carried out with variations in the particle size fraction. The size fractions used are -100+200#, -200+270#, -270+325#, -325+400# and -400#.

To determine the concentration of Au, Ag, Cu and Fe dissolved will be analyzed using the *Atomic Absorption Spectrophotometer* (AAS), which then calculates the percent extraction of each metal. In the cyanidation leach stage, sampling is conducted at 1, 2, 4, 8, 12, 24, 36 and 48 hours. Each sampling process will measure dissolved cyanide, dissolved oxygen concentration and pH of the solution.

The cyanidation experiments were carried out using themethod *bottle roll test* using variations of the fraction sizes of -100 + 200 #, -200 + 270 #, -270 + 325 #, -325 + 400 # and -400 #. Samples and water are first put into bottles, then pH measurements are taken. The pH used for the leach conditions is 10.5 - 11. If the pH is less than specified, then Ca (OH)added is until the pH matches the specified pH range. PH conditioning is done to prevent the formation of HCN gas that is harmful to the researcher and the environment and the declining gold-silver recovery due to evaporation CN-.

Sampling was carried out at 1, 2, 4, 8, 12, 24, 36 and 48 hours during the leaching process as shown in Figure III-8. Samples were taken as much as 50 ml for AAS testing and testing of free cyanide concentrations. For each sample, the concentration of free cyanide in the solution was measured by titration using silver nitrate (AgNO$_3$) solution as titrant and ρ- Dimethylaminobenzylidene Rhodanine as an indicator. Titration is stopped if there has been a change of color to pink indicating the exact whole free cyanide already saturated react with Ag $^+$ and formed complex Ag (CN) $_{2-}$. The reaction that occurs at the equivalent point is as follows:

AgNO$_3$ + 2 NaCN = NaAg (CN)$_2$ + NaNO$_3$

(a)

(b)

(c)

(d)
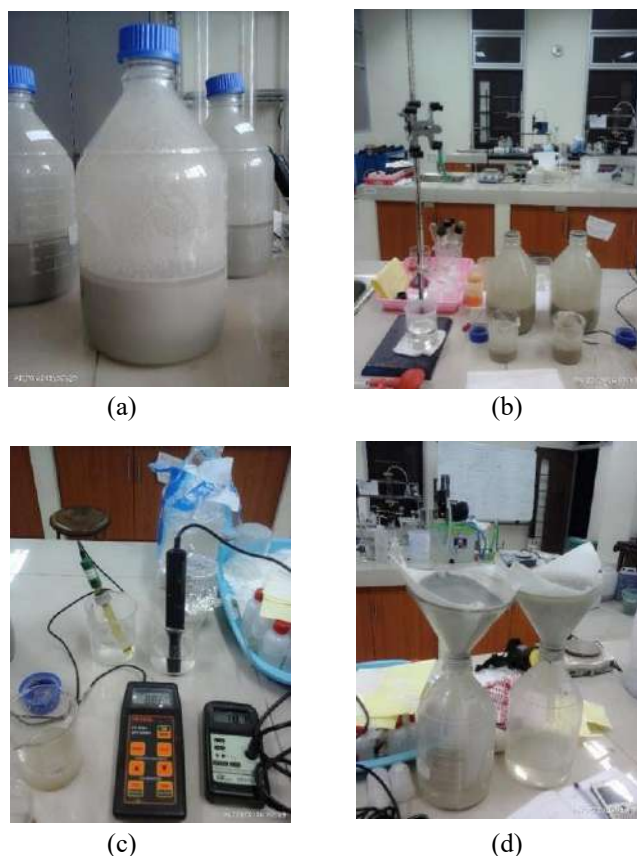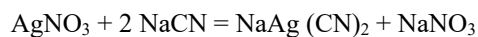
FIGURE 3. (a) *Bottle Roll* which is ready to be put in a roll system, (b) Preparation of sampling and titration (c) Measurement of pH and DO, and (d) Screening process

The research began with a mineragraphic test. Test results show that gold is in ore in the form of electrum.

RESULTS AND DISCUSSION

In this part, will explain about result of sample characterization and result of the leaching experiment using the bottle roll.

The Result of Sample Characterization

This research began with a mineragraphic test. In the analysis of mineragraphy, samples need to be made according to the preparation so that the analysis is done well. The preparation used in the analysis is a polishing incision. Shooting

is carried out in the reflection light of the Nikon Eclipse 50 iPol. From the observations of mineragraphy, it is known that the ore samples consist mostly of quartz, as well as a small amount of sulfide minerals, namely chalcopyrite, spalerite, pyrite, and covelite. Calcite is also found in this ore, which can potentially causeproperties *preg-robbing*. Megascopis gold minerals are not visible, but in observations mineragraphy found the presence of gold in the form of electrum minerals. Electrum minerals are found to be very few in number and have a creamy white appearance, measuring very fine to 5 μm that are scattered randomly and are included in quartz.

(a)   (b)
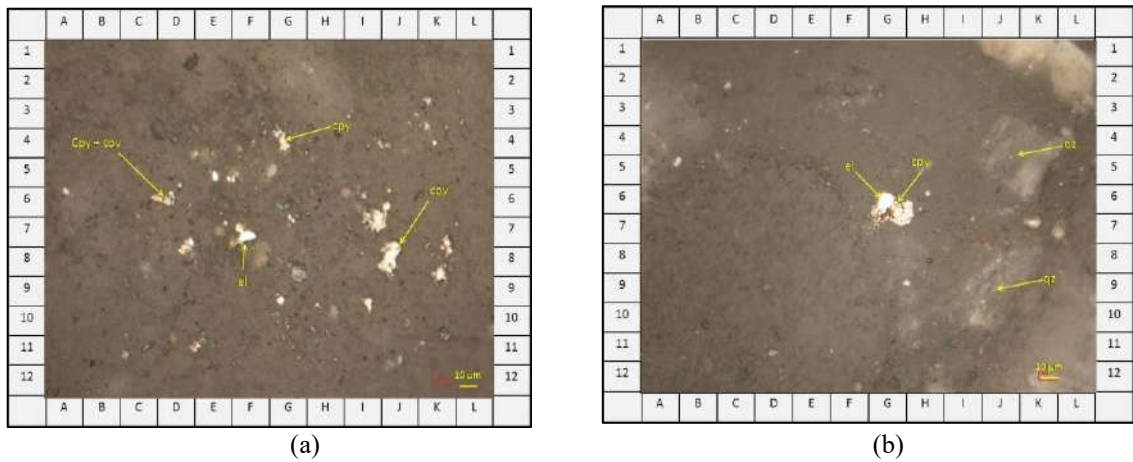
FIGURE 4. (a). Micrography of a sample A, under reflection microscope, cumulative inclusion of sulfide mineral detritus in urate quartz crystals, cov = covellite, cpy = chalcopyrite, el = electrum. (b). Micrography of a sample A, under reflection microscope, detritus sulfide containing electrum, qz = covellite quartz, cpy = chalcopyrite, el = electrum.

TABLE 1. Composition of Elements Contain in the Sample.

Compound	Composition (%)
SiO_2	65.64
TiO_2	0.259
Al_2O_3	6.66
Fe_2O_3	4.15
MnO	0.0679
CaO	9.75
MgO	2.78
Na_2O	1.00
K_2O	1.90
P_2O_5	0.132
SO_3	0.476
LOI	6.86
ZnO	0.0101

Compound	Composition (%)
CuO	0.0062
SrO	0.0714
V_2O_5	0.0132
Cr_2O_3	0.0314
BaO	0.0534
Rb_2O	0.0086
Ga_2O_3	0.0018

TABLE 2. Results of the Analysis of Fire Assay and ICP

Element	Content
Au	5.2 ppm
Ag	< 0.5 ppm

Based on the results of the fire assay analysis, it was found that Au levels in ore samples is 5.2 ppm and Ag level is <0.5 ppm. As for the preg-robbing test, ore samples have preg-robbing properties, the ore has a tendency to take back the $Au(CN)_2$ complex- disolved in solution so that can gold extraction decrease at certain hours. This preg-robbing characteristic is usually caused by the presence of carbon in the ore, for ore samples it is known that carbon is present in the form of the mineral calcite ($CaCO_3$). Carbon is one of the *carbonaceous matter* in the ore can also cause gold trapped in it, thus blocking the leaching of gold.

Based on the results of *pre-robbing test*, ore samples have preg-robbing properties that is, the ore has a tendency to reclaim the Au (CN)complex $_2$- dissolved in solution so that gold extraction can decrease at certain hours. The value of% PR is 18.7% and is expected to have a negative influence during the leach process. The possibility of thiseffect *pre-robbing* will be further evaluated from the results of the cyanidation experiment. This characteristic of *pre-robbing* is usually caused by the presence of carbon in the ore. For samples A and B it is known that carbon is present in the form of the mineral calcite ($CaCO_3$). Carbon is one of the main *carbonaceous matter* in the ore which can also cause gold to be trapped in it, thus preventing gold leaching.

The Result of The Leaching Experiments using The Bottle Roll

Process of reducing the size of the ore used as a sample in this experiment is very important because based on the results of the mineragraphic test, the electrum is of fine size and associated with quartz, chalcopyrite, covelite, calcite or digenit. The gold associated with silica must be completely liberated from silica in order to dissolve it in the leachate solution. Likewise the electrum associated with chalcopyrite and its changes.

In this experiment the leaching process was carried out using a *bottle roll test* with variations in the size fraction of -100+200 mesh, -200+270 mesh, -270+325 mesh, -325+400 mesh and -400 mesh. The experiments were carried out for 48 hours at room temperature and atmospheric pressure, 40% solids percent, cyanide concentration of 1000 ppm, dissolved oxygen concentration ≥ 8 ppm, pH range 10.5-11 and bottle rotational speed of 70 rpm. Profile of percent extraction of Au, and Ag as a function of time at various ore size fractions is shown in Figure 5 and Figure 6.
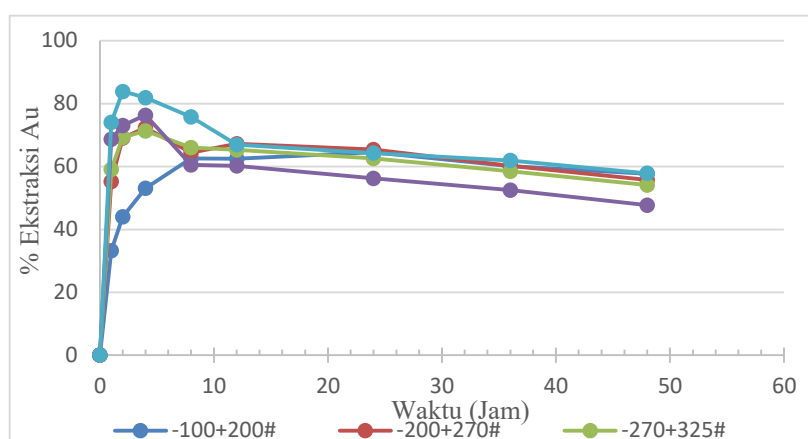
FIGURE 5. Profil of % Au extraction in various size fractions

In Figure 6 you can see the effect of size fraction on Au extraction percent. From the graph above, it can be seen that the highest gold extraction value is obtained in the fraction of -400 mesh size, which is 83.87%. In the finer size fractions, the gold extraction percent is also higher. Based on the results of mineragraphy shows that gold is in a smooth size so that in the most refined size fraction, the degree of liberation of gold will be higher. The leaching rate will increase and the extraction percent will also increase.

For all size fractions, extraction was highest when leaching occurred at the 4th hour. After that there will be a reduction in percent extraction from gold. This indicates that the ore is preg-robbing. This nature of *preg-robbing* is caused by calcite ($CaCO_3$) contained in the mineral ore as much as 8-10%. This trait will be verified by the pregrobbing test discussed in the previous chapter.
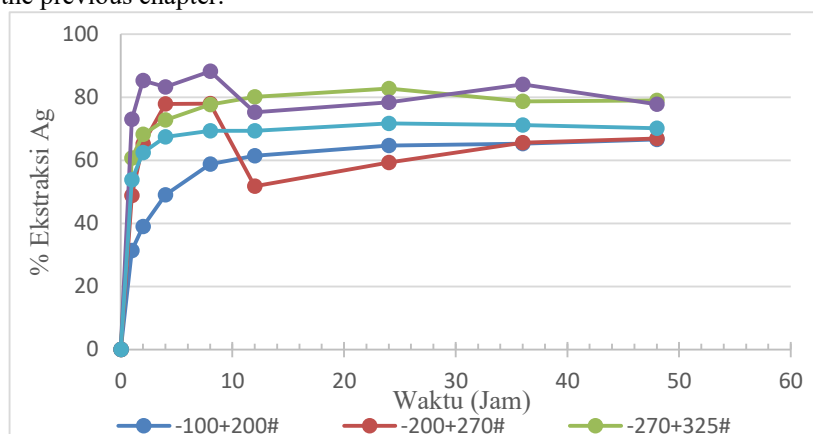
FIGURE 6. Profil of % Ag extraction in various size fractions

Based on the experimental results presented in Figure 6, the highest percent extraction value of Ag also occurred in fractions of size -325+400 mesh, which was 88.22%. The longer the leaching time, the percent extraction of Ag was also seen to decrease after the 8th hour. This further showed that the ore had a *preg-robbing property*.
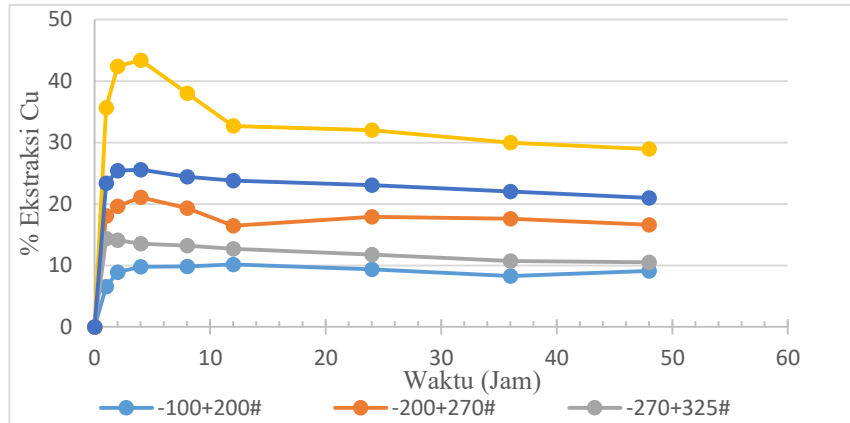
FIGURE 7. Profil of % Cu extraction in various size fractions
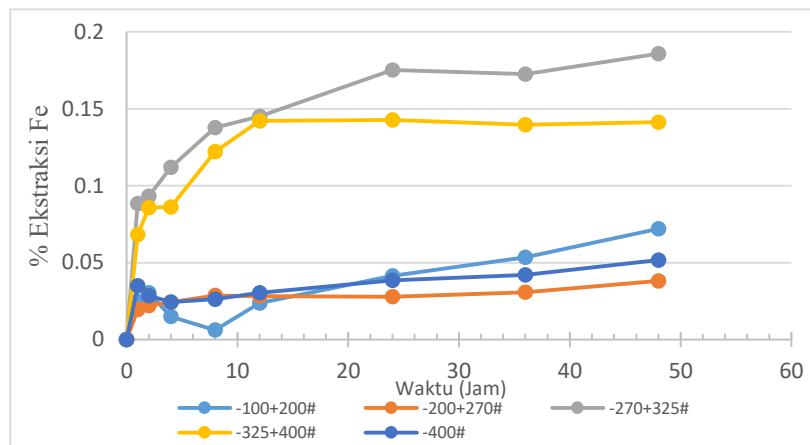
FIGURE 8. Profil of % Fe extraction in various size fractions

The highest percentage of Cu extraction is 43.39% in the fraction of size -325+400 mesh. Whereas the percentage of Fe extraction was very low at 0.18% in the fraction of the size -270+325 mesh.

CONCLUSION

Ore samples tend to be *preg-robbing* with the main content of silica, some sulfide minerals (chalcopyrite, pyrite), and calcite, where gold is very fine to 5 µm trapped in sulfide and silica minerals. The highest gold extraction value was obtained in the fraction of the size of -400 mesh, which was 83.87%. The highest value of Ag extraction also occurs in fractions of -325 + 400 mesh size, which is 88.22%.

ACKNOWLEDGMENTS

REFERENCES

1. Achmadi, S. S. 1990. Kimia Kayu. Departemen Pendidikan dan Kebudayaan. Direktorat Jenderal Pendidikan Tinggi. Pusat Antar Universitas. Ilmu Hayat. Institut Pertanian Bogor.
2. Adams, M. D. 2005. Advances in Gold Ore Processing. Elsevier.
3. Al-Saidi, H. M., 2013. The fast recovery of gold(III) ions from aqueous solutions using raw date pits: Kinetic, thermodynamic and equilibrium studies. Journal of Saudi Chemical Society, xxx, xxx–xxx
4. Behin, J. an Azizian, S. (2004), *Kinetic models of sorption: a theoretical analysis*, Journal of Colloid and Interface Science, 276(1): 47-52.
5. Braun, Patrick. Method Manual Volume 1 Gold Analysis in Alkaline Cyanide Solutions. Society of Mineral Analysts Sparks, Nevada.
6. Habashi,F., A Textbook of hydrometallurgy,metallurgie extractive, Quebec, Enrc Canada 1993.
7. Judoamidjojo, R. M., E.G. Said dan L. Hartoto. 1989. Biokonversi. Departemen Pendidikan dan Kebudayaan. Direktorat Pendidikan Tinggi. Pusat Antar Universitas Bioteknologi, Institut Pertanian Bogor. Bogor.
8. Kinoshita, T., Akita, S. S., Ozawa, S., Nii, S., Kawaizumi, F., Takahashi, K., 2004. Continuous Recovery of Gold(III) via Foam Separation with NonionicSurfactant. Journal of Minerals & Materials Characterization & Engineering, Vol. 3, No.1, 53-63.
9. Marsden, John and C. Iain House. 2006. *The Chemistry of Gold Extraction,* 2nd edition. Society for Mining, Metallurgy and Exploration, Inc. : USA.
10. Syukri. 1999. *Kimia Dasar 3*. Bandung : Institut Teknologi Bandung.

Design of Ergonomic Chairs for Railroads Installation Workers

Robertoes Koekoeh Koentjoro Wibowo[1], Priyo Agung Wicaksono[2], Hari Arbiantara Basuki[3]

[1,3] Mechanical Departmen Engineering, Engineering Faculty, Jember University
[2] Student of Mechanical Departmen Engineering, Engineering Faculty, Jember University
Jember Jln. Kalimantan 37, Jember 68121
e mail: koekoeh@unej.ac.id

Abstract. The train is a transportation that has the advantage in facilitating the movement of goods or people and masse and environmentally friendly. During 2010-2018 has been carried out the construction of new lines including double track, double track railway which some processes done manually by the workforce.
Potential hazards that can be experienced by workers one of them is the danger of ignoring ergonomic factors. Ergonomic dangers can occur when the job, body position and working conditions or put a burden on the body that can eventually cause low back pain. Low back pain is associated with the frequent carrying, lifting, and pushing of heavy items and often or long bowing, sitting or standing or other unnatural postures standing for long periods of time and lack of rest.
The Research was conducted on railroad installation worker for making ergonomic chair design that accordance with anthropometry of Indonesian. The aim of the research is to design of ergonomics chair that accordance with rail road installation workers, then analyze result of design and making chair for workers. The design and manufacture of chairs are used according to the principles of ergonomics. The method used in this research is Ergonomic Function Deployment. The method in this research is the development of Quality Function of Deployment by adding Ergonomic principle. Ergonomic Function of Deployment, which is by adding new relationship between consumer's desire with questionnaire method for railroad installation workers and ergonomic aspect of product. The new design of chair is by using width of 40.1 cm that accordance with anthropometry dimension of the 95th for hip width of workers. The resulted of the questionnaire, resulted 53.33% of railroad installation workers have experience lower back pain when working without chair. By using a new design of chair, the railway worker feels comfortable when seat on the chair during work, as many 56.6% from respondence. Another result, the existence of the chairs increasing 50% work attempt of the worker. The chair is used for rest by workers is 46.6%, design of chair is sturdy seats for workers is 63.3% and workers feel comfortable with a 60% in sitting position with the chair. However, workers still feel the pain in other parts by 60%. for rest 46.6%, sturdy seats for workers 63.3% and workers comfortable with a 60% sitting position.

Keyword: chair, ergonomics, installer, rail road

Abstract. During the period of 2010-2018 the construction of a new double track railway line using human labor was carried out. The potential hazards that workers can experience are the dangers of ignoring ergonomics factors. Injury or fatigue can occur when the type of work, body position and working conditions or placing a burden on the body not in the right position. The purpose of this study is to design, create and analyze the results of an ergonomic chair for railroad installation workers. The method used in this study is the Ergonomic Function of Deployment. The results of this study found that the anthropometric dimensions used were 95th percentile with hip width of 40.1 cm. The results of making chairs obtained data 53.33% of railroad installer workers experience lower back pain. 56.6% of railroad installation workers feel comfortable with a chair when work is in progress, as many as 50% of railroad installer workers say it is helped by the existence of a chair when working. Workers still feel pain in other parts by 60%. Workers most often use chairs to rest 46.6%, workers feel sturdy chairs to work at 63.3% and feel comfortable with a sitting position of 60%.

Keyword: Chair, Ergonomics, Railway

INTRODUCTION

Railroad transportation has advantages in facilitating mass movement of goods or people, supporting equity, environmentally friendly, supporting growth and stability as well as driving national development [1]. Train is an effective mass transportation mode, for long and close distances and can meet basic human needs in facilitating and accommodating all economic and social activities. Its existence as a means of transportation to transport various types of goods and services from one place to another can drive the community's economy [2]

In the year 2010-2018 new construction of railroad tracks has been carried out as long as 922 km, where in the process built it some work processes are still carried out manually, using human labor. Human labor is an important factor that has a major role in development because he is the subject of management and supervision in national development [3].

Occupational safety and health, it is very important to applied it at work, so that government and business entities need to pay attention to occupational safety and health in order to reduce or prevent accidents in work activities [4].

One of the potential injuries that might exist in workers is to neglect the ergonomics factor in making the design of a tool or work station. Ergonomics is engineering knowledge to achieve an adjustment and reciprocity between workers and the tools used in carrying out work. The benefits can be measured in terms of efficiency, health and well-being. [5]. The potential for injury to a worker can occur when the type of work, body position, and heavy of the load that given to the body are not appropriate given to the worker. Injuries that can occur in workers who are misplaced are back pain [5].

Lower back pain is lower back pain, which is experienced by many workers [6]. Low back pain associated with frequent carrying, lifting, and pushing heavy objects and often or for a long time when bending, sitting, or standing long or other postures that are not natural to stand for long periods [7].

Squatting and standing position is a method that is done by workers when installing a railroad in the installation work, such as welding, bolt tightening or checking the rail. Based on research found that this method significantly increases the risk of pain in the waist, knees or legs after more than 5 minutes, the pain becomes more painful when working in a crouching position [8].
Workers experience back pain due to incorrect work position or no devices that helping during working. Railroad workers who are still manually installing rails by hand will work more in a squat position. With such conditions added without tools when working to be one of the causes of low back pain in railroad installation workers. [9]
The use of a chair while working is an effort that can be done to reduce the impact of low back pain on railroad installation workers. The chair is an object to help improve posture and reduce pressure on the body when used [9].

Railroad installer workers have the potential to experience fatal injuries caused by fatigue at work and lack of rest time [10]. A short rest can reduce the symptoms of low back pain. Ergonomically designed chairs will have a positive impact on its users [11], but chairs that are not ergonomically designed will result in complaints of uncomfortable, awkward positions, to low back pain significantly on users [12].

The purpose of this research is to design and create an ergonomic chair prototype for railroad installation workers in accordance with Indonesian anthropometry.

METHODOLOGY

Firstly, this research was conducted by taking Indonesian people anthropometry data. Secondly, followed by interviews and filling out questionnaires to workers on the railroad tracks. The data obtained were analyzed using percentile and the Ergonomic Function Deployment method to obtain an ergonomic chair design in accordance with the wishes of the respondents. Anthropometric measurements were carried out on 50 male railroad installation workers. And they were asked to fill out questionnaires and were interviewed. The stages of this research are as follows:

1) Anthropometric measurements
Anthropometric measurements were carried out on 50 male railroad workers. Anthropometric measurement results data are then processed by conducting data uniformity tests and calculating percentile values for each dimension of the human body. In testing data uniformity, data must be between the Lower Control Limit and the Upper Control Limit, if there is data that is outside the control limit, the data value is more than the Upper Control Limit (UCL) or less than the Lower Control Limit (LCL), then the data must be removed. This test is carried out to facilitate the designer in making decisions during the product planning and design process. The equation used for processing anthropometric data is as follows [13]

a. Data Uniformity Test
1. Average

$$\bar{x} = \frac{\Sigma x_i}{n}$$

Where:
$\bar{x}$ = average
x_i = amount of data
n = number of observations

2. Standard Deviation of Samples

$$s = \sqrt{\frac{\Sigma(x_i - \bar{x})^2}{n-1}}$$

Where:
s = standard deviation
$\bar{x}$ = average
x_i = amount of data
n = number of observations

3. For data control limits with K = 2, then:

UCL (Upper Control Limit) $= \bar{x} + 2s$
LCL (Lower Control Limit) $= \bar{x} - 2s$

b. Percentile

K^{th} percentile $= \bar{x} \pm Z\ s$
Where:
K^{th} = Value for the desired percentile

Z = Z = Constant for the desired percentile
for 5%th percentile, the value of Z = -1,645
for 95%th percentile, the value of Z = + 1,645
for 50%th percentile, the value of Z = 0

The questionnaire was given to 50 respondents, namely railroad installer workers. The questionnaire contains the expectations of workers regarding the design of suitable seats in relation to the installation of railroad tracks. Besides that the questionnaire also inventory complaints of pain experienced by workers on their bodies when installing railroad tracks. Then the questionnaire is processed using Ergonomic Function Deployment. After the expected prototipe of seat design is finished and tested, the worker is asked for his opinion through a questionnaire about the impact felt by the railroad installer workers from the results of trying to design the seat made

3) *Ergonomic Function Deployment* (EFD)

Ergonomic Function Deployment (EFD) is a development of Quality Function Deployment (QFD), namely by adding a new relationship between consumer desires and ergonomic aspects of the product. This relationship will complete the House of Quality (HOQ) matrix form which also translates into desired ergonomic aspects [14].

4) Design and Manufacture of Railroad Seats.

The design and manufacture of ergonomic chairs begins with measuring the dimensions of the railroad track, selecting materials and the manufacturing process. Finished seats will be tested on railroad workers. The results that become parameter values are ergonomic aspects of the chair and lower back pain suffered by workers.

RESULTS AND DISCUSSION

Data on Percentile Calculation Results

The results of anthropometric measurements on railroad installation workers are given in Table 1.

Table 1. Anthropometric Measurement

No	Body Dimension	n	Dimension (cm)	s	Dimensions Percentile (cm)		
					5th	50th	95th
1	Stature (height)	50	168.26	5.401	160.8	166.5	177.6
2	Weight (kg)	50	62.18(kg)	11.62	46.2	59.0	86.4
3	Height in a sitting position	50	88.7	3.80	82.0	88.0	95.4
4	Shoulder Height in a Sitting Position	50	61.2	3.7	55.3	61.0	68.0
5	Elbow Height in a Sitting Position	50	22.6	3.8	14.5	21.7	28.9
6	Thigh Thickness	50	14.9	2.2	12,1	14,8	19.2
7	Knee Length	50	56.3	4.2	50.0	56.4	65,0
8	Popliteal length	50	45.0	3.7	38,7	44,8	51.2

No	Body Dimension	n	Dimension (cm)	s	Dimensions Percentile (cm)		
					5th	50th	95th
9	Knee Height	50	52.5	4.5	44.9	52,0	62.2
10	Popliteal Height	50	40.2	2.9	35.6	39.9	48.4
11	Shoulder Width	50	45.1	4.1	39.3	44,0	53.6
12	Upper Shoulder Width	50	36.5	3.1	31,3	37.0	41.0
13	Hip Width	50	34.4	3.2	29.0	34,0	40.1
14	Chest Thickness	50	18.6	2.4	14.6	18.4	23.5
15	Stomach Thickness	50	20.5	3.0	15,2	20.4	27,2
16	Upper Arm Length	50	37,4	3.3	31.0	37.8	43.4
17	Forearm Length	50	45.0	3.6	37,2	45,0	52.0
18	Head Length	50	18.2	2.9	16.6	18.1	20,0
19	Head Width	50	15.8	1.2	13.2	16.2	17.6
20	Elbow Length Spans	50	89.0	4,8	78,00	90,7	94.8
21	Leg Length	50	24.9	1.1	23.0	24.9	27.0

From Table 1 the 5 th and 95 th percentile values are obtained in which the present values are used to design seats for railroad workers that are in accordance with human body measurements in general.

Table 2. Questionnaire 1

No	Variabel	Attribute	Choise (√)
1	The chair the railroad worker desires	a. Lightweight chair	
		b. Flexibility stuck to the train tracks	
		c. Seat with foam pads	
		d. Height adjustable	
2	Parts of the body that experience complaints of pain when working	a. Neck	
		b. Hand	
		c. Legs	
		d. Lower back pain	
3	Do You Feel Comfortable to install rail without a seat?	a. Yes	
		b. No	
		c. I have no idea	

No.											
4	Do you experience pain in the spine while working?	a. Yes									
		b. No									
		c. I dont know									
5	Are you comfortable doing work with squatting?	a. Yes									
		b. No									
		c. I dont know									
6	Does the chair you want has a backrest?	a. Yes									
		b. No									
		c. No Opinion									
7	Have you ever suffered injuries during installation?	a. Frequenly									
		b. No									
		c. some while									
8	What color chair do you want?	a. Brown									
		b. Blue									
		c. Grey									
		d. Green									

Table 3. Questionnaire results

No.	Score					Score Pecentage (%)			
	a	b	c	d	n	a	b	c	d
1	10	18	12	10	50	20,0	36,0	24,0	20,0
2	13	12	10	15	50	26,0	24,0	20,0	30,0
3	25	10	15		50	50,0	20,0	30,0	
4	29	8	13		50	58,0	16,0	26,0	
5	17	25	8		50	34,0	50,0	16,0	
6	17	22	11		50	34,0	44,0	22,0	
7	18	25	7		50	36,0	50,0	14,0	
8	12	26	3	9	50	24,0	52,0	6,0	18,0

The red table section is not provided a question.

* = The largest number of complaints is the dominant experienced by railroad installer workers

Table 4. Results of Questionnaire From Table 3

No	Variable	Attribute	Percentage
1	The chair the railroad worker desires	Flexibility stuck to the train tracks	36.0%
2	Parts of the body that experience complaints of pain when working	Lower back pain	30.0 %
3	Do You Feel Comfortable to install rail without a seat?	No	50.0%

No	Variable	Attribute	Percentage
4	Do you experience pain in the spine while working?	Yes	58.0 %
5	Are you comfortable doing work with squatting?	No	50.0 %
6	Does the chair you want has a backrest?	No	44.0 %
7	Have you ever suffered injuries during installation?	No	50.0%
8	What color chair do you want?	Blue	52.2%

The Result of the Design of Train Installer Seats

The results of the design and manufacture of chairs are the results of the wishes of the railroad installer workers obtained from the questionnaire and then combined with processing the anthropometric measurement results data. Questionnaire processing, using the Ergonomic Fuction Deployment method
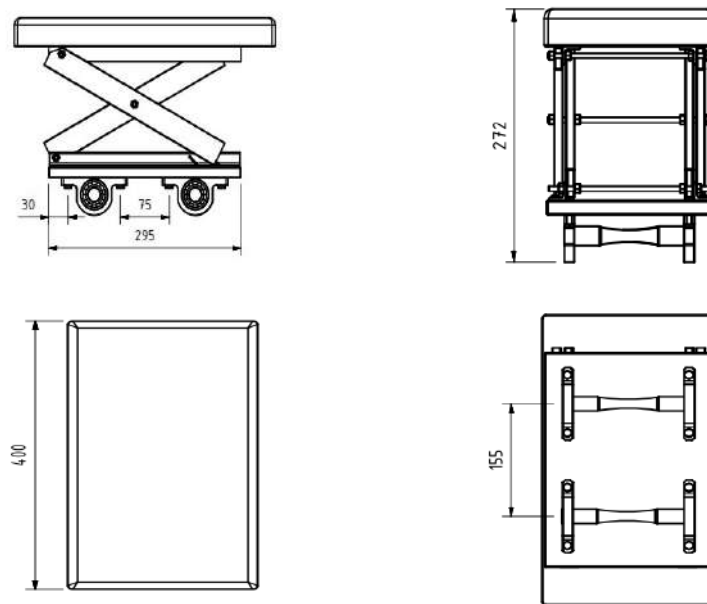
Figure 2 Rail Installer Chair

Table 5 Technical Specifications of Chairs

No	Technical specifications	Specifications
1	Chair Length	400 mm
2	Seat Width	200 mm
3	Minimum seat height	174 mm
4	Maximum Chair Height	272 mm
5	Foam material used	PVC foam
6	Wood used	Pine wood
7	Bearing type used	Aluminium KP004 Ø 20
8	Shaft	Aluminium Ø20
9	Plate	Aluminium Plate
10	Maximum Load	± 90 kg
11	Install a chair	Placed on the rail

Table 6 Questionnaire Analysis of Chair Design Results for Railroad Installation

No	Variabel	Atribut	Presentase	Atribut	Prosentase	Atribut	Prosentase
1	Chair Prototype	Comfortable	40%	Uncomfortable	20%	The chair is not strong enough	10%
2	The chair is used most often	For Rest	46,6 %	Welding	26.6%	Bolt tightening	30%
3	Still feel pain when working after using a chair	Yes	60%	No	20%	Respondents did not vote	20%
4	Still feel pain in the spine when working after using a chair	Yes	53.3 %	No	26.66 %	Respondents did not vote	20%
5	Comfortable with a chair when work in progress	Yes	56,6 %	No	23.33%	Respondents did not vote	20%
6	The chair helps workers in the installation of railroad tracks	Yes	50%	No	23.30%	Respondents did not vote	26.6%
7	Strong chairs for workers	Yes	63,3%	No	13.33%	Respondents did not vote	23.33%
8	Workers are comfortable with sitting position	Yes	60%	No	23.30%	Respondents did not vote	16.60%

CONCLUSION

1. Based on the results of the study, it was found that the anthropometric dimensions used for the ergonomic train railroad worker chair are 95th percentile with hip width of 40.1 cm.

2. From the results of the study, it was found that 53.33% of railroad installer workers still experienced low back pain. As many as 56.6% of railroad installation workers feel comfortable with the chair when the work is in progress, as many as 50% of railroad installation workers stated the existence of a chair helps do the work. Workers still feel pain in other parts by 60%. Workers most often use chairs to rest 46.6%, sturdy chairs for 63.3% workers and comfortable workers with 60% sitting position.

REFERENCES

[1]   Bappenas. Transportasi di Indonesia. Jakarta 2016 ; Badan Penerbit Dinas Perhubungan RI.

[2]   *Annual Report KAI*. Laporan tahunan kereta api Indonesia : PT Kereta Api Indonesia; 2015

[3]   Rencana Strategis Kementrian Perhubungan 2015-2019. Jakarta ; Badan Penerbit Dinas Perhubungan RI ; 2015

[4]   Sofiandi, Aldi. 2015. *Pelaksanaan Perlindungan Hukum Keselamatan Dan Kesehatan Kerja Pekerja Penjaga Pintu Perlintasan Kereta Api Di PT KAI (PERSERO) DAOP IV YOGYAKARTA*. Yogyakarta : Universitas Islam Negeri Sunan Kali Jaga. Bappenas.

[5]   Yassierli, Hardianto 2015. *Ergonomi Suatu Pengantar*. Bandung : PT Remaja Rosdakarya.

[6]   Yassierli, *Implementasion of Ergonomic programs to reduce sick leave due to low back pain among nickel minning operators*. Bandung: Bandung Institute of Technology.

[7] Fajar, Irwan. 2014. Pengaruh Posisi Kerja Terhadap Kejadian *Low Back Pain* pada Pekerja di Kampung Sepatu, Kelurahan Miji , Kecamatan Prajurit Kulon, Kota Mojokerto. Jember: Universitas Jember.

[8] Andersen et. al 2007. *Risk factors for more severe regional musculoskeletal symptoms: a two-year prospective study of a general working population*. : Netherlands.

[9]   Jaewan, K 2008. *A Case Study For The Selection Of Railway Human Reliability Analysis Method*. Korea Railroards Research Institude

[10] Clark, Calabrese Bianka et al. 2017. *Time of day effects on railroad roadway workers injury risk. US Departement of Transportation*, Cambridge : USA

[11] Peter J. Sheahan et al 2016. *The Effect of rest break schedule on acute low back pain development in pain and nonpain developers during seated work*. Queen's University. Canada

[12] Rosanna Alojado et al 2015. *Designing an ergonomic   chair for pedicurists and manicurists in Quezon City, Phlipines ;* Departement of Industrial Engineering University of Philipina , Diliman : Quezon City Philipines

[13] Adrianto, R., et al. 2014. Usulan Rancanangan Tas Sepeda *Trial* Menggunakan Metode *Ergonomic Function Deployment* (EFD). Bandung. Jurnal Online Institut Teknologi Nasional No. 02, Vol. 02.

[14] Irmai Puspita. 2016. Modifikasi kursi penumpang kereta api ekonomi yang ergonomis dengan metode *ergonomic function deployment*. (Studi Kasus Pada KA Logawa yang Diproduksi di PT. INKA). Jember : University of Jember

[15] Sophia Tetteh et. al. 2016 . *Ergonomics assessment of locally fabricated passenger seats in trotro vehicles in Accra*, Ghana. Accra : University of Ghana.

[16] Tri Novianto, Tanpa Tahun. Perancangan Dan Pengembangan Desain Produk Meja Warung/Café Lesehan Multifungsi Yang Ergonomis Menggunakan Metode Ergonomic Function Deployment (EFD). Semarang : Universitas Dian Nuswantoro Semarang

[17] Wibowo, D.P., Nasifahl L., Dan Berlianty, I. 2011. Perancangan Ulang Desain Kursi Penumpang Mobil Land Rover yang Ergonomis dengan Metode *Ergonomic Function Deployment (Efd)*. Yogyakarta: Teknik Industri, UPN "Veteran".

Petrophysics Evaluation in Tight Sand Reservoir

Eriska Eklezia Dwi Saputri[1, a]

[1]*Faculty of Engineering, University of Jember, Jl. Kalimantan 37 Kampus Tegal Boto*

[a]eriska.eklezia@unej.ac.id

Abstract. Tight sand reservoir means that reservoirs have low porosity and low permeability. Theses type of reservoirs are extremely complex, producing from multiple layers with different permeability that often enhanced by natural fracturing. Petrophysical interpretive procedures usually are described in terms of an idealized clastic reservoir or known as "Archie" reservoir. Theoretically, standard evaluation based on Archie reservoir can be used but some correction is needed because the presences of clay mineral like illite, kaolin and micas in pores. This correction is applied by calculated the volume of clay/shale. Clay/Shale volume must be determined by make an overlay between total clay data from XRD and clay/shale calculated from gamma ray log. From this step, the match or closest value will be the clay/shale volume model, which will be used for porosity calculation and other petrophysic parameters. This paper presented simple procedure to determine reservoir properties.

INTRODUCTION

Petrophysic evaluation is a crucial step in built a reservoir simulation model. Petrophysic evaluation includes evaluation of well log data, routine core analysis data or special core analysis data (SCAL), mud log data, formation testing and fluid testing. From this evaluation, we can get shale volume data, porosity, permeability, water saturation, which is used to calculated hydrocarbon saturation.

Petrophysic evaluation procedure standard is based on Archie reservoir, is which ideal clastic reservoir. Criteria of Archie reservoir are single rock type, homogeneous, clay free, slit free, intergranular porosity and so on. Actually, there is no ideal reservoir.

Tight sand reservoir means that reservoirs have low porosity and low permeability. These type of reservoirs are extremely complex, producing from multiple layers with different permeability that often enhanced by natural fracturing. The complicity of these reservoirs is attributed to a) low porosity and low permeability reservoir, b) the presence of clay mineral like illite, kaolin and micas in pores, c) the heterogeneity of the reservoir in vertical and lateral direction. Evaluation of tight gas sand reservoir represents difficult problems.

Theoretically, standard evaluation based on Archie reservoir can be used but with some correction especially shale correction. This paper presented petrophysic evaluation with simple volume shale correction for tight sand reservoir.

METHODOLOGY

Petrophysical interpretive procedures usually are described in terms of an idealized clastic reservoir, which is the textbook reference and is sometimes termed an "Archie" reservoir because it broadly matches the requirements for the application of the fundamental Archie equations that provide the quantitative basis for well log analysis (Archie 1942). A workflow for the petrophysical evaluation of an Archie reservoir is shown in Fig.1.
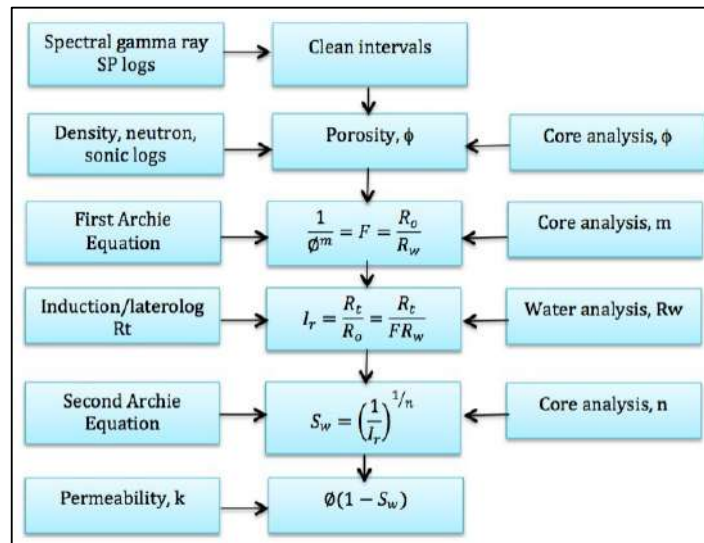
FIGURE 1. Workflow for petrophysical evaluation of Archie reservoir

For tight sand reservoir, correction of shale must be done, so the workflow for petrophysical evaluation of tight sand reservoir is shown in Fig. 2. Clay/Shale volume must be determined by make an overlay between total clay data from XRD and clay/shale calculated from gamma ray log. From this step, the match or closest value will be the clay/shale volume model, which will be used for porosity calculation.
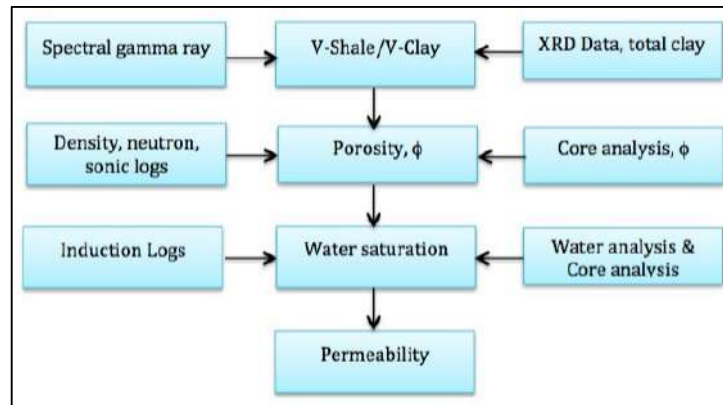
FIGURE 2. Workflow for petrophysical evaluation of tight sand reservoir

RESULTS AND DISCUSSION

Clay/Shale volume was computed using Gamma Ray index, which were then, used in several equations/methods, some of them are Linear, Curved, Clavier, Steiber, Old Rock, and Young Rock models. Gamma Ray index is obtained from Gamma Ray value of clean reservoir and Shale baselines that was assigned before. Clay volume data from XRD measurement (Table 1.) was used as reference to select the suitable method for shale volume determination. Total clay volume measured from XRD was compared with and overlaid on clay volume curved computed by various methods, as shown in Fig.3. Young Rock method gave the best match (best fit) with XRD data that can be observed in Fig.4. This clay volume is used as a correction factor for porosity calculation.

TABLE 1. Minerals Composition Measured from XRD

Depth (m)	Total Clay
2140.0	6.5
2148.5	3.8
2168.4	5.0
2180.7	5.5
2188.0	3.4
2203.2	2.3
2216.5	3.3
2243.1	5.2
4209.3	42.1
4233.7	6.1
4336.5	32.7
4348.6	43.5
4393.0	7.2
4533.3	9.4
4749.6	34.9
4805.4	49.0
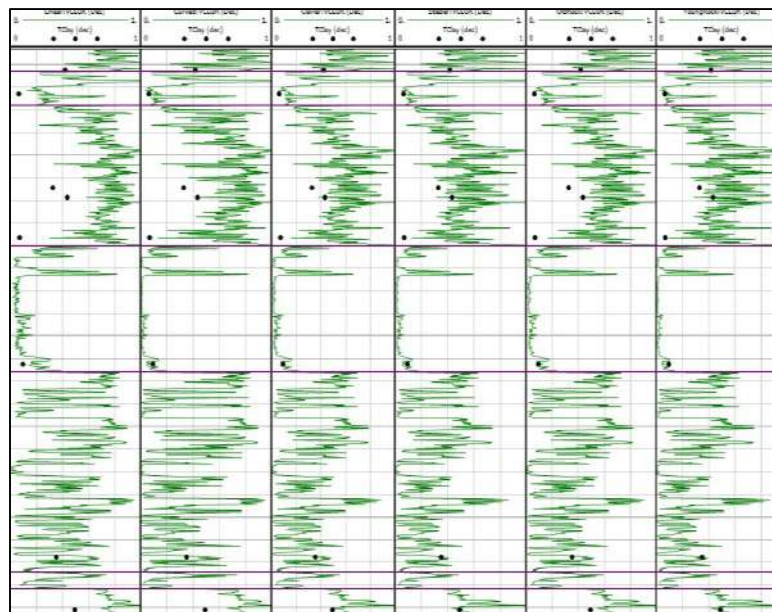
FIGURE 3. Clay/Shale Volume Calculation with Different Models
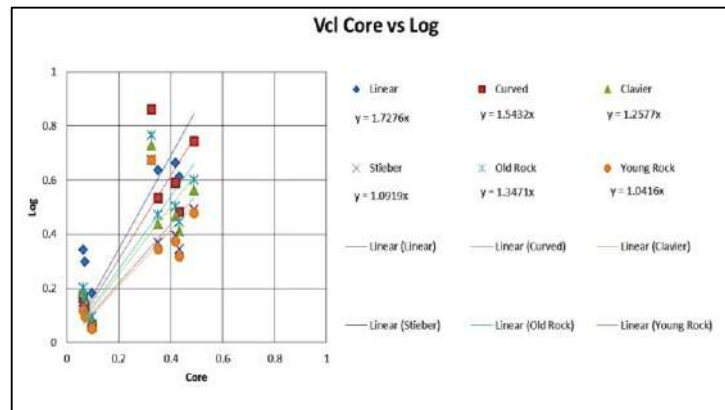
FIGURE 4. Log-Core (XRD) Cross Plot

Several methods were used in the calculation of porosity. They are Density, Neutron, Sonic, Density-Neutron and Density-Sonic. Matrix and Clay properties were obtained or estimated from core/log data. Matrix density is averagely taken from results of routine core measurement. Density of dry clay is set at 2.85 g/cc (literature suggest density of dry clay in the range of 2.65 – 2.85 g/cc). Porosity values from routine core data measurement taken from several depths (Table 2.) were used to calibrating reference for selecting the appropriate porosity computation method, as shown in Fig.5 and Fig.6.

TABLE 2. Data from Routine Core Analysis

Depth (m)	Porosity (%)
4466.8	2.9
4515.0	6.8
4567.3	7.5
4639.2	6.5
4650.5	7.7
4805.4	0.5
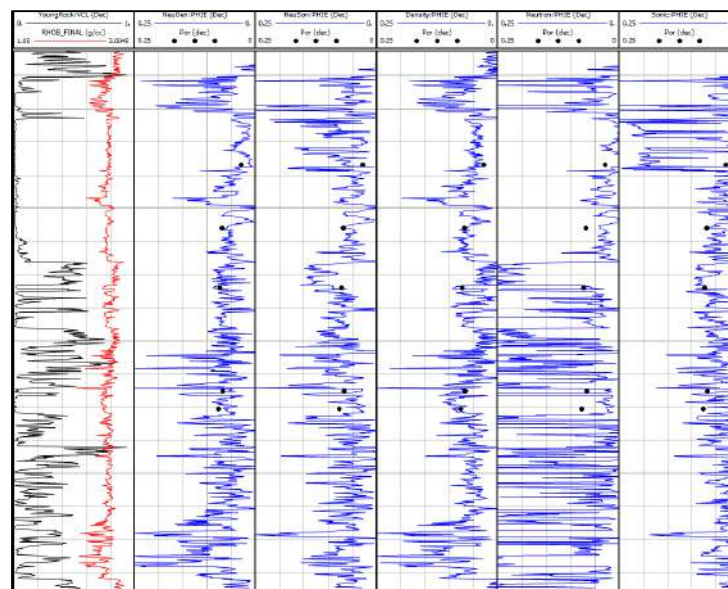
FIGURE 5. Porosity Calculation with Different Models

Proceedings of CCSE ASEAN 2019
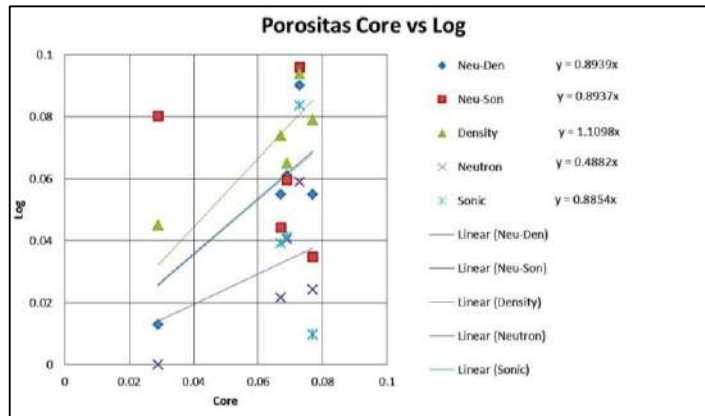
FIGURE 6. Log-Core (porosity) cross plot

Residual water saturation (irreducible) obtained from Special Core Analysis (SCAL) we used to calibrate water saturation computation from log data. However, these data should be used with caution because connate water saturation indicated by log may not necessarily the same as residual (irreducible) water saturation measured in SCAL. When depth is significantly above gas-water contact, both data can be considered similar.

Some methods were used and the results are overlaid with SCAL data. From this graph, only Simandoux, Indonesian and Woodhouse equations are considered to be stable throughout the entire depth intervals. Among the three methods, Simandoux equation gives the best fit to SCAL data, as shown in Fig.7.
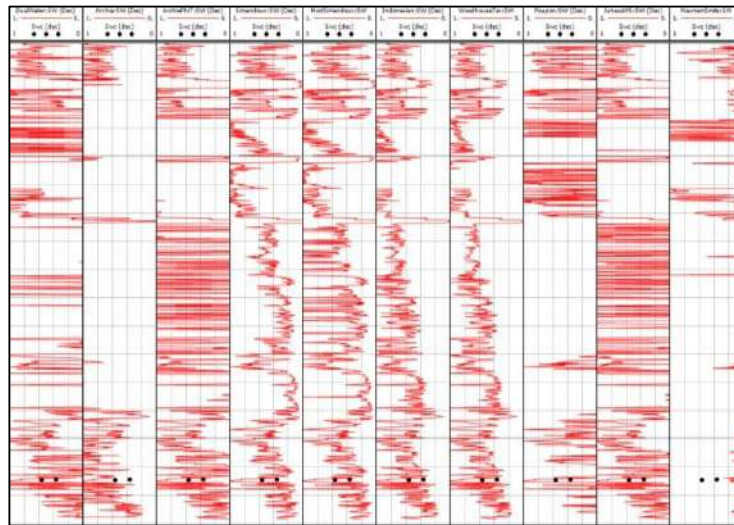
FIGURE 7. Water Saturation Calculation with Different Models

To find the permeability value, used the same method as looking for other reservoir properties. Because there is no core data for permeability sample then to determine the permeability of reservoir used simple calculation.

CONCLUSION

Tight sand reservoir not classified as "Archie" reservoir, so correction of shale is needed. The simple procedure was developed to correct reservoir properties determination. This procedure could be applied in different reservoir by considering the geological aspect.

ACKNOWLEDGMENTS

REFERENCES

11. Archie, G.E. 1942. The electrical resistivity log as an aid in determining some reservoir characteristics. In *Transactions of the American Institute of Mining and Metallurgical Engineers,* No. **142,** SPE- 942054-G, 54–62. New York City: American Institute of Mining and Metallurgical Engineers Inc.
12. Jacobi, D., Gladkikh, M., LeCompte, B., et al. 2008. Integrated Petrophysical Evaluation of Shale Gas Reservoirs. Paper SPE 114925 presented at the CIPC/ SPE Gas Technology Symposium Joint Conference, Calgary, 16–19 June. http:// dx.doi.org/10.2118/114925-MS.
13. Schlumberger, 2009, Log Interpretation Chart, 2009 edition.
14. Warner, H.R. and Woodhouse, R. 2007. Petrophysical Applications. In *Petroleum Engineering Handbook, Volume V: Reservoir Engineering and Petrophysics,* ed. L.W. Lake, 421–493. Richardson, Texas: SPE.

The Analysis of Single Row Deep Groove Ball Bearing Towards Rolling Resistance on the Prototype of Titen Electric Vehicles

Achmad Fitoyo[1, a)], Agus Triono[2, b)*], Gaguk Jatisukamto[3, c)], M. Nurkoyim[4, d)],
Nasrul Ilminafik[5, e)], M. Fahrur Rozy H[6, f)], Digdo Listyadi S[7, g)]

[1]Postgraduate Student of Mechanical Engineering, University of Jember - 68 121 Jember, Indonesia
[2, 3, etc.]Department of Mechanical Engineering, University of Jember - 68 121 Jember, Indonesia

a)achmadfittoyo@gmail.com
b)agus.triono@unej.ac.id
c)gaguk.ft@unej.ac.id
d)nurkoyin@unej.ac.id
e)nasrul.teknik@unej.ac.id
f)fahrur.teknik@unej.ac.id
g)digdo@unej.ac.id

Abstract. Energy efficient vehicle is a vehicle that is designed such that, in order to produce high efficiency levels, one of which is an electric vehicle. Electric vehicles are vehicles driven by an electric motor, the system works is to use the electrical energy stored in batteries and then supplied to the motor through the control to set fast or slow rotation of the motor. Electric vehicles are now beginning to be developed and has become a race event every year, especially at the level of energy consumption efficiency. One factor that can affect the efficiency of energy consumption is the rolling resistance. Rolling resistance is the resistance to objects that rotates due to friction against the surface. The magnitude of the rolling force that occurs depends on the magnitude of the frictional coefficient between the two surfaces. The method used in this study using response surface method, which is useful for problem modeling and analysis techniques. Based on the analysis of data processing using the software Minitab 18, it was found that the rolling resistance force will be increased with increasing force obtained and of the area of contact on a ball bearing, in addition to the bearing will suffer losses when getting round that is too high. By the method used, by using a smaller bearing obtained an efficiency increase of 4.68%, by regulating the rotational speed of bearing at 549.1717 RPM, Radial load of 145 N and axial load of 130 N.

Keywords: Rolling Resistance, Bearings, Electric Car, Response Surface Methodology

INTRODUCTION

Energy saving vehicles is a vehicle specifically designed to yield high levels of efficiency. The vehicle is expected to consume little fuel as possible, but can travel far enough. So that the depletion of fossil fuels, with energy efficient vehicles could reduce the use of fuel oil. Important factors to improve the performance of a vehicle is the mass, aerodynamic drag and rolling resistance [1].

Issues that affect the electric vehicle rolling resistance has many factors, one of which is *bearing*, In this study aims to optimize the use of rolling bearings using response surface method to fit the needs of electric vehicles. Type vehicle prototype is a vehicle specially designed shape of the fuselage, using two front wheels and one rear wheel, so as to minimize drag on the airflow.

bearing is a pivot rivet machine elements are loaded, so that the rotation or movement back and behind it can take place in a smooth, safe, and provide long life. Bearings should be sturdy enough to allow the shaft as well as other machine elements work well. If the pads are not functioning properly, then the achievements of the entire system will decrease or be unable to work properly [2]. Rolling resistance is the resistance to objects that rotates due to friction

forces [1]. Basically, the rolling resistance is the moment of the object against the direction of motion, equivalent to the force required to move an object. Response surface method is a collection of statistical and mathematical methods is useful for problem modeling and analysis techniques. In this method, The main goal is to optimize the response is influenced by a variety of process parameters. [3].

After observing and studying previous studies, it is known that many factors that affect rolling resistance, so as to try to lift a study bearing type single row deep groove ball bearing using response surface method to optimize the use of a bearing rolling in accordance with needs electric vehicle prototype.

METHODOLOGY

The method used at this stage is a response surface method (Response Surface Methodology) with the Box-Behnken experimental design.

Table 1. Design Rolling Resistance Testing by Box-Behnken Design

No	Parameter Level			Parameter (*Newton*)			Rolling Resistance			Average
	KPB	BR	BA	KPB	BR	BA	R 1	R 2	R 3	
1	-1	-1	0	512	145	140				
2	1	-1	0	552	145	140				
3	-1	1	0	512	165	140				
4	1	1	0	552	165	140				
5	-1	0	-1	512	155	130				
6	1	0	-1	552	155	130				
7	-1	0	1	512	155	150				
8	1	0	1	552	155	150				
9	0	-1	-1	532	145	130				
10	0	1	-1	532	165	130				
11	0	-1	1	532	145	150				
12	0	1	1	532	165	150				
13	0	0	0	532	155	140				
14	0	0	0	532	155	140				
15	0	0	0	532	155	140				

*R= Replikasi

Data processing is done by calculating the *ANOVA (Analysis of Variant)* using statistical software Minitab 18 to determine the effect of the rotational speed outer race, the axial force and radial force, on rolling resistance to obtain style rolling resistance on a single row deep groove ball bearing as small as possible , So it can serve as the basis for selection of the appropriate pads for a race-type electric vehicle prototype.

Cushioning material used for the test that is the type of single row deep groove ball bearing (628, 6200 and 6201) with each using C3. In this test done without giving lubricant, so every once tested, bearings used must be cleaned.

Figure 1. Rolling Resistance Test Equipment at Bearing

The tools used in this research is the Rolling Resistance of test equipment bearings by measuring the tangential force of the bearing. This tool is designed to combine the testing tool bearings in accordance with ISO / IEC 17025 [4], as well as a laboratory test equipment for rolling resistance of the tires, using a drum in accordance with ISO 8767 and 9948 [5].

In a study using three independent variables were suspected of having a significant effect on the response variable that is rolling resistance. Factors that will be used is the rotational speed bearings, axial load and radial load. Level values used can be seen in Table 2

Table 2. Variable Factors and Value Level

Factor	Level Down	Intermediate level	Level Up
Code	-1	0	+1
Speed Bearing Swivel	512 rpm	532 rpm	552 rpm
Radial load	145 N	155 N	165 N
Axial load	130 N	140 N	150 N

RESULTS AND DISCUSSION

Style Rolling Resistance Testing Results

Test method Box-Behnken design based on Response Surface Methodology which is used to determine the combination of the process parameters are rotational speed bearings, axial load and radial load, so as to determine the influence of parameters on the response, then the result showed the following results:

Table 3. Data Bearing Testing Results

No.	Parameter			Average Rolling Resistance Bearing 628 (N)	Average Rolling Resistance Bearing 6200 (N)	Average Rolling Resistance Bearing 6201 (N)
	Speed Bearing (rpm)	Radial Load (N)	Axial Load (N)			
1	512	145	140	0.1202137	0.1310333	0.2633016
2	552	145	140	0.1161199	0.1212297	0.2510019
3	512	165	140	0.1516087	0.1661348	0.3219977
4	552	165	140	0.1542641	0.1473968	0.3068767
5	512	155	130	0.1402401	0.1514193	0.2984308
6	552	155	130	0.1385527	0.1473138	0.2922164
7	512	155	150	0.1495894	0.1708925	0.3296045
8	552	155	150	0.1405167	0.1495267	0.2949549
9	532	145	130	0.1154284	0.1211384	0.2493270
10	532	165	130	0.1414019	0.1527270	0.2988675
11	532	145	150	0.1258842	0.1309303	0.2686342
12	532	165	150	0.1574451	0.1710384	0.3298199
13	532	155	140	0.1427849	0.1578719	0.3010527
14	532	155	140	0.1442233	0.1556314	0.3037911
15	532	155	140	0.1403231	0.1517036	0.2970142

Analysis of Bearing Type 628

Data processing is done in stages, that is by looking for style rolling resistance first and then do the analysis. Resistance rolling style data analysis consists of three steps, namely the establishment of a model from experimental data results, then set up a model equation for rolling resistance force. The next step is to test the suitability of the model.

Table 4. Results of ANOVA for Bearing Type 628

Source	DF	Seq SS	Adj SS	Adj MS	F	P	
Regression	9	0.002433	0.002433	0.000270	20.64	0.002	*
Linear	3	0.002216	0.002216	0.000739	56.40	0.000	*
KPB	1	0.000019	0.000019	0.000019	1.42	0.287	
BR	1	0.002018	0.002018	0.002018	154.12	0.000	*
BA	1	0.000179	0.000179	0.000179	13.65	0.014	*
Square	3	0.000185	0.000185	0.000062	4.70	0.064	
KPB*KPB	1	0.000002	0.000000	0.000000	0.01	0.941	
BR*BR	1	0.000183	0.000183	0.000183	13.97	0.013	*
BA*BA	1	0.000000	0.000000	0.000000	0.04	0.854	
Interaction	3	0.000033	0.000033	0.000011	0.84	0.529	
KPB*BR	1	0.000011	0.000011	0.000011	0.87	0.394	
KPB*BA	1	0.000014	0.000014	0.000014	1.04	0.354	
BR*BA	1	0.000008	0.000008	0.000008	0.60	0.475	
Residual Error	5	0.000065	0.000065	0.000013			
Lack-of-Fit	3	0.000058	0.000058	0.000019	4.94	0.173	
Pure Error	2	0.000008	0.000008	0.000004			
Total	14	0.002499					

R-Sq = 97.38%   R-Sq (pred) = 62.35%   R-Sq (adj) = 92.66%

* signifikan

Table 4 is the result of analysis of variance modeling parameters for rolling style reistance. Based on the table, it can be seen Fvalue at 20.64, while the F table = F (0:05, 9, 5) = 3.32. From the statistical equation if F count> F table, and the value of p value less than 0.05, it can be stated that the model is significant. It can be concluded that the variable factors have been a significant effect on the model form.

In addition to showing the results of the model, the table also shows test results using a statistical model parameters that convert into p value. Based on the results of second order equation model analysis with Minitab software, the regression model is obtained as follows:

$YR = 0.142444 - 0.001525 * KPB + 0.015884 * BR + 0.004727 * BA + 0.001687 * (CDE * BR) - 0.001846 * (CDE * BA) + 0.001397 * (BR * BA) + 0.000146 * (KPB2) - 0.007038 * (BR2) - 0.000365 * (BA2)$

Figure 2. Analysis of surface plot and contour plot

Of the three independent variables can be seen that the variables that most influence on rolling resistance force at a low rotation is radial loads, while at high rotation, radial load and axial load almost have the same value of the rolling resistance force. Radial load and axial load have a value proportional to the results of rolling resistance values of style, while for the rotational velocity of bearing has a value inversely proportional to the value of the force of rolling resistance results.

Analysis by Bearing Type 6200

Analysis of software Minitab 16 obtained the following results:

Table 5. Results of ANOVA for Bearing type 6200

Source	DF	Seq SS	Adj SS	Adj MS	F	P	
Regression	9	0.003566	0.003566	0.000396	50.26	0.000	*
Linear	3	0.002885	0.002885	0.000962	121.96	0.000	*
KPB	1	0.000365	0.000365	0.000365	46.26	0.001	*
BR	1	0.002210	0.002210	0.002210	280.33	0.000	*
BA	1	0.000310	0.000310	0.000310	39.31	0.002	*
Square	3	0.000569	0.000569	0.000190	24.05	0.002	*
KPB*KPB	1	0.000001	0.000007	0.000007	0.91	0.383	
BR*BR	1	0.000563	0.000552	0.000552	70.00	0.000	*
BA*BA	1	0.000005	0.000005	0.000005	0.58	0.480	
Interaction	3	0.000113	0.000013	0.000038	4.76	0.063	
KPB*BR	1	0.000020	0.000020	0.000020	2.53	0.172	
KPB*BA	1	0.000074	0.000074	0.000074	9.45	0.028	
BR*BA	1	0.000018	0.000018	0.000018	2.45	0.190	
Residual Error	5	0.000039	0.000039	0.000008			
Lack-of-Fit	3	0.000020	0.000020	0.000007	0.68	0.641	
Pure Error	2	0.000019	0.000019	0.000010			
Total	14	0.003605					
R-Sq = 98.91%		R-Sq(pred) = 89.94%		R-Sq(adj) = 96.94%			

*significant

Table 5 is the result of analysis of variance modeling parameters for rolling style resistance. Based on the table, it can be seen the F value at 50.26, while the F table = F (0:05, 9, 5) = 3.32. From the statistical equation if F count> F table, and the value of p value less than 0.05, it can be stated that the model is significant. It can be concluded that the variable factors have been a significant effect on the model form.

Based on the results of second order equation model analysis with Minitab software, the regression model is obtained as follows:

YR = 0.155069 - 0.006752 * KPB + 0.016621 * BR + 0.006224 * BA - 0.002234 * (CDE * BR) - 0.004315 * (CDE * BA) + 0.002130 * (BR * BA) - 0.001395 * (KPB2) - 0.012225 * (BR2) + 0.001114 * (BA2)
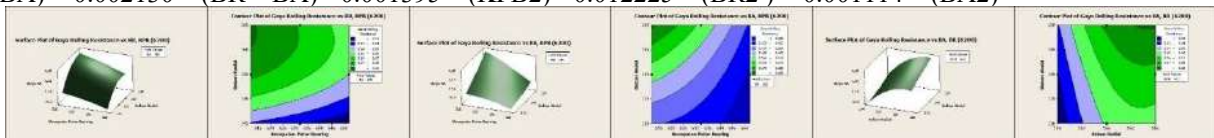
Figure 3. Analysis of surface plot and contour plot

Analysis of three independent variables, it is known that the variables that most influence on rolling resistance force at a low rotation is radial loads, while at high rotation, radial load and axial load almost have the same value of the rolling resistance force. Radial load and axial load have a value proportional to the results of rolling resistance values of style, while for the rotational velocity of bearing has a value inversely proportional to the value of the force of rolling resistance results.

Analysis by Bearing Type 6201

Analysis of software Minitab 16 obtained the following results:

Table 6. Results of ANOVA for Bearing type 6201

Source	DF	Seq SS	Adj SS	Adj MS	F	P	
Regression	9	0.009051	0.009051	0.001006	62.01	0.000	*
Linear	3	0.007813	0.007813	0.002604	160.59	0.000	*
KPB	1	0.000583	0.000583	0.000583	35.94	0.002	*
BR	1	0.006345	0.006345	0.006345	391.23	0.000	*
BA	1	0.000886	0.000886	0.000886	54.61	0.001	*
Square	3	0.001000	0.001000	0.000333	20.55	0.003	*
KPB*KPB	1	0.000017	0.000005	0.000005	0.30	0.605	
BR*BR	1	0.000967	0.000943	0.000943	58.15	0.001	*
BA*BA	1	0.000015	0.000015	0.000015	0.93	0.378	
Interaction	3	0.000238	0.000238	0.000079	4.89	0.060	
KPB*BR	1	0.000002	0.000002	0.000002	0.12	0.740	
KPB*BA	1	0.000202	0.000202	0.000202	12.46	0.017	
BR*BA	1	0.000034	0.000034	0.000034	2.09	0.208	
Residual Error	5	0.000081	0.000081	0.000016			
Lack-of-Fit	3	0.000058	0.000058	0.000019	1.66	0.398	
Pure Error	2	0.000023	0.000023	0.000012			
Total	14	0.009132					
R-Sq = 99.11%		R-Sq(pred) = 89.29%		R-Sq(adj) = 97.51%			

*signifikan

Table 6 is the result of analysis of variance modeling parameters for rolling style resistance. Based on the table, it can be seen the F value at 62.01, while the F table = F (0:05, 9, 5) = 3.32. From the statistical equation if F count> F table, and the value of p value less than 0.05, it can be stated that the model is significant. It can be concluded that the variable factors have been a significant effect on the model established, the regression model is obtained as follows:

YR = 0.300619 - 0.008536 * KPB + 0.028162 * BR + 0.010521 * BA - 0.000705 * (CDE * BR) - 0.007109 * (CDE * BA) + 0.002911 * (BR * BA) + 0.001157 * (KPB2) - 0.015982 * (BR2) + 0.002025 * (BA2)
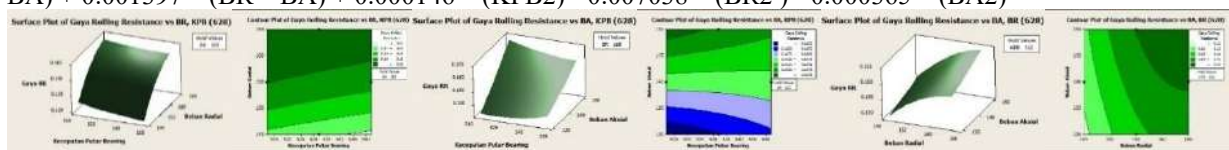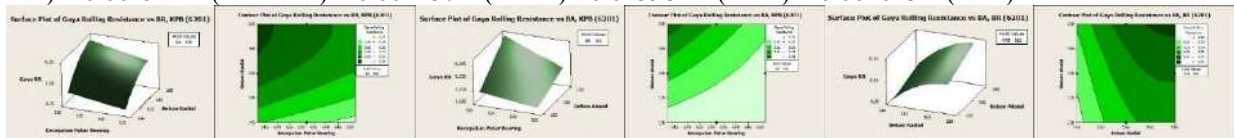

Figure 4. Analysis of surface plot and contour plot

Analysis of three independent variables, it is known that the variables that most influence on rolling resistance force at a low rotation is radial loads, while at high rotation, radial load and axial load almost have the same value of the rolling resistance force. Radial load and axial load has a value proportional to the results of rolling resistance values of style, while for the rotational velocity of bearing has a value inversely proportional to the value of the force of rolling resistance results.

Response optimization

To search for a combination of these levels of process variables that can produce responses that the optimum (target, minimum, and maximum) then used the response surface method with the approach of the function of desirability, because the function of desirability is a function obtained by combining some of the equations of the model so that the value response desired.

To enter a value of the desirability function, can be seen in the results obtained from the analysis of contour plots and surface plot. So the minimum or maximum value is known to be entered. Then the response included are as follows:

- $\hat{Y}_{628}$ = Rolling resistance on bearing 628, a score ≤ 0.12 ≤ 0.1575 $\hat{Y}$628
- $\hat{Y}_{6200}$ = Rolling resistance on the bearings 6200, earned value ≤ 0.13 ≤ 0.18 $\hat{Y}$628
- $\hat{Y}_{6201}$ = *Rolling resistance* the bearings 6201, earned value ≤ 0.26 ≤ 0.34 $\hat{Y}$628

For desirability function approach above can be solved using the software Minitab software 16. The results of the optimization software Minitab software 16, can be seen in the following chart.
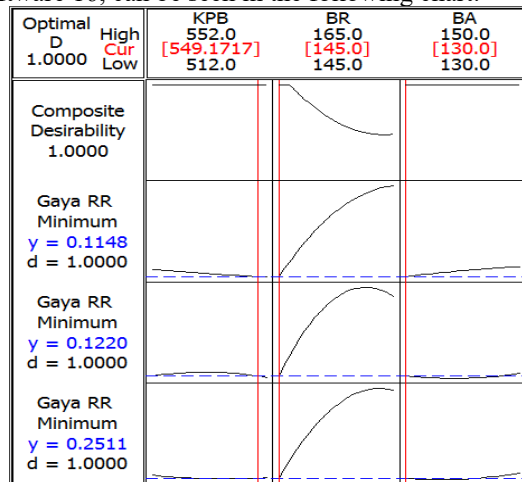
Figure 5. Graph combination of variable factors

From the combination of the above obtained optimum rolling resistance force by adjusting predictor variables as follows:

It is estimated to generate value in the bearing rolling resistance force of 0.1148 N 628 with a desirability score of 1.00, rolling resistance value in 6200 amounted to 0.1220 N bearing the desirability of 1.00, and the value of the rolling resistance on the bearings 6201 amounted to 0, 2511 N with the desirability of 1.00.

From the results obtained it can be concluded that the value of the force of rolling resistance will increase with increasing force obtained [1], as well as of the area of mutual contact on a ball bearing, and the bearing will suffer losses when getting round that is too high [6].

The increase in efficiency of Style Rolling Resistance

Table 7. Comparison of Setting Standard Setting Research

No.	Parameter	Results Standard	Research result
1	Speed Bearing Swivel (CDE)	532 rpm	549.1717 rpm
2	Radial load (BR)	155 Newton	145 Newton
3	Axial load (BA)	140 Newton	130 Newton
4	*rolling Resistance* on Bearing 628	-	0.1148 Newton
5	*rolling Resistance* on Bearing 6200	0.1551 Newton	0.1220 Newton
6	*rolling Resistance* on Bearing 6201	-	0.2511 Newton

Table7. In the table can be seen that the results of the research setting value slightly better compared with the use of standard setting for electric cars bearing prototype. This can be proved by a simple calculation which results in a standard percentage comparison of the results with the results. Percentage comparisons can be determined by the following equation:

1. A large percentage of the bearings 6200 against the results of research on bearing 628, namely:
   (0.1551 to 0.1148): 0.1551 x 100% = 25.98%
2. A large percentage of the bearings 6200 against the results of research on the bearings 6200 are:
   (0.1551 to 0.1220): 0.1551 x 100% = 21.34%
3. A large percentage of the bearings 6200 against the results of research on the bearings 6201 are:
   (0.1551 to 0.2511): 0.1551 x 100% = -61.90%

Based on these test results, to gain efficiencies can be obtained by using the following equation:
- The increase in the efficiency of the bearing type 628
  - Energy consumption = 25.98% x 0.18% = 4.68%
  - η = 4.68% x 165 km / kwh = 7.722 km / kwh
- The increase in the efficiency of the bearing type 6200
  - Energy consumption = 21.34% x 0.18% = 3.84%
  - η = 3.84% x 165 km / kwh = 6.34 km / kWh
- The increase in the efficiency of the bearing type 6201
  - Energy consumption = -61.90% x 0.18% = -11.14%
  - η = -11.14% x 165 km / kwh = -18.38 km / kwh

CONCLUSION

Based on the analysis of data processing using the software Minitab 18, it was found that the rolling resistance force will be increasing with increasing force, the contact area on the ball bearing and the magnitude of the moment of inertia and bearing will suffer losses when getting round that is too high. In 6200 and 6201 bearing all predictor variables have a greater influence on the rolling resistance force. While on the 628 bearing for variable speed rotating bearing have very little effect. In the analysis that has been done can be seen that the individual variables that most influence on the process of rolling resistance force is the radial load.

The results of rolling resistance testing of all three types of bearings, analyzed using statistical methods that optimum values obtained by adjusting the rotational speed of bearing at 549.1717 rpm, load of 145 N radial and axial load of 130 N, obtained rolling resistance force in the bearing 628 at 0 , 1148 N, in 6200 amounted to 0.1220 N bearing and the bearing 6201 amounted to 0.2511 N.

SUGGESTION

In testing the rolling resistance on the type of single row deep groove ball bearing, for the outcome variable rotational speed bearings, radial load and axial load, just as a benchmark for further testing. In this case the type of bearing is also influential in rolling resistance, ranging from contact ball bearing area of the house, and the type of ball bearing. Addition of lubrication, vibration, bearing material, service life etc., also affects rolling resistance.

For further research is needed to examine the type of bearing, lubrication, material consumption etc. Bearing age gradually. From this research can be used as a benchmark for future research and can be taken that have the optimum variables or parameters can also make additions and level on research.

REFERENCES

15. M. Juhala, au (2014). Improving vehicle rolling resistance and aerodynamics. Sciecedirect.
16. Ir. Sularso, M. (1997). Basic Element Selection Planning and Engineering. Jakarta: PT Pradnya Paramita.

17. N. Aslan, YC (2006). Application of Box-Behnken design and response surface methodology for modeling of some Turkish coals. ScienceDirect.
18. SKF. (2012). Railway technical handbook Volume 1 Axlehoxes, wheelset bearings, sensors, condition monitoring, subsystems and services. Russia: PUB 42 / P2 EN 12788.
19. Walter, AG (2005). The Pneumatic Tire. WAashington, DC: National Highway Traffic Safety Administration US Department of Transportation.
20. IM Jamadar, DD (2015). Model Development for the Investigation of Localized Defects in Taper Roller Bearings Using Matrix Method of Dimensional Analysis. ScienceDirect.

Semi-Automatic Honey Filter Machine

Choirul Hamzah[1], Budihardjo Achmadi Hasyim,[2] Sinta Putri Anisa[3]

[1] choirul.17050754042@mhs.unesa.ac.id State University of Surabaya
[2] budihardjoah_unesa@yahoo.co.id State University of Surabaya
[3] sinta.17050524010@mhs.unesa.ac.id State University of Surabaya

Abstract

Honey is a sweet liquid thick liquid produced from bees or other insects obtained from flower nectar. Jogosalam village is known for the biggest honey commodity in Malang. The problem faced by partner is that in the production process still traditional, the filtering process still uses cloth and plastic containers so that honey intersects with outside air and other objects, consequently the quality of honey decreases. The screening process lasts a long time, 1 kg of honey takes 2 hours of filtering. The next problem lies in the filling process, filtered honey is inserted into the bottle using a funnel, as a result a lot of honey is spilled out of the bottle and finally wasted. The purpose of this PKMT activity is to increase the effectiveness of honey production with indicators: the screening process is done by spinner machines, and the honey filling process is faster using a pump with a controlled filling process. The method of implementation in this activity is literature study, observation with partners, making designs, making sequences of work, procuring tools and materials, making machinery, testing machines, evaluating, implementing machinery and monitoring, publishing and submitting patents, and making reports. The results of the application of a semi-automatic honey filter machine, namely partners can improve the quality of honey and the quantity of production can increase up to 400%. Production which was originally 3 kg (6 hours working) to 25 kg of honey can be filtered every day. The honey production process becomes more hygienic so that the quality of honey is maintained, and does not require a lot of time and energy. It can be concluded that the problem of partner can be overcome because the screening and filling process of honey can be more effectively carried out in one machine.

Keywords: Honey, spinner, pump, filter

INTRODUCTION

Jogosalam is a village known for the commodity of Sugar Cane and Honey in the Malang districk. in this village we find a lot of sugar cane farms and many drums, boxes of honeybee cattle.

Jogosalam village is known for the biggest honey commodity in Malang, many SMEs are engaged in the packaging of honey to glass bottles or SMEs engaged in the field of Honey livestock, resulting in a symbiosis of mutualism between honey farmers and SMEs traders, this is what causes the continued development of the honey business and its existence is recognized by the surrounding community.

Our partner SMEs are owned by Nurhayat's address at Jalan Panglima Sudirman No.72, Gondanglegi Wetan, Gondanglegi, Malang, East Java 65174, businesses that have been running for approximately 5 years with production capacity per month 1 drum of honey or approximately 100 kg of honey.

Our partner SMEs processed original honey products without a mixture, honey that was obtained from farmers then filtered and packed into glass bottles of various sizes, the benefits expressed by Ms. Nurhayat that the business of selling honey was very profitable because 1.) Genuine honey is sought after because of many circulating honey mixed with other ingredients so it is difficult to find honey without mixture, 2.) Original honey has no expiration, 3.) The selling price of honey is relatively increasing every year.

In the production process of the honey UKM Nurhayat is still traditional, namely honey that has been obtained from farmers and then filtered using coconut milk filters and using plastic containers as a container of filtered honey, filtered honey and then transferred to a water jug and then put into a bottle using a funnel , after that it is closed and labeled.

After we discussed with Mrs. Nurhayat, it turned out that there were many obstacles experienced in the business, namely the process which was still manual, the tools were still simple and Mrs. Nurhayat complained about the length of time when filtering honey 1 kg = 2 hours. After we discussed then we analyzed the conditions in the production process at the partner SMEs, so we got the problem points in the SME partners, namely:

1. Honey intersects a lot with outside air and other objects such as (coconut milk filter, hand, plastic container, water jug)

2. The long process in the screening process of 1 kg of honey takes almost 2 hours
3. In the process of filling honey directly from the water jug then loaded into a bottle which eventually loads of honey spilling out of the bottle.

As a result of many objects (coconut milk filters, plastic containers, water teapots, etc.) that are used, honey intersects a lot with outside air and other objects so that in this screening process the quality of honey is reduced, resulting in decreased selling power. caused by problem points 2 and 3 have an impact on Productivity and Efficiency of the process because the filtering time is quite long and in the filling process there is spilled honey and finally wasted.

Fuad (2001) states that in general the production problems faced by small and medium enterprises (SMEs) in Indonesia are not suitable if solved through the application / use of sophisticated / sophisticated technology machines, but many are more suitable to be solved through the application of appropriate technology. Because the investment costs for implementing appropriate technology are relatively cheap, and mastery of technology does not require too much knowledge.

Based on these problems, the researcher intends to help overcome the production problems faced by partner SMEs. After holding intensive discussions, the SMEs will be assisted with a Semi-Automatic Honey Filter Machine. It is expected that by using these machines, the quality and quantity of SME partner production can be improved. This condition is very desirable for SMEs entrepreneurs, because the continuity and quality of production can be maintained. This will have an impact on increasing the income earned by SMEs and increasing welfare, both employers and employees.

METHODS

Activities carried out to resolve partner problems through the following stages.

Interview with SMEs Partner

Interviews were conducted to determine the quantitative portraits, profiles and conditions of partners and the problems faced by partners related to the problem of the manual stripping and cleaning process. Interviews were conducted at partner SMEs.

Team Coordination

At this stage coordination is carried out with all teams to determine the scope of work of each team member.

Design Semi-Automatic Honey Filter Machine

In designing Semi-Automatic Honey Filter Machine using Autodesk SolidWorks 2015. This machine has a length of 600 mm, width of 600 mm, height of 800 mm, and its machine is made of foodgrade material which is stainless so it is safer for consumers. This machine is driven by a 1/2 PK electric motor,

Procurement of Tools and Equipment Needs

Previously, a price survey for supporting equipment and consumables was carried out, which was then an advanced stage, namely in the form of procurement of consumables and equipment needed to support the readiness of the manufacturing process. Procurement of consumables is seen in terms of price and quality of goods to be used so that products can be achieved in accordance with both functional and structural targets and adjusting available funds.

Manufacturing and Assembly Processes

After getting all the components, equipment and materials then the team carried out the machine manufacturing and assembly process. At this stage the tool manufacturing process is carried out in the workshop of the Mechanical Engineering Department of the State University of Surabaya.

Engine Test

The machine that has been made is then tested for functions to determine the functioning of each component of the tool made. After a function test, testing is carried out by peeling and cleaning according to the engine capacity to determine the level of engine performance. If the machine that is made is felt to be less than expected, then a repair process is made on the machine made.

Engine Refinement

After testing, the Semi-Automatic Honey Filter Machine was refined by refining, structuring the electrical system, and structuring the components so that the machine made had good aesthetic value.

Application of Machinery to Partner SMEs

After carrying out a series of steps above, the engine that has been refined is then sent to the partner to be implemented, and a machine-taking data collection process is carried out to be reported in the final PKM report. At this stage training on machine operation and maintenance is also carried out.

Monitoring and Evaluation

Monitoring is done by visiting SMEs partners to find out the achievements of the programs that have been implemented. In the monitoring stage, feedback will be asked in the form of criticism and suggestions from the SMES partners who have used the technology of the results of this activity to be followed up in the improvement activities.

RESULT AND DISCUSSION
Semi-Automatic Honey Filter Machine

Semi-Automatic Honey Filter Machine and Automatic Fluid Mecanism Pack function to simplify the filtering and filling process of honey, so the process can more effective. Because with manual methods to filter the honey it takes a long time, for 1 kg of honey it takes approximately 2 hours. Semi-Automatic Honey Filter Machine and Automatic Fluid Mecanism Pack with the design as shown in Figure Semi-Automatic Honey Filter Machine and Automatic Fluid Mecanism Pack function to simplify the filtering and filling process of honey with the design as shown in Figure 1 and 2.
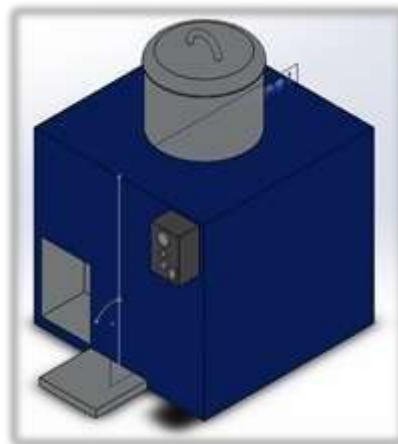
Figure 1. Semi-Automatic Honey Filter Machine 3D Design
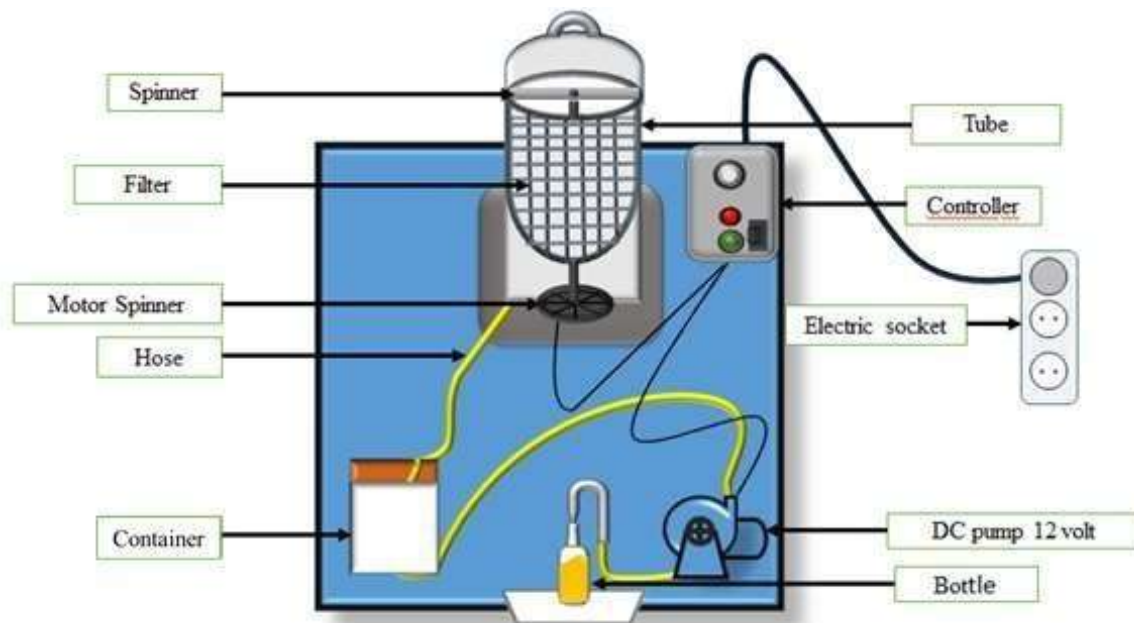
Figure 2. Semi-Automatic Honey Filter Machine 2D Design

Referring to the design above, the manufacturing process and assembly are immediately carried out with results as shown in Figure 3.

Figure 3. Semi-Automatic Honey Filter Machine

Semi-Automatic Honey Filter Machine have specifications as shown in the following table 1.

Table.1 Specifications of Semi-Automatic Honey Filter Machine
Dimensions, materials, capacity, power, and power source.

No.	Description	Information
1	Dimensions	60 cm x 60 cm x 80 cm
2	Materials	Steinless Steel, Aluminum Plate
3	Capacity	1-3 kg/ production
4	Power	70 Watt
5	Power source	Household electricity

Semi-Automatic Honey Filter Machine and Automatic Fluid Mecanism Pack will work when the motor is turned on and then the centrifugal force on the spinner will force honey through the filter that it's located on the spinner wall. Honey that passing through the filter will go into the container through the hose. The honey will be flowed with the help of DC pump 12 volt into the bottle. The closed system using food grade stainless steel materials will make honey poduced more hygienic than using manual methods.

Based on the results of engine testing, the results obtained as shown in table 2.

Table 2. Results of the application of Semi-Automatic Honey Filter Machine

No.	Number of honey	Time required	
1	1-3 kg	5 minutes	Engine capacity of 3 kg/ 5 minutes
2	1-6 kg	10 minutes	
3	1-9 kg	15 minutes	

Table 3 Comparison of Machine by Manual Method

No.	Number of honey (MERINDU SEMATI)	Time required (MERINDU SEMATI)	Number of honey (Manually)	Time required (Manually)
1	1 kg	5 minutes	1 kg	2 hours
2	6 kg	10 minutes	3 kg	6 hours

CONCLUSION

Based on the results of the application of "MERINDU SEMATI" Semi-Automatic Honey Filter Machine and Automatic Fluid Mecanism Pack is very useful for honey partner SMEs so that the honey production process becomes 72 times more effective which initially the screening process takes 360 minutes to 5 minutes, the process becomes more practical because the engine is done with an electric motor drive. While for its production capacity, which initially only 3 kg per 6 hours can now be 18 kg with approximately 30 minutes, the filling process becomes faster because it is done automatically, and the product produced is also more hygienic because the machine is made of stainless steel.

REFERENCES

Biegel. J. E. 1998. Pengendalian Produksi, Suatu Pendekatan Kuantitatif. Terjemahan. Tarsito Bandung.

Collins, J. A. 1993. Mechanical Design Of Machine Elements And Machines: analysis, prediction , prevention, 2nd ed., wiley, New York.

Erdman, J. W. and Erdman, E.A. (1982). Effect of home preparation practices of nutritive value of foods in handbook of nutritive value of foods. Miloslaw Recheign, Florida 1: 237 -263.diakses 24 September 2018.

Fuad, Ahmadi. 2001. Karakteristik Teknologi Tepat Guna balam Industri SkalaUsaha Kecil dan Menengah di Jawa Timur. Makalah yang disampaikan dalam rangka pelatihan produktivitas usaha kecil di Unesa. Tanggal 26 Juli 2001.

Wikipedia. 2018. Madu. Dikutip pada tanggal 25 September 2018 dari :https://id.wikipedia.org/wiki/Madu.

Johnson, Curtis, D. 2003.Process Control Instrumentation Technology. NewJersey: Pearson Education.

Hidayah, Mufidah Nurul dkk. 2013. Makalah Zat Dan Energi PRINSIP KERJA DONGKRAK HIDROLIK (http://hunihindra.blogspot.co.id/2014/12/vbehaviorurldefaultvmlo_12.html) diakses tanggal 26 September 2018.

Analysis of Using Lumajang Iron Sand Magnetit Nanoparticles for Increasing Heavy Oil Recovery Through Microwave Assisted Gravity Drainage (MWAGD) Method

Riska Laksmita Sari[1, a)]

[1]*Faculty of Engineering, Universitas of Jember, Jl. Kalimantan 37 Jember, INDONESIA*

[a)]Corresponding author: riska.laksmita@unej.ac.id

Abstract. Along with the increasing number of energy needs in the world, especially oil, coupled with the depletion of oil reserves in conventional reservoirs, encouraging various efforts to increase oil production in reservoirs, especially in non-conventional reservoirs. One of the non-conventional reservoirs is a Heavy Oil Reservoir. The number of heavy oil reservoirs in the world reaches 70% of the total oil reserves in the world. One of the problems related to oil production in heavy oil reservoirs is a very low primary recovery mechanism. The use of the Enhanced Oil Recovery (EOR) method is an effort to improve the recovery of heavy oil. The EOR process used sometimes uses materials / materials that have high prices, so it is less efficient in terms of economy. One of the efforts made to cost efficiency of the EOR process is through the use of abundant natural materials. In this study, laboratory analysis was carried out in order to improve the recovery of heavy oil by combining the EOR method and nanoparticle technology. The nanoparticles used were magnetite nanoparticles extracted from Lumajang iron sand and coprecipitation process. In this study, 3 analyzes of the effect of the use of iron sand nanoparticles on the increase of petroleum oil recovery were carried out, the use of Lumajang iron sand magnetite nanoparticles using MWAGD method and conventional heating and the influence of the use of micron Lumajang magnetite iron sand particles with MWAGD method. this study is the use of Lumajang magnetite iron sand nanoparticles using the Microwave Assisted Gravity Drainage (MWAGD) method resulting in a greater value of heavy oil oil recovery compared to conventional heating and the use of micron-size luminous magnetite sand particles. But what needs to be noted is that there is an optimum weight percent value of the nanoparticles used. So that when it is less or more than the optimum value, the EOR performance will be less efficient.

Keywords Heavy Oil, EOR, Nanoparticle, MWAGD

INTRODUCTION

Iron Sand is one of the abundant natural resources in Indonesia, not least in the Lumajang area, East Java. One of the efforts made in order to provide added value to the commodity is by separating its magnetite levels (Fe_3O_4 and Fe_2O_4) into ferrofluids and ferrogels. Magnetite in the form of nanoparticles will change the physical properties of magnetite so that it can increase the kinetic activation energy. Nanoparticles have many applications in the oil and gas industry, especially in the process of Enhanced Oil Recovery (EOR). Mechanisms such as changes in wetness, viscosity reduction and IFT reduction can be achieved when nanoparticles are applied (Hajir et al, 2016)

Microwave Assisted Gravity Drainage of Heavy Oils (MWAGD) is one of the nonconventional EOR methods that has several advantages, namely to minimize heat loss in oil or gas wells. In porous media saturated by water and oil, during the microwave heating process, water and oil particles will provide positive and negative magnetic charges. When the positive charge rotates 180 the negative charge rotates 180o in the opposite direction to the positive charge. This will continue so that the energy arises due to collisions, movements and friction that produces heat in the porous media. The heat energy will change the characteristics of heavy oil in terms of viscosity, wetness,

etc. (Hascakir, 2008). Combining these two methods (Use of Nanoparticles and EOR MWAGD) is expected to improve the performance of EOR in improving heavy oil recovery.

METHODOLOGY

Synthesis of magnetite nanoparticles from Lumajang iron sand using coprecipitation method with Hydrochloric Acid (HCL) as a solvent for iron sand base material. Then NH_4OH is used as a precipitate solution. Next step is fabrication of magnetite nanoferrofluid. At this stage fabrication of nanoferrofluid is carried out by mixing water with magnetite nanoparticles resulting from synthesis with various weight percent variations (0.5, 1, 1.5, and 2 wt%.). The third stage is heating with a microwave and conventional oven by applying the gravity drainage method.

RESULT AND DISCUSSION

Identification and characterization with XRF is needed because the sample used is natural material, so it is necessary to confirm the impurity that may be present in the sample. XRF (X-Ray Flourocencies) aims to obtain qualitative data of the elements contained in the sample and also by weight.

From table 1, it can be seen that the Fe compound (87.21 wt%) is the most dominant among all the identified compounds. Fe compounds in the wild form iron oxide compounds including Fe_3O_4 (magnetite) and $Fe_{3-x}Ti_xO_4$ (titanomagnetite). Iron compounds which are almost close to 90 percent by weight indicate that, iron sand has a more dominant magnetite content. In the XRF results, there are many impurities such as Al, Ca, Si, Ti, etc. This is normal because the samples used come from nature that have not been given special treatment (physical or chemical treatment). The impurity is quite small compared to Fe content. It can be said that the sample of iron sand used has a high level of Fe purity.

Table 1.Result of XRF Iron Sand

Compound	Al	Si	P	Ca	Ti	V	Cr
Conc	1 +/- 0.6	1.1 +/- 0.03	0.2 +/- 0.03	0.41 +/- 0.004	6.42 +/- 0.03	0.48 +/- 0.05	0.11 +/- 0.009
Unit	%	%	%	%	%	%	%

Compound	Mn	Fe	Ni	Zn	Br	Eu	Yb
Conc	0.50 +/- 0.02	87.21 +/- 0.75	0.06 +/- 0.01	0.06 +/- 0.004	0.34 +/- 0.002	0.72 +/- 0.101	0.0 +/- 0.03
Unit	%	%	%	%	%	%	%

Compound	Re	Bi
Conc	0.3 +/- 0.007	0.93 +/- 0.04
Unit	%	%

Qualitative and Quantitative Identification of the Magnetite Phase

The XRD technique is used to identify the crystalline phase in the material by determining the lattice structure parameters and to get the particle size. When a monochromatic x-ray beam comes on the surface of a crystal, reflections occur only when the angle of incidence has certain values. These values depend on the wavelength and crystal lattice constant, and to explain selective reflectivity in terms of interference effects, such as in physical optics.
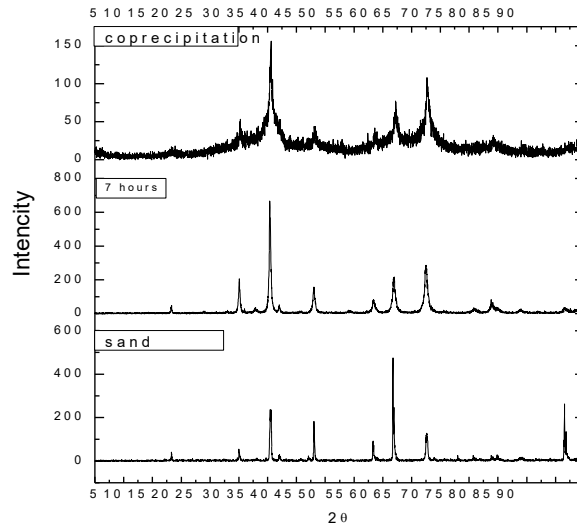
Figure 1. Graph of three XRD Test results

In Figure 1, the highest intensity is at the diffraction angle $2\theta = 350$, which is a characteristic or character pattern of Fe_3O_4 particles (Sun et al, 2006). Subsequent analysis was performed with the Rietveld method to quantitatively analyze phase compositions with the rietica software. This analysis begins with the searchmatch process to predict the phases contained in the sample.
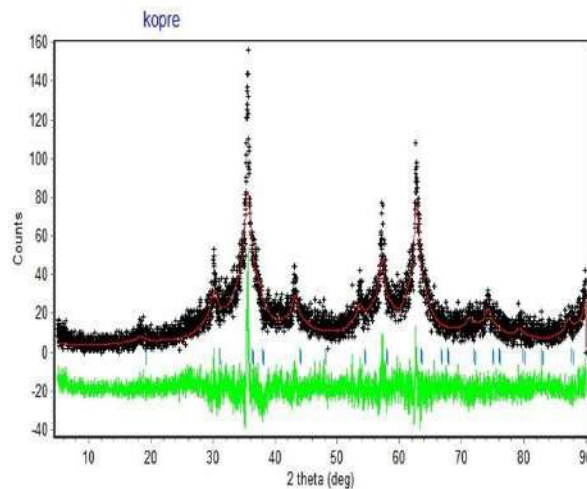
Figure 2 Patterns of the results of Fe_3O_4 refinement using the rietveld method Measured diffraction patterns are depicted with a black (+++) sign and calculated diffraction patterns are drawn with a straight red line. The bottom green curve is the plot of the difference between the measured diffraction pattern and the calculated diffraction pattern. Upright lines indicate the peak position.

After the refinement process is carried out with the method of rietveld, the matching parameters are obtained, namely GoF (Goodness of Fit). Refinement of XRD data with the Rietveld method gets a GoF value of 1.132 and a Rbragg of 5.54. From the XRD data, the crystal size of a material can also be calculated and estimated using the Schererr formulation. In the schererr formulation, we need FWHM (Full Width of Half Maximum) data on the peaks detected on the XRD graph. The value of FWHM can be seen more easily by using some software, one of which is

X'Pert HighScore Plus. The FWHM value obtained is changed in the form of new radians calculated using the Schererr formulation. From this analysis, it was found that the average crystal size of the iron sand which was compressed was 13.24 nm.

Analysis of Effect of Use of Lumajang Iron Sand Nanoparticles in the Improvement of Heavy Oil Recovery

In this study, 3 analyzes were carried out on the influence of the use of iron sand nanoparticles on the increase in oil recovery of oil between them, the influence of the use of magnetite nanoparticles of Lumajang iron sand with MWAGD method and conventional heating and the effect of using magnetite particles of Lumajang iron sand with MWAGD method.
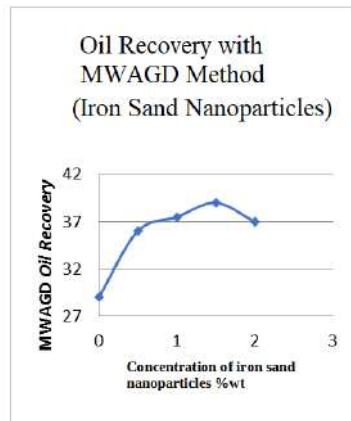
Figure 3 Average oil recovery graphs using the MWAGD method and iron sand nanoparticles

In figure 3, it appears that the weight percent value (% wt) 1.5 indicates the highest value of oil recovery. But on the increase of weight percent (% wt) 2, the value of oil recovery has decreased. As the weight percent of iron sand nanopaticles increases, oil recovery is also higher until it reaches its optimum value (In table 4, the optimum value is at 1.5% wt weight percent). At this optimum value, the viscosity of the oil emulsion decreases (Alomair, et al 2014). In weight percent (% wt) 2, the value of oil recovery decreases due to nanoparticles covering the pore so that oil is difficult to flow.
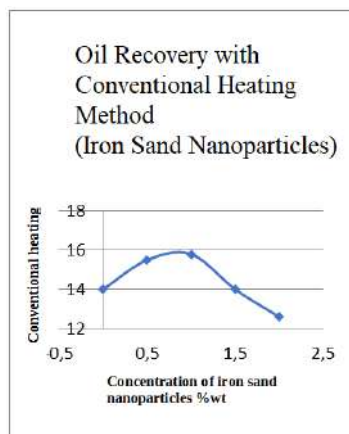
Figure 4 Average oil recovery graphs using conventional heating methods and iron sand nanoparticles

In figure 4, it appears that the weight percent value (% wt) 1 shows the highest oil recovery value. However, on the increase of weight percent (% wt) 1.5, the value of oil recovery has decreased. As the weight percent of iron sand nanopaticles increases, oil recovery is also getting higher until it reaches its optimum value (In figure 4, the optimum value at 1% wt weight percent). At this optimum value, the viscosity of the oil emulsion decreases (Alomair, et al 2014). In weight percent (wt%) 1.5, the value of oil recovery decreases due to nanoparticles covering the pore so that oil is difficult to flow.

Comparison of the use of the MWAGD method and conventional heating is shown in Figure 3 and Figure 4. The value of oil recovery using the MWAGD method tends to be greater than with conventional heating. This is because the microwave waves that are included in the heating system are faster to activate the movement of nanoparticles in the heavy oil emulsion so that the heavy oil flow through the pore is also getting bigger.
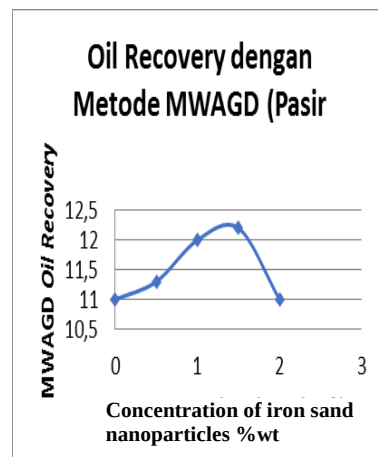
Figure 5 Graph of Average Oil Recovery using MWAGD method and ordinary iron sand particles (micron sized)

In Figure 5 compared to Figure 3 (MWAGD method), it appears that the size of the magnetite particles used affects heavy oil recovery. The use of nanoparticles further increases the value of heavy oil oil recovery. This is because the smaller the particle, the greater the surface area, so that the reaction of nanoparticles which have been heated with microwave waves on the oil emulsion will be greater so that it can reduce the viscosity of heavy oils marked by the greater value of oil recovery.

CONCLUSIONS AND RECOMMENDATION

The conclusion of this study is the use of Lumajang iron sand magnetite nanoparticles using the Microwave Assisted Gravity Drainage (MWAGD) method produces a heavy oil oil recovery value greater than using conventional heating and the use of micron sized magnetite iron sand magnetite particles. This is because heating with microwave waves and nanoparticles (greater surface area) will accelerate the rate of activation reactions so that the viscosity of heavy oil emulsions will be smaller, marked by higher oil recovery. But what needs to be noted is that there is an optimum weight percent value of the nanoparticles used. So that when less or exceeds the optimum value, EOR performance will be less efficient.

In subsequent studies, it is better to measure the resulting viscosity so that the measurement will be more accurate. In addition, further research needs to be done related to the minimization of closed pores (Pores Plugging) caused by the agglomeration of nanoparticles in the emulsion

ACKNOWLEDGMENTS

REFERENCES

1. Alomair,O.A., Matar,K.M dan Alsaeeed, Y.H . 2014. Nanofluids Applications for Heavy Oil Recovery. SPE Oil and Gas Conference, SPE, 2014.
2. Fuad Abdulloh, Renik Wulansari dkk. 2010. Sintesa dan Karakterisasi Sifat Struktur Nanopartikel$_{3-}$Fe$_x$Mn$_x$O$_4$ dengan Metode Kopresipitasi. Prosiding Pertemuan Ilmiah XXIV HFI Jateng & DIY, Semarang 10 April 2010. Hal 139
3. Hajir, Al-Farsi, Peyman Pourafshary dkk. 2016. Application of Nanoparticles to Improve The Performance of Microwave Assisted Gravity Drainage as a Thermal Oil Recovery Methode. SPE-179764-MS. Presented at the SPE EOR Conference, Oman,21-23 March 2016.
4. Acar, C. 2007. Enhancing Petroleum Recovery From Heavy Oil Fields. Middle East Technical Universities.
5. Hascakir, Berna dkk. 2008. Microwave Assisted Gravity Drainage. IPTC 12536. Presented at the International Petroleum Technology held in Malaysia, 3-5 Desember 2008.

Risk Factors of Head-Load Carriage on Farmers as Indicated by Their Physiological and Subjective Responses

Benjamin D. Rubin[1, a] and Alaine T. Liggayu[2,b]

[1,2] (*University of San Carlos-Talamban Campus*
(*Talamban, Cebu, City, Philippines*).

[a)] Corresponding author: rubenjamin35@gmail.com
[b)]liggayualaine@gmail.com

Abstract. The extent of the musculoskeletal disorder (MSD) problem is not well understood among farmers who are performing head-load carriage. Head-load carriage is still a primary mode of transporting vegetables in Mantalongon, Dalaguete, Cebu, the research locale. The purpose of this study was to investigate the risk factors associated with head-load carriage among farmers through their subjective and physiological responses. Relationship between MSD's and task-related factors, health background and individual profile were investigated for the 36 farmers. They reported that pain and discomfort in the neck (2.28) and hips (2.50) have the highest scores, although considered only as mild pain and discomfort based on a 0 to 10 rating scale. The heart rate and systolic blood pressure increased significantly before and after head-load carriage. However, the increase in diastolic blood pressure was not statistically significant. Moreover, farmers were able to carry load 147% of their body weight and rated the task as "moderate" based on the Borg scale. Results also showed that health background and individual profile did not relate statistically to the experienced pain and discomfort. There were four identified risk factors in this study: (1) load weight carried that had significant effects on the Rating of Perceived Exertion (RPE) (p=0.003), discomfort in the neck (p=0.002), discomfort in the upper back (p=0.001), and difference in heart rate (p=0.025); (2) terrain travelled for the discomfort in the upper back (p=0.025), lower back (p=0.046) and legs (p=0.031), (3) distance travelled that significantly contributed to the difference in heart rate (0.001); and (4) lifting technique for the discomfort in the lower back (p=0.023).

INTRODUCTION

Equipment and machinery in the farm make work easier and more efficient. In advanced countries, mechanization of the agricultural production is an advantage that they have over the third world countries like the Philippines where manual labor is still the predominant practice. Currently, the agriculture sector employs approximately 866 million workers which correspond to a quarter of the world's entire workforce [1]. Given the fact that most of these workers perform their job manually, problems involving agriculture-related injuries and musculoskeletal disorders (MSD) have been consistently reported at the most common of all occupational injuries and illnesses for farm workers, especially those involved in intensive manual labor tasks[2–10].

In the Philippines, 27.7% of the total workforce in the country comprises the agricultural sector as of 2017[11]. Since manual labor is still primarily observed in this sector, many labor-related injuries have been reported through the years. According to a report from the Philippine Statistics Authority (PSA) in 2017, work-related injuries in agriculture

accounted to as much as 6.35% of the entire recorded injuries in the country. Further, the injuries on the head, neck, back, arm, shoulder, and lower extremities were the most common. The leading causes of these injuries are lifting and carrying of agricultural materials and products.

In Mantalongon, Dalaguete, Cebu manual load carriage is used by the farmers as the primary mode in the transportation of vegetables. Before these vegetables reach the consumers, farmers place the vegetables inside a huge locally-designed basket called "bukag" and manually carry or transport the vegetables from the farm to the nearby access roads. The task is apparently hard labor in which the consequences are not known. However, by literature, the effects of load carriage can be measured through subjective [12–15] and physiological responses[16–18].

Studies related to load lifting and carrying suggest the need for physiological and subjective measurements [19–23]. In combination, it has been a reliable source of information about the MSD status of human workers. Recent studies and literature on load carriage are primarily focused on the subjects like military[12,13,20,24], school children[23,25–28], porters[18,22,29] and hikers[30,31]. Studies on load carriage in the field of agriculture is unrepresented in literature especially head-load carriage such as practiced by the farmers in Mantalongon, Dalaguete, Cebu; and the potential hazards attached to it.

METHODS

Participants

The participants of the study were the farmers of Mantalongon, Dalaguete, Cebu officially listed in the report of the Department of Agriculture Region VII who grow high-value crops that are common in the considered research environment. Participants were surveyed during the actual head-load carriage in harvesting the vegetables after securing approval from them.

Research Procedure

After preparing the needed tools and equipment, the researcher begin data gathering. First, the researcher searched for farms in the harvest stage. Once approval was obtained, the researcher got and recorded the pre-work or initial heart rate and the blood pressure of the farmer. Next, the farmer was observed while performing head-load carriage. At this stage, the task-related factors - the land terrain (either uphill, flat or downhill), distance traveled and the lifting technique (either pre-positioned or on-ground) were noted with the working heart rate and blood pressure. Load weight was measured after the farmer released the basket. After that, when the farmer had rested, the researcher measured his weight and height, and inquired for his age and task experience. Lastly, the farmer was asked to fill up the sheets for the rating of perceived exertion (using the scale by Borg, 1982) [32] and the pain and discomfort level for the body regions - the neck, shoulder, upper back, lower back, hips, thighs and legs (using the modified version of Borg Scale by Corlett and Bishop, 1979 and Simpson et al., 2011b)[31,33] with the assistance of the researcher. This procedure was repeated until the target sample size was reached.

Research Design

The study was of descriptive and quantitative type since it attempted to describe a phenomenon associated with head-load carriage through the effects manifested by the farmers as determined by their physiological and subjective perceptual responses. Further, this research used purely quantitative and coded qualitative data to achieve the objective of relating physiological and subjective responses from the farmers. Purely quantitative data consisted of the farmers' profile - their age, body mass index, and task experience; and the task-related factors of load weight, and carrying distance; as well as the physiological responses – heart rate and blood pressure. Coded qualitative data that was utilized in the study were composed of the task-related factors of land terrain and lifting techniques; and the subjective responses – the body map and discomfort level, and the rating of perceived exertion. The purely quantitative and coded data were made to facilitate cluster analysis.

Data Treatment

The gathered data underwent cluster analysis through SPSS v.23. Specifically, k-means clustering was used to analyze them. K-means clustering is a method of classifying or grouping items into k groups (where k is the number of pre-chosen groups)[34]. The grouping is determined by minimizing the sum of square distance among items and the corresponding centroids. Its process involves series of iterations to come-up with statistically significant clusters. The purpose of which is to group data by similarities.

In determining the optimal number of clusters in k-means clustering, the elbow method was used in the study. Elbow method is a method of interpretation and validation of consistency within clusters designed to help finding the appropriate number of clusters in a data set. In the study, the farmers' profile and task-related factors were grouped together with the corresponding physiological and subjective responses to determine significant differences that eventually led to the identification of potential hazards. T-test was applied to determine the significant differences among the physiological responses of heart rate and blood pressure. Finally, regression analysis was utilized to determine the specific risk factors associated with head-load carriage.

RESULTS AND DISCUSSION

Physical and Health Background of the respondents

Respondents' age, BMI and years of experience on head-load carriage.

There were 36 out of 53 identified farmers participated in the study, a 68% response rate. The age, height, weight, BMI and years of experience in head-load carriage are presented in Table 1. Based on the US Department of Health and Human Services[35], the average BMI of 23.08 of the farmers indicates that they are healthy. Further, the average height of the respondents is 158.17 cm which is 8 centimeters below the average height of the adult Filipino male of 165.6 cm[36].

TABLE 1. Biographic and Task-Related Data of the Farmer Respondents

Specifics	Minimum	Maximum	Mean	Std. Deviation
Age	17.00	63.00	34.7778	12.70795
Height	146.00	168.00	158.1667	6.36733
Weight	42.00	73.00	57.8611	7.71697
BMI	18.44	29.67	23.0833	2.47481
Years of Head-load carriage Experience	1.00	50.00	16.3333	12.26610
Distance Travelled (Meters)	28.00	980.00	334.8056	236.16348
Load Weight Carried (Kilograms)	38.00	118.00	84.8056	22.84334

Previously Experienced Pain and Discomfort

Prior to the study, all respondents had been experiencing body pain and discomfort. According to them, they describe this as strain or "pamaol" in the local language. Results shows that the hips and neck region are the primary locations of pain and discomfort. It suggests that the farmers' neck and hips area are more prone to MSD risks than the other body parts; which is similar to the results of the study by Lloyd et al. (2010) that compared the subjective perceptions on head and back loading. Performing the head-load carriage is a labor intensive task which requires the whole body to support the carried weight. During lifting and carrying, neck solely supports the load from the head, and the hips support the entire load from the upper body which makes the farmers more vulnerable to MSDs.

Carrying and lifting of basket full of vegetables were the primary causes of the farmers' previously experienced pain and discomfort and it was agreed by all 36 respondents. However, activities in farming other than lifting and carrying were also considered as one of the reasons why farmers had been experiencing pain and discomfort. These activities are spraying of chemicals and weeding the farm which are commonly performed by the farmers during months of cultivating vegetables.

Head-load carriage Frequency

Results shows that 52.78% of the respondents said that they carry vegetables with the basket 1 to 3 times per week, and 44.44% of the respondents expressed that they carry vegetables 4 to 6 times per week. It means that almost all of the farmers perform lifting and carrying tasks every week. Hence, transporting vegetables through baskets to the nearby access roads is part of their routine livelihood activity. It also means that the farmers are prone to bodily pain and discomforts because of this repetitive and labor taxing task of head-load carriage.

Lifting technique used during head-load carriage

In lifting the "bukag", the farmers apply two lifting techniques: the prepositioned and on-ground. On-ground technique involves the positioning of the "bukag" on a flat ground-level before carrying and lifting which makes is more difficult to lift compared to preposition lifting technique. On the other hand, the prepositioned technique, the "bukag" is placed on a flat hip-level ground, which makes it more convenient and easier to lift and carry. The pre-position lifting technique is the one commonly used by the farmers during head-load carriage according to them.

Subjective Responses

The results in Fig.1 show that the farmers rated hips and neck, 2.5 and 2.2, respectively; the highest among the body parts although interpreted only as mild pain and discomfort based on a 0 to 10 rating scale for pain and discomfort level after head- load carriage. In addition, these results reflect the same body parts previously experienced by the farmers in terms of pain and discomfort (see Fig.2). The Rating of Perceived Exertion (RPE) results show that the farmers rated head-load carriage task as 2.83 on the average (Table 3) which is considered a "moderate" task based on the Borg's Scale (1982) [32]. Looking at Table 1, the average weight of farmers is 57.86kg, while the average load weight during the actual head-load carriage is 84.8kg. This means that the farmers were able to support load 147% of their body weight which is remarkably higher than the result of Simpson et al., (2011b) who reported that the RPE rate of "hard" is already equivalent to 40% of their subjects' body weight. The result may prove that the farmers had already adapted to the task of head-load carriage physically and psychologically which is similar to the study of Malville et al. (2001) that reported porters can regulate work intensity and can carry extremely heavy loads without creating persistent medical problems. To further support this, Fig.2 shows that there are more counts on previously experienced body pain and discomfort versus after the actual head-load carriage. This could mean that some of the farmers had also already adapted to the experienced pain and discomfort. Upon verification through interview, 78% of farmers said that their bodies were already used to head-load carriage because they perform it routinely.
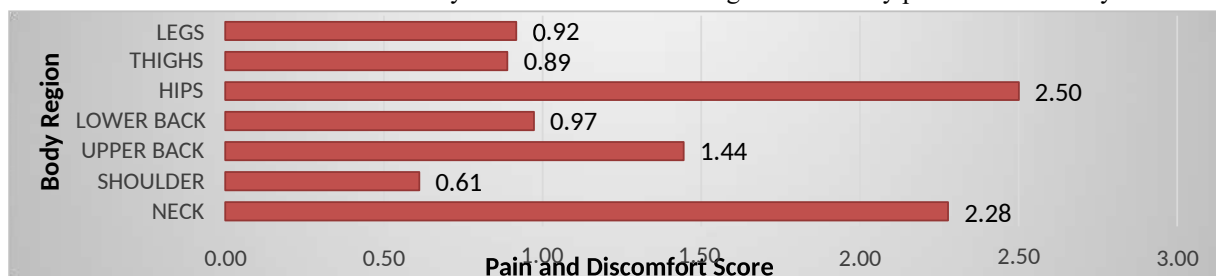
FIGURE 1. Pain and Discomfort Level After Head-Load Carriage
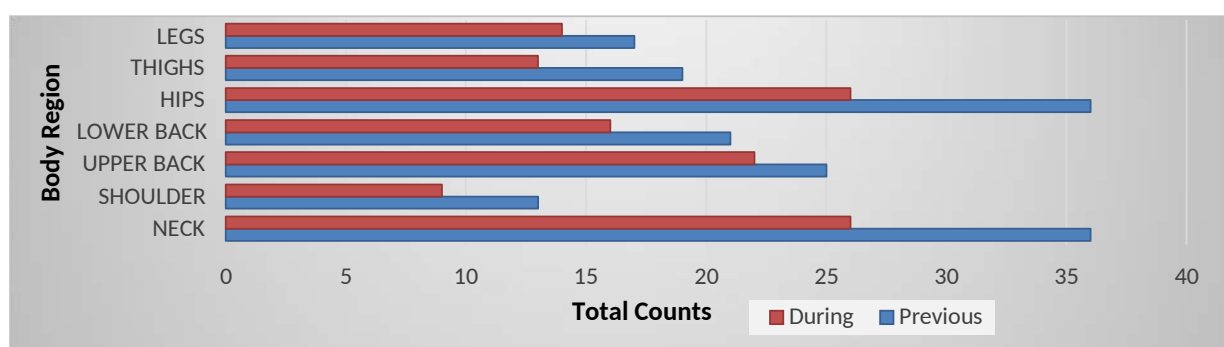
FIGURE 2. Pain and Discomfort comparisons in the Previous Experience and After Head-Load Carriage

TABLE 3. Statistical Summary of Subjective Responses After Head-Load Carriage

Subjective Responses	Minimum	Maximum	Mean	Std. Deviation
RPE Score	0.50	5.00	2.8333	1.22474
Discomfort on Neck	0.00	6.00	2.2778	1.87634
Discomfort on Shoulder	0.00	6.00	0.6111	1.24849
Discomfort on Upper Back	0.00	4.00	1.4444	1.31897
Discomfort on Lower Back	0.00	4.00	0.9722	1.15847
Discomfort on Hips	0.00	6.00	2.5000	2.10442
Discomfort on Thighs	0.00	4.00	0.8889	1.30445
Discomfort on Legs	0.00	4.00	0.9167	1.25071

Physiological Responses

Results shows that there were changes in the respondents' heart rate and blood pressure before and after head-load carriage. Average heart rate increased from 80.33 bpm to 97.97 bpm and the p-value of 0 in Table 5 suggests that the change is statistically significant ($p > 0.05$). This is comparable to the results of the study by Holewijn (1990), which reported an increase in heart rate while walking with load. Meanwhile, blood pressure was determined in two indicators, systolic and diastolic. Systolic blood pressure increased from 119.36 mmHg to 122.42mmHg and the paired t-test revealed that the change is statistically significant with p-value of 0.003. However, the diastolic blood pressure almost remained the same from 79.17mmHg to 79.5mmHg and the change was not statistically significant (p-value=0.833). These results are opposite to the studies of Bhambhani and Buckley, (1997) and Hong et al., (2000), Majumdar et al.,(2009) who concluded that there was significant increase in diastolic blood pressure of subjects during carriage of more than 20% BW of loads. These results support that the farmers have already adapted to their task of head-load carriage.

TABLE 5. Significance of Paired T-tests of Heart Rate and Blood Pressure Before and After Head-Load Carriage

Pairing		Paired Differences					t	df	Sig. (2-tailed)
		Mean	Std. Deviation	Std. Error Mean	95% Confidence Interval of the Difference				
					Lower	Upper			
Pair 1	Heartrate BEFORE – Heartrate AFTER	-17.63889	14.00847	2.33475	-22.37867	-12.89910	-7.555	35	.000
Pair 2	Systolic BEFORE - Systolic AFTER	-3.05556	5.78641	.96440	-5.01339	-1.09772	-3.168	35	.003
Pair 3	Diastolic BEFORE - Diastolic AFTER	-.33333	9.40517	1.56753	-3.51558	2.84892	-.213	35	.833

Cluster Analysis Results

Final results of cluster analysis reveal that the individual profile (Age, BMI and Task Experience) and health background of the farmers did not have significant relationships with their physiological and subjective responses at p<0.05. Only the task related factors such as the load weight carried, lifting technique used, distance and terrain travelled had significant effects on the physiological and subjective responses. The risk factors are the independent variables that had statistically significant relationships with the dependent variables determined through regression analysis. These risk factors were load weight carried, terrain travelled, lifting technique, and distance travelled shown in table 6 below.

Load weight carried contributed to as much as 50.9% to Rating of Perceived Exertion, 53.1% to discomfort in the neck, 50.2% to discomfort in the upper back, and 36.1% to difference in heart rate. This means that the weight of the load that the farmers carry through their baskets affects their perception significantly on how much effort and strength they apply to support the load. It also means that the pain and discomfort they experience in the neck, upper back, and the increase in heart rate are caused greatly by the load weight they carry.

On the other hand, terrain travelled contributed to as much as 34% to the discomfort in the upper back, 35% to the discomfort in the lower back, and 40.5% to the discomfort in the legs. The negative sign on the percent contributions indicate that as the terrain travelled by the farmers decreases or becomes downhill while performing head-load carriage, the greater are the resulting pain and discomfort in the upper back, lower back and legs. It should be noted that inclined terrain ease up the transport of load downhill[39]. Also, the back of the farmers are those that were affected due to the compression force affecting the spine and the legs while carrying load[40].

In addition, lifting technique causes discomfort in the lower back with an estimated weight contribution of 37.6%; and distance travelled affected difference in heart rate with 53.4% weight contribution. Lifting of load compresses the back bones of the body according to Niebel (2014) and walking with supported load increases heart rate[37].

TABLE 6. Risk Factors, their Related Physiological and Subjective Responses, and Statistical Significance

Dependent Variable	Independent Variable (Risk Factor)	Relational Significance of Independent Variable to the Dependent Variable	
		p-value	Standardized Coefficient (Weight Contribution)
Rating of Perceived Exertion	Load Weight Carried	0.003	0.509
Discomfort on the Neck	Load Weight Carried	0.002	0.531
Discomfort on the Upper Back	Terrain Travelled	0.025	-0.340
	Load Weight Carried	0.001	0.502
Discomfort on the Lower Back	Lifting Technique	0.023	0.376
	Terrain Travelled	0.046	-0.350
Discomfort on the Legs	Terrain Travelled	0.031	-0.405
Difference on Heart Rate	Distance Travelled	0.001	0.534
	Load Weight Carried	0.025	0.361

CONCLUSION

Although the farmers in Mantalongon, Dalaguete, Cebu may have adapted to their task of head-load carriage based on their physiological and subjective perceptual responses, there are risk factors related to the task that they have to be aware of so that injuries and serious diseases/conditions can be prevented. These risk factors are the load weight they carry, the terrain and distance they travel as they perform head-load carriage and the lifting technique they apply. Reduction of the intensities of these risk factors is advised for their future health. However, additional studies should be undertaken to explore the possible risks in their own work environment that may have influences on the ways they perform head-load carriage.

ACKNOWLEDGMENTS

REFERENCES

1. ILO. Facts on Agriculture: Http://www.ilo.org. (2017).

2. Chapman, L. & Meyers, J. Ergonomics and Musculoskeletal Injuries in Agriculture: Recognizing and Preventing the Industry's Most Widespread Health and Safety Problem. (2002).

3. Mccurdy, S. A., Samuels, Ã. S. J., Carroll, D. J., Beaumont, J. J. & Morrin, L. A. Agricultural Injury in California Migrant Hispanic Farm Workers. **235,** 225–235 (2003).

4. Meyers, J. M. *et al.* High Risk Task for musculoskeletal disorder in agricultural field of Work. (2000). doi:10.1177/154193120004402232

5. Villarejo, D. Occupational Injury Rates Among Hired Farmworkers. 39–46 (1998).

6. Kotowski, S. E., Davis, K. G., Kim, H. & Lee, K. Identifying risk factors of musculoskeletal disorders on Korean farms un rre ct pr oo f v er si o n oo un co rre ct ed. **00,** 1–9 (2014).

7. Edd, J. M. M. *et al.* Priority Risk Factors for Back Injury in Agricultural Field Work. 39–54 (2008).

8. Mccurdy, S. A. & Carroll, D. J. Agricultural Injury. **480,** 463–480 (2000).

9. Fathallah, F. A. Musculoskeletal disorders in labor-intensive agriculture. *Appl. Ergon.* **41,** 738–743 (2010).

10. Ng, Y. G. *et al.* Risk factors of musculoskeletal disorders among oil palm fruit harvesters during early harvesting stage. **22,** 286–292 (2015).

11. World Bank. Indicator: Agriculture Employees. (2017).

12. Birrell, S. a & Hooper, R. H. Initial subjective load carriage injury data collected with interviews and questionnaires. *Mil. Med.* **172,** 306–11 (2007).

13. Birrell, S. A. & Haslam, R. A. Subjective Skeletal Discomfort Measured Using a Comfort Questionnaire Following a Load Carriage Exercise. *Mil. Med.* **174,** 177–182 (2009).

14. Legg, S. J., Barr, A. & Hedderley, D. I. Subjective perceptual methods for comparing backpacks in the field. *Ergonomics* **46,** 935–955 (2003).

15. Lloyd, R., Parr, B., Davies, S. & Cooke, C. Subjective perceptions of load carriage on the head and back in Xhosa women. *Appl. Ergon.* **41,** 522–529 (2010).

16. Hong, Y., Li, J. X., Ki, A. S. & Robinson, P. D. Effects of load carriage on heart rate , blood pressure and energy expenditure in children. 37–41 (2000). doi:10.1080/001401300404698

17. Jena, S., Kumar, A., Singh, J. K. & Mani, I. Biomechanical model for energy consumption in manual load carrying on Indian farms. *Int. J. Ind. Ergon.* **55,** 69–76 (2016).

18. Nag, P. K., Nag, P. K., Sen, R. N. & Ray, U. S. Cardio-respiratory performance of porters carrying loads on a treadmill. *Ergonomics* **22,** 897–907 (1979).

19. Drain, J., Billing, D., Neesham-Smith, D. & Aisbett, B. Predicting physiological capacity of human load

carriage - A review. *Appl. Ergon.* **52,** 85–94 (2016).

20. Paul, S. *et al.* Physiological and biochemical responses during incremental uphill load carriage. *Int. J. Ind. Ergon.* **50,** 26–33 (2015).

21. Bhambhani, Y. & Buckley, S. Physiological and biomechanical responses during treadmill walking with graded loads. 544–551 (1997).

22. Malville, N. J., Byrnes, W. C., Lim, H. A. & Basnyat, R. Commercial Porters of Eastern Nepal : Health Status , Physical Work Capacity , and Energy Expenditure. **56,** 44–56 (2001).

23. Mackie, H. W. & Legg, S. J. Postural and subjective responses to realistic schoolbag carriage. *Ergonomics* **51,** 217–231 (2008).

24. Knapik, J. J. *et al.* Soldier performance and strenuous road marching: influence of load mass and load distribution. *Mil. Med.* **162,** 62–67 (1997).

25. Chow, D. H. K., Ting, J. M. L., Pope, M. H. & Lai, A. Effects of backpack load placement on pulmonary capacities of normal schoolchildren during upright stance. *Int. J. Ind. Ergon.* **39,** 703–707 (2009).

26. Mackie, H. W., Legg, S. J., Beadle, J. & Hedderley, D. Comparison of four different backpacks intended for school use. *Appl. Ergon.* **34,** 257–264 (2003).

27. Orantes-Gonzalez, E., Heredia-Jimenez, J. & Beneck, G. J. Children require less gait kinematic adaptations to pull a trolley than to carry a backpack. *Gait Posture* **52,** 189–193 (2017).

28. Porter, G. *et al.* Social Science & Medicine Health impacts of pedestrian head-loading : A review of the evidence with particular reference to women and children in sub-Saharan Africa. *Soc. Sci. Med.* **88,** 90–97 (2013).

29. Minetti, A. E., Formenti, F. & Ardigo, L. P. Himalayan porter's specialization: metabolic power, economy, efficiency and skill. *Proc. R. Soc. B Biol. Sci.* **273,** 2791–2797 (2006).

30. Simpson, K. M., Munro, B. J. & Steele, J. R. Backpack load affects lower limb muscle activity patterns of female hikers during prolonged load carriage. *J. Electromyogr. Kinesiol.* **21,** 782–788 (2011).

31. Simpson, K. M., Munro, B. J. & Steele, J. R. Effect of load mass on posture, heart rate and subjective responses of recreational female hikers to prolonged load carriage. *Appl. Ergon.* **42,** 403–410 (2011).

32. Borg, G. Psychophysical bases of perceived exertion. (1982).

33. Corlett, E. N. & Bishop, R. P. A Technique for Assessing Postural Discomfort. 37–41 (1979).

34. MacQueen, J. B. Some Methods for classification and Analysis of Multivariate Observations. (1967).

35. Centers for Disease Control and Prevention. Body Mass Index : Considerations for Practitioners. (2009).

36. Roser, M. Human Height. (2016).

37. Holewijn, M. Physiological strain due to load carrying. 237–245 (1990).

38. Majumdar, D., Bhattacharyya, M., Kumar, R. & Majumdar, D. Optimum load for carriage by soldiers at two walking speeds on level ground. *Int. J. Ind. Ergon.* **39,** 68–72 (2009).

39. Pimental, N. A. & Pandolf, K. B. Energy expenditure while standing or walking slowly uphill or downhill with loads. 37–41 (2007). doi:10.1080/00140137908924670

40. Niebel, B. Niebels Methods, Standards and Work Design. 4 (2014).

Regional Action Plan Towards SDG 6: Achieving Universal Access to Safe and Affordable Drinking Water

Dewi Junita Koesoemawati [1], Yuliana Sukarmawati [,2*], Rindang Alfiah [3]

University of Jember

[1]dewi.teknik@unej.ac.id, [2]yuliana.sukarmawati@unej.ac.id [3] rindangalfiah@unej.ac.id

Abstract

Since the establishment of Sustainable Development Goals 2030 (SDGs) to end global problems and challenges, Indonesia has demonstrated a strong commitment in achieving universal access to safe and affordable drinking water. Clearly, achieving SDG Goal 6 require synergy in the development of strategic plan and policies both at the national level and city levels. This study aims to develop regional action plan in Jember Regency which consists of annual target policies, strategies and work programs as a guideline for government and stakeholders in implementing their daily activities to support the water for all vision. Data collection method used was interviews and focus group discussion which involving all relevant stakeholders as well as the local community and to be followed by expert justification. The results show that the main problems and challenges in achieving affordable drinking water are the low coverage of access to drinking water in rural areas, limited water supply sources, and lack of the involvement from business enterprise by corporate social responsibility programs. The proposed programs are categorized into two different policy framework containing the performance improvement of drinking water management and the strengthening of water organization capacity.

Keywords SDG, clean water, action plan.

BACKGROUND

Drinking water is one of the most vital resources for life and fundamental human need. Indonesian government has been agreed to achieve universal access of water supply and sanitation in 2030. One of which, Indonesian government has been committed to reach 100% access to safe and affordable drinking water as stated in 17 goals of Sustainable Development Goal (SDG). Achieving SDG Goal 6 require synergy in the development of strategic plan and policies both at the national level and city levels. Clearly, it is now urgently needed to establish regional action plan in water supply and management in specific, measurable, attainable, and relevant goals. Thus, in this study we develop regional action plan in Jember Regency which consists of annual target policies, strategies and work programs as a guideline for government and stakeholders in implementing their daily activities to support the water for all vision.

MATERIALS AND METHODS

1. **Study area**

    The location of study is Jember Regency which consists of 31 district. This research collects data from all different types of community ranging from low-income up to high-income residential area.

2. **Data collection method**

Research data consists of primary data and secondary data as follows:

a. Primary data

    Primary data collected form surveys, observations and questionnaire. We conduct focus group discussion with sanitarian from 50 health service center from 31 district around Jember Regency to obtain their insights about current state of drinking water supply and management in Jember.

b. Secondary data

    Secondary data obtained by collecting reports and master plan documents from all relevant stakeholders such as Department of Housing, Department of Water Resources Management, Department of Environment Management, Department of Health and Department of Regional Planning, Department of Statistics.

3. Data analysis method

There are three stages in analyzing current state of drinking water supply as well as establishing regional framework to achieve safe and affordable drinking water.

1. Analyzing challenges and opportunity of the framework implementation of SDG 6 by assessing current issues and constraints
2. Defining policy framework based on goals of SDG 6 as well as medium-term national plan (RPJMN 2016-2019)
3. Establishing strategies, target policies, strategies and work programs as a guideline for government and stakeholders in implementing their daily activities to support the water for all 2030 vision as shown in Table 1.

Tabel 1. Targets and indicators of water and sanitation for all

Target	Indicator
Universal access to safe and affordable drinking water	1. Proportion of population using safe drinking water services
	2. Proportion of bodies of water with good ambient water quality
	3. Change in water-use efficiency over time
	4. Degree of integrated water resources management

Source: United Nations, 2018

DISCUSSION AND ANALYSIS

1. Potensi dan Permasalahan Akses Air Minum

Access to drinking water is almost completely sufficient, even though achieved by having communal drinking water sources. To meet the needs, it requires an integrated facilities and infrastructure for drinking water supply, or better known as SPAM. The implementation of SPAM is a series of activities in carrying out the development and management of facilities and infrastructure that follows the basic management process which includes planning, implementing, monitoring and evaluating activities in order to optimize the benefits and functions of SPAM for drinking water supply to the community. There are several types of drinking water from the regional water company (PDAM), which comes from ground water, spring, and surface water. The source of water that comes from surface water comes from the treatment of the Bedadung and Mayang rivers. Drinking water supply in Jember Regency is also served by community consisting of piped connections, which is originating from PDAM and HIPPAM and non-piping connections, originating from shallow wells, drilled wells as well as unprotected springs. HIPPAM is a water management organization in rural areas where usually utilizes existing water sources in their respective regions through assistance from the Department of Housing and Public Works. Current conditions of the HIPPAM in Jember Regency are shown in table 2.

Tabel 2. Quantity, location and current performance of drinking water supply network and reservoirs

Area	Qty	Location	Performance	Reservoirs
Jelbuk	1	Ds. Panduman	Poor	-
Arjasa	6	Ds.Darsono	Poor	Not available
		Ds.Darsono	Poor	Not available
		Ds.Darsono	Good	Available
		Ds.Darsono	Good	Available
		Ds.Kemuning Lor	Poor 50%	Poor 75%
		Ds.Biting	Poor	Not available
Silo	5	Ds.Sumber Jati	Good	Available
		Ds.Silo	Good	Available

Area	Qty	Location	Performance	Reservoirs
		Ds.Karang Harjo	Good	Available
		Ds.Karang Harjo	Good	Available
		Ds.Pace	Good	Available
Sumberjambe	3	Ds.Jambearum	Good	Available
		Ds.Cumedak	Good	Available
		Ds.Pringgodani	Good	Available
Panti	1	Ds. Kemiri	Rusak	-
Ledokombo	6	Ds.Sumberlesung	Good	Available
		Ds.Sukogidri	Good	Available
		Ds.Lembengan	Good	Available
		Ds.Sumberbulus	Good	Available
		Ds.Karangpaiton	Good	Available
		Ds.Sumbersalak	Good	Available
Semboro	14	Ds.Pondok dalem	Good	Not Available
		Ds.Pondok dalem	Good	Not Available
		Ds.Pondok dalem	Good	Not Available
		Ds.Pondok dalem	Good	Not Available
		Ds.Pondok dalem	Good	Not Available
		Ds.Pondok dalem	Good	Available
		Ds.Pondok dalem	Good	Available
		Ds.Pondok dalem	Good	Available
		Ds.Pondok dalem	Good	Available
		Ds.Pondok dalem	Good	Available
		Ds.Pondok dalem	Good	Not Available
		Ds.Pondok joyo	Good	Available
		Ds.Pondok joyo	Weak	Available
		Ds.Pondok joyo	Good	Available
Mayang	5	Ds.Tegalwaru	90%	Good
		Ds.Sidomukti	Good	2 good, 7 poor
		Ds.Seputih	Weak	Weak
		Ds.Seputih	Good	2 good, 3 poor
		Ds.Seputih	Good	5 good, 3 poor
Kaliwates	4	Kel.Kaliwates	Good	Available
		Kel.Kebun agung	Good	Available
		Kel.Kebon agung	Good	Available
		Kel.Kebon agung	Good	Available
Patrang	15	Kel.Gebang	Poor	Poor
		Kel.Baratan	Good	Available
		Kel.Bintoro	Good	Available
		Kel.Bintoro	Good	Available

Area	Qty	Location	Performance	Reservoirs
		Kel.Bintoro	Good	Poor
		Kel.Slawu	Good	Available
		Kel.Jumerto	Good	Available
		Kel.Banjarsengon	Good	Available
		Kel.Banjarsengon	Good	Available
		Kel.Banjarsengon	Good	Available
		Kel.Banjarsengon	Good	Available
		Kel.Banjarsengon	Good	Available
		Kel.Banjarsengon	Good	Available
		Kel.Banjarsengon	Good	Available
		Kel.Banjarsengon	Good	Available
Kalisat	3	Ds.Plalangan	Good	Available
		Ds.Gambiran	Good	Available
		Ds.Sumber Ketempa	Poor	Available
Pakusari	1	Ds. Subo	Good	-
Sukorambi	3	Ds.Sukorambi	Good	Available
		Ds.Karangpring	Good	Available
		Ds.Kelungkung	Good	Available
Tanggul	4	Ds.Mangisan	Weak	Available
		Ds.Darungan	Good	Available
		Ds.Tanggul Wetan	-	-
		Ds.Selodakon	Good	Available
Sumberbaru	2	Ds.Jambesari	Good	Not Available
		Ds.Karang Bayat	Good	Available
Bangsalsari	1	Ds. Bangsalsari	Good	-

Source: Jember masterplan of water supply and management, 2015

Tabel 3. Drinking water infrastructure

No.	Types of infrastructure	Qty
1	Pipe network systems	38.031
2	Non-pipe network systems	75.437
3	Shallow water well	328.032
4	Deep water well	56.225
5	Spring protector and reservoirs	14.453
6	Hydrant	5.744
7	Bore well	6.562
8	Shared drinking water well	18.692
9	Miscellaneous	911

Source: Department of Health, Jember (2018)

As stated by Department of Health, population of Jember is 2.363.016 (740.068 households) which consist of 2.111.956 (670.694 households) rural population and 2.111.956 (670.694 households) urban population. Total achievement can be calculated by comparing total population with the quantity of drinking water infrastructure, as shown in Table 3.

Tabel 3. Drinking water baseline target

No.	Types of infrastructure	Qty
1	Pipe network systems by regional water service company	36.038
2	Pipe network systems by community based-water service	75.437
3	Non-pipe network systems	430.520
	Total	541.995 (73%)

Source: Department of Health and Jember Water Service Company (2018)

Current state of drinking water supply and management can be reviewed from relevant documents such as medium-term regional plan in Jember Regency (RPJMD Kabupaten Jember), as follows:

Tabel 5. Short-term target in drinking water supply and management

Indicator	Baseline	Target 2019
Drinking water access per household	382.258 household	466.542 household

Source: Government of Jember (2018)

Tabel 6. Current achievement in drinking water supply and management

No.	Indicator	Target	Achievement
1	Pipe network systems by community based-water service	154	164

Source: Government of Jember (2018)

Based on the total population of Jember Regency, current achievement of drinking water access as shown in Table 3 is 73%, which means 16% higher than targeted by regional plan (RPJMD). To be able to completely achieved, we need to address several water-related issues, as follows:

1. Lack of updated regulation about drinking water supply and management
2. Lack of inter-sectorial policies
3. Degradation of raw water resources in quality as well as in quantity
4. Unbalancing state between population and available infrastructure
5. Lack of community awareness in hygiene because of culture
6. Limited availability of water service provider in regional level
7. Limited capability of local government in addressing water supply issues despite of the regional autonomy
8. Limited capital investment in water supply infrastructure from public and private sector

Tabel 4. Challenges and opportunity of drinking water supply and management

No.	Indicator	Challenges
1	Technical aspect	**1.** Intermittent supply of drinking water from regional water company (PDAM)
2	Social aspect	1. Lack of community awareness in hygiene because of culture 2. Lack of knowledge in the importance of drinking water access 3. Poor economy level in rural areas
3	Financial aspect	1. Lack of financial resources

		2. Lack of the local government ability in providing financial resources for drinking water supply and management
4	Management aspect	1. Lack of harmonization among stakeholders to support the improvement of drinking water supply and management 2. Lack of coordination from external parties in organizing community and social responsibility 3. Lack of private entities and community-based entities in drinking water supply sector
5	Environmental aspect	Water quality degradation because of the increasing of population density which lead to the contamination of water source by domestic wastewater

2. Policy framework in water supply and management year 2019-2024

The direction of the Regional Action Plan for Clean Water Supply and Management in Jember Regency supports the policy on drinking water sourced from the Medium-Term National Development Plan (RPJMN), the Medium-Term Regional Development Plan (RPJMD), the Public accountability report on the budget implementation presented by local government heads to the DPRDs (LPJK) and the Masterplan of Drinking Water Supply and Management Document (RISPAM). The policy for developing drinking water supply systems is based on an analysis of problems, challenges and applicable service standards. The policy directions made as a basis for the regional action plan in the supply of drinking water are described as follows.

Tabel 7. Regional Water Supply Access Policy

No	Policy Sources	Policy	Target
1	RPJMN	Development and Utilization of Appropriate Technology for water treatment / purification / drinking	The number of regions applying appropriate technology in 2019 will reach 25 regions
		Raw Water Supply and Management	Facilities and Infrastructure for the management of raw water improved
			The functions and services of raw water infrastructure are returned to normal
			Increased regional capacity in providing and managing raw water for 100% of clean water that is held
		Operation and mainteance of natural resources facilities and infrastructure	Facilities and infrastructure for managing raw water whose functions and services are maintained
		Regional Drinking Water Supply (SPAM) infrastructure development	The construction of 1.320.000 house connection for regional scale
		Urban Drinking Water Supply infrastructure development	The construction of 9.991.200 house connection for sub-district capital
			Development of 4,268,800 drinking water supply for the Capital City Expansion
		Development of rural drinking water supply infrastructure	Development of 9.665.920 community-based drinking water supply
		Drinking water supply infrastructure development in special region	Establishment of 661,000 house connection of drinking water supply in Urban Slums area
			Establishment of 66,200 connections to drinking water supply houses in the Fisherman Area
			Establishment of 1.705.920 connection to drinking water supply in water prone areas/border/outermost island

No	Policy Sources	Policy	Target
		Facilitation of drinking water supply by local water company (PDAM)	Assisted program in 174 PDAMs
			Development of the Low Income Community (MBR)- SPAM network in 4,909 regions
		Facilitation SPAM Non-PDAM	Assistance with 50 regional technical implementing units
			Development of the MBR SPAM network in 1,400 regions
		regulating, guiding and supervising the development of drinking water	the implementation, regulation and supervision of the development of drinking water
		monitoring and developing SPAM	the compilation of 1,018 monitoring and guidance reports on the implementation of SPAM
		Facilitating the development of funding sources, investment patterns for SPAM implementation, investment promotion	225 reports on facilitation for the development of financing sources, investment patterns for SPAM implementation, investment promotion
2	LKPJ	Drinking Water	The total population group of independent drinking water providers is 248 groups
3	RISPAM	Service system plan	the development of a new sub-district capital city that has a closed water service system with a target of service coverage for Jember Regency up to 2028 is 70%, both served by the Piping Network (JP), and not the Piping Network (BJP), both served by the PDAM, and by Local Drinking Water Management and Utilization Organization.
		SPAM development plan	the capital of Sumberjambe sub-district, capital of Sukowono sub-district, capital of Wuluhan sub-district, capital of Tempurejo sub-district, capital of Panti sub-district, capital of Mayang sub-district, capital of Sukorambi sub-district, capital of Silo sub-district.

3.   Target policies, strategies and work programs
Referring to the current status of clean water supply, a series of objectives, goals and strategies has been established based on the combination of SWOT analysis and SDG's universal target as stated in the Decree of President No.59 Year 2017, as follows:

1. Policy integration in increasing service level of clean water supply and sanitation
2. Developing self-management system in clean water supply
3. Optimizing the effectiveness and continuity of clean water access
4. Establishing local team project
5. Budget allocation in tourism sector for the development of clean water access
6. Balancing budget proportion for all sectors especially clean water access and infrastructure provision
7. Developing and innovating applied technology
8. Increasing participation for all stakeholders
9. Increasing the private sector participation in allocating budget for clean water access and infrastructure by CSR (Corporate Social Responsibility)
10. Enhancing campaign, promotion and education of hygiene

There are three different approaches in increasing clean water access and infrastructure provision, as stated in national plan (RPJMN) as follows:
1. Infrastructure performance optimization (supply side)
2. Increasing service efficiency (demand side)
3. Providing master plan of clean water supply

To completely achieve universal access target in clean water supply, a series of policy and program has been established in Jember Regency, as follows:

1. Action plan in increasing the performance of clean water supply and management
   a. New connection program in high-density residential area
   b. Water losses reduction plan by water meter and valve rehabilitation and water flow meter installation in transmission and production pipe network
   c. Construction of spring protection infrastructure
   d. Construction of water reservoir infrastructure to replace 17 damaged reservoir in Jember Regency
   e. Strengthening master plan of clean water supply and management as well as feasibility analysis of technology, environment, social, economic and financial.

2. Action plan in maintaining environmental quality
   a. Repetitive water quality test and assessment
   b. Preventing water body contamination by river water monitoring as guided by government regulation No.82 Year 2001

3. Action plan in enhancing the roles and responsibilities of local government
   a. Establishing local team project to assist and strengthen the roles and responsibilities of local government
   b. Community participation in clean water supply and management
   c. Community education in clean water supply and management
   d. Repetitive scheduled meeting for local team project, partner and member of stakeholders

4. Action plan in increasing the public awareness of hygiene
   a. Public talk in hygiene and sanitation
   b. Training in the budget allocation strategy in hygiene and sanitation for stakeholders
   c. Enhancing infrastructure provision in public space, schools and health service points
   d. Training for hygiene and sanitation ambassador

ACKNOWLEDGMENTS

REFERENCES

1. BAPPENAS.Agenda Nasional Pembangunan Air Minum dan Sanitasi 2015-2019. BAPPENAS: Direktorat Permukiman dan Perumahan
2. Budiantoro, Setyo. 2017. Metadata untuk Penyusunan Rencana Aksi yang Partisipatif. Jakarta: BAPPENAS
3. Direktorat Cipta Karya. 2016. Petunjuk Teknis Penyusunan, Pelaksanaan dan Pemantauan RAD AMPL Program PAMSIMAS. Jakarta: PAMSIMAS.
4. Kementerian Perencanaan Pembangunan Nasional. 2017. Ringkasan Metadata Indikator Tujuan Pembangunan Berkelanjutan (TPB)/Sustainable Development Goals (SDGs) Indonesia. Jakarta: BAPPENAS
5. Komisi Nasional Hak Asasi Manusia.Kerangka Analisis untuk Mengintegrasikan Tujuan Pembangunan Berkelanjutan (SDGs) dengan Kewajiban Pemenuhan Hak-hak Asasi Manusia untuk di Indonesia.https://sdg.komnasham.go.id/sdg-content/uploads/2017/04/Tujuan-6.pdf

6. Pemerintah Republik Indonesia. 2017. Peraturan Presiden RI No. 59 Tahun 2017 tentang Pelaksanaan Pencapaian Tujuan Pembangunan Berkelanjutan.
7. United Cities and Local Governments.Tujuan Pembangunan Berkelanjutan yang Perlu Diketahui oleh Pemerintah Daerah.https://www.uclg.org/sites/default/files/tujuan-sdgs.pdf
8. UNICEF. 2012. Air Bersih, Sanitasi & Kebersihan.
9. https://www.unicef.org/indonesia/id/A8_-_B_Ringkasan_Kajian_Air_Bersih.pdf